THE PHYSICAL REVIEW

VOLUME 89 Second Series NUMBER 3

FEBRUARY 1, 1953

Published for the

AMERICAN PHYSICAL SOCIETY

by the

AMERICAN INSTITUTE OF PHYSICS

LANCASTER, PA., AND NEW YORK, N. Y.

THE PHYSICAL REVIEW

A journal of experimental and theoretical physics established by E. L. Nichols in 1893

Published by the American Institute of Physics for the

AMERICAN PHYSICAL SOCIETY

Officers

President

J. H. Van Vleck
Harvard University
Cambridge, Massachusetts

Vice-President

Enrico Fermi
Institute for Nuclear Studies
University of Chicago
Chicago 37, Illinois

Secretary

K. K. Darrow
Bell Telephone Laboratories
Office:
Columbia University
New York 27, New York

Treasurer

G. B. Pegram
Columbia University
New York 27, New York

Local Secretary for the Pacific Coast

J. Kaplan
University of California at Los Angeles
Los Angeles, California

Managing Editor

S. A. Goudsmit
Brookhaven National Laboratory
Upton, Long Island
New York

BOARD OF EDITORS

Editor

S. A. Goudsmit

Assistant Editor

S. Pasternack

Associate Editors

Stanley Brooks	M. Goldhaber	W. P. Allis
J. F. Carlson	R. Hofstadter	F. G. Brickwedde
G. L. Critchfield	A. W. Lawson	W. B. Fretter
W. Deming	A. Pais	Corvens Hellmer
T. H. Johnson	R. Serber	H. W. Lewis
Hanna Kopfermann	C. H. Townes	Arnold Nordsieck

Manuscripts for publication should be submitted to S. A. Goudsmit, Brookhaven National Laboratory, Upton, Long Island, New York. The contributing institutions are requested to pay a publication charge of $15 per page which, if honored, entitles them to 100 free reprints. Instructions will be sent with galley proofs.

Proof and all correspondence concerning papers in the process of publication should be addressed to the Publication Manager, American Institute of Physics, 57 East 55 Street, New York 22, New York.

Subscription Price

United States and Canada.....$20.00
Elsewhere.....$22.00

Back Numbers[1]

Single back number into which complete year is available
Prior to 1949: $25.00
Thereafter: $23.00
Single copies: $3.00 each, prior to July, 1929;
$1.50 each, July, 1929–December, 1941;
$2.00 each, January, 1942–December, 1946;
$1.25 each, thereafter.
Current Index, 1975–1980: $4.00.

Subscriptions, renewals, and orders for back numbers should be addressed to the American Institute of Physics, 57 East 55 Street, New York 22, New York.

Changes of address in the case of members of the American Physical Society should be addressed to the Treasurer; in the case of other subscribers to the American Institute of Physics.

[1] Issues 1 (Series II) Physics Department, Cornell University, Ithaca, New York.

The Physical Review is published semi-monthly at Pilon and Lime Streets, Lancaster, Pennsylvania.

Entered as second-class matter March 6, 1918, at the Post Office at Lancaster, Pennsylvania, under the Act of March 3, 1879.

Acceptance for mailing at special rate of postage provided for in paragraph (d-2), section 34.40, P. L. & R. of 1948, authorized January 27, 1950.

THE
PHYSICAL REVIEW

A journal of experimental and theoretical physics established by E. L. Nichols in 1893

SECOND SERIES, VOL. 89, NO. 3 FEBRUARY 1, 1953

The Internal Pair Production of γ-Rays of Mesonic Origin; Alternate Modes of π^0 Decay*

P. LINDENFELD AND A. SACHS, *Columbia University, New York, New York*

AND

J. STEINBERGER, *Brookhaven National Laboratory, Upton, Long Island, New York, and Columbia University, New York, New York*

(Received September 15, 1952)

The internal pair creation of the γ-rays in the processes

(1) $\pi^0 \rightarrow \gamma+\gamma$,
(2) $\pi^-+P \rightarrow \gamma+N$

has been observed. The experimental conversion coefficient $\beta=0.0080\pm0.0016$ is to be compared to the theoretical prediction, 0.0063. In addition, we have obtained an upper limit on the fraction of neutral pions which decay directly into a pair: $\pi^0 \rightarrow e^+ + e^-$. The limit is one in 2000.

I. INTRODUCTION

As in lower energy phenomena, mesonic processes usually resulting in γ-ray emission may instead produce an electron-positron pair. The characteristics of this pair are calculable in good approximation on the basis of quantum electrodynamics, and there is all reason for confidence in these theoretical results.[1,2] Since some of the theoretical findings are necessary in the analysis of the experiments which are here described, they will be stated briefly. (a) The internal conversion rate is expected to be

$$\beta \cong \frac{2\alpha}{3\pi}\left[\ln\frac{E}{mc^2}-1.4\right],$$

where $\alpha=1/137$, $E=$photon energy, and $m=$electron mass. (b) The electrons are emitted with angular correlation

$$P(\theta)d\theta \simeq \text{const}\times d\theta/\theta; \quad \theta > 4mc^2/E.$$

Half of the pairs are emitted within the correlation angle $\theta_{\frac{1}{2}}=(8mc^2/E)^{\frac{1}{2}}$. For the following it may be pointed out that this distribution is slightly broader than that of pairs produced and scattered in 1 g/cm² Pb converter. (c) The electrons are emitted with a flat energy distribution from mc^2 to $E-mc^2$.

These properties are to good approximation independent of the nature of the recoil and the multipole character of the radiation.[1] In addition, it may be noticed that β is only weakly dependent on the γ-ray energy. For $E=130$ Mev, $\beta=0.0065$; for $E=70$ Mev, $\beta=0.0062$.[2] We have studied this conversion in the processes

$$\pi^0 \rightarrow \begin{cases} \gamma+\gamma & \text{(1a)} \\ \gamma+e^++e^-, & \text{(1b)} \end{cases}$$

$$\pi^-+P \rightarrow \begin{cases} \gamma+N & \text{(2a)} \\ e^++e^-+N. & \text{(2b)} \end{cases}$$

The photons of process (1) have approximately 70-Mev energy; those of process (2) have 130 Mev. Pairs of electrons, probably the result of the π^0 decay in (1b) have been observed by Daniel, Davies, Hulvey, and Perkins[3] in cosmic-ray stars and by Lord, Fainberg, Haskin, and Schein[4] in π^- induced stars.

In addition, we consider the disintegration

$$\pi^0 \rightarrow e^+ + e^-. \quad \text{(1c)}$$

From a theoretical point of view, (1c) may proceed in 3 ways: (a) There is a specific meson-electron interaction. (b) The meson, possibly with the help of

* Research supported by joint contract of ONR and AEC.

[1] J. R. Oppenheimer and L. Nedelski, Phys. Rev. **44**, 948 (1939).

[2] R. H. Dalitz, Proc. Phys. Soc. (London) **A64**, 667 (1951).

[3] Daniel, Davies, Hulvey, and Perkins, Phil. Mag. **43**, 753 (1952).

[4] Lord, Fainberg, Haskin, and Schein, Phys. Rev. **87**, 538 (1952).

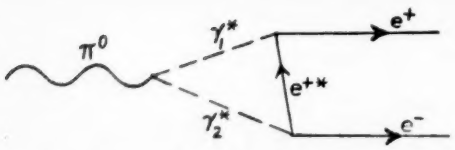

FIG. 1. Feynman diagram for the disintegration (1c) proceeding by way of two intermediate virtual photons.

intermediate nucleon states, produces a virtual photon which creates the pair. (c) The meson produces 2 virtual photons by means of the interaction responsible for 1(a) and 1(b) (see Fig. 1). The electrons are the secondaries of these photons.

Process (b) is of the same order in α as (1a) and might be expected to compete favorably. However, it may be shown that it is not possible to construct a gauge and Lorentz invariant interaction which absorbs the neutral meson of zero spin and emits a virtual photon. For spin-zero mesons, therefore, process (b) can make no contribution.[5] This is a more general statement of a result noticed on the basis of a more specific model using intermediate nucleons to obtain the coupling between meson and photon fields.[6]

Process (c) can be calculated on the basis of quantum electrodynamics. It is of the same order in α as the decay into two pairs (Fig. 2). Both processes are expected, therefore, to be $10^{-4}-10^{-5}$ times as probable as (1a).

II. EXPERIMENTAL ARRANGEMENTS

We have studied (1) and (2) experimentally, using negative mesons stopped in liquid hydrogen. It has been shown by Panofsky *et al.*[7] that on coming to rest in hydrogen, the pion is absorbed, probably from the K orbit, and the reactions (1a) and (2a) proceed at the relative rate: $0.93/1\pm20$ percent. We examine the radiation from the target in coincidence (10^{-8} sec resolving time) with the incident meson, especially as a function of the amount of lead converter between the target and the detector. Those particles observed without converter, after subtracting pairs produced in the target, target walls, and detector, are attributed to the internal conversion electrons. The experimental arrangements are shown in Figs. 3, 4, and 8. All five counters are in coincidence. It is important that the geometry is such that electrons which originate in the heavier parts of the target are excluded. This is the reason for the small vertical dimension of counter No. 3.

It is equally important to keep the radiation thickness of the target, its walls and the counter as small as possible. In our case, we have a total conversion thickness of 0.094 g/cm² Pb equivalent or, on the basis of the experiments of Lawson,[8] 0.0068 and 0.0080 mean free paths for γ-rays of processes (1) and (2), respectively. This contributes a background approximately equal to the expected effects.

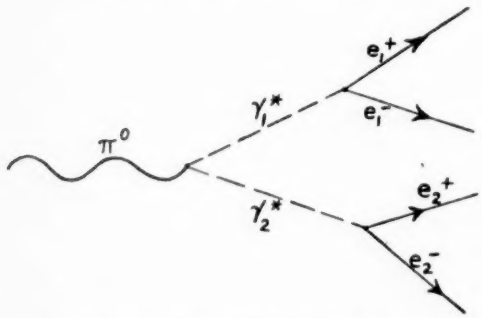

FIG. 2. Feynman diagram for the decay of a π^0 meson into two pairs.

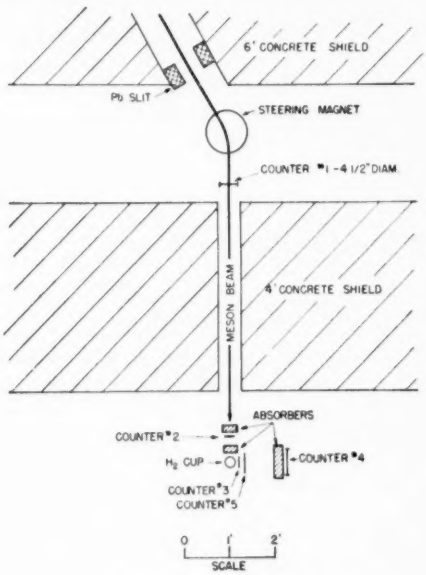

FIG. 3. Geometry, over-all.

III. EXPERIMENTAL RESULTS

A. Observed Events Caused by Mesons Stopped in H_2

The data exhibited in Fig. 5 (each point represents a subtraction filled cup−empty cup) show the variations of the coincidence rate with thickness of the absorber in the meson beam (absorber 1). The coincidences, both with and without converter, occur near the end of the range of the 70-Mev meson beam. The events are therefore produced by mesons *stopped* in hydrogen.

[5] Although for spin zero mesons these arguments forbid the decay into an electron pair by process (b), in the case of spin-one mesons, the decay into two γ-rays is forbidden and the decay into an electron pair is allowed.

[6] J. Steinberger, Phys. Rev. **76**, 1180 (1949).

[7] Panofsky, Aamodt, and Hadley, Phys. Rev. **81**, 565 (1951).

[8] T. Lawson, Phys. Rev. **75**, 433 (1949).

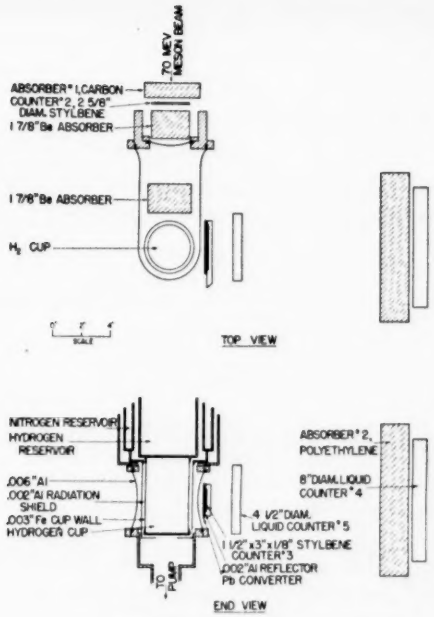

FIG. 4. Geometry, detail.

B. Conversion Characteristics

The conversion in lead of the radiation produced by the mesons stopping in hydrogen is shown in Fig. 6. Two points on this conversion curve were measured with greater accuracy to allow a more precise determination of the internal pair creation coefficient β. The data are given in Table I.

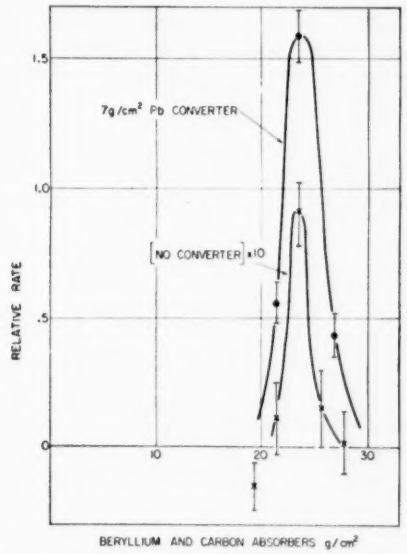

FIG. 5. Counting rates as a function of the incident meson range. Indicated errors are standard statistical fluctuation.

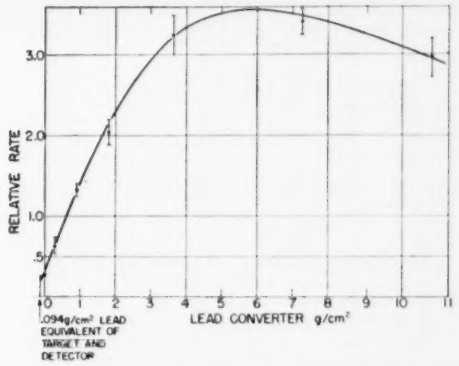

FIG. 6. Conversion characteristics of the radiation produced by mesons stopped in hydrogen. Indicated errors are standard statistical fluctuation.

The existence of the direct pairs is demonstrated in Fig. 6. If the conversion characteristics are extrapolated to that negative converter thickness which represents the conversion in the target and its walls, the remaining counting rate is the result of the internally converted pairs.

C. Electron Ranges

In Fig. 7 we present data on the attenuation in absorber No. 2 of the particles originating in hydrogen, both with and without 1 g/cm² Pb converter. Absorber thicknesses less than 55-Mev ionization loss equivalent are polyethylene, those in excess are a mixture of this and carbon.

Theoretically, we expect similar range curves with and without converter, since both the relative conversion rate of the two γ-ray groups as well as the energy spectra of the conversion electrons are very nearly the same in internal as in external conversion. This is in reasonable agreement with the experimental results.

D. 180° Coincidences

In process (1) the γ-ray or pair is accompanied by another γ-ray at an angle of between 168° and 180° in the laboratory system. The deviation from 180° is caused by the velocity of the neutral meson, approximately $(0.22\pm0.02)c$. Detection of this γ-ray can serve to distinguish between process (1) and process (2). We have detected 180° coincidences by replacing counter No. 5, Fig. 2, by a counter 8 in. in diameter, $6\frac{1}{4}$ in. from the center of the target, opposite telescope No. 3–No. 4 (see Fig. 8). The results are given in Table II.

TABLE I. Two points on the lead conversion curves. Absorber 2 is 5 g/cm² CH_2. Quoted error is standard statistical fluctuation.

Converter thickness	Counts per 10^6 incident particles		
	Target full	Target empty	Net due to H_2
None	4.95±0.31	0.47±0.13	4.48±0.34
0.96 g/cm² Pb	25.5 ±1.0	1.49±0.42	24.0 ±1.1

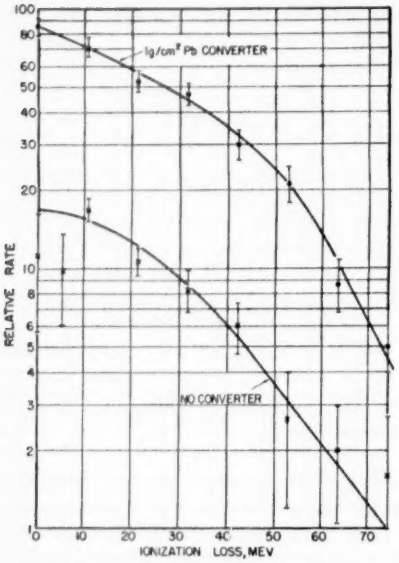

FIG. 7. Integral range of internal and external conversion electrons for two converter thicknesses. Indicated errors are standard statistical fluctuation.

IV. ANALYSIS OF THE EXPERIMENTAL DATA

A. Internal Pair Creation Coefficient β

In order to calculate the internal pair creation coefficient on the basis of the data (Table I), it is necessary to known: (a) the conversion probability of the γ-rays in the converter, (b) the conversion in the target, walls, and counters, (c) the relative efficiency for detecting the electrons produced by internal and external conversion.

Let

τ = conversion thickness of target, walls, etc.

$t = \tau$ + converter thickness = τ + 0.96 g/cm² Pb.

λ_1 = mean free path for pair creation of 70-Mev γ-rays.

λ_2 = mean free path for pair creation of 130-Mev γ-rays.

ϵ_{γ^1}, ϵ_{γ^2} = efficiency for detecting one member of the externally converted pair of processes (1) and (2).

ϵ_{e^1}, ϵ_{e^2} = efficiency for detecting one of the internally converted γ-rays of processes (1) and (2), respectively.

η = fraction of γ-rays due to process (2) = 0.35 ±0.07.[7]

$1-\eta$ = fraction of γ-rays due to process (1).

β = internal conversion coefficient.

Then the net counting rates, C.R., with and without converter, are

$$\begin{aligned}\text{C.R.}_t &= (1-\eta)\epsilon_{\gamma^1 t}(1-e^{-t/\lambda_1})+\eta\epsilon_{\gamma^2 t}(1-e^{-t/\lambda_2}) \\ &\quad +\beta[(1-\eta)\epsilon_{e^1 t}+\eta\epsilon_{e^2 t}], \\ \text{C.R.}_\tau &= (1-\eta)\epsilon_{\gamma^1 \tau}(1-e^{-\tau/\lambda_1})+\eta\epsilon_{\gamma^2 \tau}(1-e^{-\tau/\lambda_2}) \\ &\quad +\beta[(1-\eta)\epsilon_{e^1 \tau}+\eta\epsilon_{e^2 \tau}].\end{aligned} \tag{3}$$

Here we assume the thicknesses t and τ small enough so that secondary shower effects are negligible.

If

$$R \equiv \text{C.R.}_t/\text{C.R.}_\tau = 5.36 \pm 0.46,$$

then

$$\beta = \frac{(t/\lambda)\epsilon_{\gamma t} - R(\tau/\lambda)\epsilon_{\gamma\tau}}{R\epsilon_{e\tau} - \epsilon_{et}}, \tag{4}$$

where

$$(t/\lambda)\epsilon_{\gamma t} = (1-\eta)(1-e^{-t/\lambda_1})\epsilon_{\gamma^1 t} + \eta(1-e^{-t/\lambda_2})\epsilon_{\gamma^2 t} \tag{5}$$

and

$$\epsilon_{et} = (1-\eta)\epsilon_{e^1 t} + \eta\epsilon_{e^2 t}. \tag{6}$$

We proceed to the calculation of the several parameters.

(1) *Conversion in the Target and Detector* τ

The effective conversion thickness of target and detector is the following:

$\frac{1}{4}\pi \times 1.5$ in. $H_2 + (4/\pi) \times 0.0035$ in. Fe
$+0.011$ in. Al $+0.062$ in. CH.

The corresponding number of radiation lengths are

0.00172 H + 0.0063 Fe + 0.0032 Al + 0.0028 C
= 0.0140 radiation length.

$\tau = 0.0140 \times 5.9$ g/cm² $\times 1.12/0.98 = 0.0945$ g/cm² Pb equivalent, where the last factor is the measured ratio of pair creation cross sections in light elements and in lead.[8] $t = 0.96 + 0.094 = 1.055$.

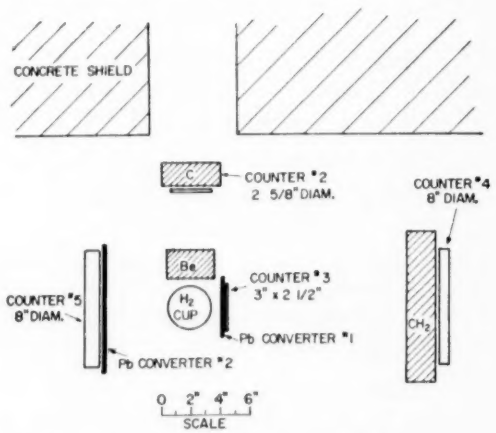

FIG. 8. Geometry of 180° coincidence experiments.

TABLE II. Experimental results on 180° coincidences (see Fig. 6). Errors tabulated are standard deviations.

Converter No. 1	Converter No. 2	Counts 1+2+3+4 per 10^6 incoming particles Target full	Target empty	Net	Counts 1+2+3+4+5 per 10^6 incoming particles Target full	Target empty	Net
none	none	21.7±1.0	9.4±1.2	12.3±1.6	0.525±0.17	0.15±0.15	0.37±0.25
1.85 g/cm² Pb	none	106 ±4.1	10.6±1.4	95 ±4.3	3.9 ±0.78	0.5 ±0.3	3.4 ±0.85
none	7.25 g/cm² Pb	23 ±1.0	8.8±0.9	14.2±1.4	1.86 ±0.26	0.13±0.09	1.73±0.28
0.96 g/cm² Pb	7.25 g/cm² Pb	65.3±2.2	10 ±1.5	55 ±2.7	10.8 ±0.9	0.2 ±0.2	10.6 ±0.9
1.85 g/cm² Pb	7.25 g/cm² Pb	112 ±4.3	9.9±1.4	102 ±4.5	16.6 ±1.7	0.33±0.25	16.3 ±1.7

(2) Mean Free Path for Pair Production λ

Again using Lawson's[8] data,

$$\lambda_1=11.8 \text{ g/cm}^2 \text{ Pb}; \quad \lambda_2=10.6 \text{ g/cm}^2 \text{ Pb}.$$

(3) Detection Efficiencies ε

The probability of detecting one of the electrons in a pair depends on the solid angle Ω of the detectors, on the probability s that the electron has sufficient range, and on the probability p that both members of the pair are detected. $\epsilon=s/(1+p)$; we drop the factor Ω which is common to all ε's, and consider a fixed photon energy. If $N(E)dE$ is the normalized energy distribution of the converted electrons, and if this corresponds to a normalized range distribution $M(R)dR$, then

$$s=\int_{R_{\min}} M(R)dR.$$

$R_{\min}$ is the minimum range necessary to traverse the counters and absorbers. If straggling is neglected in the following,

$$s=\int_{E_{\min}}^{E_{\max}} N(E)dE.$$

The factor p is the product of a geometrical factor g and a range factor r. r is the probability that particle 2 has sufficient range, given the fact that particle 1 does. Again, neglecting straggling,

$$r=\frac{1}{s}\int_{E_{\min}}^{E_{\max}-E_{\min}} N(E)dE=2-\frac{1}{s}, \qquad (7)$$

the last because of the symmetry of $N(E)$ in pair production. g is the geometrical probability of finding the second electron within counter No. 4, averaged over the position of incidence of electron 1 in this counter. We have not succeeded in solving this problem exactly, but have derived an approximate relation for a Gaussian correlation.

Let $P(r)=\exp(-r^2/a^2)$ be the distribution function of particle 2 about particle 1, where r is the distance between the particles, both r and a in units of the radius of counter No. 4. Then

$$g\cong\frac{2}{\pi}E\left(\frac{1}{a}\right)\left\{a\left[\exp\left(-\frac{1}{a^2}\right)-1\right]+(2+a)E\left(\frac{1}{a}\right)-\frac{a^2}{2}E\left(\frac{2}{a}\right)\right\}, \qquad (8)$$

where

$$E(x)\equiv\int_0^x \exp(-y^2)dy. \qquad (9)$$

For the computation of s and r, we have taken $N(E)=1/E_{\max}$, a good approximation for both external and internal pairs. $E_{\min}=17.4$ and 15.6 Mev with and without converter, respectively. The average radiation loss has been included in $E_{\min}$. Then

$$s_{1t}=0.75, \quad s_{1\tau}=0.77, \quad r_{1t}=0.67, \quad r_{1\tau}=0.70,$$
$$s_{2t}=0.87, \quad s_{2\tau}=0.88, \quad r_{2t}=0.85, \quad r_{2\tau}=0.86.$$

In evaluating g we have replaced the distribution of the internal pairs by a Gaussian with the same median. Taking into account scattering in the converter, we have from (2)

$$g_{\gamma^1 t}=0.64, \quad g_{\gamma^1\tau}=0.90, \quad g_{e^1 t}=0.36, \quad g_{e^1\tau}=0.45,$$
$$g_{\gamma^2 t}=0.81, \quad g_{\gamma^2\tau}=0.94, \quad g_{e^2 t}=0.51, \quad g_{e^2\tau}=0.59,$$

and

$$p_{\gamma^1 t}=0.43, \quad p_{\gamma^1\tau}=0.63, \quad p_{e^1 t}=0.241, \quad p_{e^1\tau}=0.315,$$
$$p_{\gamma^2 t}=0.69, \quad p_{\gamma^2\tau}=0.81, \quad p_{e^2 t}=0.43, \quad p_{e^2\tau}=0.508,$$

so that

$$\epsilon_{\gamma^1 t}=0.525, \quad \epsilon_{\gamma^1\tau}=0.473, \quad \epsilon_{e^1 t}=0.605, \quad \epsilon_{e^1\tau}=0.586,$$
$$\epsilon_{\gamma^2 t}=0.515, \quad \epsilon_{\gamma^2\tau}=0.486, \quad \epsilon_{e^2 t}=0.609, \quad \epsilon_{e^2\tau}=0.585.$$

It should be observed that only the relative efficiencies for external and internal pairs enter in the expression (4) for β. We believe that these relative efficiencies are in error by less than 10 percent.

(4) Compton Electrons

In the expression (4) for β we have failed to include the contribution of the Compton electrons. Although in lead this is only a few percent of that resulting from pair production, Compton electrons of the light elements are not negligible. We must add in the numerator of (4) the term $\frac{1}{2}[f_{Ct}-Rf_{C\tau}]$, where f_{Ct} and $f_{C\tau}$ are the

fraction of γ-rays detected by means of their Compton electrons, with and without converter, respectively. On the basis of the Klein-Nishina formula $f_{Ct}=0.0032$, $f_{C\tau}=0.0017$, and $\frac{1}{2}[f_{Ct}-Rf_{C\tau}]=-0.0030$.

(5) *Result*

We then obtain

$$\beta=\frac{(t/\lambda)\epsilon_{\gamma t}-(R\tau/\lambda)\epsilon_{\gamma\tau}-0.0030}{R\epsilon_{e\tau}-\epsilon_{et}},$$

$$=\frac{0.0453-0.0210-0.0030}{3.14-0.607},$$

$$=0.0084\pm0.0016.$$

The possible errors in β are as follows:

(a) Photons are converted in the heavier portions of the target and scattered into the telescope by the first counter. This requires a scattering through at least 30° in 0.004 radiation length, and should contribute negligibly.

(b) Electrons from μ-e decay. The μ-mesons may be either a beam contamination or else a contamination resulting from the decay of π-mesons which competes with π-capture in hydrogen. The electrons are emitted with a mean delay of 2.2×10^{-6} sec and have a probability 1/200 of occurring within the 10^{-8} sec resolving time of the coincidence circuits. The μ-meson beam contamination is 5–6 percent, and has somewhat larger range than that of the π-mesons, so that an even smaller percentage, compared to the π-mesons would stop in the hydrogen. They should, therefore, contribute at most $0.02/200=0.0001$ electron per stopped π-meson, one percent of the observed effect. The competition of π-μ decay and π-capture has been studied in the cloud chamber filled with hydrogen at 20 atmospheres by Sargent and Reinhardt.[9] No π-μ decays were observed in 20 events of stopping pions. Therefore, in liquid hydrogen, this competition cannot affect our result.

(c) The subtraction for conversion in the target, altogether 0.53 of the counting rate without converter, may be in error to the extent of the measured cross sections,[8] as well as the measured target thicknesses. We believe that altogether this should not contribute to the error in excess of 5 percent.

(d) The neglect of secondary shower effects leads to an underestimate of β. We estimate this effect to be less than 1.

Combining the errors, we have the experimental result $\beta_{\text{exp}}=0.0084\pm0.0019$, which is to be compared with the theoretical value $\beta_{\text{theory}}=0.0063$. The discrepancy is somewhat larger than the experimental uncertainty, it is also larger than a reasonable estimate of the theoretical uncertainty.

[9] We wish to thank authors Sargent and Reinhardt for these as yet unpublished results.

B. Upper Limit on the Direct Decay into Two Electrons

The data on 180° coincidences allows an upper limit to be placed on the fraction of π^0 mesons which decay directly into a pair. The fraction of such events is

$$\frac{\text{C.R. without converters, and resulting from electrons}}{\text{C.R. with converters}}\times\frac{\text{efficiency for detecting }\gamma\text{-ray pairs}}{\text{efficiency for detecting electron pairs}}.$$

The rate with converter is $16.3\pm1.7/10^6$ incoming particles, without converter it is $0.35\pm0.25/10^6$ incoming particles. It is possible, however, in this geometry to count some γ-rays converted in the heavy target walls near counter No. 5 (see Fig. 8). Even neglecting this, a rate $0.20/10^6$ incoming particles is derived from the conversion of γ-rays in the target walls and counters. An upper limit for the number of direct pairs counted may be $0.2/10^6$ incoming particles. The detection efficiency for the pair is approximately unity. The photon detection efficiency is obtained from the computations of IVA, with the help of the data of Figs. 6 and 7. We obtain 0.14 for telescope 3–4 with $\frac{3}{16}$ in. converter, and 5 g/cm^2 CH_2 absorber, and 0.30 for $\frac{1}{4}$ in. converter and no absorber. The over-all efficiency for counting the pair is therefore 0.042. We obtain

$$\frac{\text{rate }\pi^0\rightarrow e^+ + e^-}{\text{rate }\pi^0\rightarrow\gamma+\gamma}\leqslant\frac{0.2\times0.042}{16.3}=0.0005.$$

This upper limit is still larger than that expected from the production of electrons with the help of intermediate photons (Fig. 1). It is therefore only possible to state that the specific meson-electron pair interaction is smaller by at least a factor 2 000 than the meson-photon pair interaction.

C. The Branching Ratio $\pi^0\rightarrow\begin{matrix}\gamma+\gamma\\ \gamma+e^++e^-\end{matrix}$

The data of Table II also permit a separate estimate of the internal conversion rate for the γ-rays of neutral meson decay. The computation is as in Part (A) of this section; it is only necessary to make a correction for the difference in geometrical detection efficiency for the γ-ray in counter No. 5, Fig. 8. The difference is the result of a difference in the theoretical angular correlation function for the two processes, and is small because counter No. 5 subtends a large angle ($\pm33°$). We calculate a geometrical efficiency of 0.81 in the case of external, and 0.77 in the case of internal conversion. It may be noted that line 5 of Table II provides a check on the calculated efficiencies. We observe 0.160 ±0.019 γ-rays detected in counter No. 5 per γ-ray

detected in telescope 3–4. On the basis of the computations, we should expect $(1-\eta)\times 0.81\times 0.30=0.158$. (0.30 is the conversion efficiency, 0.81 the geometrical efficiency).

The data, lines 3 and 4, Table II, yield

$$R=\frac{(10.6\pm 0.9)\times 0.77}{(1.73\pm 0.28)\times 0.81}=5.83\pm 1.05;$$

$$\beta_{\pi^0}=\frac{(1-e^{-t/\lambda_l})\epsilon_{\gamma^1 l}-R(1-e^{-\tau/\lambda_l})\epsilon_{\gamma^1\tau}+\frac{1}{2}[f_{Cl}-Rf_{C\tau}]}{R\epsilon_{e^1\tau}-\epsilon_{e^1 l}},$$

$$=0.00725\begin{matrix}+0.0040\\-0.0025\end{matrix};$$

$$\frac{\text{rate}(\pi^0\to\gamma+e^+ +e^-)}{\text{rate}(\pi^0\to\gamma+\gamma)}=0.0145\begin{matrix}+0.0080\\-0.0045\end{matrix}.$$

This agrees with the theoretical prediction of 0.012,[2] and with the findings of the Bristol group.[3]

D. Absolute Counting Rates

It is not uninteresting to see whether or not the observed γ-ray flux does account for most of the incoming π-mesons. Per incoming pion we expect

$$n=1.5\times\frac{2t\epsilon_{\gamma l}}{\lambda}\times(\Omega/4\pi)\times\delta\times\text{outscattering factor},\quad(10)$$

where 1.5 is the number of γ-rays per captured pion; $t\epsilon_{\gamma l}/\lambda$ is the conversion and detection efficiency as in Sec. A and is 0.04 for 1 g/cm^2 Pb converter; Ω is the solid angle of detection and is 0.173 sterad; and δ is the fraction of mesons with proper range interval, approximately 0.16 from Fig. 5.

The outscattering factor is the hardest to estimate. If we include the effects of the size of counter No. 3 in this factor, and remember that the mesons are scattered rather badly near the end of their range, we estimate a factor $\frac{1}{6}$. Then $n=3.3\times 10^{-5}$; from Table I we see that 2.4×10^{-5} are observed. The observed photon flux, therefore, does account reasonably for the disappearance of the π^- mesons.

V. SUMMARY

We have observed the internal pair production of the γ-rays associated with π^- capture in hydrogen. The conversion coefficient is obtained on the basis of the experimental data, in conjunction with theoretical predictions on the angular correlation and energy distribution of the conversion electrons. The results are as follows: For the conversion of all photons, of which one-third result from the inverse photoeffect and are of 130 Mev, and two-thirds result from π^0 decay and are of $\sim$70 Mev, the experimental conversion coefficient is $\beta=0.0084\pm 0.0019$, in rough agreement with the theoretical result $\beta=0.0063$. For the neutral meson alone the decay into a photon and electron pair proceeds $0.0145\begin{matrix}+0.0075\\-0.0045\end{matrix}$ of the time, compared to the theoretical result 0.012. If we combine these two results, the experiment gives $\beta=0.0080\pm 0.0016$.

In addition, we have obtained an upper limit of 0.0005 on the fraction of neutral pions decaying into an electron pair alone. No such decay processes can occur through the intervention of a single virtual photon for spin-zero mesons. The number expected through the intervention of two virtual photons should be of the order of five times less than the observed limit. The experimental result, combined with experimental estimates on the half-life of the neutral mesons,[10] permits an upper limit to be placed on the direct interaction of the neutral meson with an electron pair. If this interaction is of the form $f\bar{\psi}\gamma_5\psi\phi$, where ψ and ϕ are electron and meson wave functions, respectively, then

$$(f^2/4\pi\hbar c)<10^{-11}.$$

We are indebted to M. Goldhaber, N. Kroll, and R. Serber for discussions which have materially clarified our understanding of the experimental results. H. J. Boorse kindly made his hydrogen liquifier available to us. The bombardments were carried out by the Nevis cyclotron crew under the direction of J. Spiro.

[10] The experimental results on the lifetime of the neutral meson are not entirely in agreement. Lord *et al.* [reference 4 and Phys. Rev. **80**, 970 (1950)] have evidence that $\tau<2-3\times 10^{-15}$. Daniel *et al.* (see reference 3), as well as Kaplan and Ritson [Phys. Rev. **85**, 900 (1952)] find $\tau\simeq 10^{-14}$ sec. For the purposes of this discussion we take $\tau>10^{-15}$.

The Blocked Capillary Method for Determining Melting Pressures: The Melting Curve of Helium from 1.5° to 4°K

C. A. SWENSON*
Jefferson Physical Laboratory, Harvard University, Cambridge, Massachusetts
(Received June 30, 1952)

The blocked capillary technique has been used to check previous piston displacement values for the helium melting pressure curve in the range from 1.5° to 4°K. In the course of these experiments, details of which are given, it was shown that melting pressure as given by the capillary blocking method are completely reliable, and can be very accurate. Variations of the capillary size or pressure difference across the capillary had no evident effect.

The behavior of the helium melting curve in the vicinity of the upper "triple point" is discussed in some detail. An analysis of the data indicates that it is in qualitative agreement with the assumption that the λ-transformation is of the second order.

I. INTRODUCTION

THE mechanical blocking of a fine capillary by the freezing of a liquid was first used by Kamerlingh Onnes at Leiden in his work on the melting pressure curve of hydrogen.[1,2] The method has been used rather extensively, since in the low temperature region it requires a simple experimental set-up and relatively small quantities of the substance being investigated. The accuracy of this technique, as compared with others, has never been systematically studied, and discrepancies in the work of several experimentalists can be attributed either to impurities in the substance used, or to an effect which is inherent in the method. P. W. Bridgman has pointed out that the application of shearing stresses can lead to a lowering of the melting point of a solid, and that these stresses must exist across the block in the capillary. In some experiments on carbon dioxide, Michels reduced this pressure difference to less than an atmosphere, and obtained good agreement with melting pressures obtained by Bridgman, who used the so-called "piston displacement" technique.[3]

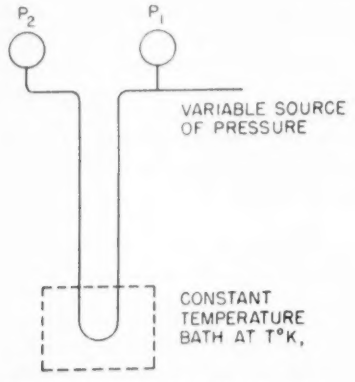

FIG. 1. A simple capillary blocking set-up.

In previously reported work, a modified form of the piston displacement method was used by the author to obtain melting pressures, latent heats of melting, and volume changes on melting for helium in the range from 1.6° to 4°K.[4] The melting pressure data were believed to be accurate to better than one-tenth of one percent, although the data as a whole were thermodynamically inconsistent in the region of the upper "triple point" on the helium phase diagram. This made it advisable for the melting pressure curve to be redetermined using an independent method, and the blocked capillary technique was chosen as the most convenient, and most likely to give accurate results. The apparatus and procedure which were found to be capable of giving reproducible capillary blocking data, in agreement with the piston displacement data, are described below. An analysis of the composite melting pressure data for helium is also given, together with quite reliable values for the entropy differences between liquid and solid helium along the melting curve.

II. EXPERIMENTAL DETAILS

Figure 1 shows the simplest version of a capillary blocking set-up.[2] The coldest point of the capillary is held at a constant temperature T, while the pressure on the liquid in the capillary is slowly increased. P_1 and P_2 will remain equal and increase together as long as the capillary is below the freezing pressure corresponding to T. Above the freezing pressure, there will no longer be continuity between the two gauges, and P_2 will give a constant reading (roughly the freezing pressure) as P_1 is increased.

Freezing points were found to be quite difficult to work with, since supercooling was often observed. A second procedure, which turned out to be more reliable, was used to measure melting points. The temperature of the loop T, was slowly lowered until the capillary was

* Now at the Cryogenic Engineering Laboratory, Massachusetts Institute of Technology, Cambridge, Massachusetts.
[1] H. Kamerlingh Onnes and W. van Gulik, Leiden Comm. **184a** (1926).
[2] W. H. Keesom, *Helium* (Elsevier, Amsterdam, 1942), p. 180.
[3] For a discussion, see P. W. Bridgman, Revs. Modern Phys. **18**, 28 (1946).
[4] C. A. Swenson, Phys. Rev. **86**, 870 (1952).

found to be blocked. T was then held constant as P_1 was gradually decreased. P_2 remained unchanged until the solid blocking the capillary was melted at the value of P_1 corresponding to the melting pressure at T. At this melting pressure, P_2 dropped rapidly, and approached P_1. It was necessary that P_2 be greater than P_1, since melting occurred initially at the lower pressure. It also had to be established that the melting pressures observed for a given temperature were independent of the pressure differences across the capillary, $\Delta P = P_2 - P_1$.

The essential features of the apparatus used, then, were a source of variable pressure, a cryostat, in which the temperature of the loop was accurately known, and a means for indicating the pressure difference across the capillary when it was blocked. P_1, the source of variable pressure, was the same pressure balance which was used in the piston displacement experiment, so that the absolute calibration of the balance was not of importance in comparing the two sets of data. Similar vapor pressure thermometers were also used in the two experiments, so that difficulties would not arise from the comparison of the temperatures.

The final design of the cryostat which was found to be satisfactory for this work is sketched in Fig. 2. It was constructed entirely from copper, and mounted in a vacuum jacket for thermal isolation. The base of the cryostat was immersed in a liquid helium bath, the temperature of which could be varied from 4° to about 1.4°K, and its top was held at a temperature near 4°. This insured that there was a small but definite temperature gradient along its length.

The capillary itself was suspended in the liquid of the vapor pressure thermometer (of about 1 cc capacity), so that the temperature of the capillary could be read accurately on a mercury of oil manometer. The ends of the capillary were connected to room temperature by $\frac{1}{2}$ mm o.d. stainless steel tubing, while the vapor pressure thermometer was connected to the manometer by a copper nickel tube, 1.5 mm i.d.

The lower heater, No. 1, was used to vary the temperature of the vapor pressure thermometer, and, hence, the temperature of the capillary, by sending a heat flow through the copper connection to the outer bath. Thus, if the outer bath was held at 1.5°, the capillary temperature could be raised as high as 1.9° by applying current to the heater. A fine control on this heater current was used to regulate the temperature of the capillary, and to compensate for slight changes in the bath temperature. Temperature fluctuations were kept to less than 0.0005 degree.

The upper heater was necessary to give reproducible results. It was found that if the temperature gradient (or heat flow) down the capillary was too small, a considerable length of time was needed for the heat of fusion to be supplied to the solid in the capillary. Checks were always made to insure that the melting point found was not a function of the heat input, or

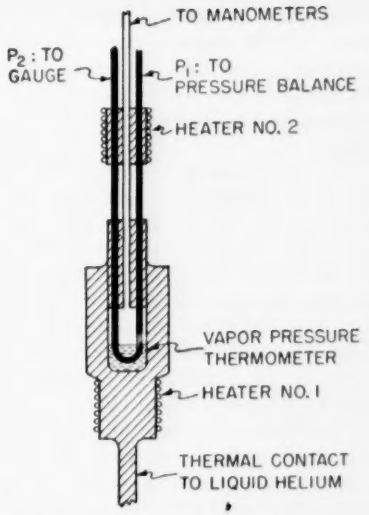

FIG. 2. The final version of the capillary blocking cryostat used.

of the rate of change of pressure. A minimum input of about 2 milliwatts seemed necessary to insure reproducibility. Below the λ-point, however, the thermal conductivity of helium II was found to be large enough so that this heater could be dispensed with.

With the experiment as set up finally, the requirements on the gauge for measuring P_2 were not very stringent. Any device that would show the disappearance of the pressure difference across the block would be satisfactory. In anticipation of other work, it was decided that the gauge would have to have a very small dead volume, and would have to be sensitive to variations in pressure of at least 0.1 atmosphere over the pressure range from 20 to 150 atmospheres. Differential monometers are usually not very rugged, and are easily blown out by careless handling. A Bourdon gauge is not quite sensitive enough, and is likely to stick within the requirements above. The final solution to the problem was simple and sturdy, and extremely sensitive.

A sketch of the gauge used is shown in Fig. 3. A steel plate, 2 mm thick, was fastened by means of six steel bolts to a brass block by a steel ring, so that a diaphragm 2 cm in diameter was formed. A pressure inlet of small diameter was made in the block under the center of the diaphragm. The constants of the diaphragm were chosen so as to give its center a rise of about 0.1 mm when a pressure of 120 atmospheres was applied to it. This rise was magnified by means of the 100:1 lever arrangement shown, and finally detected by an electrical contact between the micrometer and the end of the lever. A thyratron detection circuit of high internal resistance, attached to an indicator light, made it possible to reproduce settings to about 0.005 mm on the enlarged micrometer head, and changes of this order of magnitude were easily detected.

This meant that changes in pressure of less than 0.1 atmosphere could be observed over the usable range. It is interesting to note that the change in the height of the diaphragm caused by the change in pressure of 0.1 atmosphere is less than one-fifth of a wavelength of visible light.

The lever arrangement was first suggested by Professor K. T. Bainbridge, and was based on an original idea by Dr. D. W. Dye.[5] The center of the diaphragm made contact with a ball bearing by means of a post. The center of this ball bearing was 1 mm in front of a line through the centers of two outer ball bearings, both of which rested on a hard (glass) surface. The distance between these bearings and the electrical contact on the end of the lever was roughly 10 cm. The springs at the outer ends of the center bar were to insure that the lever pivoted on the two outer bearings, and was also in stable equilibrium with the center bearing. The counterbalance was used to supplement the springs. The combination of a mechanical lever arm, micrometer, and electrical contact, rather than the original optical arm, led to a much more convenient piece of apparatus for this purpose.

This gauge was very sensitive, and extremely rugged. Its chief usefulness comes when it can be calibrated at one point (as when the capillary was free) and used to measure changes in pressure from this value. In the absence of vibration, it was quite stable, and retained a setting during leak testing, for instance, within ± 0.005 mm on the scale for twenty-four hours or longer. Because of its sensitivity, it was not reproducible to this amount for large pressure differences (twenty or thirty atmospheres), although the drift or hysteresis was not large. The chief source of error was most likely very small irregularities either on the bearings or on the glass.

FIG. 3. The pressure gauge used to measure P_2. See the text for a description and details.

The pressure difference across the capillary ΔP was varied by altering the temperature of the blocked side of the capillary after it had emerged from the cryostat. A loop of this capillary was immersed in liquid nitrogen while the capillary was free. After the block was formed, P_2 could be increased at will by varying the length of the capillary remaining in the liquid nitrogen. This procedure was used to verify that, during a run, P_2 was always greater than P_1. It was also possible to show that the melting point at a given temperature was independent of the pressure difference across the capillary. This apperared to hold, in general, even for a pressure difference of 25 atmospheres at a melting pressure of 50 atmospheres, so no precautions were taken to insure that ΔP was any special value in the following experiments. It was usually of the order of five or six atmospheres.

The experimental procedure may now be summarized briefly. With about two milliwatts of power being supplied to the top heater, and a constant pressure in the capillary, the lower heater current was slowly decreased until there was no longer contact between the pressure balance and the pressure gauge. ΔP was increased to about five atmospheres, and the temperature of the vapor pressure thermometer regulated as closely as possible. Weights were removed from the pressure balance at the rate of about 0.01 atmosphere/minute until the pressure gauge changed suddenly, showing that the block had been broken. At the same time, a slight increase was usually noted in the vapor pressure, resulting from the sudden passage of the "hot" gas through the thermometer. The melting pressure was calculated from the constants of the balance and barometric pressure, and the temperature from the 1949 Cambridge vapor pressure scale, using a conversion factor of 15.62 between the density of mercury and Apiezon A oil.

III. RESULTS

The apparatus was first tested by making a determination of the melting curve of nitrogen, using the two techniques. Nitrogen was chosen as a convenient substance to work with, since it could be obtained relatively pure, and its triple point was easily reached experimentally. Absolute temperatures were calculated from the work of Keesom and Bijl.[6] It was found that the piston displacement and capillary blocking data were indistinguishable between 5 and 140 atmospheres, and could be represented by the equation,

$$P+882.5=0.0024703T^{3.084305} \text{ atmos.}$$

This curve is parallel to the earlier curve of Keesom and Lissman,[7] although it is displaced downwards by roughly $1\frac{1}{2}$ atmospheres.

[5] F. H. Rolt, *Gauges and Fine Measurements* (MacMillan and Company, Ltd., London, 1929), p. 339.

[6] W. H. Keesom and A. Bijl, Physica **4**, 305 (1937).

[7] W. H. Keesom and J. H. C. Lissman, Leiden Comm. **232b** (1934).

A preliminary check with helium showed that the two methods agreed between 2.5° and 4°K to within a few tenths of an atmosphere, so the remainder of the work reported here was concentrated in the region of the upper "triple point" on the helium phase diagram. Previous work, using the piston displacement method, had given consistent results which are shown as the solid curve in Fig. 4.[4] The melting pressures obtained by using the capillary blocking technique are shown as points, and it can be seen that the agreement between the two methods is quite satisfactory.

The effect of capillary size was also investigated, since it is possible, expecially in liquid helium II, that size effects (small ratios of volume to area) will become important. Three separate capillaries are represented in the data of Fig. 4 (not indicated individually), with approximately equal numbers of the points due to each. The capillaries were, in order of size, (a) copper, 0.026-inch i.d., volume/area=0.165 mm; (b) copper, 0.013-inch i.d., with a 0.009 inch steel wire down its center, volume/area=0.025 mm; (c) a copper tube, drawn down over sixty-six 0.005-inch piano wires, volume/area =0.002 mm.[8] No size effect was found, even in helium II, which is not surprising, since the spaces in the finest capillary were of the order of one hundred helium II film thicknesses. It would be of great interest to go to still smaller capillaries, but the time taken to obtain equilibrium across the finest capillary used was of the order of a minute, and this would increase considerably if a decrease of another factor of ten were attempted in the ratio of volume to area.

It was quite necessary to make the capillaries from copper because of its relatively high thermal conductivity. Initially, when stainless steel and copper-nickel capillaries were used, deviations from the piston displacement curve were observed below 1.764°. These deviations could be roughly predicted as the result of the fact that the thermal conductivity of liquid helium II under pressure was so much greater than that of the capillary material that appreciable temperature drops (of the order of a few thousandths of a degree) could appear across the walls of the capillary. These deviations, always giving melting pressures that were too high, were consistent, and seemed to disappear above 1.764°. If this effect were the result of superfluid helium II, then the temperature of the upper "triple point" given in reference 4 (1.743°) could not be correct. To check this, a more accurate determination of the λ point-pressure curve was made.

The method used was essentially a modification of that used by Schmidt and Keesom,[9] and more recently, Long and Meyer.[10] Two copper vapor pressure thermometers were connected to opposite sides of a differential oil manometer, and were joined by a 3-inch copper capillary (0.026 inch i.d.), containing liquid helium under pressure, and soldered to the sides of the thermometers. The temperature of the upper thermometer, as measured by means of an absolute oil manometer, was held constant while the bottom thermometer was kept at a slightly higher temperature by means of a heater. The pressure on the helium in the capillary was then slowly decreased by removing weights from the pressure balance until at the λ-point, the temperature difference between the gas thermometers, as shown by the differential manometer, tended to decrease. The accuracy of this method is limited because the thermal conductivity of helium II has a finite temperature coefficient at the λ-point,[11] but the data of Fig. 5 (tabulated in Table I) are probably accurate to ±0.002°. The coincidence of the upper λ-point as obtained by an extrapolation of these data (Fig. 4), and as deduced from the conductivity effect, seems to verify this assumption. The coordinates of this "triple point" can now be given with considerable assurance as

$$P_\lambda = 29.64(\pm 0.03) \text{ atmospheres},$$
$$T_\lambda = 1.764(\pm 0.003)^\circ\text{K}.$$

This is in better agreement with the original data of Keesom and Clusius.[12]

The λ point-pressure curve as determined earlier and the kink in the piston displacement melting pressure curve at 1.743° seem to be closely connected.[4] The capillary blocking data lie slightly below this curve above 1.743°, and seem to indicate that the kink does not actually exist. It is most likely that when the

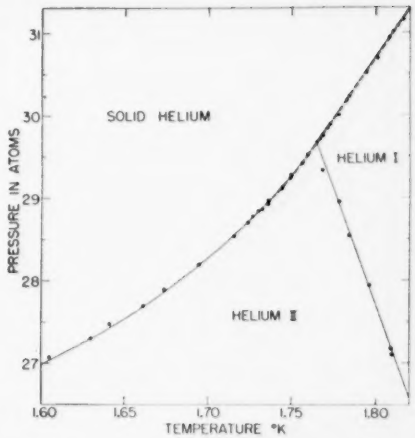

FIG. 4. The melting pressure data in the vicinity of the upper "triple point." The individual points represent capillary blocking data, while the solid line represents previous piston displacement data.

[8] For a discussion of the method used for the calibration of this capillary, see J. F. Allen and A. D. Misener, Proc. Roy. Soc. (London) **A172**, 467 (1939).

[9] G. Schmidt and W. H. Keesom, Physica **4**, 963 (1937).

[10] E. A. Long and L. Meyer, Phys. Rev. **83**, 860 (1951).

[11] J. F. Allen and E. Ganz, Proc. Roy. Soc. (London) **A171**, (1939).

[12] See reference 2, p. 225.

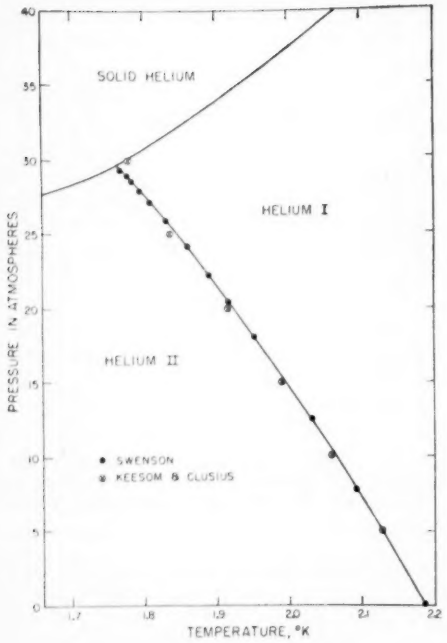

FIG. 5. The λ point-pressure curve.

thermal conductivity of the helium II became sufficiently great, a small temperature inhomogeneity inside the piston displacement cryostat was evened out. The crude λ point-pressure technique used previously could, presumably, detect only when the thermal conductivity of the helium was "sufficiently large," and not when it began to change rapidly.

The deviation of the capillary blocking points above 1.75° is slightly outside experimental error (about 0.001°). It is consistent enough, however, under various conditions, so that a fair amount of weight should be placed on it when deciding on the final smoothed melting pressure curve. The curve finally decided on is indicated by the dashed line in Fig. 4.

There also seems to be a tendency below 1.7° for the capillary blocking points to deviate towards higher melting pressures than those given by the piston displacement curve. These deviations are towards better agreement with earlier data obtained by Keesom and Miss Keesom[13] and the author.[14] It is perhaps significant that the data from all sources are in quantitative agreement from 1.75° to 1.8°, so that discrepancies at lower temperatures are most likely the result of differences in experimental technique. The maximum deviation of 0.15 atmosphere at 1.6° is between the present work and the earlier capillary blocking data obtained by the author.[14] The set-up which was used in that work was such that the thermal conductivity effect, which was mentioned previously, may be responsible for the discrepancy. The agreement between the various sources seems to become better as the temperature is lowered.

The consolidation of these differing but seemingly accurate sets of data into a reliable melting pressure curve is quite difficult. The present capillary blocking data confirm the piston displacement experiments so well that a smoothed curve incorporating the two sets of data was taken as the most likely to be correct. This curve is given in column 2, Table II, for temperatures between 1.4° and 4°K. It is not likely to be in error by more than two-tenths of one percent at any given point, and is internally consistent to a greater accuracy than that near 1.75°.

The slope of the melting pressure curve, $(dP/dT)_M$, is actually of more interest than the curve itself, since it can be combined with measurements of the change in molar volume on melting ($(\Delta V)_M = V_L - V_S$) to obtain the entropy difference between the solid and the liquid along the melting curve. The derivatives were obtained by using the first and second differences of the smoothed curve at small temperature intervals.[15] This procedure is straightforward as long as the second differences are small, but between 1.7° and 1.8° the slope of the melting pressure curve is changing very rapidly. A certain amount of arbitrariness is introduced in the way that the smoothed curve is drawn through the experimental points, and this is reflected in the $(dP/dT)_M$ curve. An obvious criterion which must be satisfied by any $(dP/dT)_M$ curve is that the area under the curve between any two temperatures must equal the experimentally observed difference in melting pressure.

The final smoothed values of $(dP/dT)_M$ are summarized in column 3 of Table II, and the data in the vicinity of the λ-point are plotted in Fig. 6. The shape of this curve resembles very closely the expected curve for a second-order transformation, with a discontinuity in its slope occurring at the upper "triple point." This discontinuity in $(d^2P/dT^2)_M$ is finite, and is of the order of -500 atmospheres/deg^2. It can also be calculated from other melting curve data by using the Ehrenfest relations for a second-order phase

TABLE I. Smoothed values of the λ point-pressure curve.

T_λ (°K)	P_λ (atoms)
2.186	0.02
2.15	3.18
2.10	7.26
2.05	11.10
2.00	14.72
1.95	18.18
1.90	21.50
1.85	24.62
1.80	27.62
1.764	29.64

[13] W. H. Keesom and A. P. Keesom, Leiden Comm. **224e** (1933).
[14] C. A. Swenson, Phys. Rev. **79**, 626 (1950).
[15] E. T. Whittaker and G. Robinson, *The Calculus of Observations* (Blackie and Son, Ltd., London, 1932), p. 62.

transformation.[4] If the new values for $(dP/dT)_\lambda = -54.5$ atmospheres/deg and $(dP/dT)_M = 27.5$ atmospheres/deg are used, $\Delta_{I,II}(d^2P/dT^2)_M$ can be computed as -220 atmospheres/deg^2.

The argeement between the two figures is such that no real decision can be made about the applicability of the Ehrenfest relations in this case. An error of a factor of two might be expected from the experimental data, since the second derivative of the melting pressure curve has been taken, and it is varying quite rapidly. The slope of the $(\Delta V)_M$ curve at the λ-point also is used, and could be in error in spite of a seeming consistency in the data.

One possibility exists which is not usually considered. If the specific heat, thermal expansion, and compressibility have infinite discontinuities at the λ-point, then $(d\Delta S/dT)_M$ would be infinite also. Previous data are so crude (except for the specific heat data) that this could have been overlooked. The ordinary equations which govern the second-order phase change would be indeterminate, with the λ point-pressure curve still existing. The values for the entropy difference between liquid and solid helium have been calculated, using previous ΔV values, and are tabulated in column 5 of Table II. The slope of the entropy difference curve in helium II at 1.764° is rather large (about 16 cal/mol-deg), but not infinite. These calculations involve the $(\Delta V)_M$ curve, however, and are, therefore, open to suspicion.

It is possible to calculate the slope of this curve directly from the observed values of $\Delta_{I,II}(d^2P/dT^2)$, $(dP/dT)_\lambda$, $(dP/dT)_M$, $(\Delta V)_M$, and the temperature at the upper λ point, using the Ehrenfest relations. The agreement is satisfactory with the above figure. What is perhaps of more interest is to calculate the magnitude of the discontinuity in the specific heat which one would find in the vicinity of the upper triple point, if these data are assumed. Using the relations which were mentioned in the previous paper,[4] the following expression for the specific heat discontinuity can be derived:

$$\Delta C_p = C_{pI} - C_{pII} = T(\Delta V)_M \Delta_{I,II}(d^2P/dT^2)_M / [1 - R(2+R)],$$

where $R = (dP/dT)_M/(dP/dT)_\lambda$. If

$$(\Delta V)_M = 1.48 \text{ cc/mol}, \quad T_\lambda = 1.764°,$$
$$(dP/dT)_M = 27.5 \text{ atmospheres/deg},$$
$$(dP/dT)_\lambda = -54.5 \text{ atmospheres/deg},$$

and

$$\Delta_{I,II}(d^2P/dT^2)_M = -500 \text{ atmospheres/deg}^2$$

are substituted into this expression, the calculated value for ΔC_p is -18 cal/mol-deg, or -4.5 cal/g-deg. This is reasonable, and of the same order of magnitude as the specific heat anomaly found in liquid helium under its saturated vapor pressure.

The final conclusions to be drawn from this melting pressure work are not clear-cut. The blocked capillary technique seems to be as capable of giving accurate results as the piston displacement method, and the two sets of data are in excellent agreement in the vicinity of the upper "triple point" for helium. The analysis of the results is more difficult, and only indications can be drawn from the experimental data. It is quite definite that the slope of the melting pressure curve is continuous at the λ-point, and that the data are in qualitative agreement with the Ehrenfest relations. If the behavior of the λ-transformation is the same at the lower "triple point" as at the upper,

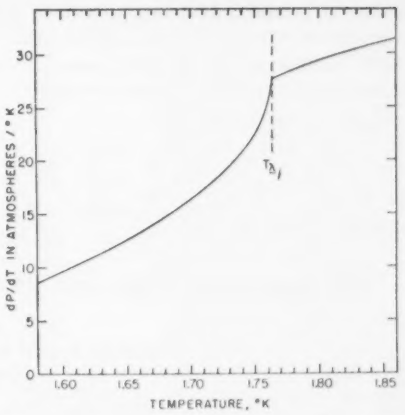

FIG. 6. The slope of the melting pressure curve $[(dP/dT)_M]$ in the vicinity of the upper "triple point."

TABLE II. Smoothed values for the melting pressure, P, the slope of the melting pressure curve, $(dP/dT)_M$, the molar change in volume on melting, $(\Delta V)_M = V_L - V_S$, and the molar entropy difference between liquid and solid helium, $(\Delta S)_M = S_L - S_S$.

T (°K)	P (atmos)	$(dP/dT)_M$ (atmos/deg)	$(\Delta V)_M$[4] (cc/mol-deg)	$(\Delta S)_M$ (cal/mol-deg)
1.40	(25.81)	4.2	2.06	0.21
1.50	26.22	6.3	2.00	0.30[5]
1.55	26.56	7.7	1.95	0.36[5]
1.60	26.99	9.6	1.89	0.44
1.65	27.54	12.3[5]	1.76	0.52[5]
1.70	28.27	16.3[5]	1.60	0.63[5]
1.72	28.63	18.2[5]	1.54	0.68
1.74	29.03	20.7	1.49	0.74[5]
1.75	29.26[5]	22.4	1.48	0.80[5]
1.764	29.63	27.5	1.47	0.98
1.80	30.70	29.2	1.45	1.02[5]
1.85	32.21	31.0	1.44	1.08
1.90	33.80	32.2	1.43	1.11[5]
1.95	35.45	33.2	1.42	1.14
2.00	37.08	34.3	1.40	1.17
2.10	40.56	35.8	1.38	1.20
2.20	44.21	37.2	1.35	1.21[5]
2.30	47.98	38.6	1.32[5]	1.24
2.50	56.3	41.0	1.28	1.27
2.75	66.7	43.6	1.22[5]	1.30
3.00	78.1	46.2	1.19[5]	1.34
3.50	102.0	51.0	1.10	1.36
4.00	128.6	56.0	1.03	1.40

then these data would lead one to expect that the discontinuities in the specific heat and thermal expansion would be finite at the normal λ-point. This is the present indication from direct measurements.[16]

[16] See reference 2, pp. 206 and 245.

This work was made possible in part by a grant from the Harvard Foundation for Advanced Study and Research. I wish to thank Mr. G. Bjorklund and Mr. E. Wilkie for their assistance in constructing the apparatus used.

PHYSICAL REVIEW VOLUME 89, NUMBER 3 FEBRUARY 1, 1953

Z-Dependence of the Pair Production Cross Section at 1.33 and 2.62 Mev

IRVING E. DAYTON*
Laboratory of Nuclear Studies, Cornell University, Ithaca, New York
(Received October 21, 1952)

The Z-dependence of the pair production cross section has been measured at 1.33 Mev for Al, Cu, Sn, and Pb, and at 2.62 Mev for Be, C, Al, Cu, Sn, and Pb. A target is used which is thick for the positrons produced in it but thin for the incident gamma ray beam. The positrons stop in the target and are detected by observing their annihilation radiation with two NaI(Tl) scintillation counters in coincidence. At both energies the Z-dependence of the cross section is best represented by an equation of the form aZ^2+bZ^4. If it is assumed that the Born approximation calculations of the cross section give the correct value in the limit of low Z, then in lead at 2.62 Mev the measured cross section is 23 percent higher than the value calculated from the Born approximation, and 104 percent higher at 1.33 Mev. All these results are in good agreement with the exact numerical calculations of Jaeger and Hulme.

The present measurement shows that near threshold the pair production cross section in lead is considerably higher than the Born approximation calculation, whereas at energies between 17 Mev and 280 Mev the value has been measured to be 10 percent to 15 percent lower than that calculated from the Born approximation. The crossover appears to occur at around six Mev.

I. INTRODUCTION

IN the years since the discovery of the production of electron-positron pairs by gamma-rays, this process has frequently been studied using the 2.62 Mev gamma-ray from ThC″.[1] These experiments have served to establish the nature of the process and to give some information about the distribution of the particles in energy and angle. But since these measurements were based on at most a few hundred cloud-chamber pictures with one or perhaps two target materials, there is no accurate data on the total cross section for pair production, and until recently nothing on the Z-dependence of the total cross section at energies below 3 Mev.

The theory of pair production is summarized in Heitler.[2] It predicts that the total cross section for nuclear pair production will vary as Z^2. At the energies involved here, it is not necessary to include the effect of screening of the nuclear Coulomb field by the atomic electrons. The theory is calculated using the Born approximation, which is expected to fail for high Z and low gamma-ray energy. Jaeger and Hulme have made a number of exact numerical calculations of the pair production cross section.[3–5] They find that in lead the exact cross section is 25 percent higher than the Born approximation value at a gamma-ray energy of 5 mc^2 and about a factor of two higher at 3 mc^2. They also find[4] that at 3 mc^2 the Z-dependence of the cross section is best represented by an equation of the form aZ^2+bZ^4. The object of the present experiment is to check quantitatively these predicted deviations from the Born approximation theory, using gamma-rays of 2.62 Mev and 1.33 Mev.

While this experiment was in progress, indications of the predicted deviations from the Born approximation theory were obtained by Cleland, Townsend, and Hughes[6] using the 2.76-Mev gamma-ray from Mg^{24}. Hahn, Baldinger, and Huber[7] have recently reported an experiment similar to this one. Their results are in general agreement with ours and with the theoretical predictions.

General Considerations

At the gamma-ray energies used in this experiment, the pair spectrometer technique, which has been used at 17.6, 88, and 280 Mev[8–10] to study pair production,

* Now at Palmer Physical Laboratory, Princeton University, Princeton, New Jersey.

[1] For references to earlier work see: W. Heitler, *Quantum Theory of Radiation* (Oxford University Press, London, 1944), second edition, p. 201; K. H. Spring, *Photons and Electrons* (John Wiley and Sons, New York, 1950), Chap. V.

[2] See Heitler, reference 1, Chap. 4.

[3] J. C. Jaeger and H. R. Hulme, Proc. Roy. Soc. (London) **A153**, 443 (1936).

[4] J. C. Jaeger, Nature **137**, 781 (1936).

[5] J. C. Jaeger, Nature **148**, 86 (1941).

[6] Cleland, Townsend, and Hughes, Phys. Rev. **84**, 298 (1951).

[7] Hahn, Baldinger, and Huber, Helv. Phys. Acta **25**, 505 (1952).

[8] R. L. Walker, Phys. Rev. **76**, 1440 (1949).

[9] J. L. Lawson, Phys. Rev. **75**, 433 (1949).

[10] DeWire, Ashkin, and Beach, Phys. Rev. **83**, 505 (1951).

is not feasible because of the low energies of the electron and positron.

The basic idea of the experiment is to use a target which is thick for positrons produced in it but thin for the incident gamma-ray beam. The positrons stop in the target and are detected by observing in coincidence their two annihilation quanta. The experimental arrangement is shown in Fig. 1. The detectors were located in a plane through the center of the target and normal to the gamma-ray beam. One of the detectors was mounted so that it could be pivoted about the target in order that the detectors could be oriented at either 180° or 90° with respect to the target. The detectors were two scintillation counters using thallium activated NaI crystals mounted on RCA type 5819 photomultiplier tubes. After amplification, the pulse from each tube was passed through a differential discriminator whose high and low biases were set to pass only pulses corresponding to the photoline from annihilation radiation. This arrangement placed a very stringent requirement on coincidences counted and considerably reduced the background coincidence rate resulting from such events as Compton scattering from one crystal to the other. It eliminated false coincidences resulting from pulses on the ac supply line and to the Compton effect in the K shell of a heavy element. In the latter case, the lower bias will always reject pulses resulting from K x-rays.

With apparatus of the above design, there are a number of effects which must be understood before valid results can be obtained. These will be mentioned briefly here, and then considered in more detail in later sections. Most fundamental of these is the fact that the coincidence counting efficiency is not constant but is a function of the distance of the annihilating positron from the line joining the centers of the two counters. Closely involved with this effect is the fact that a positron may move an appreciable distance through the target between the time it is created and the time it annihilates. Absorption of the initial gamma-ray beam

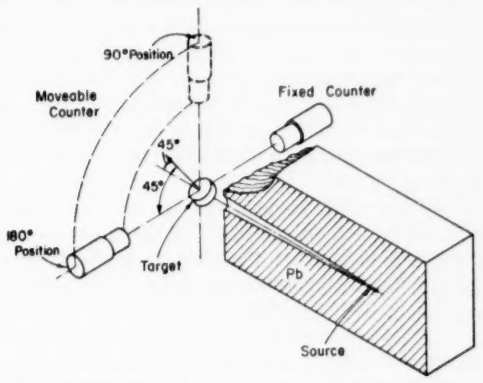

FIG. 1. Schematic drawing of the experimental arrangement. Most of the lead shielding is not shown.

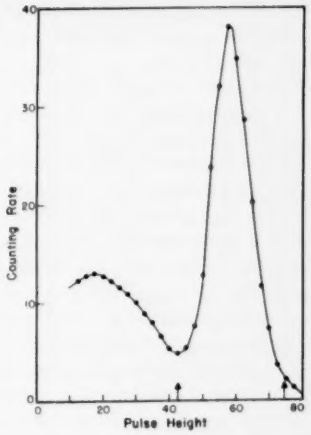

FIG. 2. Typical pulse-height spectrum from NaI (Tl) scintillation counter when exposed to annihilation radiation. Arrows show where upper and lower biases were set.

and of the annihilation radiation leaving the target must also be considered.

II. EXPERIMENTAL TECHNIQUE

Apparatus

The ThC″ source had a strength of about 60 mC and was in secular equilibrium. It was mounted 30 cm from the target behind 25 cm of lead shielding. The hole in the collimation tapered from $\frac{3}{16}$ in. in diameter at the source to 1 in. in diameter where the beam emerged. The Co^{60} source had a strength of about 2 curies, although a source of one-tenth that strength would have been adequate. It was mounted behind 75 cm of lead shielding.

Each NaI(Tl) crystal was 4 cm in diameter by 4 cm high, and was mounted in the conventional manner in mineral oil in a Lucite case which was cemented to the face of the photomultiplier tube. Each detector was 16 cm from the target.

The counters were calibrated with annihilation radiation before every run. A typical pulse-height spectrum is shown in Fig. 2. The full width of the photoline at half-maximum was about 25 percent in each counter. These counters were in use for a period of six months, and during that time a bias curve was taken at least once a week. No change in the resolution of either counter was observed during that time.

The electronics was quite simple and conventional. Each photomultiplier socket was mounted on a box containing only a voltage divider network and a few by-pass capacitors. Each box was connected to a linear amplifier whose output fed into the discriminators mentioned previously. The location of the high and low biases is indicated by the arrows in Fig. 2. The output pulses from the two discriminators were fed into a Rossi type coincidence circuit whose resolving time as measured with a sliding pulser was 0.7 μsec. The high voltage for the photomultiplier tubes was obtained from a highly stabilized supply.[11]

[11] Designed and built in this Laboratory by Leonard Walker.

The location of the dip between the photoline and the Compton edge in the pulse-height distribution gave a very sensitive way of monitoring the over-all gain of the system. It was found that a shift in over-all gain of 2 percent could be detected, and over a period of one or two weeks the change in gain never exceeded this amount. Over a period of several months the gain changed by less than 5 percent.

The targets were flat disks 2.0 in. in diameter. They were oriented so that the normal to the target made an angle of 45° with the direction of the beam and an angle of 45° with the line joining the two counters when they were in the 180° position. This orientation was chosen so that the distance through the target from any point in the target to the moveable counter would be the same whether that counter were in the 180° or the 90° position. Since the singles counting rate in each counter was the same whether the counters were in the 180° or the 90° position, the coincidence rate in the 90° position gave directly the background resulting from chance coincidences and also to such events as the double Compton effect where two truly coincident gamma-rays are produced with an isotropic distribution with respect to each other. At all times the singles rates in each counter were recorded in order to monitor the operation of the equipment, even though they were not needed in the analysis of the data.

Preliminary Measurements

Extensive survey measurements were made with the ThC″ source using six target materials, Be, C, Al, Cu, Sn, and Pb. Counting rate was measured as a function of thickness for 6 or 8 thicknesses up to about 2 g/cm². The original hope was that after applying corrections for the variation of detection efficiency over the target and the other corrections enumerated later on, the resulting curve would be a straight line whose slope could be interpreted as the rate of production of positrons in the given material. This program failed because of two effects which could be neither calculated nor measured.

Gamma-rays from the source produce pairs in the lead collimation. An unknown, but presumably constant, number of these positrons land on the front surface of the target and are counted. If the front of the target could be kept in the same place throughout the measurements, then this unknown number of positrons would be counted with the same efficiency and would not change the slope of the rate *versus* thickness curve.

A number of related effects are due to the previously mentioned fact that positrons produced in the target have a finite range, which may amount to several millimeters in the low density targets. This means, first, that a certain number of positrons made in the target are able to leave it and thus not be counted. This effect would not change the slope of the rate *versus* thickness curve (for target thicknesses greater than the maximum range of the most energetic positron produced) provided the back of the target were kept in the same position. In addition, the analysis of the data becomes complicated because positrons made at one point in the target have a distribution in range and are thus counted with varying efficiencies. An attempt was made to calculate this effect, but partly because of a lack of information about the distribution in range and scattering of the positrons from pair production at these energies, and partly because of the necessity of making simplifying mathematical assumptions, the attempt was not successful.

Experimental Procedure

The above difficulties could be overcome by insuring that all targets had identical geometry for the detection of positrons. This realization led to the following target design. Each element was made into a target 1.00 cm thick with a surface density of between 1.85 and 1.90 g/cm², which is the density of Be. In other elements this was accomplished by spacing eight or nine thin sheets with Lucite rings (except for carbon, where because of the low density the surface density was only 1.60 g/cm²). A target holder was constructed which held the target in a sandwich between two Be slugs. For the ThC″ measurements the front slug was $\frac{1}{8}$ in. thick and the back slug $\frac{1}{4}$ in. thick. For measurements with the Co^{60} source the thicknesses of both Be slugs were halved. In both cases the rear slug could have been the same thickness as the front one if two slugs of the same thickness had been available. The target holder was arranged so that the center of the target slug was on the line joining the centers of the two crystals. We believe that a good part of the difference between our results and those of the Swiss group[7] at 2.62 Mev can be explained by their failure to consider the variation of detection efficiency over the target volume.

The effectiveness of this arrangement in eliminating trouble resulting from the motion of positrons in the target depends partly on the projected range of the positron, expressed in g/cm², being independent of Z. There is a scarcity of experimental data on this subject, but measurements by Trump, van de Graaff, and Cloud[12] can be interpreted to show that the range of monoenergetic electrons in lead differs from that in aluminum by 25 percent at most. Since the effect is small, this difference can be tolerated. The fact that the difference in range for different Z is not better known introduces an error of about 1 percent in the final result.

Other features of this target design are that whether or not a target slug is in place, all the positrons from the collimation land on the first Be slug and so are counted with constant efficiency. A few of the positrons which are made in the first Be slug leave it. When the target is in place, they stop near its front surface, and when it is not in place, they stop near the front surface

[12] Trump, van de Graaff, and Cloud, Am. J. Roentgenol. Radium Therapy **XLIII**, 728 (1940).

of the second Be slug. In either case, they are counted with the same efficiency because the variation in detection efficiency was measured to be symmetrical about the line joining the centers of the two crystals. The second Be slug also serves to stop all the positrons leaving the target. A few positrons are made in the second Be slug, but they provide only a constant background.

Measurements were taken with targets of Be, C, Al, Cu, Sn, and Pb with the ThC″ source and with targets of Al, Cu, Sn, and Pb with the Co^{60} source. In order that the relative counting rates observed be proportional to the pair production cross sections in the different target materials, it is important that the detection efficiency remain constant throughout the measurement. The excellent long time stability of the apparatus has already been described. In order to eliminate the effect of short time variations in detection efficiency, an additional precaution was taken. In a few hours data were taken on all target materials with the counters in both the 90° and 180° positions. The counting times were arranged so that the desired relative statistical accuracy was obtained for each material. This "cycle" was then repeated until the desired number of counts had been obtained. All the data was obtained in three runs each lasting about 30 hours. Thus, any short time variations in efficiency would affect all targets more or less equally and cancel out. In fact, it was never possible to detect any systematic changes in counting efficiency.

Counting rates with the counters in the 180° position varied from about 5 counts per minute to about 75 counts per minute. These rates could have been increased considerably by moving the counters closer to the target, but then the chance coincidences resulting from the increased singles rates would have become too numerous.

III. TREATMENT OF THE DATA

To obtain the net counting rate resulting from positrons produced in the target, for each Z the rate obtained with counters at 90° was subtracted from that obtained with counters at 180°. From this result was subtracted the counting rate with no target in the target holder, corrected for the annihilation radiation absorbed by the target when in place. The computation of the absorption coefficients is described below. For the ThC″ source, the statistical errors on the resulting net counting rates were about 3.6 percent for Be and C and 2 percent for the other targets. For the Co^{60} source the same errors varied from 4.9 percent for Al to 2.7 percent for Pb. The corrections enumerated below were then applied to these net counting rates.

Corrections

1. When a positron annihilates in the target, its annihilation radiation must pass through the target before reaching the counters. Some of the annihilation radiation will be absorbed in the target, and it is necessary to correct for this effect. Total absorption coefficients for 0.511-Mev gamma-rays were obtained by interpolating between values calculated by White.[13] These calculations have been well verified in this energy range by the accurate experiments of Colgate.[14]

Since the detector subtended a finite solid angle, it was possible for the annihilation radiation to undergo a small angle scattering in the target and still arrive at the detector and be counted. The correction to the Compton part of the cross section was made using the Klein-Nishina formula. Since the counters defined a cone of half-angle about 6°, the Compton contribution was reduced by 1 percent. Corrections to the coherent scattering cross section were made using graphs constructed by Colgate,[15] which were in turn based on the work of Franz.[16] Eighty percent of the coherent cross section was subtracted from Pb, and up to 100 percent at lower Z. The net result of these corrections was to reduce the total absorption cross section by amounts ranging from 1 percent at low Z up to 4.4 percent for Pb. Using these absorption cross sections, the corrections to the observed counting rates ranged between 30 percent and 40 percent, except for Pb where it was 70 percent.

2. Pairs produced in the field of an electron. The calculations of Borsellino[17] were used to correct for this effect. For 2.62-Mev gamma-rays, the correction amounted to 1.4 percent in Be and much less at higher Z. Since the threshold for this process is at 2 Mev, the effect was not present in the Co^{60} measurements.

3. Impurities in the targets. The Pb, Sn, and Cu targets were made from sheets which were also used by Walker[8] for his targets. These had been analyzed both chemically and spectroscopically and showed no impurities large enough to require a correction. The aluminum target was made from grade 2S sheet which contained, according to chemical analysis, 0.6 percent Fe. A correction of 1.2 percent was made for this impurity. According to the analysis supplied by the manufacturer with the Be slug, a 1.2 percent correction was required for the impurities it contained. However, Be is notoriously difficult to analyze, and it is possible that additional undetected impurities were present. The carbon target was made from pile graphite supplied by Brookhaven National Laboratory.

4. Absorption of the primary gamma-ray beam as it passes through the target. It was assumed that one interaction removed a quantum from the beam. The targets are thin enough so that this is well justified. Absorption coefficients computed by White[13] were used. The corrections were about 7 percent at 1.33 Mev and

[13] G. R. White, Nat. Bur. Standards Report No. 1003.
[14] S. A. Colgate, Phys. Rev. **87**, 592 (1952).
[15] S. A. Colgate, Cornell University Thesis (1952) (unpublished), App. II, p. 77.
[16] W. Franz, Z. Physik **98**, 314 (1935).
[17] A. Borsellino, Helv. Phys. Acta **20**, 136 (1947).

TABLE I. Relative cross section per atom for pair production by the 1.33- and 1.17-Mev gamma-rays from Co^{60}. The data have been normalized by fitting to a curve of the form $\sigma/Z^2 = a+bZ^2$ and then setting $a=1$. On the assumption that the Born approximation is valid in the limit of low Z, the values of σ/Z^2 then give directly the departure of the cross sections from those predicted by the Born approximation. This normalization means that σ is expressed in arbitrary units.

Element	σ	σ/Z^2
Al	168.5± 8.28	0.997±0.049
Cu	934.4± 43.7	1.111±0.052
Sn	3735 ±142	1.494±0.057
Pb	13700 ±370	2.037±0.055

5 percent at 2.62 Mev, varying less than 1 percent from these values for all Z.

5. It is possible for positrons to annihilate in ways that do not give rise to two quanta 180° apart. These effects will be important in this experiment, only if they occur an appreciable fraction of the time and in addition have a Z-dependent cross section.

If a positron annihilates before becoming thermalized, then its two annihilation quanta will form an angle of less than 180° and will have, in general, different energies. Results given in Heitler[2] show that, practically independent of Z, only a small fraction of the positrons annihilate before reaching thermal velocities. This conclusion is supported by the experiment of DeBenedetti and co-workers[18] on the angular correlation of annihilation radiation. They find a small departure from 180° correlation between the two annihilation quanta which can be explained by the thermal motion of the positron and the electron with which it annihilates.

The ratio of the frequency of three-quantum annihilation to two-quantum annihilation has been calculated to be 1 to 370 in metals.[19] In addition, there is no reason for believing this ratio to be Z-dependent.

A positron may undergo one-quantum annihilation by uniting with a bound electron. This process is expected to be Z-dependent, since it depends on the strength of the binding of the electron to the nucleus. However, because of the electrostatic repulsion by the Coulomb field of the nucleus, a thermal positron cannot reach the inner electron shells. According to Jaeger and Hulme[20] the ratio of the probability of one-quantum annihilation to two-quantum annihilation in lead is of the order of 0.01.

6. The ThC″ source is supposed to contain other gamma-rays besides the one at 2.62 Mev, and these gamma-rays will produce pairs which will be recorded. If the pair production cross section could be represented by an equation of the form $\sigma(Z,E)=f(Z)\varphi(E)$, then no correction would be necessary since the other gamma-rays will produce the same fraction of the total number of pairs in all the targets. (The results given by the Born approximation calculation do satisfy the above relation, with $f(Z)=Z^2$ and $\varphi(E)$ given in Heitler.[2]) However, the calculations of Jaeger and Hulme[3-5] indicate that in the region from 3 Mev down this relation is apparently not satisfied.

Latyshev[21] has measured the gamma-ray spectrum from a ThC″ source and finds that for every 100 gamma-rays of 2.62 Mev, there are a total of 28 gamma-rays of five different energies between 1.0 and 2.2 Mev. However, Bell[22] recently pointed out that in a very pure ThC″ source there are no gamma-rays between 0.9 Mev and the principal gamma-ray at 2.62 Mev. He claims that the intermediate energy gamma-rays measured by Latyshev are the result of radium contamination of the source, which is very hard to remove chemically. Because of this fact, a rough measurement was made of the gamma-ray spectrum from our ThC″ source. A two-crystal Compton spectrometer of the type described by Hofstadter[23] was used.[24] The result was that for every 100 gamma-rays of 2.62 Mev our source had a total of 78 gamma-rays of three different energies between 1.0 and 2.2 Mev. Two pairs of lines observed by Latyshev were not resolved in this measurement, but that should not invalidate the measurement of their total intensity. Using this result, it was computed that 5 percent more positrons would be produced in lead than in low Z targets by these contaminating gamma-rays, and this correction was accordingly applied. In making these calculations it was assumed that the pair production cross section in lead is 24 percent higher than the Born approximation value at 2.62 Mev and 97 percent higher at 1.53 Mev.

For measurements taken with the Co^{60} source the situation is much more uncertain. Co^{60} emits two gamma-rays of equal strength of 1.33 and 1.17 Mev.[25]

TABLE II. Relative cross section per atom for pair production by 2.62-Mev gamma-rays. The data have been normalized by fitting the points for Al, Cu, Sn, and Pb to a curve of the form $\sigma/Z^2=a+bZ^2$ and then setting $a=1$. On the assumption that the Born approximation is valid in the limit of low Z, the values of σ/Z^2 then give directly the departure of the cross sections from those predicted by the Born approximation. This normalization means that σ is expressed in arbitrary units.

Element	σ	σ/Z^2
Be	17.21± 0.645	1.075±0.040
C	33.63± 1.19	0.934±0.033
Al	170.1 ± 3.36	1.006±0.020
Cu	866.1 ± 17.4	1.030±0.021
Sn	2702 ± 57.9	1.081±0.023
Pb	8262 ±167	1.229±0.025

[18] DeBenedetti, Cowan, Konneker, and Primakoff, Phys. Rev. **77**, 205 (1950).
[19] A. Ore and J. L. Powell, Phys. Rev. **75**, 1696 (1949).
[20] J. C. Jaeger and H. R. Hulme, Proc. Cambridge Phil. Soc. **32**, 158 (1936).
[21] G. D. Latyshev, Revs. Modern Phys. **19**, 132 (1947).
[22] P. R. Bell (private communication).
[23] R. Hofstadter and J. A. McIntyre, Phys. Rev. **78**, 619 (1950). See also James Draper, Cornell University thesis (1952) (unpublished).
[24] These measurements were made with the assistance of Dr. James Draper, who generously loaned his apparatus for the purpose.
[25] *Nuclear Data*, Natl. Bur. Standards Circular No. 499 (1950).

In order to eliminate the effect of the 1.17-Mev gamma-ray and obtain the relative cross sections at 1.33 Mev, it is necessary to interpolate between the exact point calculated by Jaeger and Hulme at 3 mc^2 and the threshold at 2 mc^2. This can be done in many different ways; there is no certain theoretical information on the shape of the exact cross section near threshold. Making widely different assumptions about this interpolation results in corrections for the 1.17-Mev gamma-ray ranging between plus 5 percent and minus 10 percent in Pb, with a value of zero fairly probable. Under these circumstances, it was decided to present the data without correcting for the presence of the 1.17-Mev gamma-ray, with the understanding that if this were done, the results would be changed little if any.

IV. RESULTS

The results are summarized in Tables I and II. The data are also exhibited in Figs. 3 and 4, where σ/Z^2 is plotted as a function of Z. If the Born approximation were valid, the points would lie on a horizontal line. The data have been fit by using least squares[26] to curves of the form $\sigma/Z^2=a+bZ^2$ and $\sigma/Z^2=a+bZ$. The points for Be and C at 2.62 Mev were disregarded in fitting the curves because of their larger statistical error and because the background was a fairly large fraction of the total counting rate. At both energies the first curve is the better fit, even though the second is by no means excluded. This agrees with the results of Jaeger[4] and Hahn, Baldinger, and Huber[7] mentioned in the Introduction. These results are in mild disagreement with those of Walker[8] who found at 17.6 Mev that his data was fit better by a curve of the form $\sigma/Z^2=a+bZ$, although the other possibility was not excluded. So far as we know, there is no general theoretical argument which tells what powers of Z might be expected in the formula for the exact cross section.

For the reasons given above, further analysis of the data is carried out using the curve $\sigma/Z^2=a+bZ^2$. For convenience the data are normalized so that $a=1$. The least squares fit then gives $b=1.59\times10^{-4}$ at 1.33 Mev and $b=3.39\times10^{-5}$ at 2.62 Mev. Since the Born approximation should give the correct result in the limit as Z approaches zero, this normalization of $a=1$ gives directly the departure of the measured cross sections from the Born approximation value. At 2.62 Mev the measured cross section in Pb is 23 percent higher than that predicted by the Born approximation. Jaeger and Hulme calculated that it should be 25 percent higher at 5 mc^2, and since they say that their calculations might be in error by as much as 10 percent, the calculations agree with experiment to well within the errors. In the case of the Co^{60} measurements, as pointed out above, comparison with theory is much more difficult. The measured cross section in Pb at 1.33 Mev is slightly more than twice the Born approximation value, and this is certainly not inconsistent with the exact calculation when the possible 5 percent error in the calculation and the slightly different energies of the measurement and calculation are taken into account.

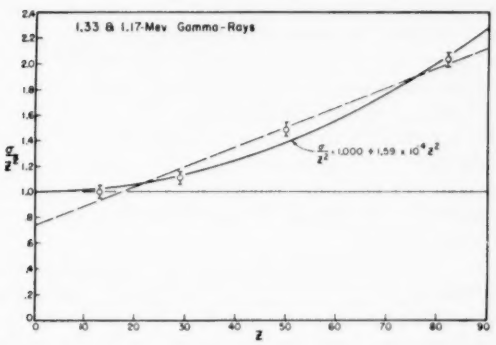

FIG. 3. Observed relative pair production cross sections for the 1.33- and 1.17-Mev gamma-rays from Co^{60}. Based on the data shown in Table I.

[26] Using the formulas given by R. T. Birge, Phys. Rev. **40**, 207 (1932).

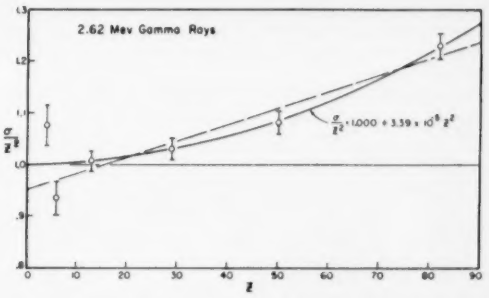

FIG. 4. Observed relative pair production cross sections for 2.62-Mev gamma-rays. Based on the data shown in Table II.

Errors

The errors quoted above are only the statistical counting errors. There are, of course, additional uncertainties in the experiment, and it is necessary to evaluate their effect on the final result. Listed below are various possible sources of error with an estimate of their magnitude in percent.

Variation of range of electrons in different materials: 1.0.

Absorption of annihilation radiation in the target: 1.0 for Pb, 0.5 for others.

Pairs produced by other gamma-rays from ThC'' source: 0.5 for Pb, negligible for others.

All the other corrections to the data are so small that errors in them are quite negligible. Since this experiment was a relative not an absolute measurement, it was not necessary to know numerical values of many other quantities, but only to know that they stayed constant during the experiment.

Combining the above errors gives an error of about

TABLE III. Ratio of the pair production cross section in lead obtained either from experiment or more accurate calculations to that calculated using the Born approximation (Bethe-Heitler theory).

Energy (Mev)	Experimental ratio	Theoretical ratio	Reference
1.33	2.04 ±0.06	···	present work
1.53	···	1.97± 5%	3, 4
2.55	···	1.25±10%	5
2.62	1.23 ±0.025	···	present work
5.3	1.046±0.019	···	28
10.3	0.932±0.014	···	28
17.6	0.865±0.012	···	28
17.6	0.845±0.016	0.800	8, 27
88	0.896±0.014	0.882	9, 27
280	0.904±0.01	0.900	10, 27

1.5 percent in lead and 1.0 percent for other materials which must be combined with the counting errors. For measurements at 2.62 Mev, a conservative estimate of the combined errors would be 4 percent for Be and C and 3 percent for the other materials. As pointed out above, the uncertainty in the contribution of the 1.17-Mev gamma-ray to the Co^{60} data completely overshadows the effects listed here.

V. FAILURE OF THE BORN APPROXIMATION

In Table III are summarized both the ratios of the experimentally observed pair production cross sections in lead to those calculated using the Born approximation, and also the results of more exact calculations at various energies. The data in this table are displayed in Fig. 5. The dashed curve is that computed by Davies and Bethe[27] and is not expected to be valid at low energies. It can be seen that near the threshold the experimental cross sections are considerably larger than those given by the Born approximation, whereas at high energies they are slightly lower. Results recently reported from Case[28] serve to locate the cross over at about 6 Mev.

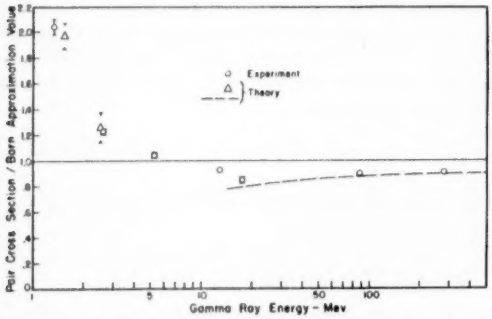

FIG. 5. Failure of the Born approximation calculations in lead. Based on data given in Table III. The dashed curve is based on the calculations of Davies and Bethe (see reference 27) and is not expected to be valid at low energies.

[27] H. Davies and H. A. Bethe, Phys. Rev. **87**, 156 (1952).
[28] Rosenblum, Shrader, and Warner, Jr., Phys. Rev. **88**, 612 (1952).

VI. NUMERICAL VALUES FOR THE CROSS-SECTIONS

In Table IV are tabulated values of the pair production cross section according to the Born approximation, and also "corrected" cross sections obtained by using the experimentally determined Z-dependence and assuming that the Born approximation gives the correct result in the limit of low Z. The Born approximation values are calculated from the formula given by Hough.[29] The corrected cross sections are calculated from the following formulas:

$$\sigma_{\text{corrected}}=\sigma_{\text{Born}}(1+1.59\times10^{-4}Z^2) \text{ at 1.33 Mev,}$$

$$\sigma_{\text{corrected}}=\sigma_{\text{Born}}(1+3.39\times10^{-5}Z^2) \text{ at 2.62 Mev.}$$

VII. REANALYSIS OF COLGATE'S GAMMA RAY ABSORPTION DATA

The results given above can be used to reanalyze some of the recent accurate gamma-ray absorption measurements of Colgate.[14] The discussion which follows refers to Sec. VII of his paper. His method of analysis was to take one of the processes which contributes to gamma-ray absorption as unknown or poorly known, and to try to find out more about it by subtracting from the experimental cross sections theoretical values for the cross sections for all the other processes. At 1.33 Mev he takes the photoelectric effect as the unknown and subtracts from the experimental cross section theoretical values for the Rayleigh, Compton, and pair production cross sections. We have followed this procedure but have substituted what we believe to be more correct values for the pair production cross section. The resulting "remainder" cross section is then compared to the theoretical photoelectric effect cross section.

TABLE IV. Pair production cross sections (in barns). "Corrected" cross sections are obtained by using the experimentally determined Z-dependence and assuming that the Born approximation gives the correct result in the limit of low Z. The Born approximation values are calculated from the formula of Hough.[a]

	1.33 Mev		2.62 Mev	
Z	σ_{Born}	$\sigma_{\text{corrected}}$	σ_{Born}	$\sigma_{\text{corrected}}$
6	0.000588	0.000592	0.0136	0.0136
13	0.00276	0.00283	0.0640	0.0644
29	0.0137	0.0156	0.318	0.327
50	0.0409	0.0571	0.946	1.026
82	0.110	0.227	2.55	3.13
92	0.138	0.325	3.20	4.12

[a] See reference 29.

At 2.62 Mev Colgate took the pair production cross section as the unknown. We believe that it is now more appropriate to take the photoelectric cross section as unknown and have accordingly analyzed the data in the same way as the 1.33 Mev data. The results are given in Table V and compared with the theory in Fig. 6. The theoretical values are obtained by multiply-

[29] P. V. C. Hough, Phys. Rev. **73**, 266 (1948).

TABLE V. Reanalysis of Colgate's data on gamma-ray absorption at 1.33 and 2.62 Mev. The data given below are corrections to Tables X and XI of reference 14. At both energies $\sigma_{\text{remainder}}$ is computed by subtracting from the experimental cross sections the theoretical Compton, Rayleigh, and corrected pair production cross sections.

	1.33 Mev		2.62 Mev	
Z	σ_{pair} $\times 10^{28}$	$\sigma_{\text{remainder}}/Z^5$ $\times 10^{33}$	σ_{pair} $\times 10^{28}$	$\sigma_{\text{remainder}}/Z^5$ $\times 10^{33}$
6	0.000592	...	0.0136	...
13	0.00283	...	0.0644	...
29	0.0156	...	0.327	...
50	0.0571	1.124±0.06	1.026	2.85±0.64
78	0.196	0.944±0.024	...	...
82	0.227	0.957±0.011	3.125	2.78±0.081
83	0.236	0.929±0.010	3.217	2.90±0.076
92	0.325	0.861±0.006	4.124	2.98±0.24

ing the K shell cross sections of Hulme, *et al.*,[30] by the ratio σ_{K+L+M}/σ_K from the Stobbe theory (see reference 13, p. 15). The contribution of the higher shells obtained in this manner is probably more realistic than that obtained by the 5/4 rule. At 1.33 Mev the values of the remainder cross section are about 5 to 10 percent lower than the theoretical photoelectric cross section; at 2.62 Mev they are about 20 percent lower. This result could mean that the energy dependence of Hulme's curves at high energies is not correct.

The author is deeply indebted to Professor W. M. Woodward for his continued interest in this experiment and for his many fruitful suggestions. He also wishes to thank Professor P. Morrison, Professor H. A. Bethe, Dr. U. Fano, and Miss Gladys White for discussions on the theoretical aspects of the problem.

APPENDIX

The value of 1.25 for the ratio of the cross section calculated by Jaeger and Hulme to that calculated from the Born approximation for lead at 5 mc^2 is obtained using the revised cross section given by Jaeger in reference 5 together with the Born approximation value calculated from Hough's formula.[29] There are numerous misprints and errors in the literature which could mislead one on this point. The values of the Born approximation cross section at 5.0 mc^2 and 5.2 mc^2 given in references 3 and 5 do not agree with other published values or with values obtained from Hough's formula. The same can be said for the Born approximation value at 5.2 mc^2 given at the top of page 259 of the second edition of Heitler. In addition, the exact value given in the same table has apparently been miscopied from the original reference. This latter error led Colgate, in plotting Fig. 8 of reference 14, to show the Jaeger and Hulme calculation as only 11 percent higher than the Born approximation value in lead at 2.62 Mev. It should also be noted that the value of the Born approximation cross section at 1.362 Mev quoted by Davisson and Evans[31] is 40 percent higher than the value computed from Hough's formula.

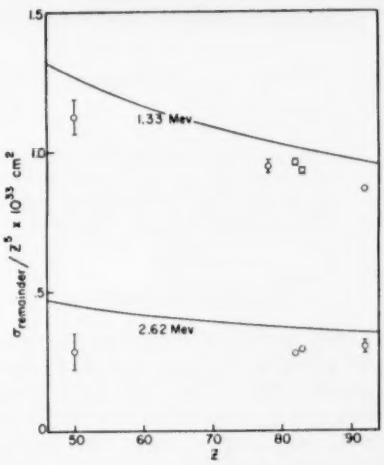

FIG. 6. Reanalysis of Colgate's data on gamma-ray absorption at 1.33 and 2.62 Mev. Curves are the theoretical photoelectric cross section/Z^5 for the respective energies. The points represent the experimental cross section minus the theoretical Compton, Rayleigh, and corrected pair production cross sections. Based on the data given in Table V.

[30] H. R. Hulme *et al.*, Proc. Roy. Soc. (London) **A149**, 131 (1935).

[31] C. M. Davisson and R. D. Evans, Revs. Modern Phys. **24**, 79 (1952).

Radiochemical Studies on the Fission of Th^{232} with Li+D Neutrons*,†

A. TURKEVICH, J. B. NIDAY,‡ AND ALTHEA TOMPKINS§
Institute for Nuclear Studies, University of Chicago, Chicago, Illinois

(Received October 14, 1952)

The fission of Th^{232} with neutrons from lithium bombarded with 7.6-Mev deuterons has been investigated radiochemically. The relative yields of fourteen mass chains, mostly in the light group, have been determined. The yields of symmetrical products are about tenfold higher than in the fission of Th^{232} with pile neutrons. Very light mass chains (very asymmetric fission) show a much smaller increase in yield.

I. INTRODUCTION

THE radiochemical investigation of the fission of Th^{232} with pile neutrons (~2.7 Mev) has recently been reported.[1] There have also been accumulated similar data over a period of years on the fission of this nuclide with fast neutrons from the Li+D reaction at the University of Chicago 37-inch cyclotron. These are the subject of this communication.

Increasing the energy of excitation of a nucleus undergoing fission is known to increase the relative yield of products of symmetrical division.[2–7] For several reasons, Th^{232} represents a good nucleus to study this effect. First, the separation of the mass peaks from the fission of Th^{232} with relatively low energy neutrons is the largest[1] of all investigated nuclei; i.e., Th^{232} fission is the most asymmetric of all. Secondly, Th^{232} has one of the highest neutron to proton ratios among fissionable nuclei. This means that even if some neutron evaporation should occur prior to the fission process with high energy neutrons, the yields of the radioactive species near stability will still represent the total mass yields.

II. GENERAL EXPERIMENTAL PROCEDURE

The thorium samples were in the chemical form $Th(NO_3)_4 \cdot 4H_2O$ (Baker's Analyzed) and weighed about seventy grams. They were packaged in two Pyrex test tubes, and wrapped in cadmium. The samples were placed directly in back of the 2 in.×3 in. water-cooled lithium target of the cyclotron.

The results reported are from fourteen bombardments varying in duration from two to eleven hours and in integrated intensities from 15 to 400 microampere hours. The variation of intensity with time during bombardment was monitored via the beam integrator of the cyclotron. Since, however, the lithium targets tended to deteriorate during a prolonged bombardment, this may be a source of error in the determination of short lived species.

The fission rate in a sample of 70 grams of $Th(NO_3)_4 \cdot 4H_2O$ under our conditions was about 2.3×10^6 per microcoulomb of deuterons on the target. It was thus about one hundred times lower in a typical bombardment than in the pile work already reported. This made it impractical to determine the yields of nuclides having fission yields less than 0.05 percent.

The samples were wrapped in cadmium in order to reduce the thermal neutron activation of Th^{232} and of uranium and other possible impurities. The thermal neutron flux inside the samples was about $5 \times 10^5 n/cm^2$ microcoulomb of deuterons on the target. It was thus less troublesome than in the pile fission of thorium.

After irradiation, the samples of thorium nitrate were dissolved in hot water containing varying amounts of nitric acid and diluted to 100 ml in a volumetric flask. Aliquots of this master solution were pipetted out for analyses for the various fission products. The determinations were usually made in duplicate and only infrequently was the same aliquot used for more than one fission product.

The general radiochemical procedure, as well as some details of analysis for fission products from thorium, has already been given.[1] The results reported here were obtained concurrently with the ones reported for the pile fission of Th^{232}. The radioactivity of the isolated samples was also measured in the same way, using cylindrical glass-walled Eck-and-Kreb type Geiger counters, and then corrected for efficiency of detection of the radiation. As before, only relative yields were determined, 53-day Sr^{89} again serving as a standard and being isolated in each bombardment. The most serious general error in this type of relative yield determination occurs in the correction for absorption

* A preliminary report of this work was presented at the December, 1947, meeting of the American Association for the Advancement of Science, Chicago, Illinois.

† The operation of the University of Chicago 37-inch cyclotron was supported during this period by the ONR.

‡ Present address: California Research and Development Company, Livermore, California.

§ Present address: Institute for the Study of Metals, University of Chicago, Chicago, Illinois.

[1] A. Turkevich and J. B. Niday, Phys. Rev. **84**, 52 (1951).

[2] Nishina, Yasaki, Kimura, and Ikawa, Phys. Rev. **58**, 660 (1940).

[3] Engelkemeir, Freedman, Seiler, Steinberg, and Winsberg, *Radiochemical Studies: The Fission Products* (McGraw-Hill Book Company, Inc., New York, 1951), Paper No. 204, National Nuclear Energy Series, Plutonium Project Record, Div. IV, Vol. 9.

[4] R. W. Spence, Brookhaven Conference Report BNL-C-9 (July, 1949), unpublished.

[5] Perlman, Goeckermann, Templeton, and Howland, Phys. Rev. **72**, 352 (1947); R. H. Goeckermann and I. Perlman, Phys. Rev. **73**, 1127 (1948).

[6] A. S. Newton, Phys. Rev. **75**, 17 (1949).

[7] Jones, Fowler, and Pachler, Phys. Rev. **87**, 174 (1952).

TABLE I. Fission yields in the fission of Th^{232} with Li+D neutrons.

(1) Mass No.	(2) Nuclide isolated	(3) No. of bombardments in which nuclide isolated	(4) $\frac{Y_x}{Y_{Sr^{89}}}$	(5) Y_x[a]	(6) Yield in pile fission	(7) $\frac{(Y_x/Y_{89})_{Li+D}}{(Y_x/Y_{89})_{Pile}}$
77	12-hr Ge—38-hr As	3	0.0034	0.022	0.009	2.7
	Total chain[b]		0.0078	0.052	0.020	
83	2.4-hr Br[c]	2	0.41	2.74	1.9	1.4
89	53-day Sr	14	(1.00)[a]	(6.7)	(6.7)	(1.00)
91	9.7-hr Sr	3	0.84	5.6	6.4	0.93
97	17.0-hr Zr—68-min Nb	2	0.74	4.95	5.4	1.0
99	67-hr Mo	3	0.46	3.1	2.9	1.0
103	42-day Ru	1	0.076[d]	0.51[d]	0.20	2.5
106	1.0-yr Ru—30-sec Rh	1	0.079	0.53	0.058	9.0
111	7.5-day Ag	3	0.094	0.63	0.052	13.1
115	2.25-day Cd—4.53-hr In	1	0.113	0.76	0.072	11.2
117	2.8-hr Cd—117-min In	1	0.055[d]	0.37[d]		
131	8.0-day I	2	0.35	2.3	1.2	2.0±1.0
132	77-hr Te—2.4-hr I	1	0.27[d]	1.8[d]	2.4	0.8±0.3
139	85-min Ba	2	1.34	9.0		
144	275-day Ce—17-min Pr	3	1.07	7.2	7.1	1.1

[a] 53-day Sr^{89} was the standard chosen in the relative yield determination. In both this work and in the pile neutron studies it was assigned a value of 6.7 percent to get absolute yields for other nuclides.
[b] The total yield of chain 77 was calculated assuming that 57 percent of the chain goes through the 59-sec Ge^{77} isomeric state (reference 1).
[c] Yield of 2.4-hr Br^{83} was calculated assuming 27/48 of the bromine came from 67-sec Se^{83} and the rest from 25-min Se^{83} (reference 1).
[d] These relative yields carry an estimated error of 50 percent.

of the beta-radiations in the counter walls. This limits the accuracy of these yields to 20 percent.

In many cases, however, the relative yields in the fast neutron fission of Th^{232} could be compared with the same quantities in the pile fission of Th^{232} with greater accuracy. This was possible because the samples were measured with the same (or very similar) Geiger tube. In this case, corrections for efficiency of detection of the radiations either cancel out completely or are much less serious than in the individual relative yield values.

The yields of fourteen mass chains, mostly in the light group of the fission products, have been determined. In all but five of these, the yields reported are averages of the results of at least two bombardments. The reproducibility from one bombardment to another was somewhat poorer than in the pile work. This was probably due to the lower intensities available—in several cases making it possible to check only crudely the purity of the isolated radioactivity by absorption methods. The lower intensities also increased the relative interference by thorium decay products. The lack of reproducibility may also be connected with slight differences in positioning of the samples during bombardment. This could give rise to variation in the yields of energy sensitive fission products.

The only reported[8] value of the cross section for the neutron fission of Th^{232} is that of 10^{-25} cm^2 at 2.5 Mev. The neutrons from a thick target of lithium bombarded with 7.6-Mev deuterons have energies ranging up to 21 Mev. The neutron distribution from such a source, however, has been determined only at low deuteron energies.[9] Theoretical calculations on what the spectrum might be at a bombarding energy of 7.6 Mev indicated that the kinetic energy of most of the neutrons should be less than 14 Mev. This result was in agreement with $Cu^{63}(n,2n)Cu^{62}$ activation experiments, which showed that for comparable cross sections[8,10] about ten percent of the fissions in Th^{232} were induced by neutrons with energy greater than 12 Mev. We estimate that the majority of the fissions under our conditions are caused by neutrons with energy between 6 and 11 Mev.

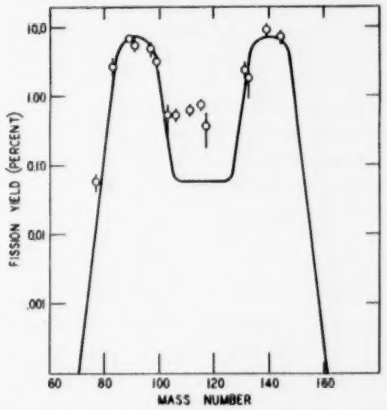

FIG. 1. Fission yields from Th^{232} with (Li+D) neutrons. The solid curve is the yield curve of Th^{232} with pile neutrons (see reference 1).

[8] Ladenburg, Kanner, Barschall, and Van Voorhis, Phys. Rev. **56**, 168 (1939).

[9] H. T. Richards, Phys. Rev. **59**, 796 (1941); L. L. Green and W. M. Gibson, Proc. Phys. Soc. (London) **62**, 407 (1949).

[10] J. L. Fowler and J. M. Slye, Phys. Rev. **77**, 787 (1950).

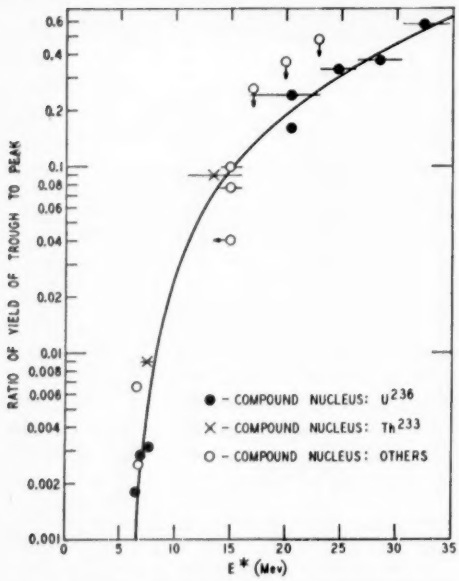

FIG. 2. Effect of energy of excitation of the compound nucleus (E^*) on the relative yield of symmetrical fission.

III. RESULTS

The results are presented in Table I. This lists for each mass number studied the long-lived radioactive members. The nuclide isolated radiochemically is underlined. The third column indicates the number of bombardments in which the nuclide studied was isolated. The fourth column gives the ratio of the yield of this nuclide to that of the standard, 53-day Sr^{89}. This is the experimental ratio of the activities corrected to an infinite bombardment and corrected for differences in detectability of the radiations.[1] The fifth column gives the yield of the chain in Th^{232} fission with Li+D neutrons, assuming Sr^{89} has a yield of 6.7 percent (the value obtained in the pile fission of Th^{232}). We assign a probable error of 20 percent to these relative yields, except for those indicated in the table, where special circumstances dictate a higher error.

The sixth column reproduces the yields in the pile fission of Th^{232} from the previous work.[1] Finally, the last column gives the ratio of the relative yield of the nuclide (referred to Sr^{89}) in fast neutron fission to the same quantity in pile fission. Unless indicated otherwise, these last ratios are believed to be good to 10 percent.

The yields in Th^{232} fission with Li+D neutrons are presented in Fig. 1. The vertical lines represent our estimate of the reliability of the yields relative to Sr^{89}. The figure shows also, for comparison, the smooth curve drawn through the yield data in the pile fission of Th^{232}. Neither of these studies on the fission of Th^{232} is accurate enough to look for the deviations from a smooth fission yield distribution indicated by recent mass spectrographic work.[11]

IV. DISCUSSION

The yield data illustrate the rise in relative yield of symmetrical fission when the energy of excitation of the nucleus undergoing fission is increased. There does not exist at present detailed information on how this probability increases for any one nucleus. The best one can do is to collect the fragmentary data at various energies for different compound nuclei and to compare them.[11] This is done in Fig. 2. The ordinate (on a logarithmic plot) is the ratio of the yield for symmetrical division to that for the most probable (asymmetric) product. The abscissa gives the energy of excitation of the compound nucleus.

Table II gives the source of the data used in constructing Fig. 2.[1,4,6,7,12–16] The energy of excitation has been calculated from the kinetic energy of the bombarding particle and the binding energy of the projectile in the compound nucleus.[17] In the case of the photofission experiments,[4,12,13] the results have been plotted

TABLE II. Data for Fig. 2.

E^* Mev	Compound nucleus	Trough yield / Peak yield	Nuclear reaction	Reference
6.50	U^{238}	0.0018	thermal neutron fission of U^{235}	14
6.50	Pu^{240}	0.0065	thermal neutron fission of Pu^{239}	14
6.74	U^{234}	0.0025	thermal neutron fission of U^{233}	15
6.9	U^{236}	0.0028	U^{235}+~0.4-Mev neutrons	4
7.7	U^{236}	0.0031	U^{235}+1.2-Mev neutrons	4
7.5	Th^{233}	0.009	Th^{232}+pile neutrons	1
11–16	Th^{233}	0.09	Th^{232}+(Li+D) neutrons	This paper
~15	Th^{233}	0.10	Th^{232}+69 Mev (max)γ	12
~15	U^{233}	0.077	U^{238}+48 Mev (max)γ	13
~15	U^{235}	0.04	U^{235}+gamma-rays	4
20.5	U^{236}	0.16	U^{235}+14-Mev neutrons	4
17	Np^{239}	<0.26	U^{238}+cyclotron protons	7
20	Np^{239}	<0.36		
23	Np^{239}	<0.48		
16.5–23.0	U^{236}	0.24	Th^{232}+α	6, 16
23.0–26.5	U^{236}	0.33		
26.5–30.5	U^{236}	0.37		
30.5–34.5	U^{236}	0.57		

[11] H. G. Thode and R. L. Graham, Can. J. Research **A25**, 1 (1947); MacNamara, Collins, and Thode, Phys. Rev. **78**, 129 (1950); Glendenin, Steinberg, Inghram, and Hess, Phys. Rev. **84**, 860 (1951).

[11] *Note added in proof:* A similar comparison has recently been made by Fowler, Jones, and Poehler, Phys. Rev. **88**, 71 (1952).

[12] D. M. Hitler and D. S. Martin, Abstract, American Chemical Society Meeting, Atlantic City, New Jersey (September, 1952).

[13] N. Sugarman and R. Schmitt, private communication.

[14] E. P. Steinberg, private communication. See also E. P. Steinberg and M. S. Freedman, Paper 219, of reference 3.

[15] Steinberg, Seiler, Goldstein, and Dudley, talk before the American Association for the Advancement of Science (December, 1947); USAEC declassified document, MDDC 1632 (January 6, 1948), unpublished.

[16] The data of Newton (see reference 6) on the yield of 43-day Cd^{115} relative to Ba^{140} as a function of depth of thorium target irradiated with 38-Mev alphas was normalized by assuming that this ratio has a value 0.00013 in the thermal neutron fission of U^{235} where the trough to peak ratio is 0.0018.

[17] G. T. Seaborg, Pi Lambda Upsilon Lecture, Ohio State University, Columbus, Ohio (March, 1952), unpublished.

at approximately 15 Mev, the reported[18] photofission resonance energy for U^{238}. The resonance is expected to be at approximately the same[19] energy in the case of Th^{232} and U^{235}. The ratios from the proton bombardment of normal uranium[7] are considered to be upper limits since the fission product selected in the work, Ag^{111}, is probably not at the bottom of the trough. These data are presented with downward arrows. With two exceptions, the remaining points lie on a reasonably smooth curve. The ratio for the thermal neutron fission[14] of Pu^{239} is definitely higher than the other data at comparable excitation. The other striking deviation is the lone experiment[4] reported on the photofission of U^{235}. It is possible that in this work the betatron energy was not sufficiently greater than 15 Mev to take advantage of the photofission resonance.[20] Within the accuracy of our knowledge of the energy of the Li+D neutrons causing fission in this study, the results reported here lie on the curve.

Figure 2 indicates the strong energy dependence of symmetrical fission and can be interpreted as an excitation curve for the formation of symmetrical products relative to asymmetrical ones in the fission of heavy elements. It would indicate, for example, that the yield of symmetrical products in spontaneous fission (if the main peaks are well separated) would be immeasurably low.

Table I and Fig. 1 also illustrate that the increase in neutron energy from pile neutrons to Li+D neutrons has a much less drastic effect on the low yields on the light side of the light peak. The yield of Ge^{77} has increased 2.7-fold; that of Br^{83} only by 40 percent. The increase in yield in this region in the case of Th^{232} can be explained semiquantitatively by the postulate that an appreciable fraction of the fissions with Li+D neutrons involve the emission (before or after fission) of one or two more neutrons than in the case of pile neutron fission. This insensitivity to energy in this region of the yield curve confirms the data of Newton.[6] In his work the same two mass chains had approximately the same yields from U^{236} excited by about 33 Mev as in U^{236} formed from thermal neutrons on U^{235}. Newton's work on U^{236} excited by 33 Mev also shows little increase in yields on the heavy side of the heavy group. Thus, both the work on Th^{232}+37.5-Mev alphas[6] and this work emphasize the difference between the restrictions preventing symmetric and very asymmetric fission.

[18] W. E. Ogle and J. McElhinney, Phys. Rev. **81**, 344 (1951).
[19] M. Goldhaber and E. Teller, Phys. Rev. **74**, 1046 (1948).
[20] R. W. Spence (private communication).

PHYSICAL REVIEW VOLUME 89, NUMBER 3 FEBRUARY 1, 1953

Ionization Probability Curves for Krypton and Xenon near Threshold

R. E. Fox, W. M. Hickam, and T. Kjeldaas, Jr.
Westinghouse Research Laboratories, East Pittsburgh, Pennsylvania

(Received October 10, 1952)

The shapes of the ionization probability curves of krypton and xenon have been determined near the ionization potential by measuring the ionization produced by nearly monoenergetic electrons in a mass spectrometer. Ionization processes associated with the $^2P_{\frac{1}{2}}$ and $^2P_{\frac{3}{2}}$ ground states of the ions are clearly resolved. Ions are observed which are attributed to auto-ionization of atoms excited to the higher states having the $^2P_{\frac{1}{2}}$ core configuration.

I. INTRODUCTION

LITTLE information is available concerning the true shapes of ionization probability curves near threshold. This is largely owing to the difficulty in obtaining an electron beam with a sufficiently narrow energy spread. Lawrence,[1] and later Nottingham,[2] in their study of the ionization probability of mercury used a magnetic analyzer to reduce the energy spread of the electron beam. In this type of experiment where total ionization is measured precautions are necessary to distinguish photoelectric effects and true ionization and to eliminate impurities in the gas sample. If, however, only the shape of the ionization probability curve is to be determined, one may use a mass spectrometer in which a positive analysis of the ions produced largely eliminates the need for these precautions.

On the other hand, the problems associated with the production of a sufficiently monoenergetic electron beam in a mass spectrometer were solved only recently. With the use of this new method it was demonstrated[3,4] that within the experimental accuracy then attainable, the ionization produced was directly proportional to the excess energy of the bombarding electrons in the region near the threshold.

In the earlier work,[3] it was reported that a slight break sometimes observed in the ionization probability curves for krypton might be attributed to the doublet ground state of the krypton ion. Since then, an increase in sensitivity, due in part to a new pulsing circuit,[5] has permitted a more detailed study of ionization prob-

[1] E. O. Lawrence, Phys. Rev. **28**, 947 (1926).
[2] W. B. Nottingham, Phys. Rev. **55**, 203 (1939).
[3] Fox, Hickam, Kjeldaas, and Grove, Proc. of the Symposium on Mass Spectroscopy in Physical Research, Natl. Bur. Standards Circular 522, January, 1953.
[4] Fox, Hickam, Kjeldaas, and Grove, Phys. Rev. **84**, 859 (1951).
[5] To be published.

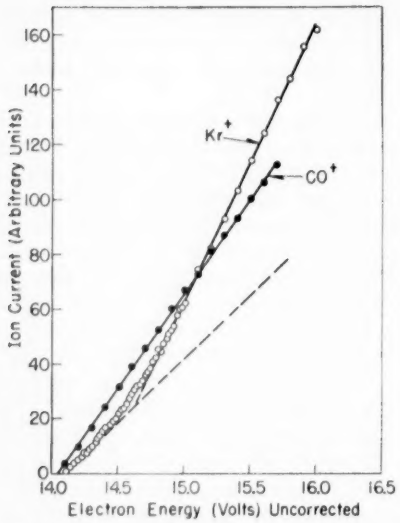

FIG. 1. Relative ionization probability curve for Kr and CO. The slight corrections necessary to establish the absolute energy scale have not been applied. The experimental probable error is indicated by the size of the data points.

ability curves. The results of studies on krypton and xenon, to be presented in this paper, reveal detailed structure of the ionization probability curves. It will be shown how these hitherto unobserved details can be correlated with information about the energy levels concerned.

II. EXPERIMENTAL PROCEDURE

The gas samples used were purchased from the Air Reduction Sales Company and were of the "spectroscopically pure" grade. No further purification was necessary since a scan of the mass spectra for these samples indicated that there were no conflicting impurities present. A pressure less than 10^{-4} mm of mercury was maintained in the ion source during observations.

The ionization studies were made using a 90° sectored magnetic field mass spectrometer similar in design to the type L-V manufactured by Westinghouse. The ion source was modified for use of the "retarding potential difference method" described in the earlier papers.[3,4] This method utilizes a retarding electrode between the filament and the ionization chamber which serves to chop off sharply the low energy electrons from the original distribution. The sharp lower boundary energy in this chopped distribution can be varied by changing the potential of this retarding electrode without appreciably affecting the rest of the distribution. The *difference* in the ion currents for two values of the retarding potential is therefore the ion current produced by electrons monoenergetic to within this change in the retarding voltage. This method then serves to eliminate effects resulting from the thermal energy spread of the electrons as well as the unknown contact potential between the filament and the ionization chamber. Since an auxiliary magnetic field is employed to align the electron beam, those electrons which have an initial transverse velocity move through the electron gun with a spiraling motion. The energy contained in this spiraling motion is adequately limited by making the slits through which the electrons pass sufficiently narrow. The effect on the electron energy owing to the electric field employed for ion removal from the ionization chamber was eliminated by giving this field and the electron beam a properly phased pulsed time dependence, so that electrons reach the ionization chamber only when the ion removal field is zero. Employing these techniques, the effective electron beam possessed a maximum energy spread of 0.06 ev and the total kinetic energy of the electrons was known to within 0.1 ev whenever an ion source with fresh surfaces was used. It was found, however, that a contact potential between the retarding electrode and the ion chamber, presumably the result of deposits from the filament, would build up with time. In the earlier work,[3,4] where ionization potentials were measured on an absolute basis, only fresh surfaces were used to minimize errors resulting from this source. Since the purpose of the present studies was to investigate the shapes of the ionization probability curves near threshold, a knowledge of the absolute energy scale was not essential; therefore, this contact potential was allowed to build up to about 0.3 volt before the ion source was removed and cleaned. For the same reason the correction for space charge in the electron beam employed in the earlier

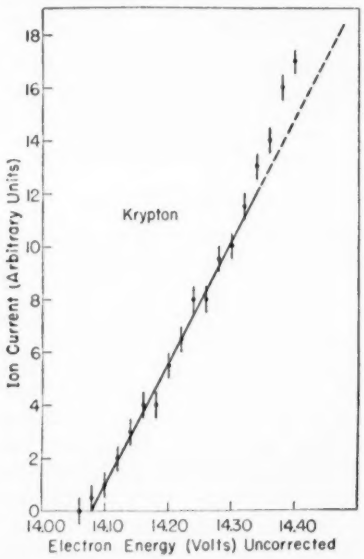

FIG. 2. The initial portion of the relative ionization probability curve for Kr on an expanded scale. The experimental probable error is indicated by the height of the lines through the data points.

work was not made. The curves shown in this paper therefore give the electron energy as uncorrected. The over-all magnitude of these corrections are small however, as can be seen by a comparison of the measured appearance potentials with the spectroscopically determined ionization potentials.

III. EXPERIMENTAL RESULTS

In Fig. 1 are shown the curves obtained for krypton and carbon monoxide. The carbon monoxide (observed at mass 28) curve is used to illustrate the linearity of ionization probability curves obtained by this method when only a single ionization process is involved. A further purpose of including the carbon monoxide curve in this figure is to indicate that the structure shown by the krypton curve cannot be caused by instrumental effects since the two curves were taken under identical conditions. It is seen from Fig. 1 that the ionization probability curve for krypton exhibits a linear portion extending from the appearance potential at 14.08 volts to about 14.3 volts. The linearity of this initial portion is demonstrated in Fig. 2 where the data have been plotted on a greatly expanded scale. It is clear that within the experimental probable error, indicated by the height of the line through the data points, this portion of the curve is indeed linear. Near 14.3 volts the curve departs from linearity for a region of about 0.6 volt after which a new linear slope is obtained (see Fig. 1).

The shape of the ionization probability curve for xenon is shown in Fig. 3. This curve exhibits a pronounced break occurring at about 1.2 volts above the onset of initial ionization. The trend of the points just below this break indicates that there may be a slight deviation from linearity in this region, although the experimental accuracy of the instrument was not sufficient to definitely establish this point. For a number of runs, the trend of the points in this region was always above the straight lines best drawn to fit the data. Here the probable error of a single measurement is indicated by the size of the data points.

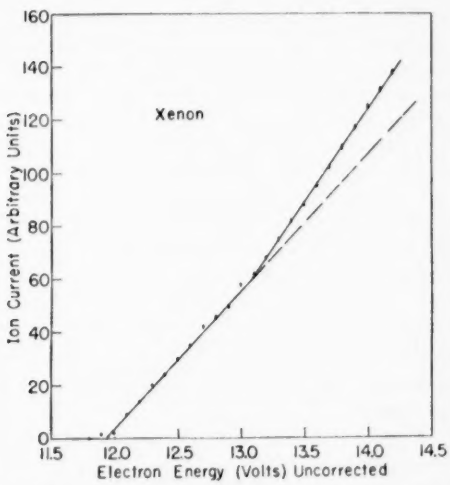

FIG. 3. Relative ionization probability curve for Xe. The probable error is indicated by the height of the data points.

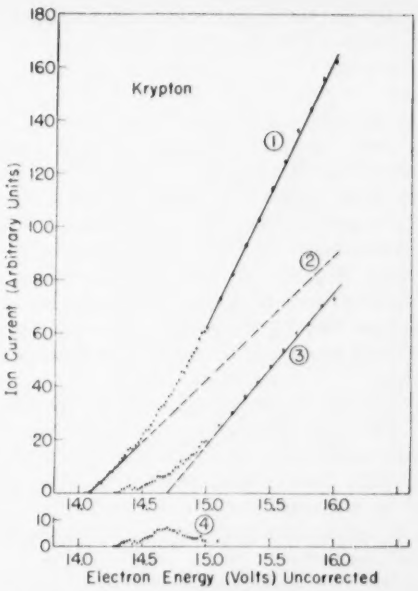

FIG. 4. Analysis of the relative ionization probability curve for Kr. (1) A typical experimental curve. (2) The straight line extrapolation of the initial linear portion of curve 1. (3) The curve obtained by subtracting curve 2 from curve 1. (4) The curve obtained by subtracting the linear portion of curve 3 and its extrapolation from curve 3.

Ionization probability curves for these gases were observed over a period of several months and under a wide range of experimental conditions. The magnetic field used for aligning the electron beam was varied by a factor of two. The pressure in the ion source was varied by a factor of five. Several electron gun-ionization chamber designs were used. The pulse frequency ranged from 50 to 200 kilocycles. The shapes of the ionization probability curves were found to be invariant under these changes.

IV. DISCUSSION

The energy level diagram of any singly charged rare gas ion, with the exception of helium, shows that the ground state of the ion is a doublet. The lowest energy state of this doublet, i.e., the true ground state of the ion, is a $^2P_{\frac{3}{2}}$ state, the other member being a $^2P_{\frac{1}{2}}$ state. In the cases of krypton and xenon, the energy separations of these doublets are[6] 0.666 ev and 1.31 ev, respectively, as determined by spectroscopic measurements.[7] The ionization probability curve for krypton

[6] Landolt-Börnstein, *Zahlenwerte und Funktionen* (Springer, Berlin, 1950), Vol. I, Part 1.

[7] Based on 8066.83 cm^{-1} per electron volt; J. W. M. DuMond and E. R. Cohen, Phys. Rev. **82**, 555 (1951).

is analyzed into its components in Fig. 4. Curve 1 of this figure shows a typical curve for krypton. The initial linear portion of this curve arises from ionization to the $^2P_{\frac{3}{2}}$ state. For gases whose ions have a single ground state the ionization probability curves obtained by the authors were linear functions of the excess energy of the bombarding electrons. On this basis it is assumed that the linear relationship holds for each member of the doublet ground state. The dashed curve 2 is then a linear extrapolation of the initial portion of curve 1, and a point by point subtraction of these curves yields curve 3. The linear portion of this curve is then the ionization to the $^2P_{\frac{1}{2}}$ state and a linear extrapolation of this curve to zero ion current yield its appearance potential.

The nonlinear portion of this curve will be discussed below. The difference between the two appearance potentials should then equal the energy separation of the doublet. And indeed, twelve runs on krypton yielded an average value for this separation of 0.66 $\pm$0.01 ev, in excellent agreement with the spectroscopic value of 0.666 ev.

A similar analysis was made on xenon. Five runs on this gas yielded an average value of 1.27$\pm$0.03 ev, as compared with the spectroscopic value of 1.31 ev.

It is interesting to compare the relative probabilities of ionization to the $^2P_{\frac{3}{2}}$ and $^2P_{\frac{1}{2}}$ states. It is apparent from Figs. 3 and 4 that the probability is higher for the $^2P_{\frac{1}{2}}$ state in krypton, while for xenon the reverse seems to hold. This somewhat surprising result has consistently been obtained from the experimental data. It may be noted that the ratio of these slopes was obtained by a subtraction method similar to the one employed in making a quantitative analysis employing ionization probability curves of a carbon monoxide and nitrogen[8] mixture, wherein the constituents were determined to better than one percent.

For the purpose of discussing the nonlinear portion of curve 3, Fig. 4, a further analysis has been made. Since the linear portion of curve 3 and its extrapolation are the result of ionization to the $^2P_{\frac{1}{2}}$ state, its contribution is subtracted from the curve yielding curve 4, Fig. 4. This curve then results from ionization not accounted for by direct ionization to the $^2P_{\frac{3}{2}}$ and $^2P_{\frac{1}{2}}$ states. This ionization is interpreted as arising by the mechanism of auto-ionization proposed by White[9] in connection with certain peculiarities observed in the optical spectra of these gases. A reference to an energy level diagram for any of these gases[9] will show that there are certain discrete excited states of the atom which lie above the beginning of that continuum resulting in ionization to the $^2P_{\frac{1}{2}}$ state. Owing to an interaction between the excited electron and the ionic core, it is possible for this ionic core to undergo a spontaneous radiationless transition to the $^2P_{\frac{1}{2}}$ configuration, the excited electron carrying off the excess energy resulting in ionization. It is this mechanism which White proposed to explain the absence of radiation arising from these levels. More recently, Beutler[10] has observed unusually strong and diffuse absorption to some of these energy levels. The absence of emission lines from, and the presence of strong and diffuse absorption lines to these levels is good evidence for the mechanism of auto-ionization.

It would be desirable to correlate the apparent structure in curve 4 with the energy levels responsible for auto-ionization. However, the accuracy of the present results does not justify this. A comparison of Figs. 3 and 4 shows that the contribution from auto-ionization is much greater in krypton than in xenon. In fact, in the latter case the auto-ionization is so small as to be barely discernible above the experimental error. This may have some relationship to the result that the ionization probability to the $^2P_{\frac{1}{2}}$ state as compared to the $^2P_{\frac{3}{2}}$ state was smaller in xenon than in krypton.

Similar studies have been made on argon. However, since the ground state doublet separation for this ion is only 0.18 ev the present accuracy of the instrumentation was not sufficient for a detailed study. It can be reported, however, that a break located at about the right energy was observed in the ionization probability curves.

SUMMARY

Relative ionization probability curves for krypton and xenon have been determined near threshold using nearly monoenergetic electrons. The detailed structure of these curves has been correlated with the energy levels obtained from spectroscopic information. The linear ionization near threshold, found to exist where ionization can proceed by a single process to a single energy level, has been applied to the analysis of the more complicated case of the singly charged ions of krypton and xenon. On the basis of a linear threshold law for each energy level, the data yield the proper energy spacing between the $^2P_{\frac{3}{2}}$ and $^2P_{\frac{1}{2}}$ ground states for these ions. Additional structure in the ionization probability curves for these ions is interpreted as arising from the process of auto-ionization.

Studies are now in progress on the doubly charged rare gas ions which possess four energy levels near the ground state. In the preliminary curves, breaks are observed which can be correlated with these energy levels on the basis of a linear threshold law for each energy level.

The authors wish to thank their colleagues in the Physics Department, especially Dr. T. Holstein, Dr. M. A. Biondi, and Dr. A. V. Phelps, for their many helpful suggestions and discussions.

[8] W. M. Hickam and R. E. Fox, J. Chem. Phys. **20**, 1055 (1952).
[9] H. E. White, Phys. Rev. **38**, 2016 (1931).
[10] H. Beutler, Z. Physik **93**, 177 (1934).

Gamma-Radiations from Zr^{95} and Nb^{95}†

C. E. MANDEVILLE, E. SHAPIRO,‡ R. I. MENDENHALL, E. R. ZUCKER,§ AND G. L. CONKLIN
Bartol Research Foundation of the Franklin Institute, Swarthmore, Pennsylvania

(Received October 14, 1952)

By employing lead absorption, coincidence counting techniques, and scintillation spectrometry, it has been shown that each beta-ray of Nb^{95} is followed by a gamma-ray of energy 0.76±0.02 Mev and that most of the beta-rays of the parent element Zr^{95} are followed by a single gamma-ray at 0.73±0.02 Mev. A disintegration scheme is proposed.

INTRODUCTION

IT has been shown that the 65±2 day Zr^{95} and the 35±1 day Nb^{95} are formed in several different nuclear reactions.[1]

In a magnetic spectrograph,[2] the energies of the gamma-rays emitted by Zr^{95} have been measured at 0.73 Mev (93 percent) 0.23 Mev (93 percent), and 0.92 Mev (7 percent). Approximately two percent of the beta-ray disintegrations of Zr^{95} have been shown to terminate at a 90-hour metastable level[3] of the residual nucleus, radioactive Nb^{95}. The energy of the isomeric transition has been measured as 0.216 Mev[4] and 0.24 Mev.[5] The radiation is totally converted. The energy of the relatively hard abundant gamma-ray of Zr^{95} has also been measured as 0.708 Mev.[4]

Spectrometric measurements have yielded quantum energies of 0.75 Mev,[6] 0.758 Mev,[4] and 0.77 Mev[7] for the single gamma-ray of Nb^{95}, the 35-day daughter element. The energy of this gamma-ray was also measured as 0.92 Mev by the method of coincidence absorption.[8] In these latter measurements, the gamma-ray which appeared to have an energy of 0.92 Mev was found in both the zirconium and niobium fractions. However, the beta-gamma coincidence rate of Zr^{95} was such as to suggest that on the average, each beta of Zr^{95} is followed by less than 0.3 Mev of gamma-ray energy. When a carefully purified source of Nb^{95} yielded a beta-gamma coincidence rate sufficiently large to account for the presence of the hard gamma-ray thought to be of energy 0.92 Mev, it was concluded that the presence of this gamma-ray in the zirconium fraction arose from an incomplete chemical separation, and that it is actually only associated with the daughter element. Because of the various conflicting reports concerning the gamma-radiations, the properties of $Zr^{95}-Nb^{95}$ have been re-investigated.

PROCEDURE AND RESULTS

A source of $Zr^{95}-Nb^{95}$ was produced in the fission process at the Oak Ridge pile. Pure separated sources of Zr^{95} and Nb^{95} were prepared repeatedly by Steinberg's oxalate procedure.[9] The gamma-rays of Nb^{95}, Zr^{95}, and $Zr^{95}-Nb^{95}$ were absorbed in lead as shown in Fig. 1. From the slopes of the curves it is evident that the gamma-rays emitted by the three different radioactive sources are essentially the same in energy. No evidence appears on any of the absorption curves to suggest the presence of any gamma-rays of lower energy and comparable intensity. Repeated chemical separations always gave absorption curves similar to those of Fig. 1. The quantum energy taken from the slope of the curve is 0.80±0.05 Mev.

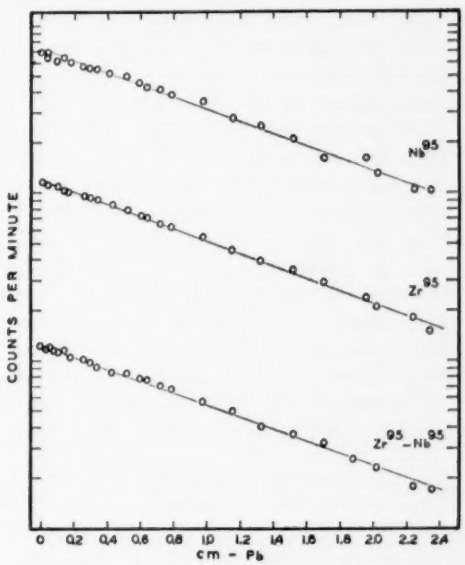

FIG. 1. Absorption in lead of the gamma-rays of Nb^{95}, Zr^{95}, and $Zr^{95}-Nb^{95}$.

† Assisted by the joint program of the ONR and AEC.
‡ At present at Tracerlab, Inc., Boston, Massachusetts.
§ Frankford Arsenal, Philadelphia, Pennsylvania.
[1] Sagane, Kojima, Miyamoto, and Ikawa, Phys. Rev. **57**, 1180 (1940); B. L. Goldschmidt and I. Perlman, *Radiochemical Studies: The Fission Products* (McGraw-Hill Book Company, Inc., New York, 1951), Paper No. 84, National Nuclear Energy Series, Plutonium Project Record, Vol. 9, Div. IV; Brady, Engelkemier, and Steinberg, Papers 85 and 88; L. Jacobson and R. Overstreet, Paper 91. The volume in which these latter references may be found will hereafter be referred to as NNES **9**.
[2] V. A. Nedzel, NNES **9**, Paper 87.
[3] D. W. Engelkemier and E. L. Brady, NNES **9**, Paper 92; E. P. Steinberg, NNES **9**, Paper 93.
[4] G. E. Hudgens and W. S. Lyons, Phys. Rev. **75**, 206 (1949).
[5] J. S. Levinger, NNES **9**, Paper 94.
[6] W. Rall and R. G. Wilkinson, Phys. Rev. **71**, 321 (1947).
[7] V. A. Nedzel, NNES **9**, Paper 90.
[8] C. E. Mandeville and M. V. Scherb, Phys. Rev. **73**, 1434 (1948).
[9] E. P. Steinberg, NNES **9**, Paper 243.

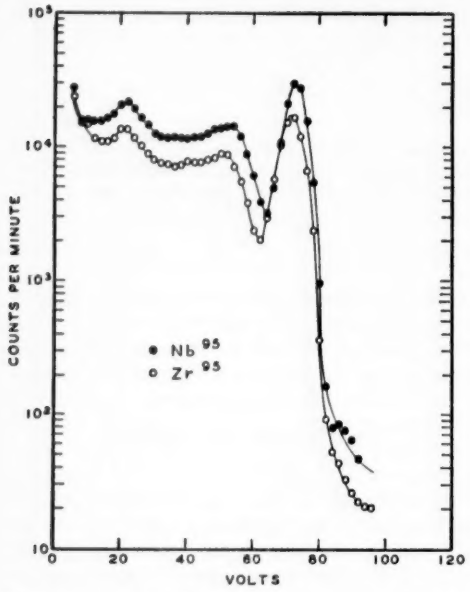

FIG. 2. Pulse-height distribution of gamma-rays from Zr^{95} and Nb^{95} on NaI(Tl).

With the aid of a scintillation spectrometer, the photoelectric lines of the gamma-rays of freshly separated Zr^{95} and Nb^{95} were observed in a crystal of NaI(Tl). The pulse-height distributions are shown in Fig. 2, where it is clear that the gamma-ray of Nb^{95} is somewhat more energetic than that of Zr^{95}. Calibration of the spectrometer with the gamma-rays from Au^{198}, Na^{22}, Cs^{137}, Sc^{46}, and Co^{60} yielded quantum energies of 0.73 ± 0.02 Mev and 0.76 ± 0.02.

The beta-gamma coincidence rates of Nb^{95}, Zr^{95}, and $Zr^{95}-Nb^{95}$, as a function of aluminum absorber thickness before the beta-ray counter, are shown in Fig. 3. It is evident that the average value of the coincidence rate is approximately the same in the three cases, confirming that most of the beta-rays of Zr^{95} are followed, on the average, by approximately the same amount of gamma-ray energy (0.71 Mev) as are the beta-rays of Nb^{95}. The beta-gamma coincidence counting arrangement was calibrated by the beta-gamma coincidence rate of Sc^{46}. In a separate group of coincidence measurements at certain selected thicknesses of absorbers before the beta-ray counter, the amounts of gamma-ray energy per beta-ray of Table I were obtained.[10,11]

TABLE I. Average gamma-ray energy per beta-ray.

Radionuclide	Absorber thickness	Gamma-ray energy (Mev)
Nb^{95}	5 mg/cm²	0.71 ± 0.09
Zr^{95}	40 mg/cm²	0.67 ± 0.08
$Zr^{95}-Nb^{95}$	40 mg/cm²	0.73 ± 0.09

THE DISINTEGRATION SCHEME

The 1.0-Mev beta-spectrum of Zr^{95} ($\Delta j=2$, yes!)[12] terminates at the 90-hr level of $Nb^{95}(p_{1/2})$;[13] so the orbital of the last odd nucleon of Zr^{95} is taken to be $d_{5/2}$. Log ft[14] for the more abundant beta-spectrum of Zr^{95} is 6.62, permitting the interpretation that the spec-

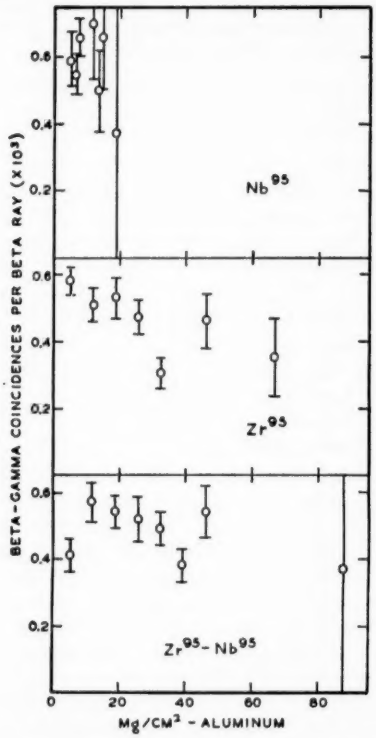

FIG. 3. Beta-gamma coincidence rate of Nb^{95}, Zr^{95}, and $Zr^{95}-Nb^{95}$ as a function of aluminum absorber thickness before the beta-ray counter.

[10] The present coincidence rates and associated gamma-ray energies are in contradiction with the previous report (reference 8) that the beta-rays of Zr^{95} are coincident with less than 0.3 Mev of gamma-ray energy. The earlier results must be ascribed to the presence of unidentified impurities having relatively low beta-gamma coincidence rates.

[11] When a radionuclide is grown from a parent element of comparable half life, it can be shown that if a chemical separation is effected at a considerable length of time after onset of growth, the disintegration rates are in the ratio of

$$C_D/C_P=\lambda_D/(\lambda_D-\lambda_P),$$

where the subscripts P and D refer to parent and daughter, and the λ's are the decay constants. For the 65-day Zr^{95} and the 35-day Nb^{95}, this ratio is 2.16 ± 0.2. In the present investigation the ratio of the gamma-ray activities was observed in both scintillation counters and Geiger counters and found to be 2.2 ± 0.1 confirming a good separation if the gamma-radiations of the parent and daughter are essentially the same.

[12] Mayer, Moszkowski, and Nordheim, Revs. Modern Phys. **23**, 315 (1952).

[13] M. Goldhaber and A. W. Sunyar, Phys. Rev. **83**, 906 (1951).

[14] A. M. Feingold, Revs. Modern Phys. **23**, 10 (1951).

trum may be once forbidden ($\Delta j=0, \pm 1$, yes!) or l-forbidden ($\Delta j=1$, no!, $\Delta l=2$). According to the former classification, the excited level at 0.73±0.02 Mev in the residual nucleus Nb^{95}, could have the orbital $p_{3/2}$, $f_{5/2}$, or $f_{7/2}$. Were it either of the first two values, a relatively intense gamma-ray of energy ~0.5 Mev would be expected to appear among the radiations of Zr^{95}, emitted in the transition between the level at 0.73±0.02 Mev and the 0.21-Mev metastable level of the 90-hr Nb^{95} (see Fig. 4). Only in the case of $f_{7/2}\rightarrow g_{9/2}$ does the probability of a transition to the ground state of Nb^{95} exceed that of a transition to the metastable level ($f_{7/2}\rightarrow p_{1/2}$). Since no gamma-radiation at 0.5 Mev is observed, the most likely of the three orbitals associated with the assumption of a once forbidden transition is $f_{7/2}$.

If an l forbidden beta-transition is assumed, the orbital assignment of the 0.73±0.02 Mev level is uniquely $g_{7/2}$. The transition $g_{7/2}\rightarrow g_{9/2}$ is, of course, far more probable than $g_{7/2}\rightarrow p_{1/2}$. Since the $f_{7/2}$ shell closes at 28 nucleons, the $g_{7/2}$ subshell, closing at 58 nucleons, is favored.

From shell model considerations and the conversion coefficients of the 0.76±0.02 Mev gamma-ray of Nb^{95}, it has been previously shown[15] that the decay of Nb^{95} to Mo^{95} can be characterized by $g_{9/2}\rightarrow g_{7/2}\rightarrow d_{5/2}$.

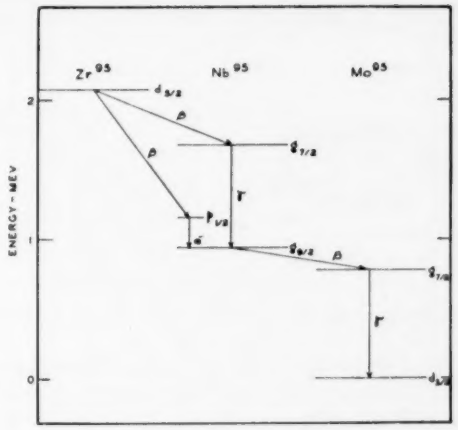

FIG. 4. Disintegration scheme of $Zr^{95}-Nb^{95}$.

[15] C. Y. Fan, Phys. Rev. **87**, 252 (1952).

PHYSICAL REVIEW VOLUME 89, NUMBER 3 FEBRUARY 1, 1953

Neutron Scattering by Coupled Paramagnetic Ions

PHILIP J. BENDT*
Pupin Physics Laboratories, Columbia University, New York, New York
(Received August 8, 1952)

The paramagnetic scattering of very low energy neutrons by MnF_2 and MnO was studied at various sample temperatures. The assumption of Van Vleck that a Gaussian distribution can be used to represent the frequency of inelastic scattering events *versus* energy transfer with the spin lattice is used, and the root mean square half-width of the distribution of energy transfer for MnF_2 is found to be 0.0020, 0.0026, and 0.0034 ev at 610°, 300°, and 126°K, respectively. Short-range order scattering modifies the scattering cross section for MnF_2 to the extent of $1.5/4\pi$ barns/steradian at 126°K, but is not observed at higher temperatures.

Measurements at 300°K indicate the magnetic scattering cross section for MnO, it if were not distorted by short-range order scattering, would be about $2.5/4\pi$ barns/steradian lower than for MnF_2. We suggest this may be accounted for by the mechanism of super-exchange between crystal ions. Rough values of a parameter indicating the range of spin order in MnO were determined at 300° and 133°K. The amount of spin order increases with decrease in sample temperature. Above the Néel temperature, it is found that most of the correlation of spin direction exists only between adjacent ions on the same sublattice.

INTRODUCTION

THE scattering of slow neutrons by crystal lattices of free paramagnetic ions has been examined experimentally.[1,2] For uncoupled ions, the magnetic scattering from each ion is incoherent relative to the nuclear scattering and the magnetic scattering from other ions. The principal feature observed is a magnetic form factor arising from the space distribution of paramagnetic electrons in the ion.

The scattering from antiferromagnetic[2] and ferromagnetic[3] materials has also been examined. For these materials, the spin state of the scatterer is assumed not to change in the scattering process, so the magnetic scattering is coherent and shows strong Bragg reflections.

Paramagnetic substances generally have a transition temperature below which there is long-range order of spin directions in the crystal lattice. This temperature T_0 is called the Curie temperature for those materials which become ferromagnetic, and the Néel temperature

* Now at the Los Alamos Scientific Laboratory, Los Alamos, New Mexico.

[1] I. W. Ruderman, Phys. Rev. **76**, 1572 (1949).

[2] Shull, Strauser, and Wollan, Phys. Rev. **83**, 333 (1951).

[3] C. G. Shull, Phys. Rev. **81**, 626 (1951).

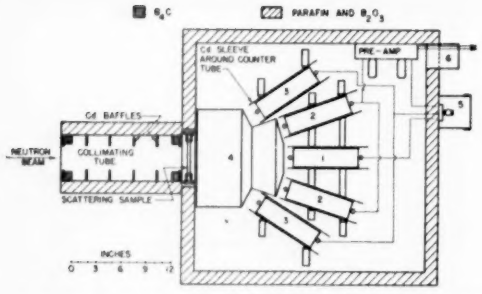

FIG. 1. Apparatus for detecting neutrons scattered at 18° and 33°.

for those materials which become antiferromagnetic. Above T_0 there is a temperature range in which the spins of neighboring paramagnetic ions are coupled.

This temperature range above T_0, where the ion spins are neither completely free nor completely locked in given directions, has not been investigated extensively. As a result of the coupling between the magnetic ions, the neutron scattering is spin-inelastic, involving energy transfer with the spin lattice. Van Vleck[4] has explained how this reduces, by two different processes, the amount of magnetic scattering which would be observed from free ions. Residual coherent scattering, derived from short-range order of spin directions among neighboring ions in a crystal lattice, contributes broad liquid-scattering type reflection patterns.

In the present experiment, measurements were made in the intermediate region above the Néel temperature of two antiferromagnetic compounds. Short-range order scattering and energy transfer between neutron and spin lattice were studied at several sample temperatures.

I. APPARATUS

The experiment was performed with a collimated beam of slow neutrons from the Columbia University cyclotron. The arc source of the cyclotron was pulsed, in order that the time-of-flight of the neutrons could be measured with the electronic Neutron Velocity Selector.[5]

The apparatus shown in Fig. 1 was built to detect the neutrons. A single BF_3 counter tube (1) is located in line with the incident neutron beam, and detects neutrons transmitted through the sample. Eight counter tubes (2) are mounted in a ring along elements of a cone having a mean half-angle of 18°. Twelve counter tubes (3) are mounted in a ring along elements of a similar cone with a half-angle of 33°. The apparatus was built to observe scattering at angles near the forward direction in order to avoid the coherent nuclear Debye-Scherrer rings.

Neutrons in the wavelength region in which measurements were made, 1.6 to 5.5 angstroms, are of sufficiently low energy that a 0.022-inch layer of cadmium provides efficient shielding. The neutron beam is defined with cadmium baffles, and the counter tubes are wrapped with cadmium, allowing neutrons to enter only through the ends. Shielding against stray neutrons is provided in the walls of the box containing the counter tubes. The collimating tube and aluminum container (4) were filled with argon gas to reduce air scattering in the vicinity of the sample. A "temperature cell" was constructed to hold samples at temperatures above or below room temperature while scattering measurements were being made. The sample temperature was measured with thermocouples.

The powder samples of anhydrous crystals of MnF_2 and MnO used in the experiment were prepared by Dr. I. W. Ruderman, and their preparation and handling are described in reference 1.

II. CALIBRATION OF THE APPARATUS

The scattering apparatus does not measure absolute cross sections, but must be calibrated with a standard scattering sample. The number of materials suitable for standards is very limited, owing to crystal structure interference effects, which strongly influence the scattering in the thermal energy region. An ideal material for a standard would be a heavy element with large incoherent scattering and negligible coherent scattering. An element which approximates the ideal standard is vanadium, which has a bound scattering cross section of 5.1 barns, a coherent scattering cross section of 0.1 barn, and a mass number of 51. Two samples of pure vanadium of different thickness were used to calibrate the scattering apparatus. A correction for multiple scattering was made by extrapolating to "zero thickness" where the ratio of multiple to single scattering goes to zero. The incoherent scattering from hydrogen in very thin sheets of polythene $(CH_2)_n$ was used to check the calibration.

The problem of separating the paramagnetic scattering from the nuclear scattering and multiple scattering

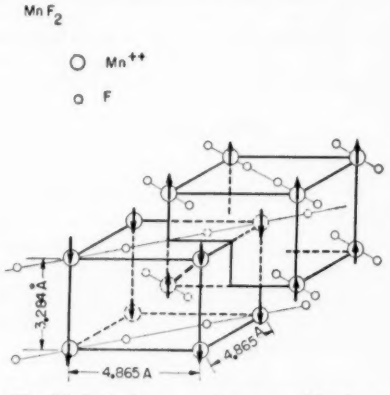

FIG. 2. The MnF_2 body-centered tetragonal lattice structure. Below T_0, the Mn^{++} ion spins are directed oppositely on the two interpenetrating sublattices.

[4] J. H. Van Vleck, Phys. Rev. **55**, 924 (1939).
[5] L. J. Rainwater and W. W. Havens, Jr., Phys. Rev. **70**, 136 (1946); **71**, 65 (1947).

must be considered. The isotope and spin nuclear incoherent scattering of Mn, F, and O are all essentially zero. The nuclear coherent scattering occurs at angles larger than 33° in the wavelength region in which paramagnetic scattering was studied. However, the nuclear coherent scattering can contribute through multiple scattering. The strongest nuclear Debye-Scherrer ring is oriented at 90° in MnF_2 at the wavelength 3.8 angstroms and at 90° in MnO at the wavelength 3.6 angstroms. As the coherently scattered neutrons near these wavelengths are traveling approximately in the plane of the sample, they have a very long path length in the sample and have a good chance of being scattered a second time. This means experimental data close to the above wavelengths have received a contribution from second-scattered neutrons. In determining the best smooth curve to fit the experimental data, the multiple scattering contribution to these points was corrected for, and therefore these points lie above the experimental curves.

At wavelengths other than those referred to above, the multiple scattering in MnF_2 and MnO is small, for two reasons. First, the samples are thin; the transmission calculated on the basis of the scattering cross section alone is about 0.9. Second, the capture cross section for Mn is large (13 barns at 1.8 angstroms), and this substantially reduces the ratio of multiple to single scattering. It is estimated that the contribution of nuclear incoherent scattering and multiple scattering is about $1/4\pi$ barns/steradian.

III. CRYSTAL STRUCTURE

MnF_2 has the body-centered tetragonal lattice shown in Fig. 2. The Mn ions are located on two inter-penetrating sublattices. In Fig. 2, the Mn spins are shown directed along the short edge of the unit crystal cell, parallel on each sublattice, and with spins opposite on the two sublattices. This is the antiferromagnetic arrangement of spins which exists in MnF_2 at temperatures below the Néel temperature 72°K as proposed by Erickson and Shull.[6]

The crystal structure of MnO resembles that of NaCl, and presents a face-centered cubic lattice of Mn ions. This can be separated into four inter-penetrating cubic sublattices of Mn ions, as shown in the top diagram of Fig. 3. Below the Néel temperature 122°K the spins are aligned alternately antiparallel on each sublattice, taken separately.[3] Consequently, each sublattice can be separated into two lattices of (+) and (−) spins, respectively, which are again f.c.c. but with a repeating distance of twice the length of the edge of a unit crystal cell. Magnetic Bragg reflections are indexed by Shull on the basis of these lattices of double size dimensions. The ion spins in Fig. 3 are directed along a crystal axis. They are parallel on alternate (1,1,1) planes and opposite on the intervening planes. This is the arrangement found by Shull, Strauser, and Wollan.[2]

[6] R. A. Erickson and C. G. Shull, Phys. Rev. **83**, 208 (1951).

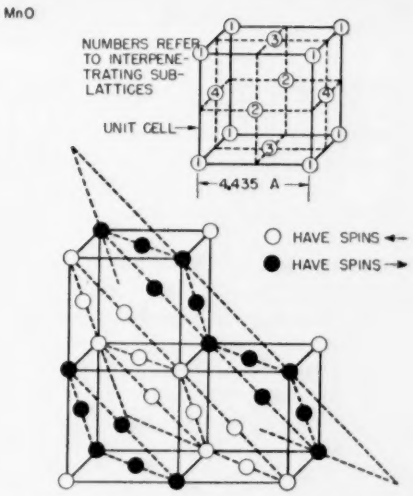

FIG. 3. The MnO face-centered cubic lattice structure. The lattice is similar to NaCl; oxygen atoms are not shown. Below T_0, Mn spins are opposite on alternate (1,1,1) planes.

Oxygen ions, not shown in Fig. 3, occur at the intersections of dashed lines with solid lines in the upper diagram, and in the center of the unit cell. Thus, each pair of adjacent Mn ions on one sublattice is separated by an oxygen ion, and ordinary quantum mechanical exchange cannot account for the antiparallel alignment of spins on the individual sublattices. The mechanism believed responsible for the spin arrangement was originated by Kramers and developed by Anderson[7] and Smart[8] for the case of f.c.c. compounds, and is called super-exchange. This involves assigning a weight in the total wave function to configurations in which a $2p$ electron from oxygen has transferred to a neighboring Mn ion. The other $2p$ electron on oxygen which has the same space wave function as the migratory electron then couples antiferromagneticly with the Mn ion directly opposite (the three ions involved are collinear). Van Vleck[9] indicates that the migratory electron goes into the $3d$ shell in Mn. Inasmuch as a paramagnetic electron is one which is not paired off with another electron having the same space wave function and opposite spin, the addition of an electron from oxygen reduces (for this excited state) the number of unpaired electrons in the Mn ion from 5 to 4. The expected reduction in magnetic scattering from Mn ions in MnO is discussed in Part VI.

IV. THEORY OF MAGNETIC SCATTERING

Halpern and Johnson[10] give the following expression for the differential cross section $d\sigma/d\omega$ for the magnetic scattering of neutrons from uncoupled paramagnetic

[7] P. W. Anderson, Phys. Rev. **79**, 350, 705 (1950).
[8] J. S. Smart, Phys. Rev. **86**, 968 (1952).
[9] J. H. Van Vleck, Lecture Notes for Grenoble Conference, 1950, unpublished.
[10] O. Halpern and M. H. Johnson, Phys. Rev. **55**, 898 (1939).

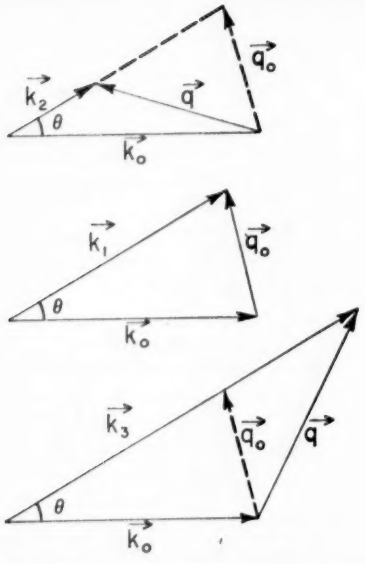

FIG. 4. Vector diagrams of neutron momentum change $\hbar\mathbf{q}$ when scattering is inelastic, elastic, and hyperelastic.

ions:

$$d\sigma/d\omega = \tfrac{2}{3}S(S+1)[e^2\gamma/mc^2]^2F. \qquad (1)$$

S is the spin of the ion, e is the charge on the electron, γ is the magnetic moment of the neutron in Bohr magnetons, m is the mass of the electron, and c is the velocity of light. F is the magnetic form factor, and is a function of the neutron momentum change. These authors derive an expression for the differential form factor F, assuming the charge distribution of the $3d$ electrons can be represented by a hydrogenic type wave function.

A theory of neutron scattering from systems of coupled ions which properly considers all the factors involved has not been developed. Halpern and Johnson indicate how the problem should be set up in a general fashion, and comment on the difficulty of evaluating the resulting expressions. Van Vleck[4] estimates the reduction in the paramagnetic scattering due to the inelastic nature of the collisions, and considers the following two processes:

(1) The total differential cross section for vanishingly weak coupling is obtained by employing sum theorems over all final states of the lattice. When the scattering is inelastic, a fraction of these final states will be energetically forbidden, since the energy changes involved are the order of magnitude of the neutron kinetic energy. The forbidden states would require the neutron to loose more than its full kinetic energy. The scattering will be reduced by the loss of these terms, and we refer to this effect as the "inelastic loss of transition states."

(2) For a given scattering angle θ, the value of the neutron momentum change $\hbar\mathbf{q}$ depends on the energy transfer, as indicated in Fig. 4. $\mathbf{k}_0$ is the incident neutron propagation vector. Three cases are illustrated: $|\mathbf{k}_1|=|\mathbf{k}_0|$ corresponds to elastic scattering for which $\mathbf{q}\equiv\mathbf{q}_0$. $|\mathbf{k}_2|<|\mathbf{k}_0|$ corresponds to an inelastic collision, where the neutron looses energy. $|\mathbf{k}_3|>|\mathbf{k}_0|$ corresponds to a hyperelastic collision, where the neutron gains energy. The importance of the diagrams is to note that $\mathbf{q}$ is always larger than $\mathbf{q}_0$ when there is appreciable energy transfer. Since the ionic form factor decreases with increasing $\mathbf{q}$, the observed cross section when the scattering is inelastic (dependent on some average value of $\mathbf{q}$) will be less than the cross section when the scattering is elastic (dependent on $\mathbf{q}_0$). We refer to this as the "inelastic effect on the form factor."

Van Vleck's paper is an important contribution to this subject; we should, however, note the limitations of his calculation. In order to estimate the effect of loss of transition states on the scattering cross section, it is necessary to assume a shape for the distribution curve of frequency of scattering events *versus* energy transfer and to calculate some parameter, such as the root mean square half-width of the distribution, designated W_{rms}. Van Vleck assumes the distribution curve is Gaussian, for which he gives justification. In order to use sum rules when calculating W_{rms}, he assigns equal *a priori* probability to all initial states of the system. This neglects the Boltzmann factor, and, consequently, his calculated value of W_{rms} is for the situation where the temperature T is much larger than the Néel temperature T_0.

It is easy to see that W_{rms} is expected to increase as the temperature is lowered toward T_0. For a simple lattice of ions such as the b.c.t. lattice of MnF_2, if only nearest neighbor interactions are considered, the energy of the spin lattice is given approximately by

$$H=\text{constant}-J\textstyle\sum_i\sum_j \mathbf{S}_i\cdot\mathbf{S}_j, \qquad (2)$$

where J is the Heisenberg exchange integral (a negative quantity in an antiferromagnetic compound like MnF_2), and $\mathbf{S}$ is the angular momentum of the Mn ion ($5/2\hbar$). The sum over i is over all ions in the lattice, and the

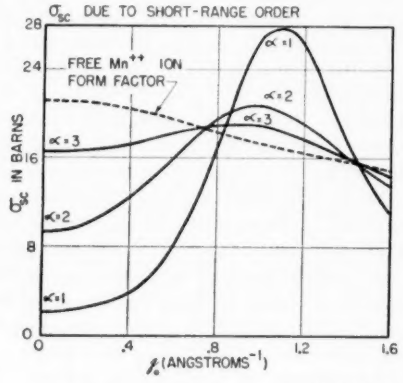

FIG. 5. Scattering cross-section curves obtained by superimposing short-range order scattering on the magnetic form factor.

sum over j is over the nearest neighbors of each ion i. The average value of $|\sum_j \mathbf{S}_j|$ of the neighboring spins of the ith ion is larger at lower temperatures, increasing from the high temperature value of approximately $Z^{\frac{1}{2}}|\mathbf{S}_j|$, where Z is the number of neighbors, to some value approaching $Z|\mathbf{S}_j|$, as T_0 is approached. Hence, the energy required to change the orientation of the ith spin in the field of its neighbors is larger at lower temperatures, and this corresponds to larger energy transfer W in an inelastic scattering event.

Probably the most serious deficiency in Van Vleck's theory is the neglect of residual coherence resulting from short-range order. Consider the equation for coherent scattering, where the scattering amplitude from the lth atom is A_l and we assume a $1/v$ detector:

$$\frac{d\sigma}{d\omega}=\frac{F}{N}\Big|\sum_l A_l e^{-i\mathbf{q}\cdot\mathbf{r}_l}\Big|^2-\frac{F}{N}\sum_l A_l^2,$$
$$\frac{d\sigma}{d\omega}=\frac{F}{N}\sum_l\sum_{l'\neq l} A_l A_{l'} e^{-i\mathbf{q}\cdot(\mathbf{r}_l-\mathbf{r}_{l'})}. \tag{3}$$

F is the form factor for a free ion, N is the number of ions in the crystal, and $\mathbf{r}_l$ is the position vector of the lth ion. For paramagnetic scattering, the essential features are obtained if we let $A_l=\pm A$. If there is correlation between the spins of the l and l' ions, one can write $\bar{A}_{l'}=g(\mathbf{w}_{ll'})A_l$. $\bar{A}_{l'}$ is the average value of $A_{l'}$ when the number of steps along the x, y, and z crystal axes separating the l and l' ions are given by the components of the vector $\mathbf{w}_{ll'}$, and where $g(\mathbf{w}_{ll'})$ is the correlation function.

After replacing $A_{l'}$ with $\bar{A}_{l'}$, we can sum over l in Eq. (3) to obtain

$$\frac{d\sigma}{d\omega}\approx FA^2\sum_{l'\neq l} g(\mathbf{w}_{ll'})e^{-i\mathbf{q}\cdot(\mathbf{r}_l-\mathbf{r}_{l'})}. \tag{4}$$

$\mathbf{r}_l$ is now any representative lattice position, not on the surface of the crystal. The sum over l' is over all ions except the lth ion. Equation (4) gives a liquid-type scattering pattern. In the present experiment, this effect causes a broad peaking of the scattering cross section curve for MnO in the region $|\mathbf{q}_0|\approx 1.23$ reciprocal angstroms and a depletion of the scattering for values of $|\mathbf{q}_0|$ less than 0.9 reciprocal angstroms. The peaking occurs around the location of the sharp magnetic Bragg reflection observed when the sample temperature is below T_0. The Bragg reflection is a result of long-range order, while the liquid-type peak results from local correlation of ion spin directions.

In order to estimate the range of spin order in the samples, we have calculated $d\sigma/d\omega$ from Eq. (4) for MnO, where alternate Mn ions on each sublattice tend to align themselves oppositely. We assumed the following form for the correlation function:

$$g(\mathbf{w}_{ll'})=(-1)^{a+b+c}e^{-\alpha(a+b+c)}. \tag{5}$$

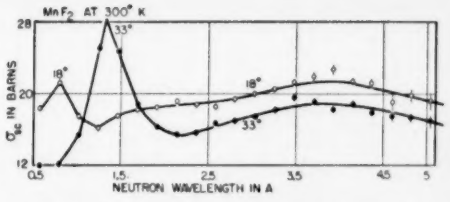

FIG. 6. Neutron scattering by MnF_2 at 300°K.

a, b, and c are the number of steps measured along the x, y, and z crystal axes which separate the two ions being considered. a, b, and c are always positive integers. α is a parameter indicating the range of order; $1/\alpha$ is the distance (in units of the crystal cell dimension 4.435 angstroms) in which the correlation drops to $1/e$. The factor $(-1)^{a+b+c}$ accounts for the alternate spin direction of ions on the sublattice.

The choice of the above function for $g(\mathbf{w}_{ll'})$ is arbitrary, but seems reasonable and allows the necessary integrations to be performed to calculate the cross-section curve. It is believed the shape of the cross-section curve is not sensitive to the exact form of $g(\mathbf{w}_{ll'})$. The curves obtained for three values of α, when the coherence is superimposed on the magnetic form factor, are shown in Fig. 5. For the values of α used in Fig. 5, practically no correlation exists between spin directions of ions separated by more than one step.

Slotnick[11] has treated the problem of coherent paramagnetic scattering, using a high temperature approximation. His results are carried to terms in $1/T^2$, and in a footnote, Slotnick observes that the rapid convergence of terms in inverse powers of T depends on the smallness of the ratio $|\Theta/T|$, where Θ is the temperature constant in the Weiss-Curie Law for the magnetic susceptibility $\chi=C/(T-\Theta)$. For MnO, Θ is -610°K, while our measurements were made at T equal to 300°K and lower. For this reason, our measurements cannot validly be compared with Slotnick's calculations.

Slotnick predicts that the maximum of the coherent scattering peak should be shifted at high temperature from the location of the antiferromagnetic Bragg reflection (determined by the spacing of next nearest neighbors). The shift is derived from nearest neighbor coupling, and the direction of the shift is to larger values of $\mathbf{q}_0$. In this experiment, we observe no shift in the location of the MnO peak. Coherent scattering by MnF_2 was observed only at 126°K, and the peak is too broad to locate the maximum.

V. RESULTS FOR MnF_2

On graphs of the experimental data, we have adopted the convention of plotting $4\pi(d\sigma/d\omega)$ and calling this quantity σ_{sc}. The total scattering cross section would equal σ_{sc} if the scattering were spherically symmetric with the same intensity as is observed in the direction of the counter tubes.

[11] M. Slotnick, Phys. Rev. **83**, 1226 (1951).

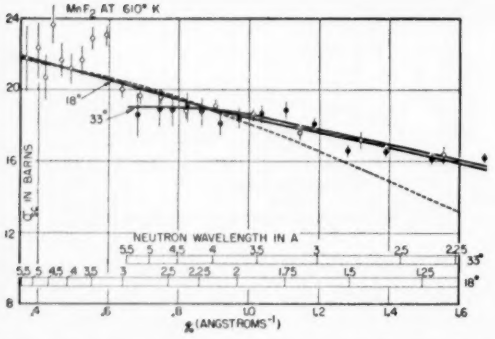

FIG. 7. Neutron scattering by MnF_2 at 610°K. The dashed line is the free ion magnetic scattering cross section calculated using expressions by Halpern and Johnson (reference 10).

Figure 6 shows the scattering data obtained from MnF_2 at 300°K as a function of neutron wavelength, and at the two angles 18° and 33°. These curves are typical of the experimental data. The large peak on the left end of each curve is the last nuclear Debye-Scherrer ring; all the other Debye-Scherrer rings come at shorter neutron wavelengths at these angles. The main contribution to the fairly smooth curves to the right of the peaks is from paramagnetic scattering, with about 1 barn contributed by nuclear incoherent and multiple scattering.

The width of the Debye-Scherrer peaks would be expected to be quite narrow if resolution broadening were absent. The time-of-flight resolution function is roughly triangular with a width at the base of between two and three times the wavelength spacing between adjacent points. In addition, these peaks are further broadened by the angular width of the rings of counter tubes. The angular width is about 4° on either side of the mean scattering angle for half-maximum detection efficiency. Since the paramagnetic scattering is generally a slowly varying function of wavelength, most of the curves are not appreciably distorted by resolution effects.

In order to study the effects of coupling between the Mn ions, the experimental data for MnF_2 at 610°, 300°, and 126°K has been plotted in Figs. 7–9 as a function of q_0, which is $1/h$ times the magnitude of the neutron momentum change for elastic scattering. It may be noted that $q_0=|\mathbf{q}_0|=2|\mathbf{k}_0|\sin(\theta/2)$, where θ is the scattering angle. $\mathbf{k}_0$ is the propagation vector of the incident neutrons, and its magnitude is 2π divided by the wavelength; hence the units of q_0 are reciprocal angstroms. On Figs. 7, 8, and 9 the positions of the experimental points are reversed left for right relative to Fig. 6. Only the part of the curve where paramagnetic scattering can be studied is shown (the nuclear Debye-Scherrer peaks are off the figures to the right). Wavelength scales for each angle are given at the bottom of the figures. For a given angle, neutron energy increases from left to right (the neutron energy E in electron volts is related to the wavelength λ in angstroms by the expression $E=0.0818/\lambda^2$).

On the plots as a function of q_0, the magnetic form factor should be the same for the two angles. The separation between the 18° and 33° curves is caused by inelastic scattering, which is different at the two angles, inasmuch as neutrons at 33° have only 0.3 the energy of neutrons at 18° for the same q_0.

The differential cross section for magnetic scattering calculated from Eq. (1), using an expression for the magnetic form factor F derived by Halpern and Johnson,[10] is shown on Fig. 7 as a dashed line.[12] In calculating F, the mean radius for the $3d$ electron probability function was taken to be 0.64 angstroms, the value determined by Ruderman.[1] Except for three points at small values of q_0, which are probably raised due to nuclear coherent scattering into the plane of the sample (see Part II), the experimental data at 18° agrees well with the dashed line in the region $q_0<0.9$. The 18° curve is essentially unaffected by coupling between ions, which is very small at this temperature (610°K). Thus the 18° curve in Fig. 7 is considered to be an experimental determination of the magnetic scattering from free ions. The agreement of experimental points with the dashed line for values of $q_0<0.9$ confirms the derivation by Halpern and Johnson of Eq. (1).

It is seen that the experimental curves lie above the dashed line for $q_0>0.9$. This indicates the radial distribution of the $3d$ electrons in Mn ions decreases faster at large radii than the free ion wave functions used by Halpern and Johnson. Shull[2] has mentioned that this compression of the wave functions may be the result of neighboring ions in the crystal lattice.

In Figs. 7–9 it is seen that the 33° curve drops below the 18° curve for $q_0<0.9$. This separation is attributed to the two inelastic processes described by Van Vleck (see Part IV). It is of interest to evaluate the half-width W_{rms}, the parameter indicating the amount of energy exchanged in inelastic collisions, using Van Vleck's assumption of a Gaussian distribution of frequency of scattering events *versus* energy transfer. This is done by assuming the fraction of the cross section at 18° which is included in the separation between the curves

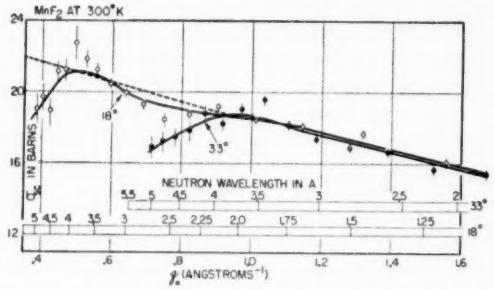

FIG. 8. Neutron scattering by MnF_2 at 300°K.

[12] The dashed line has been raised by one barn for comparison with experimental points.

equals the loss of scattering due to inelastic processes at the lower energy (33° curve). The energies for points at corresponding values of q_0 on the 18° curve are so high that they have essentially no loss of scattering. We then assume some part of this separation (for example, $\frac{3}{4}$ of the separation) is derived from the loss of transition states. This loss is that portion of a Gaussian distribution which extends to one side of the mid-point a distance greater than the incident neutron energy. From the loss of states and the incident neutron energy, the half-width of the distribution is found using tables of the Standard Error Function. The loss produced by the inelastic effect on the form factor is then calculated, making use of this tentative value of W_{rms}. If the sum of these effects does not give the observed separation between the curves, the calculation is repeated assuming a slightly different value for the loss of transition states.

For the 610°K data, the four lowest energy points (smallest values of q_0) on the 33° curve give W_{rms} equal to 0.00196, 0.00195, 0.00203, and 0.00196 ev.[13] These are in good agreement with each other and give an average for W_{rms} equal to about 0.0020 ev. On the average, the loss of transition states accounts for 80 percent of the separation between curves.

On Fig. 8, at 300°K, the four lowest energy points on the 33° curve correspond to W_{rms} equal to 0.00267, 0.00264, 0.00265, and 0.00261 ev. These values also show internal agreement and average about 0.0026 ev, which is markedly larger than the value for 610°K. The loss of transition states accounts for 73 percent of the separation between curves.

For 126°K, inspection of Fig. 9 shows that the low energy points at 33° do not form a smooth curve (the irregularity may be accounted for by statistical fluctuations). The values indicated by the seven lowest energy points are 0.00335, 0.00357, 0.00405, 0.00401, 0.00288, 0.00277, and 0.00303 ev. An average value for W_{rms} of about 0.0034 ev is indicated. The loss of transition states accounts for 74 percent of the separation between curves. The experiment confirms that W_{rms} increases as the temperature is lowered, as discussed in Part IV. The experimental values agree in order of magnitude with the value of W_{rms} calculated using Van Vleck's formulas,[4] which give, for $T \gg T_0$, $W_{\text{rms}} = 0.00285$ ev.

Mention should be made of how the above results compare with those found by Shull, Strausser, and Wollan.[2] They found no change in scattering data when they raised the temperature of their MnF_2 sample from room temperature to 400°C. This can be explained by the comparatively high energy of their neutrons, which had a wavelength of 1.057 angstroms. At wavelengths shorter than 2 angstroms, we observe no change between 300° and 610°K. Our measurements are sensitive to inelastic effects only because they are extended to include very low energy neutrons. Shull and his coworkers also mention that their MnF_2 curve falls 10 percent below the basic cross section in the forward direction of $21.2/4\pi$ barns/steradian calculated by Halpern and Johnson using Eq. (1). While there is an uncertainty of about one barn in our measurements, we appear to observe (in Fig. 7) the full value of 21.2 barns.

[13] The experimental values of W_{rms} were computed using the experimental points for 33° and the smooth curve drawn for 18°.

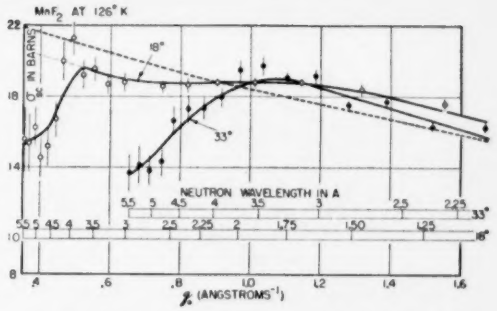

FIG. 9. Neutron scattering by MnF_2 at 126°K.

The magnetic scattering curve obtained at a scattering angle of 18° and temperature of 610°K has been drawn on Figs. 8 through 11 as a dashed line for reference purposes. An additional effect connected with the loss of scattering produced by inelastic processes may be noted on Figs. 8 and 9. By referring to the wavelength scales on these figures, points having the same wavelength, and hence the same neutron energy, may be identified on the curves at the two angles. We note the fractional separation between the curves at a particular wavelength for the 33° curve, and we add this as a correction to the 18° curve on the same figure, at the corresponding wavelength for 18°. This correction is made between 4 and 5.5 angstroms. The result of applying this correction to the data for 300°K is to bring the 18° curve up to the dashed line representing the free ion magnetic scattering curve. Apparently, inelastic scattering reduces the neutron scattering at the two angles by the same amount at corresponding neutron energies.

The consequence of applying the above correction to Fig. 9, showing data taken at 126°K, is to raise the 18° points to give a smooth curve, lying perhaps 1.5 barns below the free ion magnetic scattering curve, in the region $q_0 < 0.6$. The 18° curve, which rises above the free ion curve for $q_0 > 1.0$, then resembles the curves shown in Fig. 5. The curves in Fig. 5 were calculated to illustrate the effect of residual coherent scattering resulting from correlation of the spin directions of neighboring ions in the crystal lattice. The correction we have made is for inelastic scattering and allows the short-range order scattering to appear. An estimated value for the short-range order parameter α for MnF_2 at 126°K is about 4. Short-range order scattering is not detected in the curves at higher temperatures.

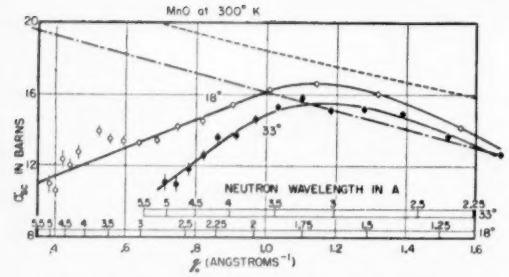

FIG. 10. Neutron scattering by MnO at 300°K.

The results obtained for MnF_2 are summarized as follows:

(1) At a scattering angle of 18° and a temperature of 610°K, the neutron scattering is essentially from uncoupled Mn ions, and the differential cross section for magnetic scattering from free ions is observed. The cross section at small values of q_0 confirms the derivation of the paramagnetic scattering by Halpern and Johnson. The shape and height of the curve for large values of q_0 show the $3d$ electron distribution in Mn^{++} decreases faster for large radii than the hydrogenic wave functions used by Halpern and Johnson.

(2) The separation between the curves at 18° and 33° plotted as a function of q_0 is attributed to inelastic scattering processes at the 33° angle, where the neutron energy is lower. Assuming a Gaussian distribution for energy transfer to the spin lattice, W_{rms} increases with decrease in sample temperature as follows:

Temperature:	610°K	300°K	126°K
W_{rms}:	0.0020 ev	0.0026 ev	0.0034 ev

(3) At 300°K and 126°K, inelastic scattering appears to reduce the scattering at the two angles by the same amount at corresponding neutron energies.

(4) Residual coherent scattering due to short-range order is not observed at 610° or at 300°K, but affects the scattering to the extent of 1.5 barns at 126°K.

VI. RESULTS FOR MnO

The cross section data at the temperatures 300° and 133°K are plotted as a function of q_0 in Figs. 10 and 11. The shape of the 18° curve at 300°K indicates it has been distorted by short-range order scattering. Shull, Strauser, and Wollan[2] also observe short-range order scattering by MnO at room temperature. As nearly as we can tell from their Fig. 1, the location and maximum of their peak are the same as we observe. The maximum cross section, when multiplied by 4π steradians, is about 15.6 barns. At the location of the maximum, their value of the cross section for MnF_2 (determined by the free ion magnetic scattering) is about 13.6 barns, while we observe 16.6 barns (the MnF_2 magnetic scattering curve is drawn as a line of short dashes in Figs. 10 and 11).[14] Therefore, while the MnO peak rises above their free ion magnetic scattering curve (as it should, due to short-range order scattering) by about 2 barns, it lies below our free ion magnetic scattering curve by about 1 barn.

We believe our curve for magnetic scattering from free ions is correct and propose an explanation for our results. The explanation is that the cross section for magnetic scattering [Eq. (1)] may be lower for MnO, as a result of the mechanism of super-exchange. As discussed in Part III, the total wave function of the Mn ion in MnO is believed to include excited states in which the number of paramagnetic electrons is reduced from 5 to 4. Referring to Eq. (1), the magnetic scattering cross section depends on $S(S+1)$, where S is the (spin) angular momentum of the Mn ion in units of $\hbar$, and therefore depends on the number of paramagnetic electrons in the ion. The situation is very complex; but, taking the simplest possible view, we conclude that if the excited state involved in super-exchange was occupied all of the time, the smaller value of $S(S+1)$ could reduce the magnetic scattering from Mn to 24/35 of its free ion value. From the shape of the 18° curve in Fig. 10, we roughly estimate that in the region of the peak, the magnetic scattering curve should lie about 1.5 barns below the peak of this curve, and thus about 2.5 barns below the magnetic scattering curve for MnF_2. A line of long dashes representing this estimate has been drawn on the figures. This reduction in magnetic scattering corresponds to occupation of the excited state about 45 percent of the time.

One would like to evaluate W_{rms} for MnO by an analysis of the separation between the 18° and 33° curves, as was done for MnF_2. This cannot be done reliably because the MnO curves are displaced by large short-range order scattering, in addition to the inelastic effects with which we would identify the separation.

The experimental curves in Figs. 10 and 11 show the peaking in the region $q_0 \approx 1.2$ increases as the temperature is lowered. The value of the cross section for $q_0 < 1.0$ is lower at the lower temperature. The depletion of the 18° curve at small values of q_0 may be a result both of larger short-range order scattering effects and of greater inelastic effects at the lower temperature.

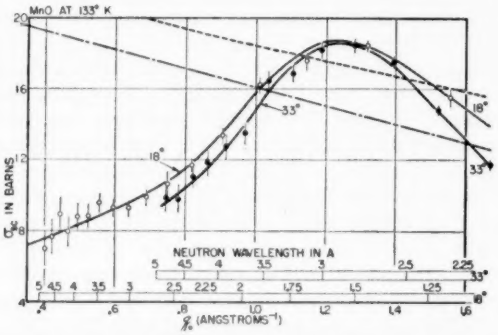

FIG. 11. Neutron scattering by MnO at 133°K.

[14] The dashed lines are raised one barn to account for nuclear incoherent and multiple scattering.

The range of spin order at 300°K and 133°K was estimated by comparing the shape of the experimental curves at 18° with the shape of the calculated curves shown in Fig. 5. In order to make the comparison, it was estimated very roughly that inelastic effects account for one-half the separation between the experimental curves and the line drawn with long dashes, in the region $q_0 < 1.0$. From the shape of the experimental curves, we estimate rough values of α to be 3 and 2, at 300° and 133°K, respectively. The amount of order is seen to increase with decreasing temperature. However, these values of α are sufficiently large to indicate that most of the correlation of spin direction exists only between adjacent ions on the same sublattice. As long-range ordering is expected below the Néel temperature, a large change in ordering apparently takes place close to the Néel temperature.

Figure 12 shows data taken at 107°K, 15° below the Néel temperature, plotted as a function of neutron wavelength λ. The peaks furthest to the left, occurring at λ equals 0.8 and 1.4 angstroms for 18° and 33°, respectively, result from nuclear Debye-Scherrer reflection from (1,1,1) planes. The two larger peaks, occurring at λ equals 1.6 and 2.8 angstroms for 18° and 33°, respectively, are produced by the magnetic Debye-Scherrer reflection from (1,1,1) planes on a double-spaced lattice. These peaks, previously observed by Shull and Smart,[15] result from long-range antiferromagnetic order of the crystal spins. They occur at $q_0 = 1.23$. The nuclear and magnetic peaks on the 18° curve are not fully resolved.

Owing to the long-range spin order below T_0, coherent effects predominate in Fig. 12. The magnetic form factor has disappeared, and the magnetic scattering is concentrated almost entirely in crystal reflections. For the 33° curve, we have compared the area under the magnetic peak with the area under the nuclear peak, and we find that the total "scattering power" of the magnetic Debye-Scherrer ring is consistant with long-range order and a unit cell of sides 8.870 angstroms. It is not possible to tell if the four sublattices are scattering coherently or independently, for theoretically the area under the Debye-Scherrer ring is the same in either case.

[15] C. G. Shull and J. S. Smart, Phys. Rev. **76**, 1256 (1949).

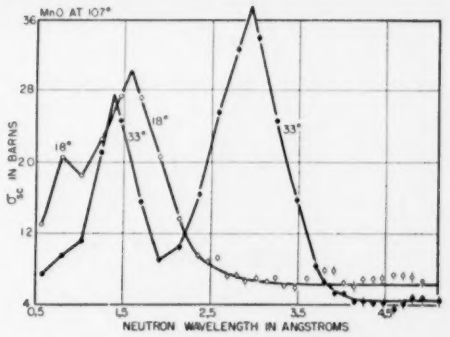

FIG. 12. Neutron scattering by MnO at 107°K.

The results for MnO are summarized as follows:

(1) The curves at 300°K indicate the magnetic scattering cross section for MnO, if it were not distorted by short-range order scattering, would be about 2.5 barns smaller than for MnF_2. We suggest this can be accounted for by the mechanism of super-exchange.

(2) Comparison of the shape of the experimental curves with calculated curves indicates values of the short-range order parameter α to be 3 and 2, at temperatures of 300° and 133°K, respectively. The amount of spin order is found to increase with decrease in temperature, but most of the correlation of spin direction exists only between adjacent ions on the same sublattice. This indicates a large change in ordering takes place near the Néel temperature.

(3) The (1,1,1) magnetic Debye-Scherrer reflection from a double-spaced lattice is observed at 107°K. This confirms long-range antiferromagnetic ordering exists below T_0.

The author wishes to express his appreciation to Professors L. James Rainwater and W. W. Havens, Jr., for real assistance they rendered to all phases of the research. He is also grateful to Dr. I. W. Ruderman for preparing the samples, and to Dr. Murray Slotnick for helpful discussions on the interpretation of results. The assistance of Janet E. Bendt, and of persons working on the cyclotron staff, is gratefully acknowledged.

The author thanks the U. S. Atomic Energy Commission for its support of this research. He is also indebted to the Vanadium Corporation of America for the loan of a pure vanadium sample.

Genetics of the Ge^{78}–As^{78} Fission Chain*

NATHAN SUGARMAN†
Los Alamos Scientific Laboratory, University of California, Los Alamos, New Mexico
(Received October 15, 1952)

The half-life of Ge^{78}, measured by isolation of the (91.0±0.6)-min As^{78}, is (86.0±1.0) min. No evidence for the ~40-min As reported in fission was found. The fission yields of Ge^{77}, As^{77}, Ge^{78}, and As^{78} are reported.

1. INTRODUCTION

IN the work described here, the genetics of the mass 78 fission chain have been re-examined, and some uncertainties presumably removed. Steinberg and Engelkemeir[1] reported a genetic relationship between a 2.1-hr Ge and a 90-min As from the slow neutron fission of uranium. They assigned this chain to mass 78 because of fission-yield considerations (0.02 percent fission yield), and the similarity between the characteristics of the 90-min As found in fission and the 80-min As^{78} produced by the (n,α) reaction on bromine.[2] Earlier, Snell[3] and Sagane and co-workers[4] had reported a half-life of 65 min for As^{78} from the (n,α) reaction. Recent work by Brightsen *et al.*[5] showed that the half-life for As^{78} from the $Br^{81}(n,\alpha)As^{78}$ reaction is 90 min by the chemical isolation of radioarsenic from bromine irradiated with fast neutrons. Brightsen and co-workers also found an arsenic activity of ~40-min half-life in fission, which they tentatively assigned to an isomeric state of the 90-min As^{78}.

In the present study it is shown that the fission chain of mass 78 is as follows:

$$(86.0\pm1.0)\text{-min } Ge^{78}\rightarrow(91.0\pm0.6)\text{-min } As^{78}\rightarrow Se^{78}.$$

No evidence for the ~40-min As was found in this work.

2. EXPERIMENTAL WORK

Two thermal-neutron irradiations of uranium salts were made in the Los Alamos Homogeneous Reactor. In the first experiment, uranyl chloride was irradiated for 10 min, and it was found that the arsenic activity isolated from separated germanium samples contained only 91-min and 38-hr half-lives, as expected for fission arsenic. However, the arsenic activity isolated directly from the irradiated material contained substantial activity of As^{76}, as well as fission arsenic, which indicated the presence of arsenic impurity in the UO_2Cl_2. Because of the contamination of some of the arsenic samples by As^{76}, it was not possible to make as complete an analysis of the data of this experiment as was done in the second experiment. In the latter case, uranyl nitrate, prepared from uranium enriched in U^{235}, was irradiated for 10 min, and all of the arsenic samples showed only the 91-min and 38-hr arsenic half-lives.

Germanium and arsenic samples were isolated from the irradiated material by procedures similar to those of Winsberg.[6] Carrier amounts of germanium and arsenic were added to an aliquot of the irradiated salt dissolved in 3*M* HCl. Arsenic was separated from this solution by first distilling $GeCl_4$ in the presence of Cl_2, adding more HCl and distilling again in order to ensure the absence of germanium in the residue. Arsenic was then separated by two distillations of $AsCl_3$ after the addition of CuCl to reduce As(V) to As(III). The carrier was precipitated as arsenic by the addition of $CrCl_2$ solution (Oxsorbent) to the $AsCl_3$ distillate.[7] The time of germanium removal from the arsenic was taken as the midpoint of the first germanium distillation which lasted about 10 min. The timing data on this sample, as well as those of the other arsenic samples, are given in Table I.

Arsenic was also separated from the germanium distilled from the original solution after allowing for an appropriate growth time of radioarsenic from the germanium activity. The $GeCl_4$ distillate removed in the analysis for arsenic in the original solution was redistilled. A precipitation of GeS_2 was made; the precipitate was dissolved in NH_4OH; a scavenging precipitation of $Zr(OH)_4$ was made, and GeS_2 was reprecipitated in the presence of NH_4I to aid in the precipitation of radioarsenic (V). The GeS_2 sample was weighed and set aside for growth of arsenic activity. The time of start of growth of arsenic was taken as the mid-point of the second germanium distillation since the subsequent operations were made in such a way as to ensure the carrying of radioarsenic by germanium. About 90 min later, arsenic carrier was added to the GeS_2 sample dissolved in NH_4OH, germanium was separated twice by distillation, and arsenic was then distilled and precipitated. This arsenic sample con-

* Performed under the auspices of the AEC during the summer of 1951 when the author was a consultant to the Los Alamos Scientific Laboratory.

† Institute for Nuclear Studies, University of Chicago, Chicago, Illinois.

[1] E. P. Steinberg and D. W. Engelkemeir, *Radiochemical Studies: The Fission Products* (McGraw-Hill Book Company, Inc., New York, 1951), Paper No. 54, National Nuclear Energy Series, Plutonium Project Record, Vol. 9, Div. IV.

[2] B. R. Curtis and J. M. Cork, Phys. Rev. **53**, 681 (1938).

[3] A. H. Snell, Phys. Rev. **52**, 1007 (1937).

[4] Sagane, Kojima, and Miyamoto, reported by G. T. Seaborg and I. Perlman, Revs. Modern Phys. **20**, 585 (1948).

[5] Brightsen, Shure, Fisher, and Coryell, Phys. Rev. **81**, 298 (1951).

[6] L. Winsberg, Paper 228 of reference 1.

[7] This procedure for the precipitation of arsenic, rather than that of the sulfide as given in reference 6, was recommended by Dr. J. W. Barnes of the Los Alamos Scientific Laboratory.

TABLE I. Activity data of arsenic samples.

Experiment	Sample	Separation time, min from end of irradiation	Growth time for arsenic, min	Activity of 91-min As^{78} at separation time, counts/min	Chemical yield	Activity corr. for chem. yield, counts/min	Aliquot, ml	Activity corr. per ml, counts/min	$A^0_{Ge^{78}}$/ml, counts/min	$A^0_{Ge^{78}}$/ml corr. for indep. As^{78}, counts/min
1	Aliquot 1, As	48	48	~215 000[a]	0.544	~396 000[a]	2	~198 000[a]	~7.95×10^5[a]	4.75×10^5
	Aliquot 2, As	323	323	228 000	0.466	490 000	5	98 000	4.96×10^5	
	Aliquot 1, Ge–As[b]	161[c]	101	107 000	0.541[d]	198 000	2	99 000	4.71×10^5	4.71×10^5
	Aliquot 2, Ge–As[b]	443[c]	92	30 200	0.627[d]	48 300	5	9660		
2	Aliquot 1, As	40	40	240 000	0.750	320 000	2	160 000	7.30×10^5	4.97×10^5
	Aliquot 2, As	245	245	1 020 000	0.690	1 478 000	10	147 800	5.36×10^5	
	Aliquot 1, Ge–As[b]	151.5[c]	92	128 000	0.606[d]	211 200	2	105 600	5.00×10^5	5.00×10^5
	Aliquot 2, Ge–As[b]	363[c]	90.5	98 000	0.520[d]	188 300	10	18 830		

Experiment	Sample	Separation time, min from end of irradiation	Growth time for arsenic, min	Activity of 38-hr As^{77} at separation time, counts/min	Chemical yield	Activity corr. for chem. yield, counts/min	Aliquot, ml	Activity corr. per ml, counts/min	$A^0_{12\text{-hr }Ge^{77}}$/ml, counts/min	$A^0_{38\text{-hr }As^{77}}$/ml (indep. of 12-hr Ge^{77}), counts/min
1	Aliquot 1, As	48	48	e						
	Aliquot 2, As	323	323	e						
	Aliquot 1, Ge–As[b]	161[c]	101	162	0.541[d]	300	2	150	5280 / 5350 → 5315	
	Aliquot 2, Ge–As[b]	443[c]	92	330	0.627[d]	528	5	105.6		
2	Aliquot 1, As	40	40	5550	0.750	7400	2	3700	(8465)[f]	3650
	Aliquot 2, As	245	245	27 100	0.690	39 280	10	3928		
	Aliquot 1, Ge–As[b]	151.5[c]	92	190	0.606[d]	314	2	157	6300 / 6600 → 6450	
	Aliquot 2, Ge–As[b]	363[c]	90.5	680	0.520[d]	1305	10	131		

[a] Activity uncertain because of presence of contaminating impurities in decay curve.
[b] Arsenic samples separated from previously isolated germanium.
[c] End of growth period of arsenic.
[d] Combined chemical yields of GeS_2 and As precipitates.
[e] Activity undetermined because of contamination by 26-hr As^{76}.
[f] Uncertain value arising from small difference of two large numbers.

tained activity descended from germanium radioactivity following the redistillation of germanium from the original solution (called "the time of start of growth" earlier).

Several hours later, another aliquot of the original irradiated solution was treated in the same way, namely, two arsenic samples were obtained, one from the original solution, the other from previously separated germanium set aside for arsenic growth. In all, there were four arsenic samples from each experiment.

Activity measurements were made using a methane-flow proportional counter with an aluminum window of 4.8 mg/cm² thickness.

3. RESULTS

The following information was obtained from activity measurements on the arsenic samples: (1) half-lives of the two arsenic species present, As^{77} and As^{78}, (2) half-life of the Ge^{78} parent of As^{78}, and (3) fission yields of the germanium and arsenic nuclides by comparison of their saturation activities with that of La^{140} grown into isolated barium samples.

In Fig. 1 are plotted the decay curves of the two arsenic samples from the first aliquot of the second experiment. Two activities are evident, a 91-min component identified as As^{78}, and a 38-hr component identified as As^{77}. Decay curve (A) is that of the arsenic isolated from the irradiated material, and (B) is that of the arsenic isolated from previously separated germanium. In each case, the curve was analyzed by subtracting the activity of 38-hr As^{77} from the total decay curve, as determined from later counting data not shown on the curve. The average half-life of As^{78} determined in this way is 91.0±0.6 min, and that of As^{77}, 38.0±0.5 hr.

The half-life of the Ge^{78} parent of 91-min As^{78} was determined from the activity data of the arsenic samples separated from previously isolated germanium from the two aliquots of each experiment. These data are given in Table I, where the samples are listed as "Aliquot 1 or 2, Ge–As." Analysis of the data of aliquots 1 and 2 yields both the half-life of Ge^{78} and the activity of Ge^{78} at the end of the irradiation, $A^0_{Ge^{78}}$. The half-life of Ge^{78} thus found in the two experiments is 86.5 min and 85.3 min. The half-live value accepted is 86.0±1.0 min, if account is taken both of the spread of the data and possible systematic errors. It is seen from Table I that the $A^0_{Ge^{78}}$ calculated from the Ge–As samples agrees with that calculated from the As samples, if a correction is made for some independent yield of As^{78} (discussed later). This result, and the fact that the half-life of the Ge^{77} parent of 38-hr As^{77}, as calculated from the activity of the same Ge–As samples, 12.4 hr in the first experiment and 13.4 hr in the second experiment, is in good agreement with the published value of 12 hr,[1,8] lend confidence to the value of 86 min found for Ge^{78}. The previously reported value for the half-life of Ge^{78} of 2.1 hr (126 min),[1] as determined directly on a sample of germanium in which arsenic activity was growing, is probably in error because of the difficulty in determining the parent half-life in a mixed sample when the parent and daughter

[8] J. R. Arnold and N. Sugarman, J. Chem. Phys. **15**, 703 (1947).

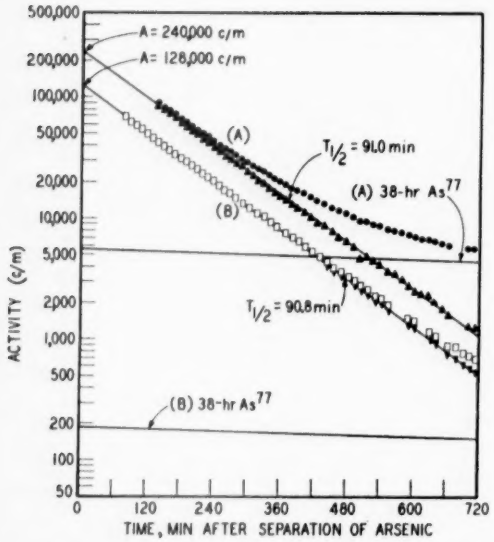

FIG. 1. Decay curves of arsenic samples from first aliquot of second experiment. (A) Arsenic isolated from irradiated material (listed as Aliquot 1, As in Table I). ●, original points; ▲, 38-hr As^{77} activity determined from later decay data subtracted from original points. (B) Arsenic isolated from previously separated germanium (listed as Aliquot 1, Ge−As in Table I). □, original points; ▼, 38-hr As^{77} activity determined from later decay data subtracted from original points.

have very nearly the same half-life. The half-life data are summarized in Table II.

The fission yields of Ge^{77} and As^{77}, as reported in Table III, measured via the As^{77} activity, are lower than those previously reported.[1,9] In this work the fission yields were determined by the following procedure. The samples were mounted on aluminum plates, covered with rubber hydrochloride, and positioned about 1 mm from the aluminum window of the counter. No absorption corrections for the counter window and sample covering were made for the As^{78}, but for As^{77} and La^{140} corrections of ~13 and 5 percent, respectively, were applied. The back- and self-scattering corrections of As^{78} and La^{140} were taken as equal,[10] whereas that of As^{77} was assumed to be about 15 percent lower[11] because of the relatively weak β-ray (0.7 Mev), and the relatively heavy sample (~20 mg/cm²). In effect, then, the saturation activity calculated from the observed activity of As^{78} was not corrected, that of La^{140} was raised 5 percent, and that of As^{77} ~28 percent. Although it is difficult to estimate the accuracy of the yields determined in this manner, they are probably as accurate as previously reported values.

One interesting feature that appeared in both experiments is an apparent independent yield for As^{78} of about 10 percent of the chain yield. The error in this yield in Table III is that calculated by assigning exaggerated timing errors to the separations of the arsenic. Another possible explanation for this apparent independent yield is that it represents a high point on the calculated decay curve of Ge^{78} as determined from the data of the half-life measurements. The major difficulty in this explanation is that the $A^0_{Ge^{78}}$ calculated from the As data of Table I is about 50 percent higher than that calculated from the Ge−As data.

TABLE II. Half-lives of germanium and arsenic nuclides.

Nuclide	Nuclide counted	Half-life observed	Half-life reported previously[a]
As^{77}	As^{77}	38.0±0.5 hr	38 hr[b]
Ge^{78}	As^{78}	86.0±1.0 min	126 min (2.1 hr)
As^{78}	As^{78}	91.0±0.6 min	90 min

[a] See reference 1 and Appendix C, *Radiochemical Studies: The Fission Products* (McGraw-Hill Book Company, Inc., New York, 1951), National Nuclear Energy Series, Plutonium Project Record, Vol. 9, Div. IV.
[b] A. Turkevich and J. B. Niday, Phys. Rev. **84**, 52 (1951).

[9] Appendix B, *Radiochemical Studies: The Fission Products* (McGraw-Hill Book Company, Inc., New York, 1951), National Nuclear Energy Series, Plutonium Project Record; Vol. 9, Div. IV.
[10] Engelkemeir, Seiler, Steinberg, and Winsberg, Paper 4 of reference 1. Engelkemeir, Seiler, Steinberg, Winsberg, and Novey, Paper 5 of reference 1.

TABLE III. Fission yields of germanium and arsenic nuclides.

Nuclide	Nuclide counted	Fission yield observed, %	Fission yield reported previously[a] %
12-hr Ge^{77}	38-hr As^{77}	2.3×10^{-3}	3.7×10^{-3}
38-hr As^{77}	38-hr As^{77}	6.7×10^{-3}	9.1×10^{-3}
86-min Ge^{78}	91-min As^{78}	1.8×10^{-2}	2.0×10^{-2}[b]
91-min As^{78} (indep.)	91-min As^{78}	$(1.8\pm0.6)\times10^{-3}$	
91-min As^{78} (total)	91-min As^{78}	2.0×10^{-2}	2.0×10^{-2}[b]
12.8-day Ba^{140}	40-hr La^{140}	6.17[c]	6.17

[a] See references 1 and 9.
[b] Fission yield calculated with 2.1-hr half-life for Ge^{78}.
[c] Assumed for fission yield calculations.

As seen in Fig. 1, the decay curves of the arsenic samples separated either from germanium (Ge−As), or directly from the irradiated material (As), showed only two fission-product activities, 91-min As^{78} and 38-hr As^{77}. No evidence for the ~40-min As reported[5] as present in fission was found. The maximum fission yield for a 40-min As determined in these experiments is 10 percent of the yield of 91-min As^{78}, whether the 40-min As is descended from 86-min Ge^{78} and is thus isomeric with 91-min As^{78}, or from a short-lived germanium parent. In the case of the data of the decay curves of Fig. 1, this limiting yield was calculated on the assumption that an activity of 6000 counts/min would have been evident at the start of counting above the 91-min As^{78} decay curves.

It is a pleasure to acknowledge the cooperation and assistance of Dr. Roderick Spence, Mr. James Sattizahn, Mrs. Pearl Neal, Mrs. Phyllis Phillips, and Mrs. Lillian Jones.

[11] W. E. Nervick and P. C. Stevenson, Nucleonics **10**, No. 3, 18 (1952).

The Isomer Rb^{84m}†

R. S. Caird and Allan C. G. Mitchell
Department of Physics, Indiana Univeristy, Bloomington, Indiana
(Received October 6, 1952)

With the help of scintillation counters information on the isomer Rb^{84m} has been obtained. The isomer was produced by an $(n,2n)$ bombardment of ordinary Rb salts. The half-life has been determined as 21 min. Three gamma-rays have been observed at 0.239, 0.463, and 0.890 Mev. The last gamma-ray occurs in the product Kr^{84}. Coincidence measurements show coincidences between the gamma-ray at 0.239 Mev and another of nearly the same energy, while coincidences between the 0.463 and the gamma-rays at 0.239 Mev are essentially negligible. A possible level scheme is discussed.

FLAMMERSFELD[1] has recently discovered an isomer of Rb^{84} which has a half-life of 23 min. The isomer was prepared by bombarding rubidium salts with fast neutrons from a Li+D reaction. In his experiments Rb^{88}(17.5 min) was always present to some extent. The experiment showed that there is a metastable state which emits internal conversion electrons of energy about 0.32 Mev, which would correspond to a gamma-ray energy of 0.335 Mev. Since experiments on the long-lived Rb^{84}(34 days) were in progress in this laboratory,[2] the present experiments were undertaken to obtain more information on the isomeric state.

The following experiments were performed with a scintillation spectrometer equipped with a differential pulse-height analyzer. $RbNO_3$, placed in a cadmium container, was bombarded with Li+D neutrons from the cyclotron. The results, Fig. 1, show two gamma-rays having energies of 0.239 Mev (discriminator setting 14) and 0.463 Mev (discriminator setting 28). The half-life of both lines was 21 min. $RbNO_3$ bombarded with Be+D neutrons slowed down in paraffin gave the same peaks, but of much weaker intensity, superimposed on a high background from the 17.5-min Rb^{88}. In order to be sure that the activity was not produced by the nitrate ion, NH_4NO_3 was bombarded with Li+D neutrons. In this case only annihilation radiation having a half-life of 11 min was seen. Finally, in order to test the purity of the rubidium, active Rb^{84}(34 days) was added to the Rb salts and these were passed through an ion exchange column. The resultant purified rubidium salts were bombarded both as RbCl and $RbNO_3$ with fast neutrons. In both cases the line at 0.239 Mev was seen to decay with a 21-min half-life. Annihilation radiation from the long-lived Rb^{84} was also present. After allowing the short-lived radiations to die out and correcting for the annihilation radiation from the Rb^{84}, we found that the line at 0.463 Mev, of 21-min half-life, was also present.

The question arises as to whether one of these gamma-rays comes as a result of a transition to an excited state of Kr^{84} or whether they are both in Rb^{84m}. Experiments[1] on Rb^{84} show a gamma-ray at 0.890 Mev. To test the two above-mentioned possibilities, a line at 0.890 Mev in Rb^{84m} was looked for and found. The half-life was 21 min but the intensity was extremely weak compared to the line at 0.463 Mev. The actual relative intensities, corrected for the photoelectric absorption in the crystal using the data of Davisson and Evans,[3] are in the ratio $I_{463}/I_{890}=7$. It, therefore, seems unlikely that the two gamma-rays are in cascade or that the line at 0.463 Mev is in the product.

Another difficulty arises if the line at 0.239 Mev is the line which governs the half-life of the metastable state. The calculated half-lives, made using the emperical formulas of Goldhaber and Sunyar[4] and including corrections for internal conversion, give $M4$, 2×10^6 sec; $E3$, 4 sec; $E4$, 2×10^4 sec. The actual half-life is 1.26×10^3

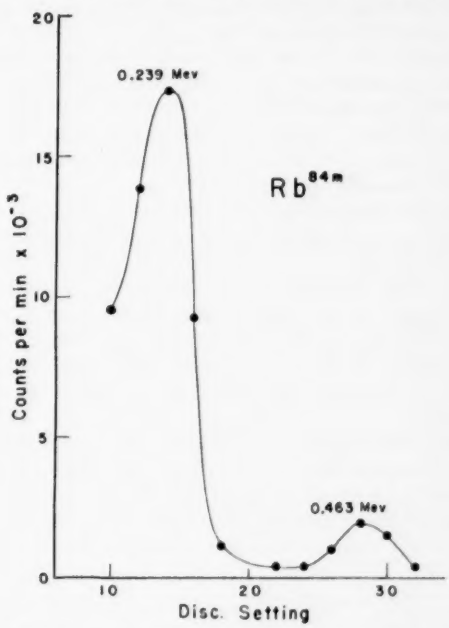

FIG. 1. Lines from Rb^{84m} (line at 0.890 Mev not shown).

† Supported by the joint program of the ONR and AEC.
[1] A. Flammersfeld, Z Naturforsch. **5a**, 687 (1950).
[2] C. M. Huddleston and A. C. G. Mitchell, Phys. Rev. **89**, 1350 (1952).
[3] C. M. Davisson and R. D. Evans, Revs. Modern Phys. **24**, 79 (1952).
[4] M. Goldhaber and A. W. Sunyar, Phys. Rev. **83**, 906 (1951).

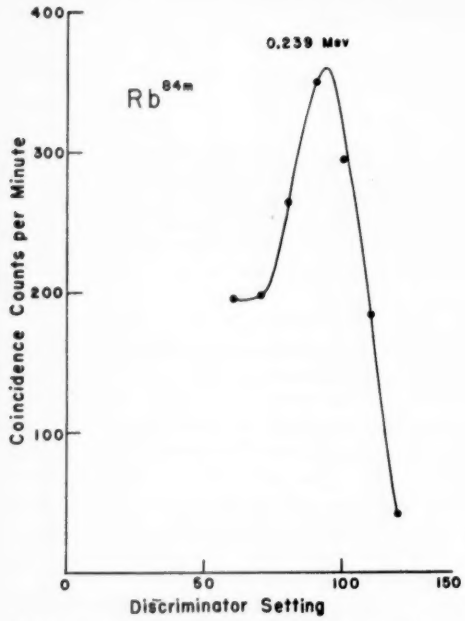

FIG. 2. Coincidence spectrum of Rb^{84m} Channel I set on line 0.239 Mev; Channel II variable.

sec. All of these are considerably longer than the observed half-life and, in addition, the internal conversion is high enough so that strong x-rays should be seen. X-rays were looked for in a proportional counter and none were seen. On the other hand, if both gamma-rays are in the parent and the line at 0.463 governs the half-life, the theoretical half-life for an $M4$ transition would be 5×10^3 sec in reasonable agreement with the observed value, and, in addition, the internal conversion coefficient would be quite small.

To test the possibility whether the line at 0.463 Mev could be in cascade with and presumably followed by that at 0.239 Mev, the relative intensities of the two lines were measured. When corrected for photoelectric cross section, the relative intensity is $I_{239}/I_{463}=2.5$. Assuming that the line at 0.463 Mev is $M4$ and that at 0.239 Mev is of low multipole order, corrections for internal conversion cannot possibly bring this ratio below 2.

Since the intensity of the line at 0.239 Mev is approximately twice that of the line at 0.463 Mev and since its energy is roughly half of the latter, it was deemed possible that there are two lines whose energies are roughly 0.239 Mev which are in cascade and that the cascade pair is in parallel with the line at 0.463 Mev. In order to test this possibility, two scintillation counters were used in a coincidence circuit. If, for example, Channel I is set on the line at 0.239 Mev and Channel II run over the line at 0.463 Mev, the coincidence rate is negligible. If, on the other hand, Channel I is set on the line at 0.239 Mev and Channel II run over this same line, a large coincidence rate was found, as shown in Fig. 2. This experiment shows that there are two gamma-rays of approximately 0.239 Mev energy in cascade and that one is not delayed appreciably behind the other.

The evidence appears to show that there are two lines of energy 0.230–0.239 Mev in cascade and that the line of energy 0.463 Mev is probably in parallel with this pair. A possible level scheme for the isomeric states, showing spins and parities, is shown in Fig. 3. Here it is assumed that the line at 0.463 Mev is an $M4$ transition and that the two lines near 0.239 Mev

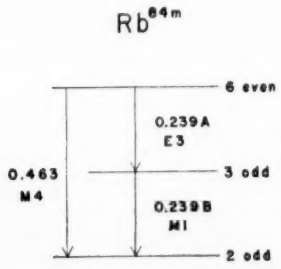

FIG. 3. Tentative level scheme for isomeric states of Rb^{84m}.

(called 0.239A and 0.239B) are $E3$ and $M1$, respectively. In order that the $M4$ transition can compete with the $E3$ transition, the square of the matrix moment of the latter must be $\sim10^{-6}$. According to Goldhaber and Sunyar,[4] the value of $|M|^2$ for $E3$ transitions varies from 10^{-3} to 10^{-6} if one uses the Weisskopf[5] transition formulas, as has been done here. It is not impossible that all three gamma-rays are in cascade with a delay greater than 10^{-6} sec between the line at 0.463 Mev and the line labeled 0.239A. It is difficult to believe that there are three metastable states above the ground level of Rb^{84} so that the parallel-cascade arrangement seems to be preferred.

Experiments are planned to make more exact measurements of the energies of the lines at 0.239 Mev as well as the K/L ratios of these and the one at 0.463 Mev.

[5] V. F. Weisskopf, Phys. Rev. 83, 1073 (1951).

PHYSICAL REVIEW VOLUME 89, NUMBER 3 FEBRUARY 1, 1953

Multiple Scattering and the Many-Body Problem—Applications to Photomeson Production in Complex Nuclei*

KENNETH M. WATSON
Physics Department, Indiana University, Bloomington, Indiana
(Received October 1, 1952)

A study is made of the scattering of fast particles by atomic nuclei. A rigorous (formal) solution to the many-body Schrödinger equation is given which has the structure of a multiply scattered wave. The relation of this solution to the "impulse approximation" is discussed. A decomposition of the wave function into "coherent" and "incoherent" parts is effected. This makes it possible to derive the familiar "optical models" directly, as well as to find systematic corrections to these models. The theory is applied to a discussion of photomeson production in complex nuclei.

I. INTRODUCTION

THE existence of high energy accelerators has made it possible to study reactions in complex nuclei induced by bombarding particles whose energies are large compared to nuclear binding energies. For such processes it is expected that the binding energy of the nucleus plays only a secondary role and that the scattering of the incoming particle by the nucleus can be described in terms of its scattering by the constituent nucleons of the nucleus individually. That is, the dynamical treatment of the many-body problem is thereby reduced to that of the two-body problem.

A number of models have been used to treat these reactions. In their study of the scattering of high energy neutrons by nuclei, Fernbach, Serber, and Taylor[1] have considered the nucleus to be a continuous "optical medium" characterized by an index of refraction and an absorption coefficient. The phase change of the incident wave is calculated as if it had followed a well-defined geometrical path through the nucleus, the total wave being the algebraic sum of the wavelets resulting from all such paths.

A somewhat more detailed application of this model has been made by Byfield, Kessler, and Lederman[2] and by Steinberger[3] in the discussion of their own experiments of meson scattering by nuclei. This involved solving the Schrödinger equation which results from expressing the meson-nucleus interaction in terms of the "optical parameters" mentioned above.

On the other hand, an elegant reduction of the many-body interactions is afforded by the use of the "impulse approximation," which has been introduced by Chew[4] and discussed in detail by Chew and Wick[5] and Chew and Goldberger.[6] The treatment given by these authors did not appear to be in the most convenient form, however, for a systematic development of the multiple scattering aspects the problem—and thus for a derivation of the optical models mentioned above.

The purpose of the present paper is to attempt the description of the multiple scattering of a fast particle in a nucleus. A rigorous formal solution to the many-body Schrödinger equation will be obtained which has the structure to be expected of a multiply scattered wave. The relation of this solution to the impulse approximation will be discussed.

On introducing a further approximation, which assumes the number of scatterers to be large, it is possible to make a separation of "coherent" and "incoherent" effects in the above solution to the Schrödinger equation. This makes it simple to derive the "optical models" mentioned above and to discuss more generally some formal relations to be expected for the scattering cross sections. Since the optical models are obtained almost directly from a rigorous solution to the Schrödinger equation, systematic corrections to these models appear to be quite straightforward.

To make the discussion of the model more specific, we shall apply it to photomeson production in complex nuclei (which includes discussion of meson scattering in nuclei). This will illustrate the flexibility of the method, since we shall also include an interaction for meson absorption (as well as for scattering). The formal arguments are quite general, however, in spite of their rather specific application in the present paper.

In Sec. II we shall introduce phenomenological interactions (and evaluate some of their matrix elements) for the photoproduction and scattering of mesons by individual nucleons, as well as for absorption by a pair of nucleons. It will then be shown that the solution to the Schrödinger equation for photomeson production involves solving the Schrödinger equation for meson scattering by the nucleus.

There appears to be ample experimental evidence[7–9] that meson scattering[2,3,10] plays a significant role in

* Supported in part by the joint program of the Office of Naval Research and Atomic Energy Commission.

[1] Fernbach, Serber, and Taylor, Phys. Rev. **75**, 1352 (1949). R. Serber [Phys. Rev. **72**, 1114 (1947)] has described the general features common to the various models employed to discuss high energy nuclear reactions.

[2] Byfield, Kessler, and Lederman, Phys. Rev. **86**, 17 (1952) (further references are given in this work).

[3] J. Steinberger (private communication).

[4] G. F. Chew, Phys. Rev. **80**, 196 (1950).

[5] G. F. Chew and G. C. Wick, Phys. Rev. **85**, 636 (1952).

[6] G. F. Chew and M. L. Goldberger, Phys. Rev. **87**, 778 (1952).

[7] McMillan, Peterson, and White, Science **110**, 579 (1949).

[8] R. F. Mozeley, Phys. Rev. **80**, 493 (1950).

[9] R. Littauer and D. Walker, Phys. Rev. **86**, 838 (1952).

[10] G. Bernardini and F. Levy, Phys. Rev. **84**, 610 (1951).

photomeson production. The observed variation of the cross section with atomic mass number A is $A^{\frac{1}{3}}$, which is proportional to the cross-sectional area of the nucleus and would seem to imply that only those mesons produced in the surface of the nucleus are able to get out. On the other hand, those mesons which are produced and re-absorbed in the nucleus will lead to high nuclear excitation. One would consequently expect to see an increase in the cross section for producing nuclear stars by γ-rays at about the threshold for meson production, which has also been observed.[11–13] (In a subsequent paper by Reff[14] a detailed comparison of the consequences of the present theory with the observed phenomena will be made.)

In Sec. III the scattering of a meson by the nucleus will be discussed. As a multiple scattering type of theory, we shall see that the model can be well described in terms of meson scattering at a point in the nucleus, followed by a scattering at a different point, followed by a scattering at a third point, etc. We shall neglect specifically "field effects" which correspond to recreation of an absorbed meson, so once the meson is absorbed the multiple scattering process ends. We shall repeatedly encounter averages of certain operators with respect to the nuclear wave functions. These expectation values can be expressed in terms of nucleon density in the nucleus, nucleon momentum distributions, and correlation in nucleon positions within the nuclear structure.

The interpretation of such expectation values with respect to the ground state of the nucleus can be made on very reasonable physical grounds. The interpretation of expectation values with respect to excited nuclear states is more ambiguous in general. However, this will not cause difficulty for the following reason: We consider the meson to be sufficiently energetic that its velocity is of the order of c, the velocity of light. The velocity of the heavier nucleons will be appreciably less than this ($\simeq c/10$). We imagine the meson to be produced (or scattered) at a point. The meson leaves this point with a velocity of about c, while the "shock wave" carrying nuclear excitation will proceed from this same point at a much lower velocity. When the meson reaches the position at which it is to be scattered again, it is expected to have "outrun" the nuclear excitation and will find the structure of the nuclear medium in the vicinity of the point of subsequent scattering to be essentially the same as in the nuclear ground state. The expectation value of operators localized at this second point will thus be replaced by expectation values with respect to the ground state of the nucleus.

[11] R. D. Miller, Phys. Rev. **82**, 260 (1951).
[12] J. Keck, Phys. Rev. **85**, 410 (1952).
[13] S. Kikuchi, Phys. Rev. **86**, 41 (1952).
[14] I. Reff (to be published). See also, Phys. Rev. **87**, 207 (1952), for a preliminary account.

II. FORMULATION OF THE PROBLEM

A. Preliminary Definitions

We seek to describe the mesonic processes in complex nuclei in terms of elementary interactions between subunits of the many-body system. The first of these is the interaction of the electromagnetic field with individual nucleons to produce a meson. This we write as

$$H'=\sum_{l=1}^{A}\exp(-i\mathbf{q}\cdot\mathbf{Z}_l)N_l, \tag{1}$$

where $\mathbf{q}$ is the momentum of the produced meson, $\mathbf{Z}_l$ is the coordinate of the lth nucleon, and N_l is a function of $\mathbf{q}$, spin and isotopic spin operators, and the photon energy and polarization. The sum is over the A nucleons in the nucleus. N_l has nonvanishing matrix elements for those charge states of the meson and nucleon which conserve charge.

As we are considering photomeson production from a nucleus, we shall need the Hamiltonian and eigenfunctions of the nuclear system. Let the Hamiltonian be H_N, so the eigenfunctions ψ_I satisfy

$$H_N\psi_I=\epsilon_I\psi_I \tag{2}$$

for a state of binding energy ϵ_I. The process of photomeson production leads in general from an initial nuclear state A to a final nuclear state F, possibly through intermediate nuclear states I.

The wave function for a meson in a plane wave state of momentum $\mathbf{q}$ is (we use as units $\hbar=c=1$)

$$\lambda_q=(2\pi)^{-\frac{3}{2}}\exp(i\mathbf{q}\cdot\mathbf{Z}). \tag{3}$$

The Schrödinger equation for this state is

$$h\lambda_q=\epsilon_q\lambda_q, \tag{4}$$

where h is the kinetic energy operator of the meson and $\epsilon_q\equiv q_0=(q^2+\mu^2)^{\frac{1}{2}}$ is the kinetic energy of the meson, whose rest mass is μ.

Expressing the energy operator of the electromagnetic field by H_γ, we define

$$H_0\equiv h+H_N+H_\gamma. \tag{5}$$

The eigenvalues of H_0 are written as E_I; and, in particular, the energy of the ground state of the nucleus plus the incident photon is called E_A.

Now, if the meson were to leave the nucleus without interaction, the Hamiltonian would be

$$H=H_0+H',$$

and the cross section for photomeson production would be

$$\sigma=(2\pi)^4S\langle H'\delta(E_A-H_0)H'\rangle. \tag{6}$$

By the symbol $\langle\cdots\rangle$ we mean the average with respect to the ground state of the nucleus. The symbol S designates an average with respect to initial polarization states. If we neglect correlations between nucleon

positions and the energy of excitation of the nucleus, use of Eq. (1) leads to

$$\sigma=(2\pi)^4 S\sum_l\langle N_l^+\delta(\epsilon_q-h)N_l\rangle$$
$$=A\sigma_f, \tag{7}$$

where

$$\sigma_f=A^{-1}[Z(\sigma_p^+ +\sigma_p^0)+(A-Z)(\sigma_n^- +\sigma_n^0)].$$

σ_p^+ is the cross section for producing a π^+ meson from a free proton, σ_p^0 that for a π^0 meson, etc. Z is the number of protons in the nucleus, so σ_f is the effective "average cross section" per nucleon for producing a meson. For brevity of notation in Eq. (7), we have summed over individual cross sections.

Equation (7) is based on the assumption that the produced meson does not interact with the nucleus. Finding the corrections to Eq. (7) resulting from such interactions will be our primary concern. It is known that the meson can be scattered as well as absorbed in nuclear matter. The scattering will be assumed to arise from an interaction of the meson with one nucleon at a time (i.e., we neglect many-body interactions). The absorption (to conserve energy and momentum) must, however, be a many-body interaction. We assume for reasons discussed previously[15] that it involves an interaction of the meson with a pair of nucleons. Although these interactions could be formally derived from a field theoretic approach, it seems preferable to introduce them in a phenomenological manner, as was the electromagnetic interaction of Eq. (1).

The scattering interaction of the meson with the αth nucleon we designate by

$$V_\alpha=(\mathbf{Z}'-\mathbf{Z}_\alpha|V_\alpha|\mathbf{Z}-\mathbf{Z}_\alpha), \tag{8}$$

which is assumed to be diagonal in the nucleon coordinate $\mathbf{Z}_\alpha$ because the mass of the nucleon is considerably larger than is that of a meson. $\mathbf{Z}$ and $\mathbf{Z}'$ represent the space coordinate of the meson. From the algebraic analysis of Chew and Goldberger[6] we obtain the transition operator for the scattering arising from V as

$$t_\alpha^0=V_\alpha+V_\alpha(\epsilon_b+i\eta-h-k_\alpha-V_\alpha)^{-1}V_\alpha. \tag{9}$$

Here ϵ_b is the energy of the meson and nucleon and k_α is the kinetic energy operator of the αth nucleon. The use of "η," as a positive parameter which goes to zero after the integrations are done, follows the convention of Lippmann and Schwinger.[16] Again, because of the large mass of the nucleon, we shall assume that in a coordinate representation t_α^0 takes the form[17]

$$t_\alpha^0=(\mathbf{Z}'-\mathbf{Z}_\alpha|t_\alpha^0|\mathbf{Z}-\mathbf{Z}_\alpha). \tag{9}$$

Transforming to a meson momentum representation, we have

$$(2\pi)^{-3}\int\exp(-i\mathbf{q}'\cdot\mathbf{Z}')t_\alpha\exp(i\mathbf{q}\cdot\mathbf{Z})d^3Zd^3Z'$$
$$\equiv\exp[-i(\mathbf{q}'-\mathbf{q})\cdot\mathbf{Z}_\alpha](q'|t_\alpha^0|q), \tag{10}$$

where $(q'|t_\alpha^0|q)$ is independent of $\mathbf{Z}_\alpha$.

The scattering interaction for a nucleus containing A nucleons is

$$V=\sum_{\alpha=1}^{A}V_\alpha. \tag{11}$$

It is understood that the isotopic spin dependence of V_α and t_α^0 corresponds to the observed scattering phenomena for the various charge states of the meson and nucleon.

The interaction for absorption has been discussed previously[15,18] and is obtainable from that for producing mesons in nucleon-nucleon collisions. We assume that the absorbing pair of nucleons has a relative coordinate $\mathbf{r}$ and a center-of-mass coordinate $\mathbf{x}$. Then the absorption operator R_μ, corresponding to absorption by the μth pair of nucleons is approximately[19]

$$(\mathbf{r}',\mathbf{x}'|R_\mu|\mathbf{Z},\mathbf{r},\mathbf{x})=R_\mu^0(\mathbf{r}',\mathbf{Z}-\mathbf{x})\delta(\mathbf{x}-\mathbf{x}')\delta(\mathbf{r}). \tag{12}$$

The $\delta(\mathbf{r})$ approximates a short-range interaction and has been discussed in detail in references 15 and 18. R_μ also contains a corresponding term to produce mesons. When the meson is absorbed in the nucleus by two nucleons, they are expected to recoil with an energy of about 140 Mev. We suppose that these two recoil nucleons have a relative momentum $\mathbf{p}$ and a total momentum $\mathbf{G}$ and that their wave function is a plane wave. Transforming R_μ^0, we have

$$(2\pi)^{-3}\int\exp(-i\mathbf{p}\cdot\mathbf{r}')R_\mu^0(\mathbf{r}',\mathbf{Z}-\mathbf{x})\exp(i\mathbf{q}\cdot\mathbf{Z})d^3r'd^3Z$$
$$\equiv\exp(i\mathbf{q}\cdot\mathbf{x})R_\mu^0(\mathbf{p},\mathbf{q}). \tag{13}$$

The absorption operator for the nucleus is the sum of R_μ over all nucleon pairs:

$$R=\sum_\mu R_\mu. \tag{14}$$

To avoid a discussion of field emission and absorption effects, we shall include R in the Hamiltonian of the system, but shall treat it as a small perturbation so that it will indeed be a transition operator. One-half the transition rate for absorption in the nucleus is then (neglecting correlations between pairs)

$$\Delta_0\equiv\pi\sum_\mu\langle R_\mu\delta(E_A-H_0)R_\mu\rangle, \tag{15}$$

where it is understood that the first R_μ absorbs and the second R_μ reproduces the meson. As before[15] we approximate E_A-H_0 by ϵ_q-p^2/M, where M is the nu-

[15] Brueckner, Serber, and Watson, Phys. Rev. **84**, 258 1(951).
[16] B. Lippmann and J. Schwinger, Phys. Rev. **79**, 469 (1950).
[17] A discussion of this point has been given by Fernbach, Green, and Watson, Phys. Rev. **84**, 1084 (1951).
[18] K. Watson and K. Brueckner, Phys. Rev. **83**, 1 (1951).
[19] This follows from the form given in reference 15 when $\mu/2M$ is neglected compared to unity (W is the nucleon mass). A specific assumption about the form of t and R is not, of course, necessary for the general theory of the next section.

cleonic mass. To calculate the matrix element $(q'|\Delta_0|q)$, we first consider the absorption of the meson by nucleons "1" and "2," so [see Eq. (12)]

$$\mathbf{r}=\mathbf{Z}_1-\mathbf{Z}_2, \quad \mathbf{x}=\tfrac{1}{2}(\mathbf{Z}_1+\mathbf{Z}_2). \tag{16}$$

Then

$$\langle R_{(12)}\delta(E_A-H_0)R_{(12)}\rangle$$

$$=\int\psi_A(\mathbf{r}', \mathbf{x}, \mathbf{Z}_3\cdots\mathbf{Z}_A)\delta(\mathbf{r}')R^{0+}{}_{(12)}(\mathbf{p}, \mathbf{q}')$$

$$\times d^3p\delta(\epsilon_q-p^2/M)R^0{}_{(12)}(\mathbf{p}, \mathbf{q})\delta(\mathbf{r})\ \exp[-i(\mathbf{q}'-\mathbf{q})\cdot\mathbf{x}]$$

$$\times\psi_A(\mathbf{r}, \mathbf{x}, \mathbf{Z}_3\cdots\mathbf{Z}_A)d^3r'd^3rd^3xd^3Z_3\cdots d^3Z_A$$

$$=\int\langle R^{0+}{}_{(12)}(\mathbf{p}, \mathbf{q}')d^3p\delta(\epsilon_q-p^2/M)R^0{}_{(12)}(\mathbf{p}, \mathbf{q})\rangle$$

$$\times P(O, x)\ \exp[-i(\mathbf{q}'-\mathbf{q})\cdot\mathbf{x}]d^3x, \tag{17}$$

where $P(O, x)$ is the joint probability of finding the nucleons "1" and "2" at the same point and of finding their center-of-mass at the point $\mathbf{x}$. It is convenient to write

$$P(O, x)=P_0v(x)/V_A. \tag{18}$$

P_0 is a factor describing correlation in nuclear structure and was discussed in reference (15), $v(x)$ is the probability density of the center-of-mass of the nucleons "1" and "2" when they are at the same point. It is normalized according to

$$\int v(x)d^3x=V_A, \tag{19}$$

the nuclear volume. Equations (18) and (19) are in agreement with the unit normalization of the nuclear wave functions.

To obtain $(q'|\Delta_0|q)$ we multiply Eq. (17) by the number of absorbing nucleon pairs, N_p. We now evaluate Δ_0 by three methods, the first two being approximations to Eq. (17). It is apparent that (except for the smallest nuclei) Δ_0 will be nearly diagonal in q. Consequently, for the two approximations we replace $R^{0+}(\mathbf{p}, \mathbf{q}')$ by $R^{0+}(\mathbf{p}, \mathbf{q})$ in Eq. (17). Then following the arguments of reference 15, Δ_0 is related to the mean free path for absorption, λ_a, in the nucleus by

$$(q'|\Delta_0|q)=\frac{v_\pi}{2\lambda_a}(2\pi)^{-3}\int v(x)\exp[-i(\mathbf{q}'-\mathbf{q})\cdot\mathbf{x}]d^3x, \tag{20}$$

where v_π is the velocity of the pion before absorption. If constant nuclear density were assumed, we would have

$$\begin{aligned} v(x)&=1 \quad \text{inside nucleus,}\\ v(x)&=0 \quad \text{outside nucleus.}\end{aligned} \tag{21}$$

This assumption is not necessary, but is the one most commonly chosen. For specific calculations in this paper we shall assume Eq. (21).

Then, if the nucleus is very large, the integral in Eq. (20) becomes a δ-function:

(Approximation I)

$$(q'|\Delta_0|q)=(v_\pi/2\lambda_a)\delta(\mathbf{q}'-\mathbf{q}). \tag{22}$$

As will be seen later, this approximation leads to the model of Fernbach, Serber, and Taylor[1] and to that of reference 15.

The second approximation involves using Eq. (20) as it stands. This equation can be simplified in a coordinate representation, if we consider $v_\pi/2\lambda_a$ to be evaluated at the energy of the meson in the nuclear medium and remove it from under the integral below:

(Approximation II)

$$(Z'|\Delta_0|Z)=(2\pi)^{-3}\int\exp(i\mathbf{q}'\cdot\mathbf{Z}')(q'|\Delta_0|q)$$

$$\times\exp(-i\mathbf{q}\cdot\mathbf{Z})d^3q'd^3q$$

$$\simeq(v_\pi/2\lambda_a)v(Z)\delta(\mathbf{Z}'-\mathbf{Z}). \tag{23}$$

We shall see in Sec. III that this leads to the model used by Lederman[2] and by Steinberger.[3] Evaluation of Eq. (17) keeping an arbitrary q' in $R^{0+}(p, q')$ leads to an expression which can be formally written as

(Approximation III)

$$(Z'|\Delta_0|Z)=(v_\pi/2\lambda_a)v(Z', Z). \tag{24}$$

(We have assumed that the nucleus is infinitely heavy and that its center is at the origin of the coordinate system.)

The diagonal element of $t_a{}^0$ [Eq. (9)] with respect to the nuclear coordinates can be found by the same method. Writing $t_C\equiv\sum_\alpha\langle t_\alpha{}^0\rangle$ we obtain

$$(q'|t_C|q)=\sum_\alpha\int\langle(q'|t_\alpha{}^0|q)\rangle$$

$$\times\exp[-i(\mathbf{q}'-\mathbf{q})\cdot\mathbf{Z}_\alpha]P(Z_\alpha)d^3Z_\alpha. \tag{25}$$

$P(Z_\alpha)$ is the probability per unit volume of finding nucleon "α" at the point Z_α. We express $P(Z_\alpha)$ as

$$P(Z_\alpha)=v_0(Z_\alpha)/V_A\simeq v(Z_\alpha)/V_A. \tag{26}$$

On summing over α, we obtain a factor of A. Approximations I and II are made as for Δ_0. Using the general theorem[16] relating the imaginary part of the scattering amplitude in the forward direction to the total scattering cross section, we obtain (since the total spin of the nucleus is much less than $A/2$)

$$(A/V_A)(2\pi)^3\langle(q|t_\alpha{}^0|q)\rangle=V_0-iv_\pi/2\lambda_S\equiv B_S, \tag{27}$$

where λ_S is the mean free path for a scattering in the nucleus and V_0 is

$$V_0=(2\pi/q_0)\ \mathrm{Re}(a_S)A/V_A.$$

$\mathrm{Re}(a_S)$ is the real part of the meson scattering amplitude in the forward direction (actually the average for the neutrons and protons in the nucleus). Then by our three approximations for Δ_0, we have [Eq. (27)]

$$\begin{aligned} &\text{I:} \quad (q'|t_C|q)=B_S\delta(\mathbf{q}'-\mathbf{q});\\ &\text{II:} \quad (Z'|t_C|Z)=B_S v_0(Z)\delta(\mathbf{Z}'-\mathbf{Z});\\ &\text{III:} \quad (Z'|t_C|Z)=B_S v_0(Z',Z). \end{aligned} \tag{28}$$

To anticipate the conclusions of Sec. III, we note that V_0 is the "effective well depth" of the nucleus as seen by the meson.[20] It should be remarked that V_0, λ_S, and λ_a are "operators" in the charge coordinates of the meson, their eigenvalues being the appropriate numerical values of these parameters for the three charge states of the meson.

B. Solution of the Schrödinger Equation

The Hamiltonian for the system is

$$H=H_0+R+V+H', \tag{29}$$

where the various terms are defined by Eqs. (1), (5), (11), and (14). The wave function of the system corresponding to an initial state, ϕ_A, containing a photon and the initial nucleus is

$$\chi_A=\Phi\phi_A. \tag{30}$$

Φ is the wave matrix introduced by Møller.[21] In the Lippmann-Schwinger[16] formulation, the Schrödinger equation for Φ can be written as (we omit the symbol "+" on Φ)

$$\Phi=1+a^{-1}(H'+R+V)\Phi, \tag{31}$$

it being understood that this equation operates on ϕ_A. The quantity a is defined as

$$a\equiv E_A+i\eta-H_0. \tag{32}$$

Spontaneous creation of virtual mesons by R is expected to be small, so we assume that R vanishes when operating on the state ϕ_A. (V obviously does so.) We also treat H' as a small perturbation, since it involves an electromagnetic interaction. Then

$$\Phi=1+\Omega a^{-1}H', \tag{33}$$

where

$$\Omega=1+a^{-1}(R+V)\Omega. \tag{34}$$

Ω is seen to describe the scattering of a meson in the nucleus, so our next problem is to study the solution to Eq. (34).

III. THE SCATTERING OF A MESON BY THE NUCLEUS

A. Basic Multiple Scattering Equations

We turn our attention to the solution of Eq. (34). The quantity R is to be considered as a small perturbation.[22] Spontaneous creation of mesons by R is to be neglected. Thus the first occurrence of R in Ω (reading from right to left) will correspond to absorption of a meson. The next occurrence of R must then correspond to creation of a meson. Neglect of "spontaneous creation" implies that the re-creation must occur immediately from the same pair of nucleons. This means that an expression such as

$$\Delta\equiv Ra^{-1}R \tag{35}$$

can be written as

$$\textstyle\sum_\mu R_\mu a^{-1}R_\mu$$

[Eq. (14)]. Also, following a single R interaction, there is no meson so V vanishes. Now, Δ is the lowest order transition operator for meson scattering arising from R. This is a many-body effect and is expected to be negligible compared to the scattering arising from V. (Experimental studies of meson scattering in hydrogen and deuterium[23] support this hypothesis that the interaction is primarily between the meson and one nucleon at a time.) However, we cannot quite neglect terms like Δ, because this quantity contains the "shadow" cast by true absorption. This arises from the imaginary part of Δ that is diagonal in the nuclear coordinates. We shall then assume that ["Im$(\cdots)$" means "imaginary part of $(\cdots)$"]

$$\begin{aligned} \Delta\simeq i\,\mathrm{Im}(\langle\Delta\rangle)\simeq&-i\pi\textstyle\sum_\mu\langle R_\mu\delta(E_A-H_0)R_\mu\rangle\\ =&-i\Delta_0. \end{aligned} \tag{36}$$

Δ_0 is defined by Eq. (15). We shall henceforth use Δ and $-i\Delta_0$ interchangeably in our equations.

A quantity b is defined as

$$b=a-\Delta. \tag{37}$$

We note that, following an R which absorbs a meson,

$$b=a, \tag{38}$$

since Δ vanishes when operating on a state that does not contain a meson.

As a first step in the solution of Eq. (34), we solve the integral equation

$$\Omega_S=1+b^{-1}V\Omega_S. \tag{39}$$

In the special case that $R=0$, Eqs. (34) and (39) are identical. That is, Ω_S evaluated for $\Delta=0$ describes the scattering of the meson in the absence of absorption.

To solve for Ω_S we introduce two subsidiary functions:

$$t_a'=V_a+V_a(a-V_a)^{-1}V_a, \tag{40}$$

$$t_a=V_a+V_a(b-V_a)^{-1}V_a. \tag{41}$$

We shall wish to identify t_a' and t_a with t_a^0 [Eq. (9)]—the scattering from a free nucleon. The identification of t_a' with t_a^0 is the impulse approximation. We shall not discuss this in detail since it would be largely a

[20] From their experiments Byfield *et al.* (reference 2) and Steinberger (reference 3) find that $V_0\simeq 20$ Mev and $(1/\lambda_S+1/\lambda_a)\simeq 10^{+13}$ cm^{-1}. These values are dependent upon the "optical model" which was used—i.e., approximation II in our notation.

[21] C. Møller, Kgl. Danske. Videnskab. Selskab, Mat.-fys. Medd **23**, No. 1 (1945).

[22] This restriction is not necessary [K. Brueckner and K. Watson, to be published].

[23] Anderson, Fermi, Nagle, and Yodh, Phys. Rev. **86**, 413 (1952).

repetition of the analysis of Chew and Goldberger[6] (although our statement of the problem differs somewhat from that of these authors). The essential point is the observation that a [Eq. (32)] and $\epsilon_b+i\eta-h-k_\alpha$ [Eq. (9)] differ only by the excitation imparted to the remainder of the nucleus. This is expected to be a small correction for high energy scatterings, such as we are considering. That $t_\alpha \simeq t_\alpha'$ is demonstrated later in this section.

The solution to Eq. (39) is

$$\Omega_S=1+\sum_{(\alpha)}\frac{1}{b}\Big\{t_{\alpha_1}+t_{\alpha_1}\frac{1}{b}t_{\alpha_2}+\cdots+t_{\alpha_1}\frac{1}{b}t_{\alpha_2}\frac{1}{b}\cdots\frac{1}{b}t_{\alpha_n}+\cdots\Big\}. \quad (42)$$

Here the index "α_i" on t_{α_i} ($\alpha_i=1, 2, \cdots A$) refers to the scattering of the meson by the α_ith nucleon. The summation over the α's (designated by $\sum_{(\alpha)}$) is a summation over all indices "α_i" independently (from 1 to A), except that *no two adjacent* indices can have the same value. Thus, if there were only the one nucleon "α," Ω_S would reduce to

$$\Omega_S=1+(1/b)t_\alpha.$$

Once we identify t_α with t_α^0, we see that Ω_S represents true multiple scattering,[24] since the meson is scattered first by one nucleon then by another, etc.—and this is summed over all possible ways that such can occur. To see that Eq. (42) is a rigorous solution to Eq. (39), we substitute the former into the right hand side of the latter. We obtain terms like

$$\frac{1}{b}V\sum_{(\alpha)}\frac{1}{b}t_{\alpha_1}\frac{1}{b}t_{\alpha_2}\cdots\frac{1}{b}t_{\alpha_n}=\sum_{(\alpha)}\frac{1}{b}V_{\alpha_0}\frac{1}{b}t_{\alpha_1}\frac{1}{b}t_{\alpha_2}\cdots\frac{1}{b}t_{\alpha_n}+\sum_{(\alpha)}\frac{1}{b}V_{\alpha_1}\frac{1}{b}t_{\alpha_1}\frac{1}{b}t_{\alpha_2}\cdots\frac{1}{b}t_{\alpha_n}, \quad (43)$$

where the index α_0 is never equal to α_1 in the summation. Using the identity

$$\frac{1}{b-V_{\alpha_1}}-\frac{1}{b}=\frac{1}{b}V_{\alpha_1}\frac{1}{b-V_{\alpha_1}}, \quad (44)$$

we find that (from Eq. (41))

$$V_{\alpha_1}\frac{1}{b}t_{\alpha_1}=t_{\alpha_1}-V_{\alpha_1}$$

holds as an identity. Thus the second term on the right-hand side of Eq. (43) is

$$\sum_{(\alpha)}\frac{1}{b}t_{\alpha_1}\frac{1}{b}t_{\alpha_2}\cdots\frac{1}{b}t_{\alpha_n}-\sum_{(\alpha)}\frac{1}{b}V_{\alpha_1}\frac{1}{b}t_{\alpha_2}\cdots\frac{1}{b}t_{\alpha_n}. \quad (46)$$

[24] We might call t_α the "effective scattering amplitude" from a bound nucleon.

Relabeling the summation indices of the first term of Eq. (43) as $\alpha_0\to\alpha_1$, $\alpha_1\to\alpha_2\cdots\alpha_n\to\alpha_{n+1}$ and summing over n, we find that the second terms of Eq. (46) and the first terms of Eq. (43) cancel in pairs. The first terms of Eq. (46) are just those terms occurring in Eq. (42), so Eq. (39) is indeed satisfied.

Let us return now to the basic scattering equation (34). The solution is

$$\Omega=(1+a^{-1}R)\Omega_S(1+b^{-1}\Delta). \quad (47)$$

To see that this satisfies Eq. (34), we substitute into the right-hand side of (34) to obtain

$$\Omega=1+(1/a)\{V\Omega_S+R\Omega_S+R(1/a)R\Omega_S\}\{1+(1/b)\Delta\}. \quad (48)$$

[$V(1/a)R=0$ since R absorbs the meson.] Now

$$1/a=(1/b)-(1/a)\Delta(1/b) \quad (49)$$

and $(1/b)V\Omega_S=\Omega_S-1$ [Eq. (39)]. We also write the term $R(1/a)R$ in Eq. (48) as

$$R(1/a)R=\Delta \quad (50)$$

by Eq. (35). Equation (48) then reduces to

$$\Omega=(1+a^{-1}R)\Omega_S(1+b^{-1}\Delta)-(1/b)\Delta+(1/a)\Delta+(1/a)\Delta(1/b)\Delta=\Omega, \quad (51)$$

by Eq. (49). Thus Eq. (47) is the required solution to Eq. (34).

To show that t_α' and t_α are nearly equal, we observe that

$$t_\alpha-t_\alpha'=t_\alpha'(1/a)\Delta(1/b)t_\alpha. \quad (52)$$

By Eq. (36) we replace Δ by $-i\Delta_0$. In b we use Eq. (22) for Δ_0. In the numerator, we use Eq. (20). Referring to Eq. (10) and to the definitions of Δ_0, we see that (if we neglect the energy of excitation of the nucleus)

$$\int\exp(i\mathbf{q}_1\cdot\mathbf{Z}_\alpha)\left(q_1\left|\frac{1}{a}\Delta\frac{1}{b}\right|q_2\right)\exp(-i\mathbf{q}_2\cdot\mathbf{Z}_\alpha)d^3q_1d^3q_2$$
$$=(2\pi)^{-3}\left(\frac{-iv_\pi}{2\lambda_\alpha}\right)\int_{V_A}d^3xd^3q_1d^3q_2\frac{\exp[i\mathbf{q}_1\cdot(\mathbf{Z}_\alpha-\mathbf{x})]}{\epsilon_q+i\eta-q_{01}}\times\frac{\exp[-i\mathbf{q}_2\cdot(\mathbf{Z}_\alpha-\mathbf{x})]}{\epsilon_q+i\eta-q_{02}+i\dfrac{v_\pi}{2\lambda_\alpha}}\simeq-(2\pi)^2\frac{\epsilon_q}{2\lambda_\alpha}, \quad (53)$$

on the assumption that the nucleus is large. In terms of the scattering amplitude a_S,

$$t_\alpha'=a_S/[(2\pi)^2\epsilon_q]. \quad (54)$$

Therefore

$$t_\alpha-t_\alpha'=t_\alpha'(1/a)\Delta(1/b)t_\alpha\simeq(a_S/2\lambda_\alpha)t_\alpha. \quad (55)$$

This is a correction to t_α of about 2 to 3 percent at the meson energies for which a_S and λ_α have been measured.

B. Decomposition of the Scattering into Coherent and Incoherent Parts

Referring to Eq. (42) we see that Ω_S can be written as

$$\Omega_S = 1+\frac{1}{b}\sum_{\alpha_1} t_{\alpha_1}\Omega_S(\alpha_1),$$

$$\Omega_S(\alpha_1) = 1+\frac{1}{b}\sum_{\alpha_2\neq\alpha_1} t_{\alpha_2}\Omega_S(\alpha_2). \tag{56}$$

These equations have the formal structure of the multiple scattering equations introduced by Foldy[25] and generalized by Lax.[26] These authors introduced the equations on grounds of physical plausibility and considered the coordinates of the scatterers to be adiabatic parameters. On the other hand, Eqs. (56) represent rigorous (formal) solutions to the many-body problem. The adiabatic approximation is obtained from Eqs. (56) by (1) assuming the impulse approximation and identifying t_α with $t_\alpha{}^0$; (2) neglecting nuclear excitation in the energy denominators. The use of Eqs. (56) to improve the second approximation leads to corrections which can be expressed in terms of momentum distributions of the nucleons in the nucleus.

The coherent scattering arises from that part of Ω_S which is diagonal in the nuclear coordinates, or

$$\Omega_{SC} \equiv \langle \Omega_S \rangle. \tag{57}$$

Using the first of Eqs. (56) to find Ω_{SC}, we encounter

$$\langle t_{\alpha_1}\Omega_S(\alpha_1)\rangle.$$

This represents scattering by nucleon α_1 of the incident wave plus the scattered waves from all the other nucleons. We expect that these previous scatterings will also have been coherent to a good approximation, for otherwise the scattering at particle α_1 would have to react in such a way as to return to their place in the ground state of the nucleus the other nucleons which had been raised to excited levels by previous inelastic scatterings. This possibility would require very strong correlations in nuclear structure and will be neglected by us. Thus we can write

$$\langle t_{\alpha_1}\Omega_S(\alpha_1)\rangle = \langle t_{\alpha_1}\rangle\langle \Omega_S(\alpha_1)\rangle. \tag{58}$$

Now $\langle \Omega_S(\alpha_1)\rangle$ differs from $\langle \Omega_S\rangle$ by the removal of one nucleon for the last scattering. If the number of nucleons is large, we can replace $\langle \Omega_S(\alpha_1)\rangle$ by $\langle \Omega_S\rangle$. Then Ω_{SC} satisfies the equation [t_C is defined in connection with Eq. (25)]

$$\Omega_{SC} = 1+(1/b)t_C\Omega_{SC}, \tag{59}$$

since a and b are "coherent quantities." In this equation (when operating on the ground state of the nucleus) b has the value

$$\epsilon_q + i\eta - h + i\Delta_0.$$

[25] L. Foldy, Phys. Rev. **67**, 107 (1945).
[26] M. Lax, Revs. Modern Phys. **23**, 287 (1951).

Thus [using the techniques of Chew and Goldberger[6] to solve Eq. (59)]

$$\Omega_{SC} = 1+\frac{1}{b-t_C}t_C$$
$$= 1+(1/e)t_C, \tag{60}$$

where we have introduced the new quantity

$$e \equiv b - t_C. \tag{61}$$

To find the coherent part of Ω [Eq. (47)] we observe that the R term is incoherent and recall that only the coherent part of Δ (i.e., $-i\Delta_0$) is kept in any case. So

$$\Omega_C \equiv \langle\Omega\rangle = (1+(1/e)t_C)(1+(1/b)\Delta)$$
$$= 1+(1/e)(t_C+\Delta). \tag{62}$$

The wave function of the scattered meson is

$$\phi_q(Z) = \Omega_C\lambda_q(Z)$$

[see Eq. (3)]. From Eq. (62) we see that ϕ_q satisfies the Schrödinger equation

$$[h+t_C+\Delta]\phi_q = \epsilon_q\phi_q, \tag{63}$$

where [Eqs. (23), (29), and (36)]

$$t_C+\Delta = \left[V_0 - \frac{iv_\blacktriangledown}{2}(1/\lambda_S+1/\lambda_a)\right]v(Z)$$
$$\equiv Bv(Z). \tag{64}$$

Equation (63) has been studied by Lederman *et al.*[2] and by Steinberger[3] in connection with their own experiments.

The expression[27]

$$C \equiv \langle t_\alpha\rangle \tag{65}$$

($t_C = AC$) is independent of α.

$$I_\alpha \equiv t_\alpha - C \tag{65'}$$

represents purely inelastic scattering. We replace t_α by $I_\alpha+C$ in Eqs. (56). Quantities such as $C\Omega_S(\alpha_1)$ occur, which we approximate by

$$C\Omega_S(\alpha_1) \simeq C\Omega_S. \tag{66}$$

This assumes that the number of scatterers is large (as can be seen from the arguments of Appendix A). Thus Eqs. (56) become

$$\Omega_S = 1+(1/b)t_C\Omega_S+(1/b)\sum_{\alpha_1} I_{\alpha_1}\Omega_S(\alpha_1);$$
$$\Omega_S(\alpha_1) = 1+(1/b)t_C\Omega_S+(1/b)\sum_{\alpha_2\neq\alpha_1} I_{\alpha_2}\Omega_S(\alpha_2). \tag{67}$$

[27] Actually, C should be defined as $C=\Sigma_I\langle I|t_\alpha|I\rangle\Gamma_I$, where Γ_I is the projection operator on the nuclear state I. This does not modify the formal arguments which follow. The approximation of Eq. (65) follows from the arguments of the Introduction.

To solve these equations, we introduce the functions

$$F=1+(1/e)\sum_{\alpha_1} I_{\alpha_1}F_{\alpha_1},$$
$$F_{\alpha_1}=1+(1/e)\sum_{\alpha_2\neq\alpha_1} I_{\alpha_2}F_{\alpha_2}, \tag{68}$$

where e is defined by Eq. (61). The desired solutions to Eq. (67) are

$$\Omega_S=F(1+(1/e)t_C),$$
$$\Omega_S(\alpha_1)=F_{\alpha_1}(1+(1/e)t_C), \tag{69}$$

as may be seen from substituting these expressions into the right-hand side of Eqs. (67). [To satisfy the second of these equations we must approximate t_CF_α, by t_CF, essentially the same approximation as that made in Eq. (66).]

Finally,

$$\Omega=(1+(1/a)R)\Omega_S(1+(1/b)\Delta)$$
$$=(1+(1/a)R)F\Omega_C, \tag{70}$$

where Ω_C is given by Eq. (62).

We note that the operator F is

$$F=1+(1/e)\sum_{(\alpha)}\{I_{\alpha_1}+I_{\alpha_1}(1/e)I_{\alpha_2}+\cdots\}, \tag{71}$$

an expression much like that of Eq. (42), except that all coherent effects are in the propagation functions, $1/e$. The physical interpretation of Eq. (71) is that the wave is propagated in a refracting medium between inelastic scatterings. That R is only on the left in Eq. (70) reflects the fact that once the meson is absorbed there will of course be no more meson scattering. The appearance of Ω_C on the right in Eq. (70) shows that the "effective incident wave" is the coherent wave rather than the actual wave of incoming mesons.

It is instructive to substitute Eq. (70) into the right-hand side of Eq. (34) to verify that we have indeed found a solution to the original equation (to within the approximation that the number of scatterers is large). This is done in Appendix A. In Appendix B it is shown that Eq. (69) can be very simply obtained when the scattering can be treated in Born approximation.

Before returning to the photomeson phenomena, we shall briefly discuss the scattering according to approximation I [Eqs. (22) and (29)] for $t_C+\Delta$. We consider first the coherent scattering:

$$\Omega_C=1+(1/e)(t_C+\Delta). \tag{62'}$$

In e we keep only the diagonal part of $t_C+\Delta$:

$$(q'|\,t_C+\Delta\,|q)=B\delta(\mathbf{q}'-\mathbf{q}). \tag{72}$$

[B is defined in Eq. (64).] In the numerator we can use approximation II:

$$(q'|\,t_C+\Delta\,|q)=\frac{B}{(2\pi)^3}\int_{V_A}\exp[-i(\mathbf{q}'-\mathbf{q})\cdot\mathbf{x}]d^3x. \tag{73}$$

[See, for instance, Eq. (20)]. Then

$$\int(q'|\,(1/e)(t_C+\Delta)\,|q)\exp(i\mathbf{q}'\cdot\mathbf{Z})d^3q'$$
$$=\frac{B}{(2\pi)^3}\int d^3q'\int_{V_A}d^3x\frac{\exp[i\mathbf{q}'\cdot(\mathbf{Z}-\mathbf{x})]}{q_0+i\eta-q_0'-B}\exp(i\mathbf{q}\cdot\mathbf{x}). \tag{74}$$

Now,

$$\int d^3q'\frac{\exp[i\mathbf{q}'\cdot(\mathbf{Z}-\mathbf{x})]}{q_0+i\eta-q_0'-B}=-(2\pi)^2(q_0/\Lambda)$$
$$\times\exp(iq\Lambda)\exp\left(-i\frac{q_0}{q}B\Lambda\right), \tag{75}$$

where $\mathbf{\Lambda}=\mathbf{x}-\mathbf{Z}$, and it is assumed that the nucleus is large enough that Λ is much greater than the wavelength of the meson. By this same assumption, we find

$$\int\left(q'\left|\frac{1}{e}(t_C+\Delta)\right|q\right)\exp(i\mathbf{q}'\cdot\mathbf{Z})d^3q'$$
$$=-\exp(i\mathbf{q}\cdot\mathbf{Z})\left[1-\exp\left(-i\frac{q_0}{q}BD\right)\right], \tag{76}$$

where use is made of the fact that B has a negative imaginary part. D is the distance from the point $\mathbf{Z}$ to the boundary of the nucleus[28] along the direction of the vector—$\mathbf{q}$. The coherent scattering is described by the transition operator:

$$T_C=(t_C+\Delta)\Omega_C. \tag{77}$$

Using Eqs. (73) and (76),

$$(q'|\,T_C\,|q)=\frac{B}{(2\pi)^3}\int_{V_A}\exp[-i(\mathbf{q}'-\mathbf{q})\cdot\mathbf{Z}]$$
$$\times\exp(-iq_0/qBD)d^3Z$$
$$=(-i/(2\pi)^2q_0)f(\theta), \tag{78}$$

where θ is the angle between $\mathbf{q}$ and $\mathbf{q}'$ and $f(\theta)$ is given by Eq. (7) of the paper by Fernbach, Serber, and Taylor.[1] The model of these authors thus follows from the use of approximation I in the propagation function $1/e$.

We can also, in the same approximation, obtain the integral equation describing the diffusion of the meson density in the nuclear medium. To simplify matters, we assume isotropic scattering and neglect the difference in the scattering by neutrons and protons, as well as charge exchange scattering (we intend merely to illustrate the application of our equations). Referring

[28] Eq. (76) has a direct physical interpretation. The first term is canceled by the "unity" term in Eq. (62'), showing that the incident wave is "extinguished" within the nucleus. The remaining term shows a net phase shift, from which the index of refraction is seen to be $n=1-(q_0/q^2)B$.

to Eqs. (68) and (69) for Ω_S, we have (for a large nucleus)

$$\psi(Z)\equiv\int(q'|\Omega_S|q)\exp(i\mathbf{q}'\cdot\mathbf{Z})d^3q'$$
$$=\int\exp(i\mathbf{q}'\cdot\mathbf{Z})(q'|\Omega_C|q)d^3q'$$
$$+\sum_{\alpha_1}\int\frac{\exp[i\mathbf{q}'\cdot(\mathbf{Z}-\mathbf{Z}_{\alpha_1})]}{\epsilon_q+i\eta-q_0'-B}\bar{I}_{\alpha_1}\psi_{\alpha_1}(Z_{\alpha_1}),\quad(79)$$

where $\bar{I}_{\alpha_1}$ is the matrix of I_{α_1} on the energy shell and $\psi_{\alpha_1}(Z_{\alpha_1})$ represents the scattered wave from the nucleons other than that indicated by α_1. The meson density is given by

$$\rho(Z)=\langle\psi^*\psi\rangle.\quad(80)$$

Substituting Eq. (79) into Eq. (80), the cross terms approximately vanish (as they are essentially incoherent). Using Eq. (75), we obtain

$$\rho(Z)=\rho_C(Z)+\frac{\sigma_{in}}{4\pi}\frac{A}{V_A}$$
$$\times\int_{V_A}\frac{\exp(-|\mathbf{Z}-\mathbf{Z}_{\alpha_1}|1/\lambda)}{|\mathbf{Z}-\mathbf{Z}_{\alpha_1}|^2}\rho(Z_{\alpha_1})d^3Z_{\alpha_1},\quad(81)$$

where ρ_C is the "coherent density," $1/\lambda\equiv1/\lambda_S+1/\lambda_a$, and $\sigma_{in}=2(2\pi)^5q_0^2\langle\bar{I}_{\alpha_1}{}^\dagger\bar{I}_{\alpha_1}\rangle$ is the scattering cross section from a single nucleon (minus the coherent scattering). This is Foldy's integral equation.[29] We have approximated $\psi_{\alpha_1}(Z_{\alpha_1})$ by $\psi(Z_{\alpha_1})$ in Eq. (81) for reasons similar to those leading to Eq. (58).

IV. PHOTOMESON PHENOMENA

A. Evaluation of the Cross Sections

The wave matrix for the photomeson problem is given by Eq. (33):

$$\Phi=1+\Omega(1/a)H'$$
$$=1+[1+(1/a)R]F\Omega_C(1/a)H'$$
$$=1+[1+(1/a)R]F(1/e)H',\quad(33')$$

since $\Omega_C(1/a)=(1/e)$ is an algebraic identity.

The transition operator is

$$T=(H'+R+V)\Phi$$
$$=H'+(V+\Delta)F\Omega_C(1/a)H'+RF(1/e)H',\quad(82)$$

to first order in H', remembering that $(R+V)$ vanishes when operating on the initial state (which does not contain a meson). To simplify the second term, we note that $(V+\Delta)F\Omega_C$ is just the transition operator for meson scattering in the nucleus (less the absorbing part). So

$$(V+\Delta)F(1/e)H'=\{(t_C+\Delta)$$
$$+[1+(t_C+\Delta)(1/e)]\sum_{\alpha_1}I_{\alpha_1}F_{\alpha_1}\}(1/e)H'.\quad(83)$$

Equation (82) is consequently split into three parts:

$$T=T_\pi+T_S+T_a,$$
$$T_\pi=[1+(t_C+\Delta)(1/e)]H',$$
$$T_S=[1+(t_C+\Delta)(1/e)]\sum_{\alpha_1}I_{\alpha_1}F_{\alpha_1}(1/e)H',$$
$$T_a=RF(1/e)H'.\quad(84)$$

To find the cross section for producing a meson which is neither absorbed nor scattered inelastically, we need just T_π. For a transition to a state of nuclear excitation I, this is

$$\langle I|T_\pi|A\rangle=\langle I|1+(t_C+\Delta)(1/e)|I\rangle\langle I|H'|A\rangle.\quad(85)$$

According to the arguments advanced in the Introduction (that the meson "outruns" nuclear excitation), we can replace $\langle I|\cdots|I\rangle$ in Eq. (85) by $\langle|\cdots|\rangle$, or the average with respect to the ground state of the nucleus. The transition operator for "elastic" photomeson production is now

$$(Iq|T_\pi|A\gamma)=(\lambda_q,\Omega_C{}^{(-)\dagger}\langle I|H'|A\rangle),\quad(86)$$

where

$$\Omega_C{}^{(-)\dagger}=1+(t_C+\Delta)(1/e),\quad(87)$$

and λ_q is a plane wave. Recalling the wave function ϕ_q given by Eq. (63), we define

$$\phi_q{}^{(-)}=\Omega_C{}^{(-)}\lambda_q,\quad(88)$$

as another "coherent scattering" wave function. By approximation II, $\phi_q{}^{(-)}$ is related to ϕ_q by

$$\phi_q{}^{(-)}=\phi_{-q}{}^*\quad(89)$$

("$-q$" means $-\mathbf{q}$). Equation (86) thus can be expressed as

$$(Iq|T_\pi|A\gamma)=(\phi_q{}^{(-)},\langle I|H'|A\rangle).\quad(90)$$

For the sake of illustration, let us assume that [Eq. (1)] the photomesons are produced into S-states (not unreasonable for charged mesons) and that

$$H'\simeq\sum_l\delta(\mathbf{Z}-\mathbf{Z}_l)N_l\quad(91)$$

in a coordinate representation. Then

$$\sigma_\pi=4\pi(2\pi)^4qq_0S\sum_l|(Iq|T_\pi|A\gamma)|^2$$
$$=A\sigma_f\frac{1}{V_A}\int_{V_A}d^3x|\phi_q{}^{(-)}(x)|^2,\quad(92)$$

if we keep only the diagonal terms in the sum over l [Eq. (91)] in Eq. (92). Uniform nuclear density is

[29] See, for instance, Eq. (6.37) of Lax's paper (reference 24).

assumed here. Equation (92) is more general than is apparent from the simplifying assumptions made [such as Eq. (91)]. If there were neither scattering nor absorption, $|\phi_q^{(-)}|^2=1$, so Eq. (92) would agree with Eq. (7).

(It might be emphasized that we need not of course have summed our cross sections over meson charge states, but could have written separate cross sections for the three meson charge states. The equations were written as given in order to save enumeration of the individual cross sections.)

One-half the probability that the meson is absorbed is obtained from

$$P_a\equiv\pi\langle T_a{}^\dagger\delta(E_A-H_0)T_a\rangle$$
$$=\pi\langle H'(1/e^\dagger)F^\dagger R\delta(E_A-H_0)RF(1/e)H'\rangle. \quad (93)$$

Writing $F=1+(1/e)\sum_{\alpha_1}I_{\alpha_1}F_{\alpha_1}\equiv 1+(F-1)$, and neglecting the small contribution from the cross terms (which are essentially "incoherent"), P_a becomes

$$P_a=\langle H'(1/e^\dagger)\Delta_0(1/e)H'\rangle$$
$$+\langle H'(1/e^\dagger)(F^\dagger-1)\Delta_0(F-1)(1/e)H'\rangle. \quad (94)$$

We have replaced $\pi R\delta(E_A-H_0)R$ by Δ_0 in Eq. (94).

Similarly, one-half the probability that the meson is scattered inelastically before getting outside the nucleus is

$$P_S\equiv\pi\langle T_S{}^\dagger\delta(E_A-H_0)T_S\rangle. \quad (95)$$

T_S is given by Eq. (84). An evaluation of P_a or P_S would involve a discussion of the multiple scattering in some detail. This might be approximated, for instance, by the methods leading to Eq. (81). On the other hand, the sum of P_a and P_S is relatively simple. $2(P_a+P_S)$ is the probability that the meson is either scattered inelastically or absorbed. For want of a better name, we shall call $2(P_S+P_a)$ the probability for "star production," since it is expected to correspond to considerable nuclear excitation. To evaluate P_S+P_a, we first simplify Eq. (95). Now,

$$\pi\delta(E_A-H_0)=\tfrac{1}{2}i(1/a-1/a^\dagger). \quad (96)$$

Using this relation, we obtain after some algebra [see Eq. (87)]:

$$\pi\Omega_C{}^{(-)}\delta(E_A-H_0)\Omega_C{}^{(-)\dagger}=\tfrac{1}{2}i\{(1/e-1/e^\dagger)$$
$$+(1/e^\dagger)[t_C{}^\dagger+\Delta^\dagger-(t_C+\Delta)](1/e)\}, \quad (97)$$

which occurs in Eq. (95). We assume that approximation I or II is valid, so [see Eq. (64)]

$$\tfrac{1}{2}i[t_C{}^\dagger+\Delta^\dagger-(t_C+\Delta)]=\mathrm{Im}(t_C)-\Delta_0. \quad (98)$$

Then

$$P_S=\sum_{\alpha_1,\alpha_2}\tfrac{1}{2}i\langle H'(1/e^\dagger)F_{\alpha_1}{}^\dagger I_{\alpha_1}{}^\dagger(1/e-1/e^\dagger)I_{\alpha_2}F_{\alpha_2}(1/e)H'\rangle$$
$$+\langle H'(1/e^\dagger)(F^\dagger-1)[\mathrm{Im}(t_C)-\Delta_0](F-1)(1/e)H'\rangle. \quad (99)$$

The major contribution to the first term above comes from the terms for which $\alpha_1=\alpha_2$ (in the double summation) and will be the coherent (i.e., diagonal in the nuclear coordinates) part of

$$\tfrac{1}{2}iI_{\alpha_1}{}^\dagger(1/e-1/e^\dagger)I_{\alpha_1}\simeq\pi I_{\alpha_1}{}^\dagger\delta(E_A-H_0)I_{\alpha_1}, \quad (100)$$

since $1/e$ can be replaced by $1/a$ for essentially the same reason that $t_a\simeq t_a'$ [Eq. (55)]. F_{α_1} operating to the left on a coherent quantity can be replaced by F, for reasons discussed in connection with Eq. (66). The coherent part of Eq. (100) when summed over α_1 becomes $(-1)\mathrm{Im}(t_C)$. Thus, the first term of Eq. (99) is

$$-\langle H'(1/e^\dagger)F^\dagger[\mathrm{Im}(t_C)]F(1/e)H'\rangle.$$

Replacing F by $1+(F-1)$ and neglecting the "incoherent" cross terms, we see that the part bilinear in $(F-1)$ is canceled by the corresponding term involving "$\mathrm{Im}t_C$" in the second half of Eq. (99). On adding P_S and P_a, the Δ_0 term in Eq. (99) cancels the corresponding term in Eq. (94) to give

$$P_S+P_a=\langle H'(1/e^\dagger)[\Delta_0-\mathrm{Im}(t_C)](1/e)H'\rangle, \quad (101)$$

in which the complex functions F do not appear.

The cross section for "star formation" is

$$\sigma_{\mathrm{star}}=2(2\pi)^3(P_S+P_a). \quad (102)$$

A straightforward evaluation along the lines of the analysis leading to Eq. (78) (using approximation I for the propagation functions, $1/e$) gives

$$\sigma_{\mathrm{star}}=A\sigma_f(1-f_a), \quad (103)$$

where σ_f is defined in connection with Eq. (7). The function f_a was given by Eq. (6) of reference 15 and goes to zero as $A^{-\frac{1}{3}}$ for large nuclei. A similar analysis, using approximation I, of the "elastic" photoproduction leads to

$$\sigma_\pi=A\sigma_f f_a \quad (104)$$

in agreement with Eq. (5) of reference 15. Comparison with Eq. (92) shows that in approximation I, f_a and the average of $|\phi_q^{(-)}(x)|^2$ over the nucleus, are identical. We notice that the sum of σ_π and σ_{star} is equal to Eq. (7). This is proved more generally below.

B. General Relationships between the Cross Sections

We shall continue to assume that approximation I or II is valid. Then one-half the probability for "elastic" meson production is

$$P_\pi\equiv\pi\langle T_\pi{}^\dagger\delta(E_A-H_0)T_\pi\rangle$$
$$=\tfrac{1}{2}i\langle H'(1/e-1/e^\dagger)H'\rangle$$
$$+\langle H'(1/e^\dagger)[\mathrm{Im}(t_C)-\Delta_0](1/e)H'\rangle, \quad (105)$$

using Eq. (84) for T_π and Eqs. (97) and (98). Then, using Eq. (101),

$$P_\pi+P_S+P_a=\tfrac{1}{2}i\langle H'(1/e-1/e^\dagger)H'\rangle. \quad (106)$$

If only the diagonal terms in the sum over nucleons are kept in Eq. (106), $1/e$ can be replaced by $1/a$, as in

Eq. (100). By Eq. (96), we then obtain

$$P_\pi+P_S+P_a=\pi\langle H'\delta(E_A-H_0)H'\rangle, \quad (107)$$

or, in the notation of Eqs. (103) and (104),

$$\sigma_{\text{total}}=A\sigma_f. \quad (108)$$

This result depends upon the use of Eq. (98) which holds only in approximations I and II.

Corresponding to a true absorption process, there must be elastic scattering. In the present case this is the elastic scattering of photons by the entire nucleus. From Eqs. (33′) and (82), it is seen that the transition operator for this is

$$T_\gamma=H'F(1/e)H'. \quad (109)$$

The coherent (and diagonal) part of T_γ is

$$\begin{aligned}\langle T_\gamma\rangle&=\langle H'F(1/e)H'\rangle\\ &\simeq\langle H'(1/e)H'\rangle\\ &=\tfrac{1}{2}\langle H'(1/e+1/e^\dagger)H'\rangle+\tfrac{1}{2}\langle H'(1/e-1/e^\dagger)H'\rangle, \quad (110)\end{aligned}$$

[neglecting $(F-1)$, as before]. Comparing with Eq. (106), we have

$$\text{Im}\langle T_\gamma\rangle=-[P_\pi+P_S+P_a] \quad (111)$$

in agreement with the corresponding general theorem[16] relating the scattering amplitude in the forward direction to the total scattering.

It should be observed that the functions F which describe the real complexity of multiple scattering phenomena have not appeared in the final results of the problems considered in this section. This is because we have asked only the simplest questions of the theory—i.e., we have studied just total cross sections and coherent phenomena. Had we studied the multiple scattering in detail (for instance, had we sought the angular and energy distribution of the emitted mesons), then the greater complexity of the F's would have been called for.

V. FINAL COMMENTS

We have confined applications of the theory largely to a derivation of the conventional "optical models." Since the discussion has been rather formal, it appears worthwhile to review the approximations involved and to consider the possibility of improving these.

Phenomenological interactions, V and R, were introduced to describe the meson scattering and absorption. We can suppose these to have been derived from a field theory by solving the one meson—one nucleon problem to find V. R can be imagined to be the leading term left over which is not diagonal in the meson occupation numbers.

Equations (56) are rigorous (but formal) solutions to Eq. (39). The solution for Ω given by Eq. (47) is also a rigorous solution to the Schrödinger equation.

The second of Eqs. (56) represents a set of A coupled integral equations. When the number of scatterers A is small it would appear feasible to attack these directly. On the other hand, when A is large the form (69) for Ω_S seems to be more useful. As is shown in Appendix A the error involved in this expression for Ω_S is of the order of A^{-1} times Ω_S. In Appendix B it is shown that Eq. (69) is valid for all values of A if the individual scatterings can be treated in the Born approximation. The fact that either of these two independent conditions is sufficient to insure the validity of Eq. (69) suggests that the error in this equation may be less than we have estimated it to be.

For a detailed study of the inelastic scattering the diffusion equation (81) provides probably the simplest approach, but is of limited validity in that it involves approximation I. A straightforward approach using Eqs. (69) and (70) is feasible if the multiplicity of the scatterings is small, and if one can either neglect the excitation energy of the nucleus or assume that it is that of a plane wave state of the struck nucleon.[30]

The optical model [Eq. (63)] is obtainable directly from Eqs. (69) and (70) if the effects of correlation between nucleon positions are neglected. Lax[31] has shown that a correction for these effects can be obtained by modifying $(t_C+\Delta)$ by a numerical factor. Using Eq. (69), such correlations arise from the coherent contribution from $(F-1)$.[32] The correlations may be taken into account exactly in the optical model, as will be shown in a subsequent publication in which a quantitative study of this model will be made.

It would thus seem that the optical model has considerable validity for the analysis of meson phenomena in complex nuclei. In this connection the term "optical model" is somewhat ambiguous. This ambiguity arises in connection with our approximations I, II, and III [Eq. (28)]. Approximation III takes into account the variation of the matrix elements of $(t_C+\Delta)$ for scatterings off the energy shell. The mean free path seems to be sufficiently long, however, that this is probably not a very important correction. On the other hand, Lederman *et al.*[2] and Steinberger[3] have found considerable differences between approximations I and II. In the analysis of their data they found that approximation II implies a mean free path for interaction which is about twice as large as that obtained from approximation I. We thus are led to expect that approximation II is fairly reliable, but that approximation I is of limited applicability.

---

[30] E. Henley, Phys. Rev. **85**, 204 (1952).
[31] M. Lax, Phys. Rev. **85**, 621 (1952).
[32] For instance,

$$\left(q''\left|\left\langle I_{\alpha_1}\frac{1}{e}I_{\alpha_2}\right\rangle\right|q\right)\simeq\delta(\mathbf{q}''-\mathbf{q})(2\pi)^3\int d^3q'\frac{t_{qq'}t_{q'q}}{\epsilon_q+i\eta-q_0'}$$
$$\times\int d^3Z_{\alpha_1}d^3Z_{\alpha_2}[P(Z_{\alpha_1},Z_{\alpha_2})-P(Z_{\alpha_1})P(Z_{\alpha_2})]$$
$$\times\exp[-i(q'-q)\cdot(\mathbf{Z}_{\alpha_1}-\mathbf{Z}_{\alpha_2})]$$

Here the P's are nucleon probability densities. In the absence of correlation this expression vanishes, since then $P(Z_{\alpha_1},Z_{\alpha_2})=P(Z_{\alpha_1})P(Z_{\alpha_2})$.

APPENDIX A

Remarks Concerning the Validity of Equation (69)

We wish to substitute Eq. (69) for Ω_S into Eq. (39) to see how well the latter equation is satisfied. However, a better solution is obtained if we modify the definition of t_α. Instead of using the definition given by Eq. (41), we shall in what follows assume that

$$t_\alpha = V_\alpha + V_\alpha \frac{1}{e - V_\alpha} V_\alpha. \tag{A-1}$$

The relation between the present t_α and the previous t_α is similar to that between the definitions given in Eqs. (40) and (41) [see also Eq. (55)].

The expression (69) for Ω_S is modified in that we suppose t_α now to be defined by Eq. (A-1). The physical interpretation of this is that the scattering amplitude is evaluated for the energy of the particle in the scattering medium.

If then the result of substituting Eq. (69) into the right-hand side of Eq. (30) is designated by $(\Omega_S)_1$, we have

$$\begin{aligned}(\Omega_S)_1 &\equiv 1 + (1/b) V \Omega_S \\ &= 1 + \frac{1}{b} V \left[1 + \frac{1}{e} \sum_{\alpha_1} I_{\alpha_1} F_{\alpha_1} \right] \left(1 + \frac{1}{e} t_C \right).\end{aligned} \tag{A-2}$$

Now,

$$\frac{1}{e} V \frac{1}{e} I_{\alpha_1} = \sum_{\alpha_0 \neq \alpha_1} V_{\alpha_0} \frac{1}{e} I_{\alpha_1} + V_{\alpha_1} \frac{1}{e} I_{\alpha_1}. \tag{A-3}$$

Expressing I_{α_1} in terms of t_{α_1}, and C by Eq. (65′), we obtain

$$\begin{aligned}\frac{1}{e} V_{\alpha_1} \frac{1}{e} I_{\alpha_1} &= V_{\alpha_1} \frac{1}{e} t_{\alpha_1} - V_{\alpha_1} \frac{1}{e} C \\ &= t_{\alpha_1} - V_{\alpha_1} - V_{\alpha_1} \frac{1}{e} C,\end{aligned} \tag{A-4}$$

using Eq. (45) with b replaced by e. (This is the reason for the definition (A-1) of t_α.) We note that

$$V + \sum_{\alpha_0, \alpha_1 (\alpha_0 \neq \alpha_1)} V_{\alpha_0} (1/e) I_{\alpha_1} F_{\alpha_1} - \sum_{\alpha_1} V_{\alpha_1} F_{\alpha_1} = 0 \tag{A-5}$$

These arise from the first part of the second term of Eq. (A-2), the first term of Eq. (A-3), and the second of Eq. (A-4).

Inserting the t_{α_1} term of Eq. (A-4) back into Eq. (A-2) and writing $t_{\alpha_1} = I_{\alpha_1} + C$, we obtain

$$\begin{aligned}\sum_{\alpha_1} (1/b) t_{\alpha_1} F_{\alpha_1} &= (1/b) t_C + (1/e) \sum_{\alpha_1} I_{\alpha_1} F_{\alpha_1} \\ &\quad + (1/A)(1/b - 1/e) \sum_{\alpha_1} I_{\alpha_1} F_{\alpha_1}.\end{aligned} \tag{A-6}$$

The last term of Eq. (A-4) becomes

$$\sum_{\alpha_1} V_{\alpha_1} (1/e) C F_{\alpha_1} = (1/A) \sum_{\alpha_1} V_{\alpha_1} (1/e) t_C F_{\alpha_1}. \tag{A-7}$$

By Eq. (76), $(1/e)t_C$ is expected to be of order unity. The quantities V_{α_1} and t_{α_1} can be assumed to be of the same order of magnitude, so Eq. (A-7) is of order $A^{-1}(\Omega_S)$. The same is true of the last term of Eq. (A-6). Finally,

$$1 + \frac{1}{b} \left(1 + \frac{1}{e} t_C \right) = 1 + \frac{1}{e} t_C. \tag{A-8}$$

Combining our results, we see that

$$(\Omega_S)_1 = \Omega_S + (1/A) \text{ times the order of } (\Omega_S). \tag{A-9}$$

Our modified form of Eq. (69) is thus seen to be a solution to the Schrödinger equation if A is large. In Appendix B it is shown that this solution (with a minor modification) holds independently of A if the Born approximation is valid—i.e., if $t_\alpha \simeq V_\alpha$.

APPENDIX B

The Born Approximation

The multiple scattering analysis is considerably simplified when the individual scattering processes can be treated in the Born approximation. For simplicity we assume only scattering without absorption, so the Hamiltonian is

$$H = H_0 + V. \tag{B-1}$$

As before,

$$V = \sum_\alpha V_\alpha. \tag{B-2}$$

Let the coherent part of V, that is $\langle V \rangle$, be called V_d. Then

$$V = \sum_\alpha v_\alpha + V_d, \tag{B-3}$$

where v_α is the "incoherent part" of V_α (i.e., is not diagonal with respect to the nuclear states). Then

$$\Omega = 1 + (1/a) V \Omega \tag{B-4}$$

is the integral equation for the scattering, where a is the same as previously.

Now define

$$\begin{aligned} f_\alpha &= v_\alpha (1/d_\alpha) v_\alpha, \\ F_\alpha &= \sum_{\beta \neq \alpha} f_\beta, \\ F &= F_\alpha + f_\alpha, \end{aligned}$$

and

$$\begin{aligned} d_\alpha &= a - F_\alpha - V_d. \\ d &= a - F - V_d. \end{aligned} \tag{B-5}$$

Then

$$\begin{aligned}\Omega = 1 + (1/d) V + \{ \sum_{(\alpha)} (1/d_{\alpha_1}) [v_{\alpha_1} + v_{\alpha_1} (1/d_{\alpha_2}) v_{\alpha_2} + \cdots \\ + v_{\alpha_2} (1/d_{\alpha_1}) v_{\alpha_2} \cdots (1/d_{\alpha_n}) v_{\alpha_n} + \cdots] \} (1/d) V.\end{aligned} \tag{B-6}$$

Here we use the same summation convention as was used for Eq. (42).

This is a rigorous formal solution to Eq. (B–4), as can be seen from substitution into the right-hand side of that equation. When we can apply the Born approximation to treat V_α as the inelastic scattering amplitude (i.e., set $v_\alpha = I_\alpha$) from the αth nucleon, we can also replace f_α in the energy denominators by

$$f_\alpha \simeq -i\pi\langle v_\alpha \delta(E_A - H_0) v_\alpha\rangle. \qquad \text{(B–7)}$$

Then $V_d + F_\alpha$ coincides with the t_C used in the text [except that $\mathrm{Im}(t_C)$ is corrected by a factor of $(1-A^{-1})$], and the equivalence of Eq. (B–6) to Eq. (69) readily follows.

PHYSICAL REVIEW VOLUME 89, NUMBER 3 FEBRUARY 1, 1953

A Quasi-Relativistic Theory of Gravitation

MARVIN G. MOORE
Mathematics Department, Bradley University, Peoria, Illinois
(Received August 31, 1951)

Rays of gravitons, as well as rays of photons in a gravitational field, have transverse vibrations, and a light ray has its velocity decreased by the presence of a gravitational ray. The decrease is twice as much when they are traveling in the same direction as when they are perpendicular (and, therefore, share one dimension of vibration rather than two). Introduction of a harmonic function for the square of the velocity of light leads to Schwarzschild's equation for, first, a light ray, and then, by way of its electromagnetic field, for a particle of matter. If the sun is moving through the ether, the action of the field is relativistic, except that the angle between the light ray and the gravitational ray is measured with respect to the ether. The acceptance of Miller's ether drift data would lead, then, to perturbations of the planets, including the major part of that observed in the nodes of Venus.

1. INTRODUCTION

WE introduce here a theory of the interaction of gravitons and photons which leads to results very similar to those of the general theory of relativity. If we take the gravitational field of the sun to be stationary, the departure from Einstein's equations is especially small, and, in particular, his three well-known results must follow. Our theory leads naturally to the view, however, that motion of the field through space has significance for gravitational phenomena and gives new results dependent on the direction and magnitude of such motion.

Since ether drift is to play an important role in our theory, we consider past experiments which have given indications of the magnitude and direction of such a drift.

It is not generally realized that the fringe shifts of the Michelson-Morley experiment were not believed by all experimenters to be negligibly small, and that Morley and Miller, and then Miller alone, continued the work carefully and repeatedly over a period of 30 years. The results were still small, but the variation in the direction of the effect as the earth moved in its orbit led Miller finally to reach the definite conclusion that the solar system is moving through the ether with a velocity of 208 km/sec toward a point in the southern sky with right ascension 4 hr, 54 min and declination $-70° 33'$.[1]

It is possible that Miller's results may prove to be spurious, especially in view of their apparent contradiction of those of other experimenters, particularly Joos and Kennedy. It is also possible, however, that the differences in design (and perhaps in method) made Miller's interferometers better able to detect his effect. Miller himself has suggested that others might have obtained positive results if they had sought to analyze their small fringe-shifts in terms of direction in the detailed manner in which he did his own. The question of the admissibility of Miller's evidence is considered by informed opinion to be still open, and, in view of the unsettled situation, our use of it in the present paper must be considered to be highly speculative.

It may be well to recall here that the special theory of relativity has discarded the ether, or privileged frame of reference, not because of any lack of compatibility, but only because such an ether is without value to the special theory.[2]

2. THE STATIONARY GRAVITATIONAL FIELD

For simplicity, we consider the sun to be concentrated at a point which is stationary in the ether. We further suppose that the gravitons of its field, moving in rays directed out from and in toward the sun, decrease the velocity of photons through an interaction of the transverse vibrations which we find it convenient to associate with the two types of elementary particles. We suppose further that the velocity of a plane-polar-

[1] D. C. Miller, Revs. Modern Phys. **5**, 203 (1933). Miller includes accounts of several similar experiments by others, including Joos and Kennedy. See also N. Rosen, Phys. Rev. **57**, 154 (1940), where the idea is presented that motion with respect to the stars may be responsible for the Miller effect.

[2] See R. B. Lindsay, Sci. Monthly **67**, 50 (1948). Also R. B. Lindsay and H. Margenau, *Foundations of Physics* (John Wiley and Sons, Inc., New York, 1936), p. 354, where reference is made to work by Page and Sparrow connected with the Miller effect.

ized ray of light is reduced only if there is a vibration of a gravitational ray along the perpendicular to the plane of polarization.

If the plane of polarization is perpendicular to a gravitational ray, then, there is no gravitational effect on a polarized ray, while the full effect is registered if the plane contains the gravitational ray.

We suppose that the square of the velocity of light is a harmonic function. Then we may write

$$r^2(d\theta/dt)^2+(dr/dt)^2=c^2(1-4m/r) \tag{1}$$

for a ray A whose plane of polarization passes through the sun. Rewriting Eq. (1),

$$c^2dt^2=r^2d\theta^2/(1-4m/r)+dr^2/(1-4m/r), \tag{2}$$

and applying Fermat's principle,

$$\int dt=\min, \tag{3}$$

we find that the ray follows a hyperbolic path past the sun, the total bending being just twice that indicated by Newton's law of gravitation if mc^2 is taken as the gravitational constant for the sun.

For a ray B whose plane of polarization is perpendicular to that of A, the corresponding equation is

$$c^2dt^2=r^2d\theta^2+dr^2/(1-4m/r), \tag{4}$$

and the application of (3) again leads to a total bending of twice that indicated by Newton's law, although the path is no longer hyperbolic.

There seems now to be a real possibility that gravitation may be capable of breaking up a light ray into two plane-polarized components. Experiment would seem to be incapable, at the present time, of detecting the effect.

If it is possible to combine A and B into one unpolarized ray, we note that the potentials associated with the mutually perpendicular directions indicated by dr and $d\theta$ are the arithmetic means of those occurring in (2) and (4), so that we are led to the equation

$$c^2dt^2=r^2d\theta^2/(1-2m/r)+dr^2/(1-4m/r),$$

or, for m/r small,

$$c^2dt^2=r^2d\theta^2/(1-2m/r)+dr^2/(1-2m/r)^2, \tag{5}$$

which is Schwarzschild's equation for a light ray in the general theory of relativity. If A and B refuse to cohere into one ray, we still find it convenient to describe their average behavior by (5).

Whether we use Eqs. (2) and (4) separately or employ (5) alone to represent a light ray grazing the sun, we arrive at the result obtained by the general theory of relativity; i.e., if we suppose the time between two points of the path of a ray to be a minimum, our ray must bend through an angle of 1.75″.

We are indebted to Schwarzschild for the knowledge that an observer moving with a particle would detect no local acceleration of the rays of its electromagnetic field if the rays were governed by (5) and (3) and if he moved according to the equation

$$ds^2=c^2(1-2m/r)dt^2-r^2d\theta^2-dr^2/(1-2m/r), \tag{6}$$

where $\int ds$ is a maximum; i.e., if he thought of space and time measurements as made up according to (6) and did not accelerate with respect to the resulting frame. Employing (6), we are then led to the same rotation of the perihelion of Mercury and red shift of the spectral lines in a gravitational field as given by the general theory of relativity.

Before leaving the case of the stationary field, let us consider the speed v of a light ray still further. From (5) to a sufficiently close approximation,

$$v^2=c^2[1-(2m/r)(1+\cos^2\tau)],$$

where τ is the angle between the radius vector from the sun and the direction of the light ray. Holding τ constant and differentiating,

$$vdv/dr=(mc^2/r^2)(1+\cos^2\tau),$$

or, approximately,

$$dv/dr=(mc/r^2)(1+\cos^2\tau)$$

and

$$dv/dt=(mc^2/r^2)(1+\cos^2\tau)\cos\tau. \tag{7}$$

As has been pointed out by Schwarzschild and Levi-Civita, the rate of change of the velocity of a light ray in (5) can be thought of as caused by a curvature of space and a curvature of time. From our viewpoint, these are nothing more than convenient ways of referring to changes of the speed of light as related to change in direction (relative to the gravitational rays) and change in position, respectively. Without space curvature, the gradient of v (with τ constant) is independent of τ, while absence of both curvatures implies a zero gradient. The space curvature factor plays no part in the larger effect given by Newton's law or in the slowing of the apparent time flow observed in the gravitational field of a heavy star, but is responsible for the departure of Mercury's orbit from an ellipse, and accounts for the part of the bending of the light ray not suggested by Newton's law.

We may further describe the situation as follows: if a light pulse is sent out in all directions from the center of a small spherical mirror in a gravitational field, the rays will not be returned simultaneously to the center without both an adjustment of the form and an acceleration of the mirror. The change in shape is required by the space curvature, while the acceleration is demanded by the curvature of time.

We shall be interested in the time curvature factor in the next section, and in the alteration of its direction caused by the ether drift.

3. THE FIELD IN MOTION

We have been considering the sun as stationary in the ether and have obtained results which will not be greatly modified by its motion through that medium.

With the sun in motion, we again think of the gravitons as going out and in with the velocity of light. As a result, a light ray is slowed by gravitons whose directions of motion have been altered by the motion of the field, and the directions of photons associated with a particle of matter have also changed. We suppose the gravitational field to be completely relativistic except for the effect of these changes in direction on the angles between the light rays and the gravitational rays, and we shall wish next to determine the resulting shift in direction of the acceleration of the particle or planet in the field.

In Eq. (7) we have focused attention on the rates of change of the speeds of the light rays going in different directions through a point, thus arriving at a method of examining the space curvature. It is the factor $1+\cos^2\tau$ which is associated with this curvature and must then be eliminated by a transformation before we arrive at the correct expression for the acceleration of the particle.

Distance in the direction $\tau=\frac{1}{2}\pi$ is unaffected by the transformation. We take it to be still unchanged when the field is moving. We thus suppose that it is a shear, rather than a rotation, of the deformation represented by the factor $1+\cos^2\tau$ which must enter our calculations. We are led to such a supposition, of course, through considerations of changes in the velocity of light.

Each direction will here be considered separately, and an angle of shear τ_0 will be determined from the equation

$$[1+\cos^2(\tau+\Delta\tau)]\cos\tau=[1+\cos^2(\tau+\tau_0)]\cos(\tau+\tau_0), \quad (8)$$

where $\Delta\tau$ is the change in τ produced by the ether drift. The left side of (8) represents the component of the deformation factor $1+\cos^2(\tau+\Delta\tau)$ in the direction $\tau=0$. The right side expresses the idea that this arises from a shear of the deformation factor $1+\cos^2\tau$. Solving for the small angle τ_0,

$$\tau_0=2\cos^2\tau\Delta\tau/(1+3\cos^2\tau).$$

We may conveniently think of τ_0 as the shift in the fixed direction $\tau=0$ of our transformation, and note that it depends on both τ and $\Delta\tau$. However, following the spherical mirror analogy, we take opposite rays in combination, never considering space measurement in terms of a single ray. We later make allowance for this in setting up our integrals.

The acceleration perpendicular to the radius vector (from the sun) and in the plane of the angle τ becomes after the reduction in acceleration in the radial direction

TABLE I.

	α	β	γ
Mercury	23.35	44.30	201.7
Venus	36.05	10.78	204.7
Earth	20.96	15.60	206.3
Mars	−31.93	9.25	205.3

TABLE II. Final discordances in the secular motions of Mercury and Venus.

Mercury	Newcomb	Explained by Einstein	Explained by Q-rel.	Final discordance Einstein	Final discordance Q-rel.
$D_t\varepsilon$	−0.88″ ±0.50″	0″	−0.55″	−2.6 P.E.	−0.97 P.E.
$eD_t\pi$	8.48 ±0.43	8.84	8.05	−1.2	1.5
$D_t i$	0.38 ±0.80	0	0.21	0.70	0.31
$\sin i D_t\Omega$	0.61 ±0.52	0	0.94	1.7	−0.94
Venus					
$D_t\varepsilon$	0.21 ±0.31	0	−0.23	1.01	2.1
$eD_t\pi$	−0.05 ±0.25	0.06	−0.01	−0.65	−0.25
$D_t i$	0.38 ±0.33	0	0.14	1.7	1.1
$\sin i D_t\Omega$	0.60 ±0.17	0	0.38	5.24	1.9

(and not perpendicular to it)

$$(mc^2/r^2)[\tau_0-\tau_0(1+\cos^2\tau)]=-(mc^2/r^2)\tau_0\cos^2\tau$$
$$=-2(mc^2/r^2)\Delta\tau\cos^4\tau/(1+3\cos^2\tau). \quad (9)$$

To find the angle $\Delta\tau$, we first employ the Lorentz equations to calculate the increment $\Delta\varphi$ added to the angle φ between a ray and the direction of the solar system through the ether by motion through that medium. It follows that for velocity v

$$\sin(\varphi+\Delta\varphi)=\frac{\sin\varphi(1-v^2/c^2)^{\frac{1}{2}}}{1-(v/c)\cos\varphi},$$

$$\cos(\varphi+\Delta\varphi)=\frac{\cos\varphi-v/c}{1-(v/c)\cos\varphi}, \quad (10)$$

$$\sin\Delta\varphi=-(v/c)\sin\varphi+\tfrac{1}{2}(v^2/c^2)\sin\varphi\cos\varphi.$$

Considering the rotation of the gravitational rays alone and taking the angles τ and ψ to be spherical coordinates, with $\tau=\frac{1}{2}\pi-\varphi_0$ and $\psi=0$ in the direction of motion of the sun, we find the acceleration of the planet perpendicular to the radial direction, and in the plane of the radius and drift, to be

$$\frac{mv^2\sin\varphi_0\cos\varphi_0}{4\pi r^2}\int_0^{2\pi}\cos^2\psi\int_0^{\pi}\frac{2\cos^4\tau\sin\tau d\tau d\psi}{1+3\cos^2\tau}$$
$$=0.0336(mv^2/r^2)\sin\varphi_0\cos\varphi_0. \quad (11)$$

This is directed toward the plane through the sun and perpendicular to the drift.

When we consider the rotation of the light rays associated with the planet, taking

$$Q=\cos\tau\cos\varphi_0\cos\psi+\sin\varphi_0\sin\tau,$$

we find that the change in the angle τ may be written

$$\Delta\tau=-Q\csc\varphi\Delta\varphi-\tfrac{1}{2}\cot\varphi(Q^2\csc^2\varphi-1)(\Delta\varphi)^2.$$

Applying Eqs. (9) and (10), we find a second acceleration to combine with (11). It is

$$\frac{mc^2}{2\pi r^2}\int_0^{2\pi}\int_0^{\pi}\frac{\cos^4\tau}{1+3\cos^2\tau}\left[\frac{v}{c}Q+\frac{1}{2}\frac{v^2}{c^2}(\sin^2\varphi\cot\tau - Q^2\cot\tau - Q\cos\varphi)\right]\cos(\psi+\Delta\psi)\sin\tau d\tau d\psi$$

$$=\frac{4mv^2}{\pi r^2}\sin\varphi_0\cos\varphi_0\int_0^{\pi/2}\int_0^{\pi/2}\frac{\cos^4\tau}{1+3\cos^2\tau}\times(\tfrac{1}{2}\cos 2\tau\cos^2\psi+\sin^2\psi)\sin\tau d\tau d\psi$$

$$=0.0779(mv^2/r^2)\sin\varphi_0\cos\varphi_0. \quad (12)$$

If the motion of the planet in its orbit is neglected, the acceleration (12) is directed oppositely to that in (11). Appropriate modifications must be made, however, because of the change in direction of the motion of the planet through the ether caused by its orbital velocity.

As mentioned earlier, Miller obtained a velocity for the ether with respect to the sun of 208 kilometers per second away from the point in the southern sky with right ascension 4 hr 54 min and declination $-70°\,33'$. Taking α to be the component of the ether velocity along the line of apsides from aphelion to perihelion, β the component in the plane of the orbit 90° to the east, and γ the component perpendicular to the orbit plane, we set up Table I.

The employment of Miller's data in conjunction with the results of our calculations as given in (11) and (12) leads to the numerical results given in Table II, where they are compared with the corresponding ones springing from Einstein's general theory, as well as with the irregularities to be accounted for, as given in Newcomb's well-known table.

The probable errors are obtained by multiplying the mean errors given in Table II by the factor 0.6745.

$D_t\pi$ for Mercury, according to our quasi relativity, is 39.1″ per century, which is closer to Leverrier's 38.3″ than to Newcomb's 41.24″. Newcomb's value not only contains an error of 1″ (which, after correction, would change the 1.5 in our last column to 2.3), but is only one of several values obtained by Newcomb at different times. Grossmann goes as far as to suggest that the correct value may be as small as 34″, while Chazy,[3] after analyzing the situation, suggests that the uncertainty is from $\frac{1}{10}$ to $\frac{1}{5}$ of the value. There has, then, been ample justification for the authors who have given the disturbance as "about 40 seconds per century."

Since the above was written, our attention has been called to some results obtained by Clemence,[4] who has made estimates of the motions of the perihelia of Mercury and the earth designed to replace Newcomb's. For Mercury he gives a motion of 42.56″ per century with a probable error of 0.94″. Adoption of this result would replace the number 1.5 in the last column of Table II by 4.1, implying a need for further examination of our theory, especially as it pertains to perihelia and eccentricities. There is considerably greater complexity here than in the treatment of the nodes and inclinations, so that the implication can hardly be ignored.

We have made no allowance for any error in Miller's data. Each of our final discrepancies, as obtained from Newcomb's results, is thus an even smaller proportion of the probable error then indicated in Table II. If we accept Miller's own estimates of his errors, however, a rough calculation shows that each of the numbers in the last column of Table II should be numerically decreased by not more than 0.1. It is possible, of course, to accept his general conclusions while still believing that unknown factors may have increased his error.

The theory of errors requires that, for a large number, half the errors be greater than the probable error, while an eighth must be greater than about 2.3 times the probable error. It is, then, in quite satisfactory agreement with the last column of Table II. The error of 4.1 P.E. mentioned above in connection with Clemence would, on the contrary, be expected once in 175 cases, while the 5.24 P.E. occurring in the next to the last column should be met only once in 2400.

[3] Jean Chazy, *La Theorie de la Relativité et la Mécanique Céleste* (Gauthier-Villars, Paris, 1928), Tome 1.

[4] G. M. Clemence, Revs. Modern Phys. **19**, 361 (1947).

Pion-Nucleon Scattering When the Coupling Is Weak and Extended*

GEOFFREY F. CHEW
Department of Physics, University of Illinois, Urbana, Illinois, and Brookhaven National Laboratory, Upton, New York
(Received October 20, 1952)

The symmetrical pseudoscalar meson theory, with an extended pseudovecto coupling to the nucleon and neglect of nucleon recoil effects, is shown to be capable of explaining the existing data on the P-wave pion-nucleon scattering. The required sizes of the source radius and coupling constant correspond to a relatively weak pion-nucleon coupling, but reactive effects in the scattering are nevertheless so important that the lowest order approximation in a perturbation treatment is completely inadequate. The Dancoff approximation, on the other hand, is accurate to within 10 or 20 percent.

THE point-coupling *perturbation* theory prediction for the symmetrical pseudoscalar pion-nucleon P-wave scattering phase shifts can be stated as follows:

$$\alpha_{33}=2y, \quad \alpha_{13}=\alpha_{31}=-y, \quad \alpha_{11}=-4y, \tag{1}$$

where

$$y=\tfrac{2}{3}(f^2/\mu^2)(k_0^3/\omega_0), \tag{2}$$

if k_0, ω_0, and μ are the momentum, total energy, and mass, respectively, of the pion, and f is the pion-nucleon coupling constant. The first phase shift subscript refers to $2T$ and the second to $2J$, if T and J are the total isotopic and ordinary angular momenta, respectively. Nucleon recoil has been neglected so that S and D scattering is ignored in this discussion. The purpose of this note is to point out that the formulas (1), (2), based on a second-order perturbation calculation, do not necessarily represent a correct evaluation of the theory even when the coupling is weak, so that their failure to agree with experiment is no indication that a weak coupling approach is invalid. Indeed, a straightforward correction of the most obvious defects of (1), (2) leads to theoretical predictions in good agreement with experiment.

In the first place, the above formulas correspond to a point interaction between pion and nucleon. With neglect of nucleon recoil, such a theory does not exist in any sense. It is absolutely necessary to spread out the region of interaction, or in other words to introduce a cutoff in momentum space, in order that the theory be meaningful. The extended source or cutoff in familiar in strong coupling theory,[1] but it is just as necessary in weak coupling if the nucleon is to be held fixed. An immediate result of introducing a cutoff is to replace the function $y(k)$ by

$$x(k)=v(k)y(k), \tag{2'}$$

where $v(k)$ is the cut-off factor, i.e., the Fourier transform of the source function. ($v(k)$ is usually taken to be a monotonically decreasing function of k, normalized to unity at $k=0$.) A much more important consequence of the cutoff, however, is that it allows an evaluation of higher order effects in the scattering. Such an evaluation[2] shows that even under conditions of coupling normally characterized as "weak," that is, $f^2/\mu a \ll 1$, where a is the source "radius," it is possible for reactive effects in the scattering to be extremely important. This situation comes about because of higher order intermediate states containing only a single pion. When the single intermediate pion has an energy close to that of the incident one, the associated energy denominator becomes very small and the size of the higher order term anomalously large. The contribution of terms in which the intermediate energy is *exactly* equal to the incident energy is sometimes called the Heitler damping.[3] These terms can be taken into account by replacing each of the phase shifts in formulas (1) by its tangent. As is well known, however, the Heitler damping terms are out of phase with the first-order terms, so that the "in phase" contribution of terms near but not on the energy shell can be equally if not more important.

To calculate the reaction due to higher order one-pion states, the Dancoff approximation[4] is appropriate. In its application to pion-nucleon scattering, one neglects configurations containing three or more pions but treats the zero, one, and two pion problem "exactly." Such a procedure leads to an integral equation, which is to be discussed in a forthcoming paper by Lee and Christian.[5] In the case of interest here, i.e., when $f^2/\mu a \ll 1$, this equation is closely equivalent to an extremely simple problem: the scattering of a pion by a velocity and spin-dependent potential, the matrix elements of which are just the usual second order scattering matrix elements calculated without damping. It will be recognized that this result is analogous to the widely used procedure of using as the nucleon-nucleon potential an operator whose matrix elements are given by a weak coupling meson theory calculation without reaction.

The results of the calculation of the "potential" scattering of pions are as follows[6]:

* This research was supported by the Office of Naval Research and Atomic Energy Commission.

[1] See, for example, W. Pauli, *Meson Theory of Nuclear Forces* (Interscience Publishers, Inc., New York, 1946), p. 12.

[2] J. S. Blair and G. F. Chew (to be published).

[3] W. Heitler, Proc. Cambridge Phil. Soc. **37**, 291 (1941); also see M. L. Goldberger, Phys. Rev. **84**, 929 (1951) for a recent discussion of the Heitler damping.

[4] S. M. Dancoff, Phys. Rev. **78**, 382 (1950).

[5] T. D. Lee and R. Christian (to be published).

[6] The formulas (1′) are based on a variational principle which will be discussed in a forthcoming paper by Chew and Low. In the

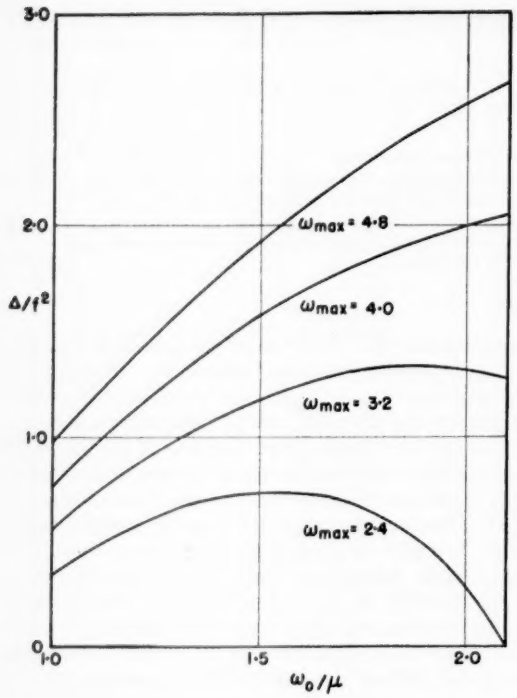

FIG. 1. The reaction function, Δ/f^2, as a function of ω_0 for a "square" cut-off factor. The cutoff occurs at a pion energy denoted by ω_{max}.

$$\tan\alpha_{33}=2x/(1-2\Delta),$$

$$\left.\begin{matrix}\tan\alpha_{31}\\ \tan\alpha_{13}\end{matrix}\right\}=-x/(1+\Delta), \qquad (1')$$

$$\tan\alpha_{11}=-4x/(1+4\Delta),$$

where

$$\Delta=\frac{2}{3\pi}\frac{f^2}{\mu^2}\int_\mu^\infty d\omega\frac{k^3}{\omega^2}\frac{\omega_0}{\omega-\omega_0}v^2(k); \qquad (3)$$

the principal value of the integral is to be taken. The coupling constant, f, is to be assigned its renormalized value, in the conventional sense of perturbation theory.

For fairly low values of ω_0, the quantity Δ is positive, so that if Δ can be as large as 0.2 the violent disagreement with experiment of the nondamped results can be removed, that is, α_{33} can become substantially larger than α_{11} in absolute value. If Δ were as large as 0.5, there would be a "resonance" in the $\frac{3}{2}$, $\frac{3}{2}$ state as was proposed by Brueckner[7] on the basis of strong coupling results. The possibility of a resonance in this one state can be traced to the sign of the nondamped phase shifts (1). The only positive phase shift is α_{33}, showing that only in the $\frac{3}{2}$, $\frac{3}{2}$ state is the "potential" effectively attractive.

In Fig. 1, the quantity Δ/f^2 is plotted as a function of ω_0 for a "square" cut-off factor, i.e., $v(k)=1$ for $k<k_{max}$, $v(k)=0$ for $k>k_{max}$. Four different values of $\omega_{max}=(k_{max}^2+\mu^2)^{\frac{1}{2}}$ are shown. Definite values of f^2 and ω_{max} were fixed by the experimentally measured total cross sections for the scattering of positive and negative pions by protons.[8–10] Choosing $f^2=0.2$ and $\omega_{max}=3.2\mu$ gives the fit shown in Fig. 2, which seems satisfactory.[11] Since S and D scattering is ignored in the preliminary calculations, a detailed fit to the angular distribution (which depends much more on the S and D phase shifts than does the total cross section) has not yet been attempted. However, it has been verified that the main features, except for the asymmetry about 90°, are correctly given. An attempt is now being made to include the S and D scattering in a simple way.

It remains to be checked that the required values of f^2 and k_{max} satisfy the requirement that 3-pion and higher configurations are actually unimportant. The direct perturbation calculation[2] shows that fourth-order contributions of this kind tend to increase α_{33} and decrease α_{11} still further, but the effect is only 10 percent in the former case and 20 percent in the latter (at 135 Mev). α_{13} and α_{31} are both increased by 6 percent.

The fact that ω_{max} is considerably less than the nucleon rest energy means that our nonrelativistic treatment of the nucleon has been justified *a posteriori*. A lack of important nucleon recoil effects has also been outstanding in the observed anomalous electromagnetic properties of single nucleons, i.e., the anomalous magnetic moments and the photopion production cross

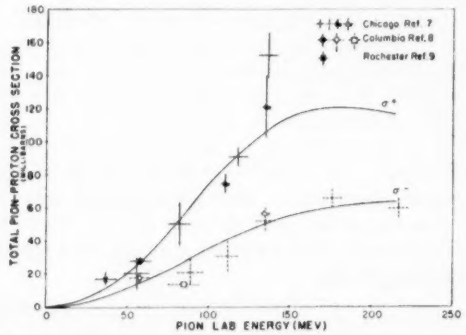

FIG. 2. Comparison of theory with the experimental pion-proton total cross sections. The solid crosses are the positive pion and the dashed crosses the negative pion experimental values.

present application the accuracy of these formulas is believed to be better than 10 percent.

[7] K. Brueckner, Phys. Rev. **86**, 106 (1952).

[8] Anderson, Fermi, Long, Martin, and Nagle, Phys. Rev. **85**, 934 and 936 (1952); Anderson, Fermi, Nagle, and Yodh, Phys. Rev. **86**, 793 (1952).

[9] Chedester, Isaacs, Sachs, and Steinberger, Phys. Rev. **82**, 958 (1951); Isaacs, Sachs, and Steinberger, Phys. Rev. **85**, 803 (1952).

[10] Barnes, Clark, Perry, and Angell, Phys. Rev. **87**, 669 (1952).

[11] In our computations, we have taken ω_0 equal to the pion energy in the center-of-mass system.

sections.[12] It is perhaps worth mentioning at this point, therefore, that the absolute value of the *mesonic* contribution to the nucleon magnetic moments, given by the above values for f^2 and k_{max} is 1.8 nuclear magnetons.[13] An analysis of the photopion production problem, as well as the neutron-electron interaction, is proceeding on the same basis.

In conclusion, it should be emphasized that even if the success of the calculations reported here is not accidental, the particular form of the Yukawa theory (e.g., pseudoscalar or pseudovector coupling) has by no means been established. *Any theory with a coupling linear in the pion field, which has a nonrelativistic limit for the nucleon,* will lead to the results described here.

The author is indebted to R. Serber and T. D. Lee for the idea of using the Dancoff approximation. Discussion with J. S. Blair, K. Brueckner, and N. Kroll also contributed significantly to the progress of the problem. Complete details of the calculations reported here, together with applications of the same general approach to other problems, will be published at a later time.

[12] J. S. Blair and G. F. Chew, Ann. Rev. Nuc. Sci. **2** (1952).
[13] M. H. Friedman (to be published).

PHYSICAL REVIEW VOLUME 89, NUMBER 3 FEBRUARY 1, 1953

Heat Conduction of the Boundary Layer in Liquid Helium II*

DAVID WHITE, O. D. GONZALES, AND H. L. JOHNSTON
Department of Chemistry, Ohio State University, Columbus, Ohio
(Received August 18, 1952)

In experiments on the thermal conductivity of liquid helium II, an anomalous heat conduction has been found in the vicinity of the heat source. The magnitude of this effect is given as a function of temperature and is shown to be independent of the heat flux. The effect has been ascribed to a thin layer of liquid helium in the vicinity of the energy source having a poor heat conduction. The existence of this layer is probably a consequence of the finite rate of conversion from superfluid to normal particles.

AN investigation carried out in this laboratory[1] on the thermal conductivity of liquid helium II and He^3–He^4 mixtures yielded, in the former case, anomalously low values of heat conduction without the characteristic maximum between 1.2°K and the λ-point. The apparatus used in this connection (solid lines in Fig. 1) consisted of a thin-walled Monel capillary, 0.01-cm inner diameter and 17.5 cm long, with the lower end embedded 0.635 cm in a copper block on which were wound a heater and phosphor bronze thermometer. After exit through the vacuum jacket, the capillary passed through another copper block in contact with a liquid helium bath. The observed temperature differences between these two blocks were used to calculate the values of thermal conductivity. In order to determine unambiguously that the low results arose from an end effect originating in the heat input wall, the measurements were repeated with the following changes:

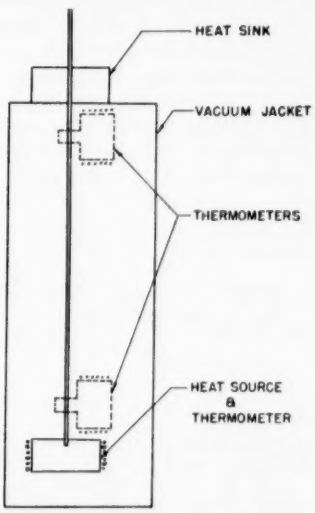

FIG. 1. Diagram of apparatus.

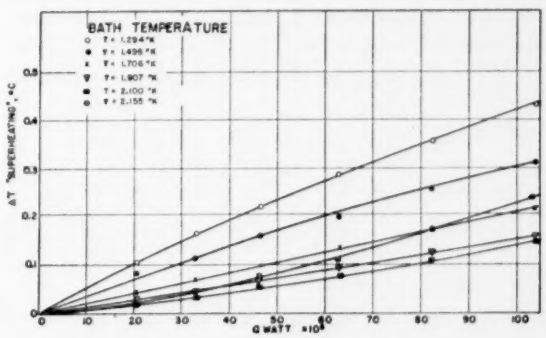

FIG. 2. "Superheating", ΔT, as a function of energy input Q and temperature T.

* This work was supported in part by the Office of Naval Research under contract with the Ohio State University Research Foundation.
[1] R. E. Probst, Massachusetts Institute of Technology Low Temperature Conference (1949), unpublished.

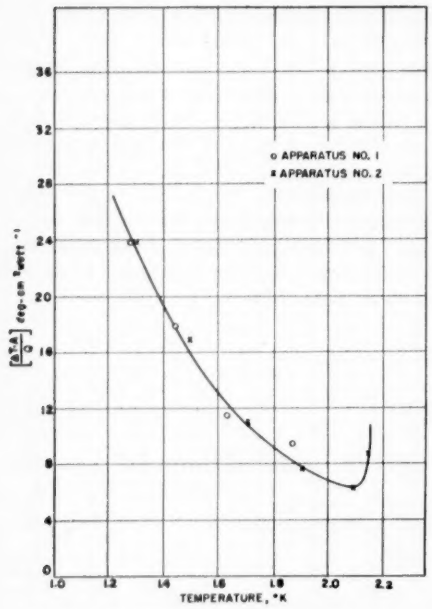

FIG. 3. $\Delta T \cdot A/Q$ as a function of temperature.

(a) adding two thermometer stations (dotted lines, Fig. 1) 1 cm from the heat source and the heat sink, and (b) changing the area of contact of the capillary with the heat source by embedding it, in a second series of experiments, only 0.079 cm in the lower copper block.

When ΔT's are measured by the two thermometer stations, shown by the dotted lines for various energy inputs at various temperatures, no anamolous thermal conductivity is found, and the data so obtained are very similar to those of Allen and Ganz.[2] However, a large temperature difference between the energy input block and the thermometer station 1 cm above it was still noticed. This "superheating" is shown in Fig. 2 as a function of energy input and temperature for the case where the capillary was embedded 0.079 cm. The plot of ΔT *versus* Q gives almost straight lines except at the highest temperatures. Assuming these are straight lines for every temperature, a plot of $\Delta T \cdot A/Q$ *versus* temperature is shown in Fig. 3 for the two series of experiments where the capillary was embedded (1) 0.635 cm and (2) 0.079 cm. A is the inner area of the capillary, and hence also of liquid helium, in contact with the energy input block. Since the data of both sets of experiments fall on the same curve, this indicates that the "superheating" must arise from this area of liquid helium in contact with the heat source. An examination of the magnitude of the effect verifies the above, since this excludes the possibility of the "superheating" arising across the boundary between the heater and the copper block, the copper block itself, or the wall of the Monel capillary. It must be then the result of a film of poorly conducting helium.

The dependence of $Q/\Delta T \cdot A$ on temperature is as $T^{2.6}$, if one excludes the point very near the λ-point. These results are very similar in magnitude and temperature dependence to those reported by Kapitza[3] for a similar series of experiments. He ascribed the effect to the low thermal conductivity of helium II which does not take part in mass transfer. Assuming a static layer of liquid helium II in our case, one can calculate the film thickness. Using the extrapolated thermal conductivity of normal helium for the thermal conductivity of the film, one gets a thickness of 2.5×10^{-4} cm at 2.0°K. This film is thicker by several orders of magnitudes than either the Rollin film or a static film produced by absorption on the wall.

The manner in which this film is formed and the question as to whether the thickness remains constant cannot be quantitatively deduced from these experiments. Since it is well known that some of the conversion of superfluid atoms to normal atoms takes place at the energy input wall, it is probable, as Gorter[4] has already pointed out, that the film results from a finite conversion rate. If this mechanism is correct, Gorter predicts that this effect will cause the attenuation of second sound, with a relaxation time of approximately 5×10^{-5} sec near the λ-point. This is not inconsistant with existing experimental results. It should also be interesting to repeat these experiments using different capillary sizes. One should expect the magnitude of this effect to vary, since the rate of heat transfer, and hence the amount of conversion at the wall, varies with capillary size.

[2] J. F. Allen and E. Ganz, Proc. Roy. Soc. (London) **A171**, 242 (1939).

[3] P. Kapitza, J. Phys. U.S.S.R. **4**, 181 (1941).

[4] C. S. Gorter, Proceedings of the International Conference on Low Temperature Physics, Oxford, August, 1951.

Nuclear Gyromagnetic Ratios. IV*

YU TING AND DUDLEY WILLIAMS
Department of Physics, Ohio State University, Columbus, Ohio
(Received October 16, 1952)

The super-regenerative oscillator techniques described in earlier reports have been employed to observe nuclear magnetic resonance absorption by B^{10}, N^{14}, Cl^{35}, Cl^{37}, As^{75}, In^{113}, In^{115}, and Bi^{209}. Nuclear g factors and magnetic moments of these nuclei are tabulated for comparison with corresponding values obtained by other techniques.

EARLIER reports from this laboratory[1–3] have described super-regenerative oscillator techniques for observing nuclear magnetic resonance phenomena. The present paper gives a resume of results obtained on nuclear species not treated in the earlier papers.

The apparatus employed in the present study was essentially the same as that reported earlier[3] except for certain improvements in electronic circuitry. These improvements include the use of a cascode preamplifier[4] between the radiofrequency circuit and the narrow-band amplifier and the use of a phase-sensitive detector between the narrow-band amplifier and the chart recorder. The introduction of these new amplifier units has resulted in the improvement of signal to noise ratios by a factor of at least 4.

In Table I are listed the observed ratios of resonance frequencies of various nuclei in the same applied magnetic field. Each value listed in the table is the mean of at least ten independent determinations. The uncertainties given are the systematic errors involved in the instrumentation and in the matching of resonance line centers in the somewhat complicated line patterns given by the super-regenerative techniques.[5] Although the side bands may be well resolved in the chart displays for the unknown and the "standard" nuclei, it is necessary that the operating conditions of the oscillator be the same for the two nuclei. In the case of each resonance listed in the table, the statistically most probable error is smaller than the indicated systematic error.

In three of the samples listed in Table I small amounts of magnetic catalysts have been used. Although the use of catalysts may produce slight shifts in resonance frequency,[6] it was found necessary to employ catalysts in those three cases in order to obtain similar line shapes for comparison purposes in the standard and the unknown. In all cases catalyst concentration was very low, and on the basis of Dickinson's studies it can be assumed that any shifts in resonance frequency result in uncertainties smaller than those listed in Table I.

The "standard" nuclei used in the present study are D^2, Sc^{45}, and Rb^{85}. The ratios of the resonance frequencies of these secondary standards to the proton frequency are given in Table II.[7–10]

In order to compare the present experimental results with those of other workers, it is desirable to express all results as ratios of resonance frequencies to the resonance frequency of the proton in the same applied magnetic field. This has been done, and these ratios are shown in Table III.[2,11–14]

Brief comments on the results obtained for the various nuclear species are given below:

The agreement between the present results for B^{10} and the early results of Bitter[11] is excellent. Of the two values of the ratio obtained in the present work, the value based on Rb^{85} is believed to be more accurate, since the Rb^{85} frequency is closer to the B^{10} frequency and since the Rb^{85} line shape is somewhat better than the line shape obtained for D^2.

The values for N^{14} and Cl^{35} are in excellent agreement with values obtained by Proctor and Yu[12]; the Cl^{37} ratio obtained in the present study is slightly higher,

TABLE I. Resonance frequency ratios.

Nuclei compared	Resonance frequency ratio	Samples (aqueous solutions)
B^{10} to D^2	0.700065±0.00007	$Na_2B_2O_4$, $D_2O+NiCl_2$
B^{10} to Rb^{85}	1.11282 ±0.00005	$Na_2B_2O_4$, RbCl
N^{14} to Rb^{85}	0.74837 ±0.00004	HNO_3, RbCl
Cl^{35} to Rb^{85}	1.01481 ±0.00005	LiCl, RbCl
Cl^{37} to Rb^{85}	0.84477 ±0.00005	LiCl, RbCl
Cl^{35} to Cl^{37}	1.20128 ±0.00006	LiCl
As^{75} to D^2	1.11569 ±0.00005	Na_2HAsO_4+NaOH, $D_2O+NiCl_2$
In^{115} to In^{113}	1.00213 ±0.00004	$In(NO_3)_3$
In^{115} to Sc^{45}	0.901877±0.00005	$In(NO_3)_3+Mn(NO_3)_2$, $ScCl_3$
Bi^{209} to D^2	1.04684 ±0.00005	$Bi(NO_3)_3$, D_2O

* This work has been supported by a contract between Wright Air Development Center, Flight Research Laboratory, and the Ohio State University Research Foundation.

[1] J. R. Zimmerman and D. Williams, Phys. Rev. **76**, 350 (1949).
[2] W. H. Chambers and D. Williams, Phys. Rev. **76**, 638 (1949).
[3] R. E. Sheriff and D. Williams, Phys. Rev. **82**, 651 (1951).
[4] Wallman, MacNee, and Gadsden, Proc. Inst. Radio Engrs. **36**, 700 (1948).
[5] A detailed discussion of line shapes will be published elsewhere.
[6] W. C. Dickinson, Phys. Rev. **81**, 717 (1951).
[7] G. Lindstrom, Phys Rev. **78**, 817 (1950).
[8] Smaller, Yasaitis, and Anderson, Phys. Rev. **80**, 137 (1950).
[9] D. M. Hunten, Phys. Rev. **78**, 806 (1950).
[10] E. Yasaitis and B. Smaller, Phys. Rev. **82**, 750 (1951).
[11] F. Bitter, Phys. Rev. **75**, 1326 (1949).
[12] W. G. Procter and F. C. Yu, Phys. Rev. **81**, 20 (1951).
[13] S. S. Dharmatti and H. E. Weaver, Jr., Phys. Rev. **84**, 367 (1951).
[14] Jeffries, Loeliger, and Staub, Phys. Rev. **85**, 478 (1952).

TABLE II. Resonances used as standards.

Ratio[a]	Resonance frequency ratio used as standard
D^2 to H^1	0.153506
Sc^{45} to H^1	0.242939±0.000003
Rb^{85} to H^1	0.0965521

[a] The value for the D^2/H^1 ratio is taken from Lindstrom (see reference 7) and Smaller, *et al.* (see reference 8); Hunten's Sc^{45}/H^1 ratio (see reference 9) is assumed; the Rb^{85}/H^1 ratio is based on the work of Yasaitis and Smaller. (See reference 10.)

but agrees with the Proctor-Yu measurement within experimental errors.

The As^{75} ratio obtained in the present work is slightly higher than the value obtained by Dharmatti and Weaver[13] and slightly lower than the ratio obtained by Jeffries, Loeliger, and Staub.[14] However, the three ratios agree within the limits of experimental error.

The ratios of the In^{113} and In^{115} to the proton frequency as obtained in the present study are slightly lower than the Proctor-Yu[12] values but agree within the limits of error.

The Bi^{209} ratio is in excellent agreement with the value obtained by Proctor and Yu.[12] It might be remarked that several determinations of the Cl^{35}/Cl^{37} and In^{115}/In^{113} frequency ratios were made in the present investigation. The present value of 1.20128 ±0.00006 for the Cl^{35}/Cl^{37} ratio is in agreement with the Proctor-Yu value[12] of 1.2014±0.0001, and with the recent value 1.2013±0.0001 obtained by Watkins and Pound.[15] The In^{115}/In^{113} frequency ratio of 1.00213 ±0.00004 checks closely with the ratio 1.0021±0.001 obtained by Proctor and Yu.[12] It might be noted that, since $I=\frac{3}{2}$ for both Cl^{35} and Cl^{37} and $I=9/2$ for both In^{113} and In^{115}, the above frequency ratios are also the ratios of the magnetic moments for the pairs of isotopes.

The values of nuclear g factor cannot be determined directly from the observed frequency ratios since, owing to the diamagnetic effects of atomic electrons, the local fields at the nuclei being compared may be slightly different even though the applied fields may be the same.

TABLE III. Ratios of nuclear resonance frequency to the proton frequency in the same magnetic field.

Nucleus	Sample	Ratio	Uncertainty (percent)	Intermediate standard	Reference
B^{10}	$Na_2B_2O_4$	0.107464	±0.010	D^2	Present study
	$Na_2B_2O_4$	0.107445	0.005	Rb^{85}	
		0.10745	0.04	B^{11}	11
N^{14}	HNO_3	0.072257	0.005	Rb^{85}	Present study
	HNO_3	0.072255	0.010	D^2	12
Cl^{35}	LiCl	0.097982	0.005	Rb^{85}	Present study
	HCl	0.097978	0.010	D^2	12
	LiCl	0.09799	0.07		2
Cl^{37}	LiCl	0.081564	0.007	Rb^{85}	Present study
	HCl	0.081553	0.014	Cl^{35}	12
As^{75}	Na_2HAsO_4 +NaOH	0.171265	0.005	D^2	Present study
	Na_2HAsO_4 +NaOH	0.17125	0.030	Na^{23}	13
	Na_3AsO_4 +NaOH	0.17129	0.018		14
also	Na_3AsS_4				
In^{113}	$In(NO_3)_3$	0.21863	0.010	In^{115}	Present study
	$In(NO_3)_3$	0.21865	0.014	Na^{23}	12
In^{115}	$In(NO_3)_3$ +cat	0.219101	0.006	Sc^{45}	Present study
	$In(NO_3)_3$	0.21911	0.014	Na^{23}	12
Bi^{209}	$Bi(NO_3)_3$	0.160696	0.006	D^2	Present study
	$Bi(NO_3)_3$	0.16069	0.010	D^2	12

TABLE IV. Nuclear g values and nuclear magnetic moments.

Nucleus	Diamagnetic correction	Nuclear g value	Spin (I)	Nuclear magnetic moment
B^{10}	1.00017	0.60033±0.00006[a]	3	1.80099±0.00018[a]
		0.60022±0.00005	3	1.80066±0.00015
N^{14}	1.00028	0.40369±0.00003	1	0.40369±0.00003
Cl^{35}	1.00110	0.54786±0.00003	3/2	0.82180±0.00005
Cl^{37}	1.00110	0.45606±0.00003	3/2	0.68410±0.00005
As^{75}	1.00284	0.95929±0.00005	3/2	1.43893±0.00008
In^{113}	1.00490	1.2272 ±0.0001	9/2	5.5222 ±0.0005
In^{115}	1.00490	1.22976±0.00008	9/2	5.5339 ±0.0004
Bi^{209}	1.0104	0.90689±0.00008	9/2	4.0810 ±0.0004

[a] Uncertainties in diamagnetic corrections are not included.

However, by applying the Lamb diamagnetic correction,[16] one can obtain g factors in terms of the proton g factor. In Table IV are listed the g factors and nuclear magnetic moments obtained from the present experimental measurements after application of the indicated diamagnetic correction on the basis of the proton moment $\mu=2.79268\pm0.00006$ nm obtained by Sommers, Thomas, and Hipple[17] and the values of nuclear spin I given in Mack's recent survey paper.[18]

The authors take pleasure in expressing their appreciation to Commander Forrest R. Biard for his assistance in the N^{14}, Cl^{37} and In^{115} measurements and to Edward Manring and Henry Cox for helpful discussions on instrumentation. This work was supported in part from funds granted to the Ohio State University by the Research Foundation for aid in fundamental research.

[15] G. D. Watkins and R. V. Pound, Phys. Rev. **82**, 343 (1951).
[16] W. E. Lamb, Phys. Rev. **60**, 817 (1941).
[17] Sommers, Thomas, and Hipple, Phys. Rev. **80**, 487 (1950).
[18] J. E. Mack, Revs. Modern Phys. **22**, 64 (1950).

PHYSICAL REVIEW VOLUME 89, NUMBER 3 FEBRUARY 1, 1953

Some Points of the Theory of Liquid Helium II

LOUIS GOLDSTEIN
University of California, Los Alamos Scientific Laboratory, Los Alamos, New Mexico
(Received September 22, 1952)

Some of the limitations of the hydrodynamic model of liquid He II are being studied in this paper. It is shown that the vortex or roton phase alone, without mutual interaction, undergoes a first-order phase change. The phonon-roton system does not have such a phase change if the zero-point energy or pressure is included explicitly in its formalism. In the high temperature or roton region the model has a normal state surface and does not account for the unusual equilibrium properties of liquid He II such as the anomalous expansion coefficient, the entropy increase and decrease in isothermal pressure and volume increases, respectively. The possibility of the abnormal liquid to become normal again at very low temperatures, where the entire thermal excitation is concentrated over the phonons, is briefly discussed.

I. INTRODUCTION

THE hydrodynamic model proposed by Landau[1] appears to be successful in describing in a fairly quantitative way some of the bulk properties of liquid He II when in equilibrium with its vapor. These are the specific heat, entropy, the superfluid-normal fluid division, and the associated velocity of propagation of temperature or second-sound waves. In order to obtain a better insight into its equilibrium properties, a more complete statistical thermodynamic study was made of the model. The approach is, however, heuristic throughout in so far as the basic assumptions concerning the distributions of the liquid atoms over the different types of states of motion are accepted as defining the model. A series of difficulties of a qualitative character will thus be disclosed in that temperature range where the phonon contribution to the equilibrium properties of the fluid is quite small or negligible in comparison with that due to the elementary vortices or rotons. A superposition of the distributions of both types of elementary excitations reduces somewhat the difficulties originating in the roton distribution alone, without eliminating them. It appears that the explicit use of the phonon type of zero-point energy or pressure is hereby necessary, while it has been consistently omitted so far from the formalism of the model. Throughout the temperature region, $1.0 \leqslant T \leqslant 2.19°\mathrm{K}$, the state surface of the model has a qualitatively different shape from the observed one. Recent experimental work[2] on the specific heat of liquid He II seems to confirm the existence of a practically pure phonon excitation region, at $T \leqslant 0.6°\mathrm{K}$. This temperature region will be discussed in view of the possibility that the equilibrium properties of the liquid may here become normal in contrast with the higher temperature or pretransition region which is anomalous with a negative volume expansion coefficient and anomalous isothermal entropy variations with volume or pressure. An experimental verification of this return to normalcy of liquid He II at low temperatures, though arduous, appears to be of great interest.

[1] L. D. Landau, J. Phys. (U.S.S.R.), **5**, 71 (1941).
[2] H. C. Kramers, Proc. Int. Conf. Low Temperature Phys., Oxford (1951); Kramers, Wasscher, and Gorter, Physica **18**, 329 (1952).

II. STATISTICAL THERMODYNAMICS OF THE ELEMENTARY VORTICES

In the present model, it will be assumed that the individual elementary vortex or roton spectrum is given by

$$\epsilon_r = \Delta + p_r^2/2\mu, \tag{1}$$

p_r denoting the linear momentum and μ the effective mass of the roton; Δ is, with μ, a second characteristic parameter of the model, the activation energy of the rotons. In statistical equilibrium, both μ and Δ are assumed to be constants, i.e., independent of the statistical variables. Their numerical values are to be derived empirically so as to obtain a good numerical fit in the description of the properties of the model. Since Δ turns out to be quite large in comparison with the temperatures in the He II range, it seems justified to consider the roton system as forming an ideal Maxwell-Boltzmann gas, in a first approximation, that is at low roton concentrations. Indeed, the number of rotons available, at equilibrium, in a state defined by the variables such as temperature, volume, or pressure, for instance, is a measure of the thermal excitation of the liquid. This number is thus a function of the variables of state, the temperature, among others. The number of rotons of the system not being an invariant means that the chemical potential or the Gibbs free energy per roton vanishes. Hence, the ideal roton distribution function over the states of the spectrum (1) at temperature T, in a volume V, is

$$d\nu_r = 4\pi(V/h^3)p_r^2 dp_r \exp(-\epsilon_r/kT). \tag{2}$$

The roton concentration $r(T)$, or the number of rotons per unit volume, depends thus uniquely on the temperature, and

$$r(T) = (2\pi\mu kT/h^2)^{\frac{1}{2}} \exp(-\Delta/kT). \tag{3}$$

An elementary calculation yields, with (1) and (2), the energy of the roton gas as

$$E_r(T, V) = \nu_r(T, V)\eta_r(T) = r(T)V(\tfrac{3}{2}kT + \Delta); \tag{4}$$

$\nu_r(T, V)$ or $r(T)V$ is the total number of rotons at temperature T in volume V, and $\eta_r(T)$, the mean thermal energy per roton, is the classical term $(\frac{3}{2}kT)$ augmented by the activation energy Δ.

The constant volume heat capacity of the system is thus

$$\begin{aligned} C_{V,r} &= (\partial E_r/\partial T)_V \\ &= \nu_r(T, V)k(\Delta/kT)^2[1+3(kT/\Delta)+(15/4)(kT/\Delta)^2] \\ &= \tfrac{3}{2}\nu_r(T, V)k+\eta_r(T)(\partial\nu_r/\partial T)_V, \end{aligned} \quad (5)$$

showing, with (4), that the heat capacity is the sum of the classical term and one originating in the change of the number of rotons. Their temperature rate of increase is, at constant volume, with (3),

$$\begin{aligned} (\partial\nu_r/\partial T)_V &= V(dr/dT) \\ &= [\nu_r(T, V)/T](\Delta/kT)[1+\tfrac{3}{2}(kT/\Delta)] \\ &= V(2\pi\mu kT/h^2)^{\frac{3}{2}}(\Delta/kT^2) \\ &\quad \times[1+\tfrac{3}{2}(kT/\Delta)]\exp(-\Delta/kT), \end{aligned} \quad (6)$$

which is exponential essentially.

In the present model the enrichment of the roton gas corresponds to the thermal excitation of the He atoms which are lifted from their lowest energy state into the high energy roton states. Since there are (μ/m) atoms per roton, m being the mass per helium atom, the activation energy per atom is $(m\Delta/\mu)$. One of the fundamental assumptions of the theory is that the nonexcited atoms are responsible for the superfluid properties of liquid He II. They thus form the superfluid component or phase and this is the reservoir of He atoms which, on thermal excitation, form the disordered roton or normal phase. The above assumption is the two-fluid hypothesis, according to which liquid He II is a mixed phase, the mixture of the superfluid and normal phases. Since for the moment we neglect the fraction of the excited atoms participating in compressional or longitudinal wave motions, the normal phase is formed by rotons.

The enrichment of the roton phase, at the expense of the superfluid phase, increases with temperature until this ordered phase is exhausted. The lowest temperature at which all the He atoms have been converted into the disordered phase is the transition temperature. Let T_0 be this temperature. Then T_0 is the root, asymptotically, of the equation

$$r(T_0) = n(T_0)(m/\mu) = (2\pi\mu kT_0/h^2)^{\frac{3}{2}}\exp(-\Delta/kT_0), \quad (7)$$

according to (3), and where $n(T_0)$ is the actual liquid He II atomic concentration at temperature T_0. This definition of the transition temperature is far from being precise. Before entering, however, into its discussion, we should like to complete briefly the description of the roton phase.

The entropy of the rotons is found to be, after an elementary calculation,

$$S_r(T, V) = \nu_r(T, V)(\Delta/T)[1+(5/2)(kT/\Delta)]. \quad (8)$$

The work function is

$$A_r(T, V) = E_r(T, V) - TS_r(T, V) = -\nu_r(T, V)kT. \quad (9)$$

Hence, the equation of state of the roton gas, to the approximation of the present treatment, is

$$\begin{aligned} p_r(T, V) &= -(\partial A_r/\partial V)_T \\ &= \nu_r(T, V)kT/V \\ &= r(T)kT \\ &= (2\pi\mu kT/h^2)^{\frac{3}{2}}kT\exp(-\Delta/kT), \end{aligned} \quad (10)$$

which is independent of the volume.

The asymptotic character of the equation of definition (7) lies in the fact that it takes no direct account of the difficulty arising from the rapid exponential increase of the roton concentration and the attendant breakdown in the "ideal" roton gas approximation. The lack of precision of the definition (7) is associated with the fact that to any value of the liquid concentration n the model supplies a transition temperature T_0, since (7) always has a single finite root for any n. Since the latter is taken to be an empirically determined constant, the $T_0(n)$ curve resulting from (7) has only a finite segment of physical significance. The limiting transition temperatures are defined by the two limiting atomic concentrations n_l and n_u, the lower and upper limits of concentrations at which the lambda-transitions are experimentally observed in liquid helium. It is seen at once that dT_0/dn is positive, i.e., the transition temperature increases with concentration. This variation of the transition temperature of the present model is similar to the one exhibited by the condensation temperature of different Bose-Einstein (B.E.) fluid models,[3] in contrast with the observed variation of the lambda temperatures of liquid He under pressures higher than its saturating vapor pressure.

The lack of precision in the definition of the transition, mentioned above, is also due to its being one-sided, inasmuch as the transformation can only be defined on its low temperature side. The present model being restricted to the He II range only, a complete definition of the transition line as the intersection of the state surfaces of liquid He II and liquid He I is outside the scope of the present theory. It is clear, however, that only through the geometrical properties of these surfaces in the vicinity of their intersection would the characteristic changes exhibited by the thermal properties of the liquid in crossing the transition be completely determined.

We return now to the discussion of the equation of state of the rotons, Eq. (10). It is seen that throughout the roton range the isobars coincide with the isothermals, the pressure being independent of the volume. In the ideal roton gas approximation the model behaves as a class of modified or nonideal B.E. fluids exhibiting

[3] L. Goldstein, J. Chem. Phys. **9**, 472 (1941).

coincident isothermals and isobars in their condensation region.[4]

We are now prepared to discuss fully the equilibrium properties of the hydrodynamic model. Clearly, the omission of the phonons has to be kept in mind, together with the asymptotic validity only of the roton approximation at the approach of the transition. The non-ideality of the roton gas limits thus the validity of the following discussion to temperatures not too close to the transition temperature.

Let us consider a constant pressure and constant temperature transformation of the fluid represented by the equation of state (10). Let this be associated with $(p, T, V_i) \rightarrow (p, T, V_f)$, and assume δV or $(V_f - V_i) > 0$. Since the roton concentration $r(T)$, defined by (4), is independent of the volume, the change in the total number of rotons, is

$$\delta \nu_r(T, V_i, V_f) = r(T)(V_f - V_i) = r(T)\delta V. \quad (11)$$

The energy which has to be supplied to the fluid in this transformation is

$$\delta E(p, T, V_i, V_f) = \int_{V_i}^{V_f} T(\partial p_r/\partial T)_V dV = T(dp_r/dT)\delta V, \quad (12)$$

since p_r is independent of the volume and depends only on the temperature. On the other hand, the entropy increase of the system is, with Eqs. (8) and (11), $(\partial S/\partial V)_T$ being (dp_r/dT),

$$\delta S_r(p, T, V_i, V_f) = r(T)\delta V(\Delta/T)[1 + (5/2)(kT/\Delta)]. \quad (13)$$

Hence, in this constant pressure, constant temperature transformation, the energy absorbed is

$$\delta E(p, T, V_i, V_f) = T\delta S_r = T(dp_r/dT)\delta V, \quad (12a)$$

as a direct calculation shows using the equation of state (10) together with (12) and (13). The preceding transformation with

$$(\partial p_r/\partial T)_V = (dp_r/dT) = (\partial S_r/\partial V)_T \quad (14)$$

being independent of the volume is strictly a first-order phase change, with a latent heat of roton production, per roton, being

$$l_r(p, T) = \delta E(p, T, \delta V)/\delta \nu_r(T, \delta V) = (5/2)kT + \Delta. \quad (15)$$

The equation of state (10) is thus associated with the high temperature phase of the two-phase region which exists below the transition line. To the present approximation, the low temperature or superfluid phase does not contribute to the pressure and is the source of the roton or high temperature phase. Strictly speaking, the preceding discussion is limited to such conditions where the mixed phase is present already. The properties of the superfluid phase remain undetermined because, to the present approximation, they do not enter into the equilibrium formalism of the model.

In the pressure-volume plane, the transition or saturation line is, with (7) and (10),

$$p_r(T_0) = (m/\mu)NkT_0/V, \quad (16)$$

i.e., an ideal gas hyperbola. The region of the (p, V) plane limited by this curve and the two axes is the transition region with coincident isothermals and isobars which are straight lines parallel to the volume axis. The model does not define that portion of the preceding region which should describe the superfluid phase. The transition region is further restricted by the finite arc of the critical hyperbola whose end points correspond to the observed limiting densities at which the transformation actually occurs. If n_1 and n_2 denote the smallest and largest atomic concentrations at which the transition is observed, then the effective length of the transition line is defined by

$$(m/\mu)n_1kT_{01} \leqslant p_r(T_0) \leqslant (m/\mu)n_2kT_{02}. \quad (17)$$

T_{01} and T_{02} are the lower and upper transition temperatures, respectively.

At any rate, the production of rotons in the present theory is equivalent to a first-order phase change, and liquid He II is represented here as an actual two-phase or mixed-phase system, the two phases being associated with He atoms distributed over different types of states of motion. Most transformations of the model are accompanied by interconversion of one phase into the other. The exceptions are provided by transformations proceeding along lines of constant roton "quality" x_r defined as the fraction of the roton phase or $r(T)/n(T)$, $n(T)$ being the mean atomic concentration at temperature T. These transformations are similar to those along constant "vapor quality" lines of the mixed liquid-vapor phases, for instance.

An immediate consequence of the equation of state (10) is the infinitely large constant pressure heat capacity as in ordinary mixed phase systems where the interconversion is a first-order phase change.

The preceding analysis of the equilibrium properties of the model shows that the claims made on the "second-order" character of the transition exhibited by it,[1] the phonon states of motion being entirely omitted, are not justified. Since the enrichment of the high temperature or roton phase was continuous, with increasing temperature, up to the presumed transition point, it was claimed that the transition was a second order one, involving no latent heat.[1] Furthermore, the jump in the specific heat at the transition temperature was claimed to be a consequence of the second-order phase change. However, in any mixed or two-phase system where the interconversion is of the first order, as is the case, to the present approximation, of the model, the

[4] L. Goldstein, J. Chem. Phys. **14**, 276 (1946). The above class of B.E. fluid models also includes those with the individual energy spectrum of the form $dn/dp = Ap^l$, p being the linear momentum of the fluid atoms, A and l being constants, $l \geq 2$. These models have been first considered by F. London, J. Phys. Chem. **43**, 49 (1939).

enrichment of one of the phases at the expense of the other is always continuous up to the transition line, where one of the phases has been exhausted. Also, the specific heat will undergo a discontinuity at the transition line, along almost any path which was followed in the approach of the transition line, with the exception of the constant entropy path and of the constant pressure path, along which the specific heat is infinite. We have proved,[4] in this connection, that modified or nonideal B.E. fluids, undergoing a normal first-order phase change, have a λ-point in their constant volume specific heat at the transition line. A complete statistical proof of the thermodynamic formula, of the Ehrenfest type,

$$\Delta C_V = -T(dV/dT)\Delta(\partial p/\partial T)_V; \quad \Delta x = x_+ - x_-, \quad (18)$$

has been given for such B.E. fluids undergoing first-order phase changes.[4] For normal fluids, the existence of constant volume specific heat λ-points at the saturation line has also been proved[4,5] to be given by Eq. (18). These λ-points are associated with constant volume transformations from the mixed phase (vapor+liquid) regions into the pure vapor phase, at volumes larger than the critical volume, $V > V_c$, or into the pure liquid phase at $V < V_c$. These thermodynamic results have been verified by us, indirectly, using the data on the constant volume specific heats of saturated liquid water and its saturated vapor, the temperature coefficient of the volume of the saturated phases together with the constant volume temperature coefficients of their pressures. A direct experimental verification of Eq. (18) has been performed recently on carbon dioxide,[6] both at $V < V_c$ and $V > V_c$.

The present studies thus prove, that as far as the roton gas approximation of liquid He II is concerned the model exhibits inconsistencies. These originate in the first-order character of the transformation undergone by the model and the ensuing infinite constant pressure heat capacity. To these one should add the incorrect trend of variation of the approximate transition temperatures as a function of the liquid density. This leads in turn to other difficulties which will be considered in the next section, where the roton and phonon excitations will be discussed simultaneously.

III. THE EQUATION OF STATE RESULTING FROM VORTICES AND COMPRESSIONAL WAVES

The liquid He II model postulates, beside the elementary vortices or rotons, the existence of thermal excitations whereby the atoms participate in quantized longitudinal or compressional type of wave motions or phonons. It is of interest that the longitudinal characteristic temperature Θ_L when computed directly using the plausible asymptotic low temperature value[7] of sound velocity s of 237 meters/sec, and the value n of the atomic concentration measured at the lowest temperature[8] of 2.18×10^{22} atoms/cm^3, is found to be

$$\Theta_L = (hs/k)(3n/4\pi)^{\frac{1}{3}} = 19.7^\circ\text{K}, \quad (19)$$

while the observed value,[2] which is necessarily uncertain at present because of the experimental difficulties at $T < 0.6^\circ$K, appears to be about 19°K. This agreement, which should be confirmed with improved specific heat measurements tends to justify the validity of the Debye picture of liquid He II at sufficiently low temperatures.

The low temperature formalism, $T \ll \theta$, of the Debye model applied to longitudinal phonons leads to the energy of agitation,

$$E_\varphi = \tfrac{3}{8}Nk\theta + (\pi^4/5)NkT(T/\theta)^3, \quad (20)$$

where θ is the longitudinal characteristic temperature and where the zero-point motion has been included. The phonon entropy is

$$S_\varphi = (4\pi^4/15)Nk(T/\theta)^3. \quad (21)$$

The work function is

$$A_\varphi = E_\varphi - TS_\varphi = \tfrac{3}{8}Nk\theta - (\pi^4/15)NkT(T/\theta)^3, \quad (22)$$

and the pressure

$$p_\varphi = -(\partial A_\varphi/\partial V)_T = \tfrac{1}{8}(Nk\theta/V) + (\pi^4/15)(NkT/V)(T/\theta)^3. \quad (23)$$

Here, explicit use has been made of the definition (19), giving $(-\theta/3V)$ for the partial derivative $(\partial\theta/\partial V)_T$. As a result, the pressure depends on the volume through the zero-point term alone. The total pressure of the phonon-roton system is then

$$p = p_\varphi + p_r, \quad (24)$$

the roton pressure p_r being given by (10). The volume dependence of the total pressure is now assured through the zero-point pressure. Had the latter been omitted, the phonon-roton system would have had coincident isothermals and isobars in the pressure-volume diagram. It should be noted here that θ depends on the volume only, to the present approximation. That is, at constant volume, θ is independent of the temperature only in this approximation, because the sound velocity s decreases first slowly and then at increasing rate at the approach of the λ-point. Up to the temperature closest to the λ-point where s was measured,[7] the maximum variation in s from its asymptotic low temperature limit amounts to about ten percent.[9]

The phonon-roton system cannot undergo constant

[5] L. Goldstein, J. Washington Acad. Sci. **40**, 97 (1950).
[6] A. Michels and J. C. Strijland, Physica **16**, 813 (1950).
[7] K. R. Atkins, Proc. Low Temp. Phys. Conference, Oxford (1951), p. 60.
[8] See the monograph of W. H. Keesom, *Helium* (Elsevier Publishing Company, Amsterdam, 1942) for the diagrams of state data.
[9] While the measurements in reference 7 have been made at a frequency of 14 megacycles/sec, unpublished measurements of H. L. Laquer, in this laboratory, at 5 Mc/sec show a similar decrease of s at the approach of the λ-point.

pressure-constant temperature transformations of the type $(T, p, V_i)\rightarrow(T, p, V_f)$ because it has no coincident isothermals and isobars. In the isothermal transformation $(T, p_i, V_i)\rightarrow(T, p_f, V_f)$, the energy absorbed is found to be

$$\delta E(T, p_i, V_i, p_f, V_f) = \Delta\{r(T)[1+(5/2)(kT/\Delta)] + (16/45)(kT/\Delta)(kT/hs)^3\}\delta V, \quad \delta V = V_f - V_i. \quad (25)$$

The roton term is the dominant one in the high temperature or the roton range. Clearly, the system does not exhibit anymore a first-order phase change. One can derive here easily the constant pressure heat capacity of the system. Using the thermodynamic relation, R being the ideal gas constant,

$$(C_p - C_V)/R = (T/nk)[(\partial p/\partial T)_V]^2 \times[-V(\partial p/\partial V)_T]^{-1}, \quad (26)$$

one finds in the roton range where

$$(\partial p_r/\partial T)_V \gg (\partial p_\varphi/\partial T)_V,$$

with

$$(\partial p/\partial T)_V = (\partial p_r/\partial T)_V = r(T)k(\Delta/kT)[1+(5/2)(kT/\Delta)], \quad (27)$$

and

$$-V(\partial p/\partial V)_T = \chi_T^{-1} = \tfrac{1}{6}nk\theta, \quad (28)$$

resulting from the zero-point pressure only, χ_T being the isothermal compressibility which, in the present model, is practically constant over the roton range where $n(T)$ varies only very slowly,

$$(C_p - C_V)/R \cong 6(r/n)^2(\Delta^2/k^2T\theta)[1+(5/2)(kT/\Delta)]^2. \quad (29)$$

Since one of the best choices of the parameters μ and Δ/k seems to be $8m$ and 8°K, respectively, the preceding formula yields about $(0.4R)$ for the molar heat capacity difference at the transition point where its validity is the most restricted. At lower temperatures, this difference decreases rapidly because of the exponential decrease of $r(T)$, Eq. (3). While still somewhat large, the heat capacity difference of $0.4R$ is some six percent of the heat capacity C_s of the liquid along the saturation line, at the λ-point. C_s should be quite close to C_p. Thus, the phonon-roton system has a constant pressure heat capacity rather close to its constant volume heat capacity provided that the zero-point motion is included into its formalism. Actually, the temperature dependent properties of the phonons are practically negligible in comparison with those of the rotons at $T \gtrsim 1.3$°K, but the inclusion of the zero-point properties of the system as a whole is indispensable for the elimination of the first-order character of the phase change of the rotons alone. One finds, nevertheless, that the compressibility $(nk\theta/6)^{-1}$ is considerably larger than the observed one. It is seen on the definition of θ_L, Eq. (19), that the latter is determined by all the atoms of the fluid, whether superfluid or not, and whether in the phonon or roton states of motion. This point should be further justified, since, *a priori*, it is not quite clear why all the atoms distributed over the different states of excitation should have the same zero-point energy, essentially the one of a linear harmonic oscillator.

We have already noted above, Sec. II, that the pure vortex model leads to a qualitatively incorrect variation of the transition temperature with liquid density, Eq. (7). The approximation involved in Eq. (7) concerns the ideality of the roton gas. The roton concentration increasing very rapidly at the approach of the transition, the ideality of the roton gas cannot be justified. While the superposition of the phonon and roton excitations eliminates the first-order transformation of the model, this does not help in correcting the qualitatively wrong variation of the transition temperature with density. It should be noted here that the one-sided definition of the transition is insufficient to prove that the phonon-roton system has a well-defined transformation of a second order. The lifting of the first-order phase change of the rotons has been proved above, while the order of the actual phase change of the phonon-roton system remains still undetermined.

Since the pressure depends on the volume through the zero-point pressure only, which to the present approximation does not depend on the temperature, one finds that

$$(\partial p/\partial T)_V = (\partial S/\partial V)_T = f(T) > 0, \quad (30)$$

which is a behavior opposite to the one observed[8] in liquid He II above 1.25°K. Not only does the model show the wrong temperature dependence of the pressure but its temperature coefficient is independent of the volume, as if it were a two-phase mixture with a first order type interconversion. Since $(\partial p/\partial T)_V$ or dp/dT is positive, the phonon-roton system also has a normal volume expansion coefficient or $(\partial V/\partial T)_p > 0$, again in contrast with the data at temperatures $T \gtrsim 1.25$°K, where the phon excitations play a rather minor role.

Another consequence of the formalism of the system is the wrong variation of the constant volume heat capacity with volume or density. Indeed,

$$(\partial C_V/\partial V)_T = T(\partial^2 p/T^2)_V = T(d^2p/dT^2) > 0, \quad (31)$$

while experimentally $(\partial C_V/\partial V)_T < 0$.

The preceding anomalies of the liquid He II are particularly emphasized when considering the entropy derivatives, $(\partial S/\partial V)_T$ equivalent to $(\partial p/\partial T)_V$, or $(-\partial S/\partial p)_T$ equivalent to $(\partial V/\partial T)_p$. In the temperature range under discussion, an isothermal volume increase decreases, while an isothermal pressure increase increases the entropy of liquid He II in utter contrast with the behavior of normal fluids. The state surface of the model in the (p, V, T), (S, V, T), or (S, p, T) spaces has thus a qualitatively different shape from that of the actual state surface of liquid He II. The phonon-roton system is thus most successful in repre-

senting with fair approximation some of the bulk properties of liquid He II in equilibrium with its vapor, that is along a single line of the state surface.

Having discussed some of the limitations of the hydrodynamic model in its description of the equilibrium properties of liquid He II, we should like to make two remarks on some possible improvements of the theory.

First of all, the equation of state should be completed by inclusion of a potential energy or pressure term associated with the static interaction of the He atoms in their position of equilibrium. This could be done along the same line as in the theory of the equation of state of ideal isotropic monatomic solids. The total energy would thus be

$$E=U(V)+E_\varphi(T)+E_r(T), \tag{32}$$

where $U(V)$ depends only on the volume, while E_φ and E_r are the thermal excitation energies of the phonons and rotons, respectively, Eqs. (20) and (4). The static pressure term p_s is $-\partial U/\partial V$, and the zero-point energy or pressure can then be included in $U(V)$ or p_s. However, such a static term does not help to reshape the state surface of the model. It does not enter into the expression of the entropy and, hence, the derivatives $(\partial S/\partial V)_T$, $(-\partial S/\partial p)_T$, or $(\partial p/\partial T)_V$ and $(\partial V/\partial T)_p$ remain the same as in the absence of $U(V)$.

In the high temperature or roton range, where, practically, the rotons determine alone the properties of the model, one has with (10),

$$(\partial p/\partial T)_V=r(T)k+kT(\partial r/\partial T)_V, \tag{33}$$

the second term on the right-hand side due to the temperature rate of increase of the roton concentration is here the dominant term. It is seen that an attempt to compensate for this term so as to make $(\partial p/\partial T)_V$ negative may require a rather drastic modification of the work function of the system. Such a modification seems to involve the roton phase, in some way, perhaps through their interaction. It appears that the incorrect state surface of the present model is to be ascribed partially, at least, to an incomplete treatment of the roton phase.

It is interesting to recall here a qualitative attempt by London,[10] within the framework of the Bose-Einstein theory of weakly interacting atoms, to explain the remarkable anomalies of liquid He II evidenced by the signs of the partial derivatives of the different state variables. The gas-like behavior was assumed and the anomalies appeared as resulting from a compromise between the opposing effects on the system of the ever attractive statistical forces and the ordinary interatomic repulsive forces at close distances.

So far, all observations of the characteristic anomalies of liquid He II have been limited to temperatures $T\gtrsim 1.0°\mathrm{K}$, which is the roton range of the present model. In this range, the equilibrium properties of the liquid appear, so to speak, tuned to the approaching anomaly of the transition, whereby the ordered or superfluid phase becomes completely exhausted. Most of the data on the equilibrium properties indicate that the anomalies become accentuated at the approach of the transition, while they become attenuated at the low temperature end of the interval more easily accessible to experimentation. At very low temperatures, $T\lesssim 0.5°\mathrm{K}$, or the phonon range, recent specific heat measurements,[2] together with those on second sound,[11] appear to vindicate the suggestion[1,12] that liquid He II is a Debye liquid with a superfluid phase. The quantization of the compressional waves appears here fully achieved in contrast with classical liquids. This suggests that the mean free path of the thermally excited compressional waves cannot become very much less than the dominant wavelength of these waves in the spectrum at these low temperatures.[13] Now, the equilibrium bulk properties of a Debye liquid exhibiting the T^3 law for the variation of its heat capacity could be expected to be normal, i.e., the derivatives $(\partial p/\partial T)_V$, $(\partial V/\partial T)_p$, or $(\partial S/\partial V)_T$ and $(-\partial S/\partial p)_T$ could become all positive. This means, that the pressure, at constant volume or density, should have a maximum, while the density, at constant pressure, should have a minimum, when represented as a function of the temperature, at $0.5°\mathrm{K}\lesssim T\lesssim 1.0°\mathrm{K}$. These extrema might, however, be quite broad. Also, the isothermal variations of the entropy should become normal. Liquids He II could thus approach the absolute zero as a normal system, exhibiting though the characteristic propagation of thermal or second sound waves because of the superfluid character of its ordered phase.

[10] F. London, J. Chem. Phys. **11**, 203 (1943).

[11] K. R. Atkins and D. V. Osborne, Phil. Mag. **41**, 1078 (1950).

[12] R. Bleaney and F. Simon, Trans. Faraday Soc. **35**, 1205 (1939); see L. Tisza, J. phys. et radium [8] **1**, 164, 350 (1940).

[13] This also suggests that the increasingly large absorption of sound waves down to about 1.2°K, observed by Atkins (see reference 7), has to change trend and may become normal to the phonon range.

High Energy Photoproton Production by 322-Mev Bremsstrahlung

J. W. ROSENGREN* AND J. M. DUDLEY
Radiation Laboratory, Department of Physics, University of California, Berkeley, California
(Received October 20, 1952)

The ejection of high energy protons from various materials by 322-Mev bremsstrahlung has been investigated using a detector telescope consisting of three liquid scintillators. Protons, above a minimum energy of 65 Mev, were distinguished from other particles by their dE/dx at a fixed range. At 70 Mev the angular distribution appears to be independent of nuclear complexity; the relative distributions from Li, C, and Ta have about the same shape. Distributions from C at 77, 127, and 174 Mev were measured between 11° and 45°. The data do not fit the predictions of a quasi-deuteron model, but adequate calculations require more knowledge of the deuteron photodissociation process. The yield at 45° for 72- and 142-Mev protons from various materials was found to be directly proportional to Z. The energy spectra of photoprotons from C have been measured at 45° and 90°. The absolute differential cross section for production of 72-Mev protons from C at 90° has been measured.

A STUDY has been made of the high energy photoprotons emitted from various targets when bombarded with the 322-Mev bremsstrahlung beam of the Berkeley synchrotron. The object was to extend to higher proton energies an earlier investigation made by Levinthal and Silverman[1] with the same beam. Recently, somewhat similar high energy measurements have been reported by Keck.[2]

Protons above a minimum energy of 65 Mev were detected with a counter telescope consisting of three liquid scintillators (terphenyl in toluene) viewed by RCA 1P21 photomultiplier tubes. This counter was constructed in cooperation with W. S. Gilbert and is described in a report of an investigation of the photodisintegration of the deuteron at high energies.[3] A particle's range was specified by demanding that it pass through the first counter and stop in the second. The protons were then distinguished from less heavily ionizing particles (e.g., mesons and electrons) by requiring a certain minimum pulse height in the first counter. By this method a deuteron would be recorded as a proton, but at the high energies investigated (corresponding to deuteron energies >90 Mev), it is doubtful that the deuteron contribution was appreciable. To vary the mean energy of the protons detected, copper absorbers were placed in front of the first counter.

By adjusting the rf accelerating voltage of the synchrotron, the so-called long beam pulse was obtained in which the electrons are made to spill into the internal 0.020-inch platinum target over a period of about 3000 μsec. Since the magnetic field is varying as a 30-cycle sine wave during the beam pulse the electrons strike the target at various energies, ranging from 298 to 324 Mev.

The bremsstrahlung beam was collimated by a ¾-inch diameter hole in a 9-inch thick lead wall, the various targets employed being placed in the beam about 50 inches beyond this wall. To monitor the beam, use was made of two ionization chambers which were part of the standard synchrotron installation and which had been calibrated absolutely by Blocker and Kenney.[4] The counter telescope was installed in a lead house with 3-inch thick walls, a 1½-inch diameter hole in the front wall of the house defining the effective solid angle subtended by the detector. The lead house was mounted on a carriage that could be revolved about the center of the x-ray target.

The angular distributions of protons of energy near 70 Mev from lithium, carbon, and tantalum were measured in the range from 30° to 150°. The results are given in Fig. 1, plotted taking $d\sigma/Qd\Omega dE=1$ at 90°. Each point represents a total angular interval of 6°. For measurements made with $\theta \leqslant 90°$, the targets were along the line at $\theta=135°$; for $\theta>90°$, the targets were along the line at $\theta=45°$. The data were adjusted (<5 percent correction) to take into account variation of proton energy losses in the target due to variation with angle of emission and the use of various target thicknesses.

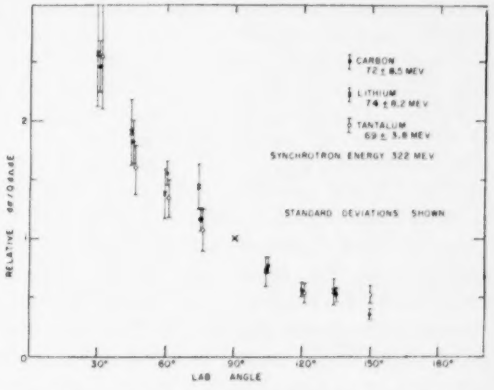

FIG. 1. Angular distributions of photoprotons near 70 Mev produced from Li, C, and Ta by 322-Mev bremsstrahlung.

* Now at Department of Physics, Massachusetts Institute of Technology, Cambridge, Massachusetts.

[1] C. Levinthal and A. Silverman, Phys. Rev. **82**, 822 (1951).

[2] J. C. Keck, Phys. Rev. **85**, 410 (1952).

[3] W. S. Gilbert and J. W. Rosengren, Phys. Rev. **88**, 901 (1952).

[4] Blocker, Kenney, and Panofsky, Phys. Rev. **79**, 419 (1950); McMillan, Blocker, and Kenney, Phys. Rev. **81**, 455 (1951).

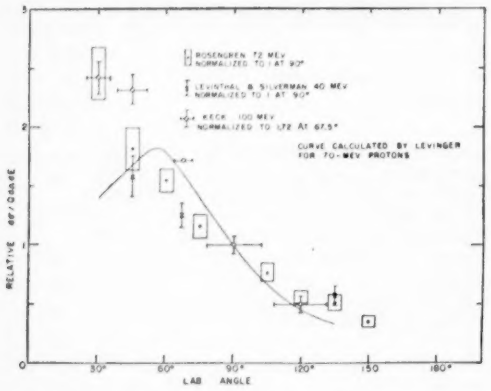

FIG. 2. Angular distributions of photoprotons from carbon.

Apparently the differences in complexity between the heavy tantalum nucleus and the light lithium and carbon nuclei have little effect upon the angular distribution. The observed distributions are within the precision of the measurements identical for all three elements. In Fig. 2 the carbon data have been plotted separately for comparison with the carbon data of Levinthal and Silverman at a lower proton energy (40 Mev) and those of Keck at a higher proton energy (100 Mev), all obtained at a synchrotron energy of about 300 Mev. The comparison indicates the distributions in this angular range become steeper with energy. Also plotted in Fig. 2 is the curve calculated by Levinger[5] for 70-Mev photoprotons from carbon using a quasi-deuteron model. Actually, this curve is for a synchrotron energy of 200 Mev, but the curve for 300-Mev synchrotron energy would be the same except at the largest angles where it would be somewhat higher. The position of the peak in the calculated distribution is in obvious disagreement with the data. Levinger's calculations, which considered the photodisintegration of a two-nucleon substructure (quasi-deuteron) moving inside the nucleus, utilized an extrapolation of the Schiff[6] and the Marshall and Guth[7] calculations of the electric dipole and quadrupole photodisintegration of the deuteron. This extrapolation has been found, however, to disagree with recent experiments.[3,8]

The distributions measured at 70 Mev, as shown in Figs. 1 and 2, may represent contributions from more than one process. Meson production from a static free nucleon by 300-Mev photons will lead to 70-Mev recoil nucleons at 30°. The motion of a nucleon inside the nucleus will make it possible to have some 70-Mev recoil protons at angles greater than 30°. Also the reabsorption of a meson inside the nucleus in which it is produced could lead to some high energy protons. The forward angular distribution of the protons shows this latter, which would give an isotropic distribution, cannot be a primary process.

The angular distributions of photoprotons from carbon at smaller angles were measured at three proton energies. The results are shown in Fig. 3, all plotted to the same scale of relative cross section. In order to get to small angles, the detector system was moved to a distance of 40 inches from the target; at all points the counter telescope aperture subtended an angle of 2°. Precautions were taken to operate at a beam intensity which was low enough to eliminate pile-up of pulses in the electronics.

The solid curves given in Fig. 3 are those calculated by Levinger for 130-Mev and 175-Mev protons produced from carbon by 300-Mev bremsstrahlung (taken from Keck's article). The normalization of the curves is arbitrary. As for the case of 70-Mev protons the distributions calculated by Levinger underestimate the small angle contributions.

The dotted curves represent calculations of the yield of protons from the disintegration of a *static* deuteron under the assumption of a cross section for deuteron dissociation that above 180 Mev is constant and isotropic. Such an assumption perhaps more closely approximates recent findings[3,8] than the theoretical values used by Levinger, and the slightly better fit (in spite of the disagreement for 174-Mev protons) suggests that Levinger's fundamental quasi-deuteron model, cor-

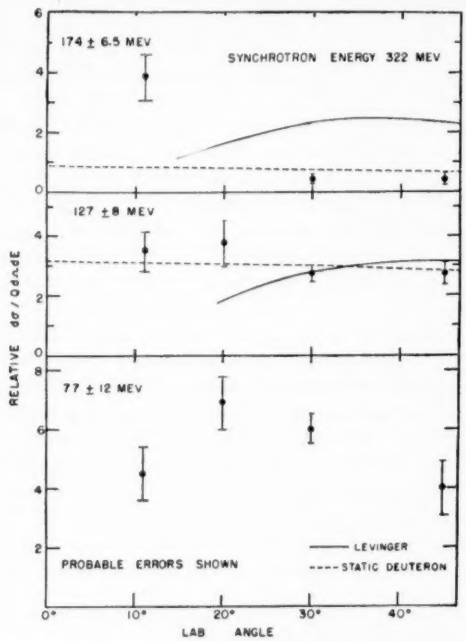

FIG. 3. Angular distributions of photoprotons from carbon at small angles. All experimental points are plotted to the same relative scale.

[5] J. S. Levinger, Phys. Rev. **84**, 43 (1951).
[6] L. I. Schiff, Phys. Rev. **78**, 733 (1950).
[7] J. F. Marshall and E. Guth, Phys. Rev. **78**, 738 (1950).
[8] T. S. Benedict and W. M. Woodward, Phys. Rev. **85**, 924 (1952); S. Kikuchi, Phys. Rev. **85**, 1062 (1952); R. Littauer and J. Keck, Phys. Rev. **86**, 1051 (1952).

rected by more accurate data for the high energy photodisintegration of the deuteron, may yet prove fruitful.

An investigation of the Z dependence was made at an angle of 45° by measuring the yields of 72-Mev protons from eleven elements, from lithium to zinc, and of 142-Mev protons from six elements, from beryllium to lead. The results are shown in Fig. 4. For both energies the yield was approximately directly proportional to Z; the curves in Fig. 4 are proportional to $Z^{1.06}$. The same data, plotted with the abscissas (NZ/A) and $(NZ/A^{7/6})$ (the former suggested by Levinger, the latter by Keck), show a greater deviation from proportionality than when plotted against Z. For both energies the yield was approximately proportional to $(NZ/A)^{1.09}$ or to $(NZ/A^{7/6})^{1.32}$.

The energy spectra of the photoprotons ejected from carbon by the 322-Mev bremsstrahlung were measured at 45° and 90° for energies above about 70 Mev. The results, shown in Fig. 5, have been corrected for nuclear absorption of the protons in the copper absorber used to vary the mean energy of the protons detected. A cross section equal to the geometrical area was used, giving a mean free path in copper of 112 g/cm². The results seem to be a smooth continuation of the $E^{-1.7}$ spectrum observed at 90° by Levinthal and Silverman at energies below 70 Mev. Keck found a break in the spectrum that he observed from carbon at 67.5°, and interpreted the fact that it occurred at half the energy of the upper limit of the bremsstrahlung distribution as confirmation of a deuteron model for the dissociation process. A proton recoiling from a neutron would carry off about half the energy for angles near 90°. Under such an interpretation, the energy of this break should depend on angle, as determined by the kinematics of deuteron disintegration. A 300-Mev photon would give a 123-Mev proton at 90° and a 197-Mev proton at 45°. However, what might be called breaks in the curves in Fig. 5 *both* occur near 140 Mev, which suggests that an interpretation cannot be so easily made.

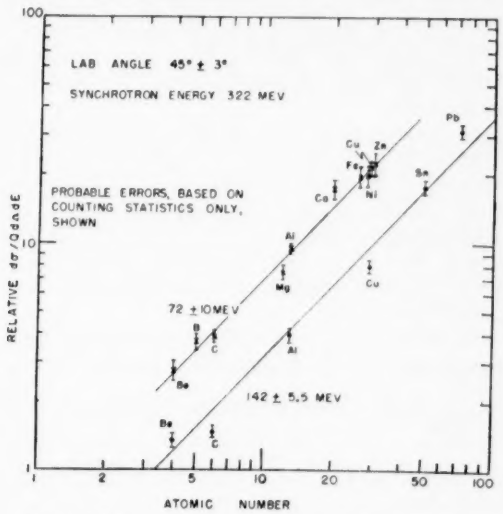

FIG. 4. Z dependence of photoproton production. Curves shown are proportional to $Z^{1.06}$.

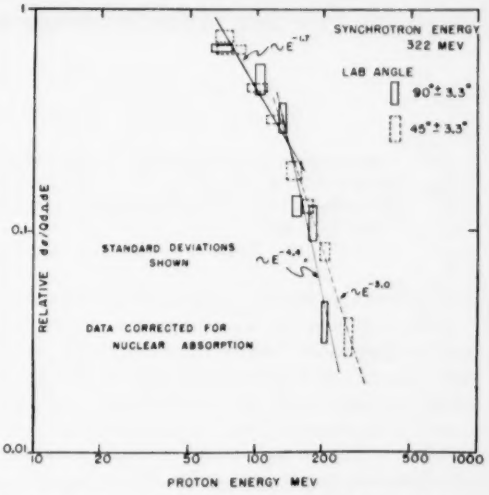

FIG. 5. Energy spectra of photoprotons from carbon, arbitrary normalization.

The absolute differential cross section for the production of 72-Mev protons from carbon at 90° was measured to be 0.72 ± 0.29 μb/Q Mev sterad, which is in good agreement with the value 0.74 ± 0.022 found by Keck at approximately the same proton and bremsstrahlung energies, but is considerably higher than the value 0.15 (±factor of 2) measured by Levinthal and Silverman. Levinger gives 0.29 μb/Q Mev sterad as the result of his calculations.

In general, over our ranges of energy and angle the absolute values calculated by Levinger appear to be roughly a factor of four too small. At energies above the meson threshold (~140 Mev) the extrapolation employed by Levinger of the calculations of Schiff and Marshall and Guth of the total cross sections for photodisintegration of the deuteron disagrees with experiment.[3,8] The cross section near 200 Mev has been found to be five to ten times higher than predicted. Thus one might expect a closer agreement between experiment and predictions from the quasi-deuteron model of the nucleus after appropriate corrections are made in that theory for both the observed angular distribution and the excitation function for deuteron photodissociation above 140 Mev.

The authors wish to acknowledge the continued interest and advice of Professor A. C. Helmholz. They appreciate the cooperation provided by Dr. W. S. Gilbert, Mr. John Barale, and the synchrotron crew directed by Mr. George McFarland. This work was supported by the Atomic Energy Commission.

Hyperfine Structure in the Paramagnetic Resonance of the Ion $(SO_3)_2NO^{--}$†

J. TOWNSEND, S. I. WEISSMAN, AND G. E. PAKE
Washington University, St. Louis, Missouri

(Received September 26, 1952)

Paramagnetic resonance spectra of the free-radical ion $(SO_3)_2NO^{--}$ in dilute solutions were observed in fields up to 50 oersteds and at frequencies up to 120 Mc/sec. The observed pattern of absorption lines agree well with that calculated for an s-electron coupled to a N^{14} (spin 1) nucleus. The zero-field splitting is 54.7 ± 0.5 Mc/sec.

THE present results represent a continuation of the work reported earlier under the same title.[1] Resonance absorption lines were studied at low values of magnetic field to further verify the mechanism of hyperfine splitting by the N^{14} nucleus, and to measure more accurately the zero-field splitting, $\Delta\nu$.

The ion was studied in the form of solutions of tetraphenyl stibonium peroxylamine disulfonate in pyridine. The concentrations were in the neighborhood of 0.1 M, giving absorption lines about one oersted wide between points of maximum slope. These solutions decompose rather rapidly after an interval of a few hours, and it was found, during the course of the experiments, that the decomposition could be delayed by the addition of a small amount of a base, such as NaOH.

The magnetic fields were produced by a pair of Helmholtz coils aligned with the earth's field, and calibrated by means of a polycrystalline sample of the free radical tris-p-nitrophenyl methyl, whose g value has been compared with that of the proton at low fields, and has been found to be independent of field.[2] The detector used is a variation of the transitron circuit,[3] used with magnetic field modulation and a phase-sensitive detector.

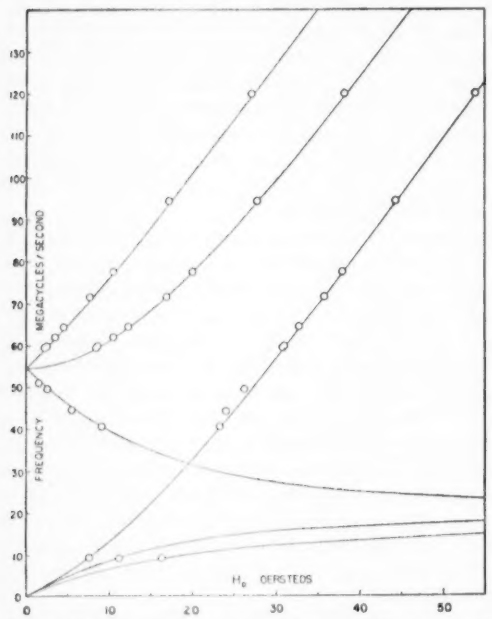

FIG. 1. Resonances of the peroxylamine disulfonate ion. The curves are calculated according to the Breit-Rabi formulas using $\Delta\nu=54.7$ Mc/sec.

The centers of the observed resonances are plotted in Fig. 1. The three points at 9.21 Mc/sec were obtained previously.[1] The curves are computed from the Breit-Rabi formulas[4,5] and fitted to the data using the single adjustable parameter $\Delta\nu$, whose value was found to be 54.7 ± 0.5 Mc/sec. The six curves given are those for transitions in which $\Delta m=\pm1$, the π-transitions, which are expected when the rf magnetic field is perpendicular to the static field,[5] as was the case in this experiment. The σ-transitions, $\Delta m=0$, induced if the rf and steady fields are parallel, would lie along two additional curves not shown. The σ-transitions, as expected, did not appear. It was impossible to make measurements of the relative intensities of these transitions, due to the decomposition of the solutions.

The bumps appearing on the sides of the 9.21-Mc/sec resonance curves in reference 1 have not been explained. Similar bumps, as many as six in number and of very low relative intensity, have appeared on the 9000-Mc/sec resonance spectrum when the sensitivity was increased.

The value of $\Delta\nu$ for this hyperfine splitting may be compared with the results of Beringer and Castle[6] for NO and of Hutchison, Pastor, and Kowalsky[7] for dilute solutions of diphenyl picryl hydrazyl. These measurements correspond to respective zero-field splittings of 44.7 Mc/sec and 42 Mc/sec. Such data, of course, impose a condition on the wave function of the unpaired electron.

Part of the equipment used was provided through a grant-in-aid from the Research Corporation.

† Assisted by the joint program of the Office of Naval Research and Atomic Energy Commission. This work has been reported by one of the authors (G.E.P.) at the American Physical Society Meeting, Columbus, Ohio, March, 1952.

[1] Pake, Townsend, and Weissman, Phys. Rev. **85**, 682 (1952).

[2] N. A. Schuster, thesis, Washington University (1951) (unpublished).

[3] H. W. Knoebel and E. L. Hahn, Rev. Sci. Instr. **22**, 904 (1951).

[4] G. Breit and I. I. Rabi, Phys. Rev. **38**, 2082 (1931).

[5] J. E. Nafe and E. B. Nelson, Phys. Rev. **73**, 718 (1948). The notation of this paper is followed here.

[6] Robert Beringer and J. G. Castle, Jr., Phys. Rev. **78**, 581 (1950).

[7] Hutchison, Pastor, and Kowalsky, J. Chem. Phys. **20**, 534 (1952).

Electron-Induced Showers in Copper*

ASHER KANTZ AND ROBERT HOFSTADTER
Department of Physics and Microwave Laboratory, Stanford University, Stanford, California
(Received September 18, 1952)

An experimental determination has been made of the radial and longitudinal distribution of energy produced in showers initiated by electrons of 118 Mev and 157 Mev in copper. A small crystal CsBr(Tl) coupled to a thin light pipe and photomultiplier was used as a probe. Graphs of the radial distributions are given from which, by numerical integration, transition curves are determined. Calculations are made for an approximately optimum design of scintillation crystal [e.g., NaI(Tl)] to capture a large fraction of the energy within a shower.

I. INTRODUCTION

SHOWER theory has been of continuing interest for more than a decade. The earliest calculations appear to have been made by Carlson and Oppenheimer[1] and by Bhabha and Heitler.[2] Among the latest calculations are those of Wilson.[3] It is quite difficult to formulate a theory in closed form when the primary energy of electrons (or photons) is not large compared to the critical energy (ϵ) in the material.[4] For example, in copper and lead the critical energies are 22.4 Mev and 7.0 Mev, respectively; at energies of 100–200 Mev the calculations, even excluding the Compton effect, are very difficult to carry out. For this reason Wilson[3] has recently used the Monte Carlo method to calculate transition curves in lead at energies from 20 to 500 Mev.

The experimental data on showers are extremely sparse, especially in the energy range of a few hundred Mev. Transition curves for photons about various (γ,n) energy thresholds were studied by Strauch.[5] Transition curves have also been obtained by Blocker, Kenny, and Panofsky[6] who investigated in C, Al, Cu, and Pb the longitudinal distribution of showers initiated by bremsstrahlung gamma-radiation from the synchrotron operated at 330 Mev. Rose[7] has investigated the angular distribution of copper (γ,n) threshold gamma-rays in the early stages of primary bremsstrahlung initiated showers in copper and lead.

The availability of nearly monochromatic electron beams from the Stanford linear accelerator has allowed us to study both the longitudinal and the radial distribution within the showers. By using electrons the shower producing component is simple and definite, and no assumption need be made about the quality of the primary beam. As far as we know, this study presents the only experimental investigation of radial distributions within showers at low energies other than that of Rose carried out with bremsstrahlung spectra.

A theory of the radial distribution has been given by Moliere[8] and by Blatt[9] for the case of air showers. These theories apply to the very high energies observed in the large cosmic-ray air showers and would not be expected to apply to the relatively small showers discussed below.

There is a great deal of interest at the present time in the distribution of energy inside a shower because of the possibility of using a large scintillator crystal to capture the whole of the shower and, thereby, measure the energy of the primary particle. In particular we have been interested in employing a large crystal of NaI(Tl) for this purpose. The shape and size of such a crystal must be considered carefully because of the difficulty and expense involved in obtaining such a large crystal. Partially for this reason, and also for its

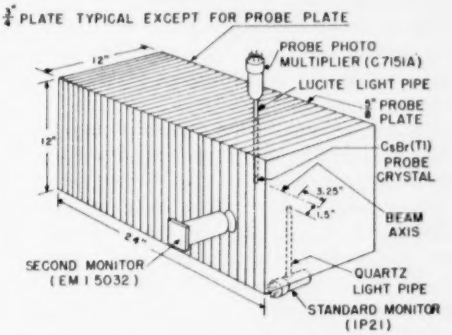

FIG. 1. Schematic arrangement of the pile of copper plates showing the positions of the probe and monitor crystals. The internal monitor was maintained 3¼ in. from the front face of the copper pile. When the probe plate was placed in front of the monitor plate, copper sheets of small thickness were inserted to make up the standard 3¼-in. monitor distance. In the "zero depth" position of the probe plate, i.e., first plate, the mean position of the probe crystal falls at ½×⅜ in. = 3/16 in. of copper. Thus, "zero" longitudinal depth refers to a shower that has developed through about 0.54 radiation lengths of copper.

* This work was aided by the joint program of the Office of Naval Research and Atomic Energy Commission.

[1] J. F. Carlson and J. R. Oppenheimer, Phys. Rev. **51**, 220 (1937).

[2] H. J. Bhabha and W. Heitler, Proc. Roy. Soc. (London) **159**, 432 (1937).

[3] R. R. Wilson, Phys. Rev. **86**, 261 (1952).

[4] B. Rossi and K. Greisen, Revs. Modern Phys. **13**, 240 (1941). The Rossi-Greisen article presents an excellent summary of the physical basis of shower theory and the definitions of terms in common usage.

[5] K. Strauch, Phys. Rev. **81**, 973 (1951).

[6] Blocker, Kenny, and Panofsky, Phys. Rev. **79**, 419 (1950).

[7] J. W. Rose, Phys. Rev. **82**, 747 (1951).

[8] G. Moliere, Naturwiss. **30**, 87 (1942); W. Heisenberg, *Cosmic Radiation* (Dover Publications, New York, 1946); see also J. Roberg and L. W. Nordheim, Phys. Rev. **75**, 444 (1949), who discuss the average radial spread of showers.

[9] J. Blatt, Phys. Rev. **75**, 1584 (1949).

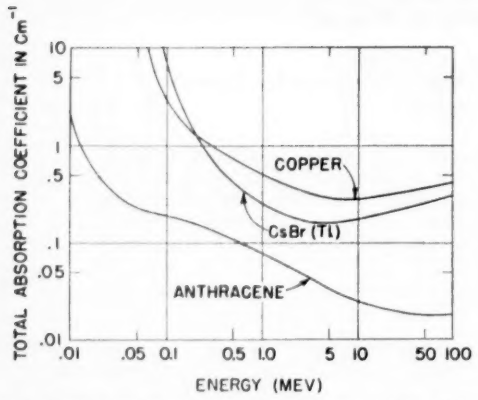

FIG. 2. Total absorption coefficients for copper CsBr(Tl) and anthracene (assumed carbon of density 1.25 g/cm³).

intrinsic interest, we have carried out the shower study described below.

II. DISCUSSION OF THE METHOD

We have employed copper as a representative substance because of its availability in pure form, high density (shower contained in relatively small volume), and relative proximity to NaI(Tl) in atomic number. To study the nature of the shower process, we have inserted a small scintillation crystal, which we call a probe, and a light pipe in a cylindrical well of diameter $\frac{7}{16}$ in. bored in a copper plate $\frac{5}{8}$ in. thick. The radial position of the probe samples the specific energy loss at the given position in the plate. By moving the plate to different positions in the shower, the longitudinal distribution can be studied. Figure 1 shows the experimental situation in a schematic way. The bulk of the copper was made up of $\frac{3}{4}$-in. thick plates, each 12 in. $\times$12 in.

In any method employing a probe it may be asked whether the probe measures the desired physical quantity. In this particular case we wish to measure the energy loss at any radius and any depth. We inquire therefore (a) whether the well and probe distort the shower, (b) whether the crystal probe measures the energy loss which would occur in a similar volume of copper, or, equivalently, something proportional to that loss.

We have made a partial attempt to answer these questions. As far as (a) is concerned, experimental data below will show that except perhaps at the beginning of the shower, so to speak, "in the direct beam," there is no significant distortion due to the well and probe.

Question (b) is more difficult to answer. If an instrument with practically zero stopping power (in the limit, a vacuum) were used to measure the number of electrons passing through it, for example, an ion chamber, the projected electrons, being finally responsible for actual energy loss, would furnish in the chamber a sampling of their presence in the copper and hence would give a true picture of energy loss within the copper.

At the other extreme, if it were possible to obtain a fictitious scintillating crystal of copper and a fictitious "copper light pipe" the true distribution of energy would be obtained. We have employed an intermediate case between these two extremes. Our probe has been made of CsBr(Tl), and has been a cylinder of length 0.125 in. and diameter 0.250 in. A Lucite light pipe of diameter 0.300 inch has been used to conduct light from the probe to the photomultiplier. For purposes of comparison we have also used an anthracene crystal (0.125-in. diameter and 0.25-in. length) as a probe with the same light pipe.

In order to simulate copper exactly it would be necessary for the probe to have (1) the same stopping power for gamma-rays throughout the effective gamma-ray region, say 100 kev–10 Mev, (2) the same stopping power for collision loss, i.e., direct ionization loss by electrons. Items (1) and (2) imply the same conversion properties for transforming gamma-energies into electron energies.

Figure 2 shows a comparison of the gamma-ray absorption coefficient *versus* energy for CsBr(Tl), Cu and anthracene (assumed pure carbon of the density of anthracene) for comparison.

It may be seen that although the fit is not perfect the agreement between Cu and CsBr(Tl) is surprisingly good, considering how different the substances really are. Anthracene demonstrates how different the comparison can be.

Figure 3 shows a similar comparison of electron energy loss per centimeter due to collisions. In this case the comparison between Cu and CsBr(Tl) is less favorable but again better than between Cu and anthracene.

Let us now consider in more detail the comparative behavior of crystal probe materials for gamma-rays.

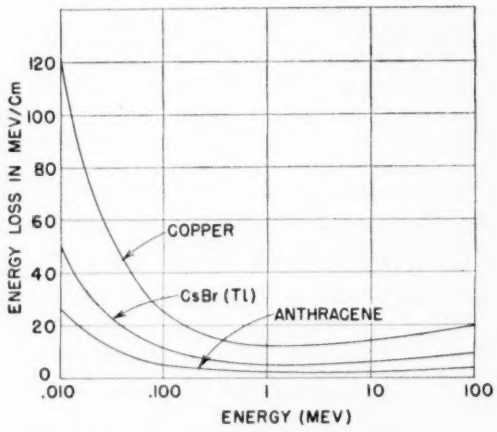

FIG. 3. Energy loss for copper, CsBr(Tl) and anthracene (assumed carbon of density 1.25 g/cm³).

In a shower initiated by electrons, the chief component at the beginning of the shower will be electrons. At the peak of the transition curve (~1.6 radiation lengths for these energies in copper), we shall find a mixture of electrons and gamma-rays. Towards the end of the shower, in the exponential tail of the transition curve, we shall find principally gamma-rays of energy close to 8.0 Mev for copper.

It is, therefore, appropriate to compare different regions of the curves in Figs. 2 and 3 for various parts of the shower in order to gain an appreciation of the similarity or dissimilarity of CsBr(Tl) and anthracene to copper. More specifically, it is not enough to use Figs. 2 and 3 as the basis of comparison, for in scintillation detectors the quantity measured is the energy absorbed by the crystal detector. Therefore, curves showing absorbed energy are really required.

Figures 2 and 3 offer a basis for calculating the energy absorbed in the detectors. Using the known relations in the Compton effect[10] for determining the amount of energy absorbed by struck electrons, we have computed the curves of Fig. 4. These curves show the energy absorbed by one centimeter of detector plotted against energy of the incident quantum. On the high energy side, we have cut off the increase of absorbed energy due to the finite size of our probe crystals. The cut-off regions are indicated by the dashed lines.

A comparison of energy absorbed can now be made as follows. Figure 5 shows the ratio of absorbed energy per cm in CsBr(Tl) to that in copper for various fractional compositions of electrons and gamma-rays;

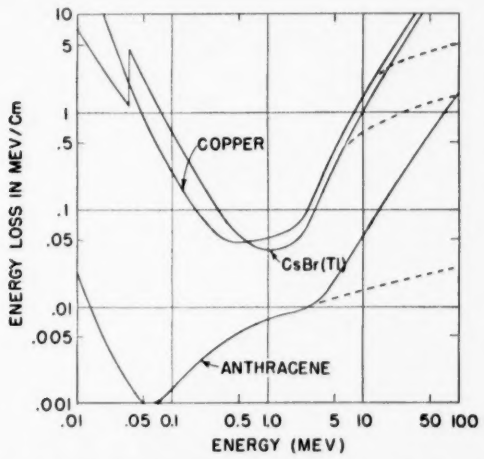

FIG. 4. Energy loss of gamma-rays in one centimeter of material. The curves show the energy absorbed by a layer of material one cm thick, taking into account the energy transferred to electrons in the Compton effect. The energy absorbed from electrons created by pair production is limited by the finite size of the absorbing sample. The limit is shown by the dashed lines in the appropriate cases. The discontinuity in the CsBr(Tl) curve is due to the absorption edge in Cs near 36 kev.

[10] C. M. Davisson and R. D. Evans, Revs. Modern Phys. **24**, 79 (1952).

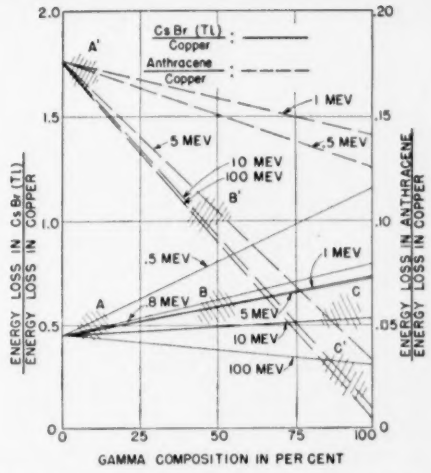

FIG. 5. Comparative energy loss of a probe crystal of CsBr(Tl) or anthracene and energy loss in a sample of copper of the same length. The scale of ordinates for CsBr(Tl) lies to the left, that for anthracene to the right.

in other words, the abscissa is the ratio of the number of gamma-rays to the sum of the number of electrons and gamma-rays of the same energy. Figure 5 also shows a similar plot for anthracene and copper. For example, at the left, zero abscissa means that the ratio of energy absorbed is purely due to collision loss by electrons and is essentially a function of density ratio. At the right, unity abscissa means the composition is purely gamma-rays. The beginning of an electron shower will be approximated by the region near the symbol A, the transition region by the symbol B, and the tail of the shower by symbol C. Corresponding regions for anthracene are given by A', B', C'.

While these considerations are mainly pictorial, they are indicative of the results to be expected with the different detectors. It may be seen that the ratio: energy absorbed in CsBr(Tl)/energy absorbed in copper is considerably more uniform over the entire shower range than the corresponding ratio for anthracene. Thus, CsBr(Tl) would appear to be a much more satisfactory probe material for copper than anthracene, though, of course, not ideal. A measure of perfection would be the degree of coalescence of all lines of different energy into one common horizontal line. CsBr(Tl) does show approximately this behavior for the range of energies 0.8 to 100 Mev.

In any case the distortion of the true radial and longitudinal curves resulting from the choice of probe is not critical. Using anthracene as a probe crystal under experimental conditions identical with those of CsBr(Tl) runs, we have found that the main features of the radial distributions are similar to those of CsBr(Tl) runs, especially at depths greater than 5 inches in the copper pile. At smaller depths the saturation of the photomultiplier-anthracene combination

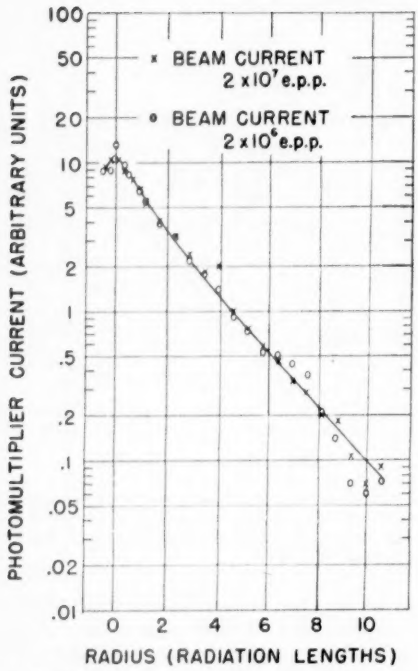

FIG. 6. Radial distributions at the same longitudinal position for two beam intensities differing by a factor of 10. For ease of comparison the curve taken at lower beam current was raised by a factor 10. Beam current is given in electrons per pulse.

made an accurate comparison difficult. Nevertheless, when it was certain that this combination was not saturating, the radial runs at smaller depths were similar to CsBr(Tl), except that anthracene showed a tendency to give higher relative readings at the center of the shower, perhaps by as much as a factor two or so, than those of CsBr(Tl). For such comparisons the CsBr(Tl) and anthracene curves were normalized at a radius of four inches.

Since the radial runs show large changes (see Figs. 12 and 13) for small changes of radius, the behavior of the radial distributions will not be expected to be critically different for different probe materials, which is just what the experiments show.

It will be seen later that the experimental transition curves obtained with CsBr(Tl) check those previously observed with an ion chamber.[6] This agreement gives us some confidence in using CsBr(Tl) as a probe material.

CsBr(Tl) has been chosen for another important reason. In these experiments the Stanford linear accelerator produced pulses lasting about 0.3 μsec. Were an organic crystal similar to anthracene used (decay constant 0.03 μsec), the emission of light from the crystal could saturate the photomultiplier and/or reduce the voltage at several points on the chain of dynode resistors. By using CsBr(Cl) (decay constant about 5 μseconds), the possibility of saturation is greatly ameliorated. The CsBr(Tl) crystal acts like a storage device and releases light to the photomultiplier at times when the linear accelerator pulse is over. To take advantage of the storage principle, we have used a galvanometer or equivalent dc amplifier to measure the current from the photomultiplier.

A third reason for choosing CsBr(Tl) is that the luminous output, integrated over the complete duration of the light pulse, is as large as that given by NaI(Tl) and perhaps a trifle larger. This material is therefore highly suitable for dc work.

A fourth reason has to do with convenience. CsBr(Tl) is not deliquescent to any appreciable degree and so may be mounted without an air-tight protective cover. Considering the fact that a seal with the light pipe must be made, this fortunate stability of CsBr(Tl) is not of small value.

The CsBr(Tl) samples we have used[11] are slightly phosphorescent when stimulated by visible light. All operations have been conducted after the phosphorescence had decayed to negligibly small values. We have not noticed a phosphorescence due to shower or gamma-ray stimulation, and no background correction for this effect need be made.

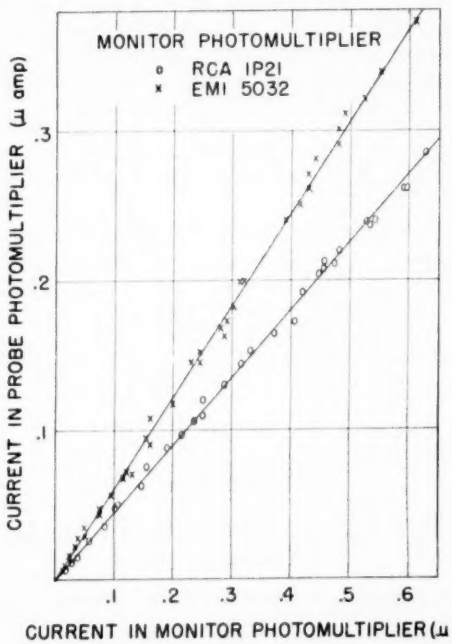

FIG. 7. Linearity runs for the various monitors. The probe photomultiplier was never used under conditions requiring more than 0.1 microampere.

[11] Kindly supplied to us by Mr. K. E. Long of the Harshaw Chemical Company, Cleveland, Ohio.

Effect of the Light Pipe

There is a possibility that the light pipe may emit luminous radiation when exposed within a shower because of the Čerenkov effect or possibly because of direct luminescence. Such light would come from the whole length of the pipe in varying degrees and falsify the readings of the probe crystal. Luminous effects in the light pipe were looked for but were found to be negligible, unless the light pipe passed through the direct beam. Even in this case the effect is small.[12] Tests made of the luminous radiation from the 0.300-in. diameter light pipe under conditions actually used show that the contribution of the light pipe when the CsBr(Tl) crystal is in the beam at the start of the shower amounts to less than 1 percent of the crystal probe reading. At the edge of the copper plate where the crystal emerges from the probe-well, the contribution of the light pipe is undetectable. The effect of the light pipe is therefore considered negligible.

Monitoring

The radial runs were taken preferably at constant accelerator beam current. The beam was not always steady, and hence, a monitor was used to which all readings could be referred.

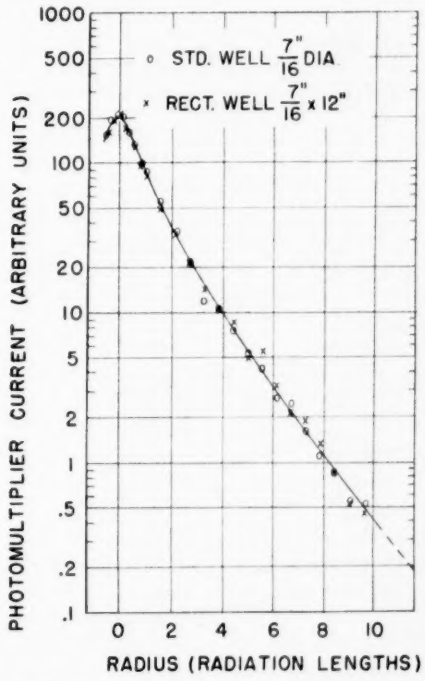

FIG. 8. Comparison between runs taken with standard $\frac{7}{16}$-in. well and with an entire $\frac{7}{16}$-in. plate removed from the copper pile. The data were taken at a depth of approximately five inches in the pile.

[12] See Fig. 9 and the associated discussion in the text.

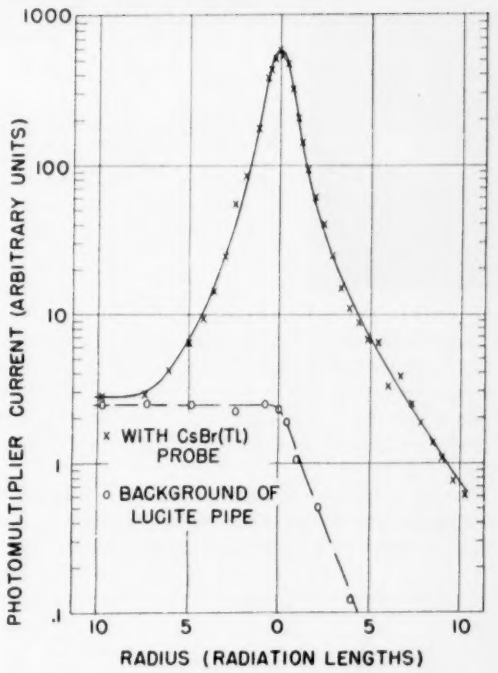

FIG. 9. Radial distribution measured with a 13 in. long light pipe. The light emitted from the pipe is probably due to Čerenkov radiation.

The monitor crystal was on most occasions a second CsBr(Tl) crystal although in some cases a KI(Tl) crystal was used. The monitor current was read by a second galvanometer. The monitor CsBr(Tl) crystal was 0.25 in. in diameter and 0.625 in. long. A quartz light pipe conducted the light to a 1P21 photomultiplier. The monitor crystal and probe were stationed permanently in a plate $3\frac{1}{4}$ in. of copper behind the first plate, and the crystal was positioned 1.5 in. from the shower axis, as shown in Fig. 1. A second monitor was used outside the copper pile on many occasions and is also shown dotted in Fig. 1 in its usual position. In special tests an EMI 5032 photomultiplier and CsBr(Tl) were used in combination as an external monitor.

Tests of Linearity

It is essential for correlation of the data taken in one longitudinal position of a plate with another that the readings of the monitor (s) and probe be linear with respect to the beam current.

A test of linear response of the probe crystal was made by first taking a radial run at a given longitudinal position in the shower and later changing the beam current by a large factor, say 10, as judged by the monitor crystal or by an ionization chamber in front of the copper pile, and comparing runs. Figure 6 shows two sets of runs in the same longitudinal position but with beam currents changed by a factor 10. The run

FIG. 10. The electron beam as it entered the copper pile. The beam was approximately an ellipse of height $\frac{1}{4}$ in. and width $\frac{1}{2}$ in.

at lower beam current has been shifted in the figure by a factor 10 for better comparison. It will be seen that the runs superpose within the experimental error, and the fact that they do so over ranges of greater than 10^2 in probe readings is a strong indication of exact linearity over a wide range.

Further evidence of linearity may be obtained by plotting the probe crystal readings against the monitor (or both monitors') readings. Figure 7 shows typical plots of probe and monitor readings. The use of three different photomultipliers (C7151A, 1P21, 5032) in taking linearity curves lends confidence to the method, since the saturation properties of all three types cannot be identical.

An additional piece of less direct data on linearity was obtained by plotting an ion chamber reading against probe current in a fixed position as the beam intensity was changed. The ion chamber in this case was placed ahead of the copper pile so that the primary beam struck the ion chamber first. At low beam currents $<10^6$ electrons/pulse, the curve was linear. At higher beam currents the ion chamber reading flattened off, suggesting that the ion chamber saturated. On increasing the ion chamber field, the curve straightened out but flattened off at still higher beam currents. The fact that the ion chamber saturated in just the region found in this work was also found independently in this laboratory by Panofsky[13] in another connection, who calibrated the chamber in terms of induced radioactivity in carbon.

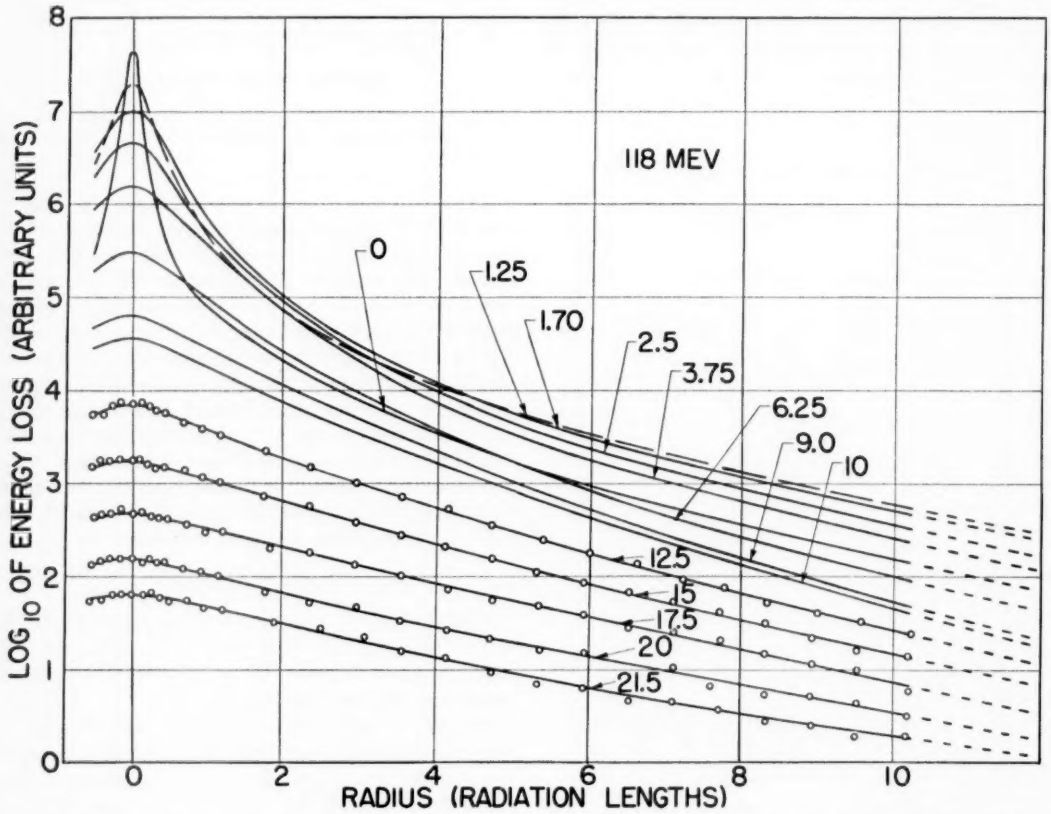

FIG. 11. Radial distributions at 118 Mev. Experimental points are indicated on the lower curves. Because of possible confusion of the close-lying curves, the experimental points are omitted from the upper curves. The figures pointing to the appropriate curves refer to the longitudinal depth in the pile in terms of radiation units. Zero depth refers to showers passing through $\frac{5}{16}$-in. Cu (see Fig. 1).

[13] W. Panofsky, private communication.

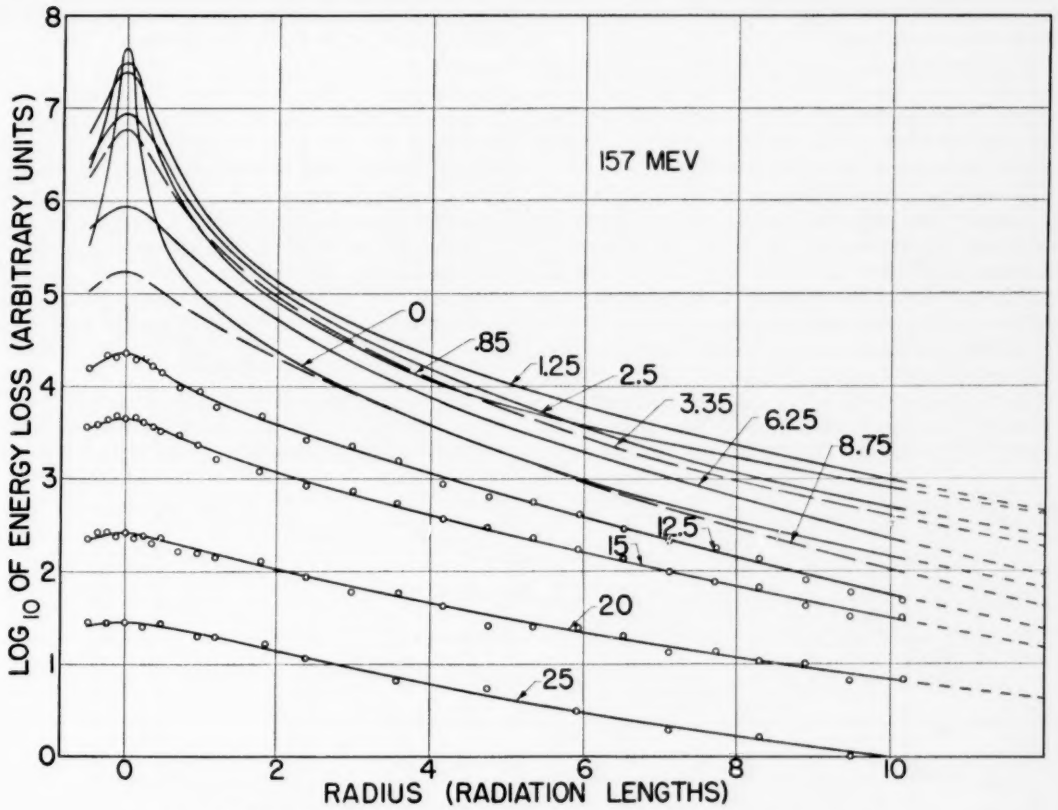

FIG. 12. Radial distributions at 157 Mev. Data presented are similar to those in Fig. 11.

When trials were first made to observe linearity, definite departures were found from the straight lines of Fig. 7. This condition was corrected by placing large capacitances (0.1 μf) at the 6th, 7th, 8th, 9th dynodes across the voltage divider resistances (0.47 megohm). Nevertheless, because of the high light-emitting speed of anthracene, we have observed definite evidence of nonlinearity when anthracene is used in moderately high beams. Under comparable conditions the CsBr(Tl)-photomultiplier combination shows no evidence of saturating.

Effect of Well Size

We have made several experiments with various diameters of wells in the 6th longitudinal plate position (about 5 in. in the copper pile). The data are unchanged for various diameters, and in fact show negligible change even when the probe plate is completely removed. It appears from this work that the gap left by the probe plate is small enough that the shower is not distorted by its presence in the neighborhood of the 6th plate. Figure 8 shows radial plots with a $\frac{7}{16}$ in. well and with probe plate removed.

Experiments with 6 and 9 inches of well refilled with copper plugs also showed no significant changes in radial distributions.

Small changes might have been expected if the probe-well had been inserted before or near the shower maximum. Because of lack of operating time, a complete investigation was not possible. However, enough data were observed under conditions of varying geometry which convince us that the effect of the probe-well is very slight in all cases.

Symmetry of Radial Curves

The probe crystal was moved from top to bottom of the probe plate to determine whether the radial distribution had proper symmetry about the beam. Below the center of the plate the light pipe is itself in the beam. A thirteen-inch light pipe was used in these tests. A typical curve is shown in Fig. 9. It may be seen that the curve is symmetrical until a point is reached where the shower intensity at the probe is reduced to a value equal to that of the Čerenkov light in the light pipe (which is now struck by the beam). The limiting plateau on the left is exactly what has been found when the effect of the light pipe was investigated by itself,

i.e., without a probe crystal. The light pipe plateau is shown in the lower part of Fig. 9.

In all final runs an 8 inch long light pipe was used and the data were taken from top to center and 1 in. beyond center on the lower side. This method of taking runs checked the fact that the center of the shower axis was at the center of the copper plates.

In this connection the line-up of the central axis of the copper pile with the beam axis was made by photographing the beam at the front and back of the platform supporting the copper pile both at the beginning and end of the experiment. In both cases the copper was, of course, removed from the beam.

The size and shape of the primary electron beam as it struck the first copper plate is shown in Fig. 10. The beam was produced by a $\frac{1}{4}$-in. diameter lead collimator followed by a magnet and a second $\frac{1}{4}$-in. (approx.) tapered lead collimator. Each collimator was 24 inches long. The horizontal width of the beam is due to the dispersive effect of the magnetic analyzer. The energy spread in the beam is about 3 percent, thus 3.5 Mev in 118 Mev and 4.7 Mev in 157 Mev. The elliptical shape of the beam proved to be a slight disadvantage in measuring the early parts of the transition curve (see below). It hoped that future experiments will be made with a circular beam.

The energy of the beam was measured by following the course of the beam in the magnet with a flux coil and integrating the resultant field over the path. Calibration of the flux coil was made with a proton moment apparatus. The estimated error is 1.5 percent.

III. RESULTS

Composite sets of radial intensity runs are shown in Figs. 11 and 12 for 118 Mev and 157 Mev, respectively. When the radial intensity is multiplied by $2\pi r dr$

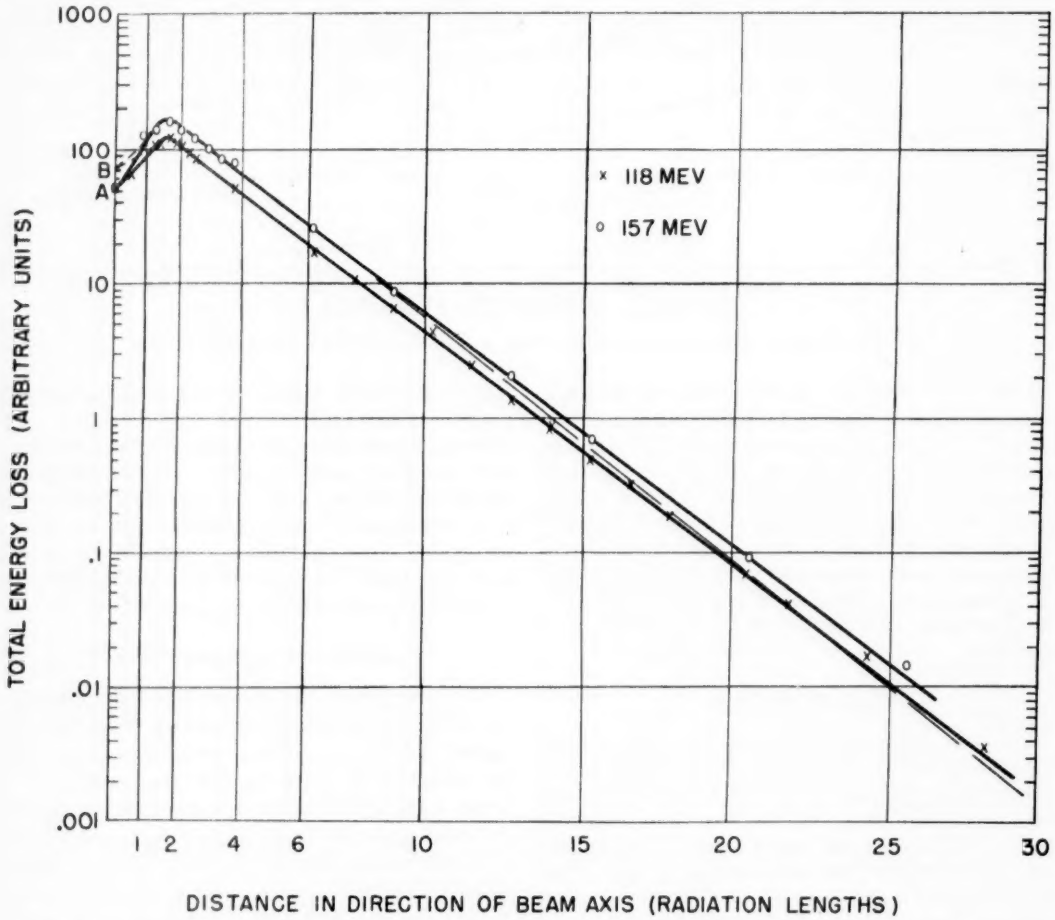

FIG. 13. Transition curves for electron initiated showers in copper at 118 and 157 Mev. Zero depth refers to showers passing through $\frac{1}{16}$-in. Cu (0.54 radiation lengths). Dotted portions of curves at left represent the uncertainty in the numerical integrations due to the elliptical beam shape. The dashed line between the transition curves represents the exponential absorption of gamma-rays at the minimum of the curve of absorption coefficient for gamma-rays (see Fig. 2).

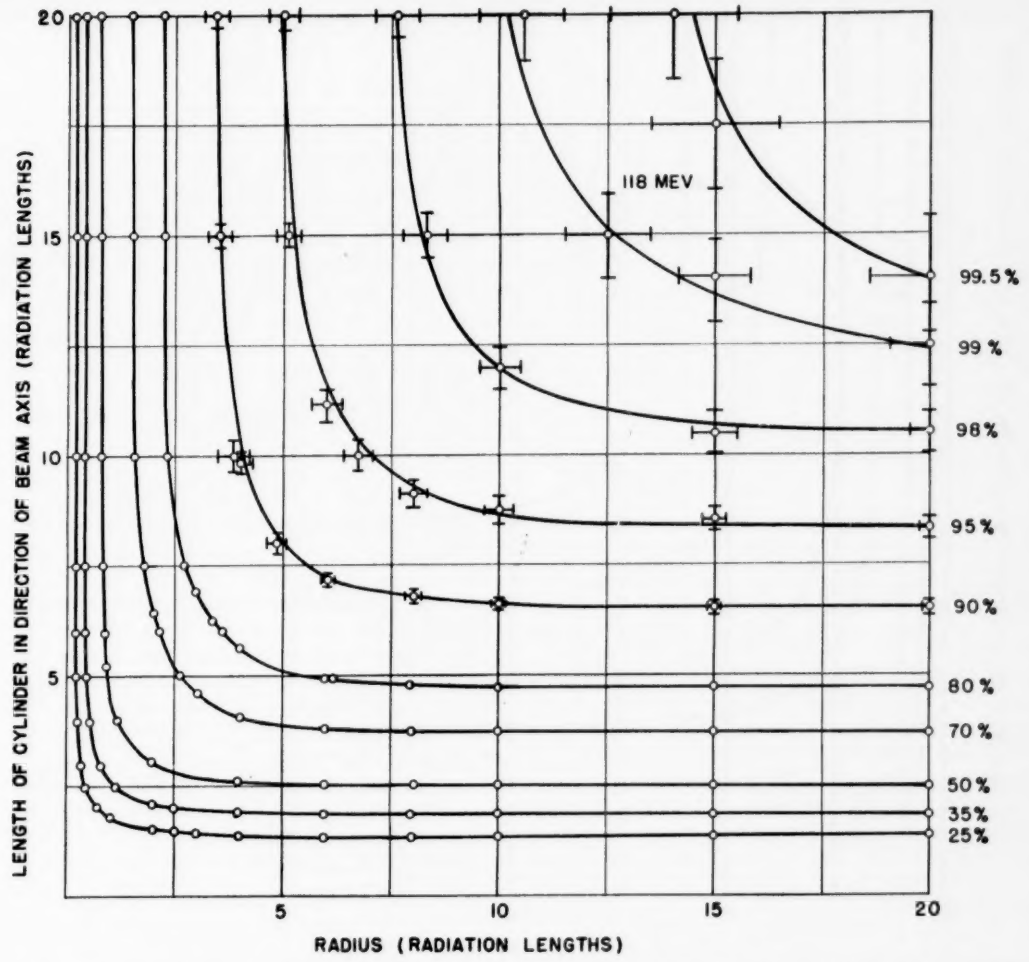

FIG. 14. Average total energy loss in copper cylinders of various dimensions for incident electrons of 118 Mev. These curves were calculated from the data in Fig. 11. The curves might be termed "isoenergetic curves."

(r = radius) the energy content within the ring dr at r can be obtained. Integration over all rings within a copper plate will give the total energy dissipated in a plate. A plot of the energy per plate as a function of depth within the shower gives what is known as a "transition curve." Transition curves for 118 and 157 Mev are given in Fig. 13. The points in Fig. 13 were actually obtained by extrapolating to infinity the tails of the radial curves, which are essentially exponential in the regions considered. The extrapolation to infinity does not add more than 2.2 percent for the first plate and a maximum figure of 30 percent for the 25th plate.

The far end of the exponential tail of the transition curve should have a slope approximately equal to the absorption coefficient of gamma-rays at the minimum of the theoretical gamma-ray absorption curve. A curve with this slope has the dotted appearance in Fig. 13. The absorption coefficient data are taken from the Bethe-Heitler theory. It will be noticed that the slope differs by 5 percent from that given by Bethe-Heitler and corresponds to a smaller absorption coefficient. Of interest is the fact that Blocker, Kenny, and Panofsky[6] have also found a deviation of approximately the same amount. It is not known at present if the discrepancy between the experimental and theoretical results is significant.

In Fig. 13 the dotted portions of the transition curves to the left of the maxima represent the present uncertainty in the data caused by the elliptical shape of the beam (see above). It is not believed that the radial distributions are affected by the deviation from a circular beam because of the small beam size relative to the dimensions of the plates. However, the integrations were made over circular rings, assuming equal intensity over the rings. This is clearly not so within the beam or while the beam has not yet spread signifi-

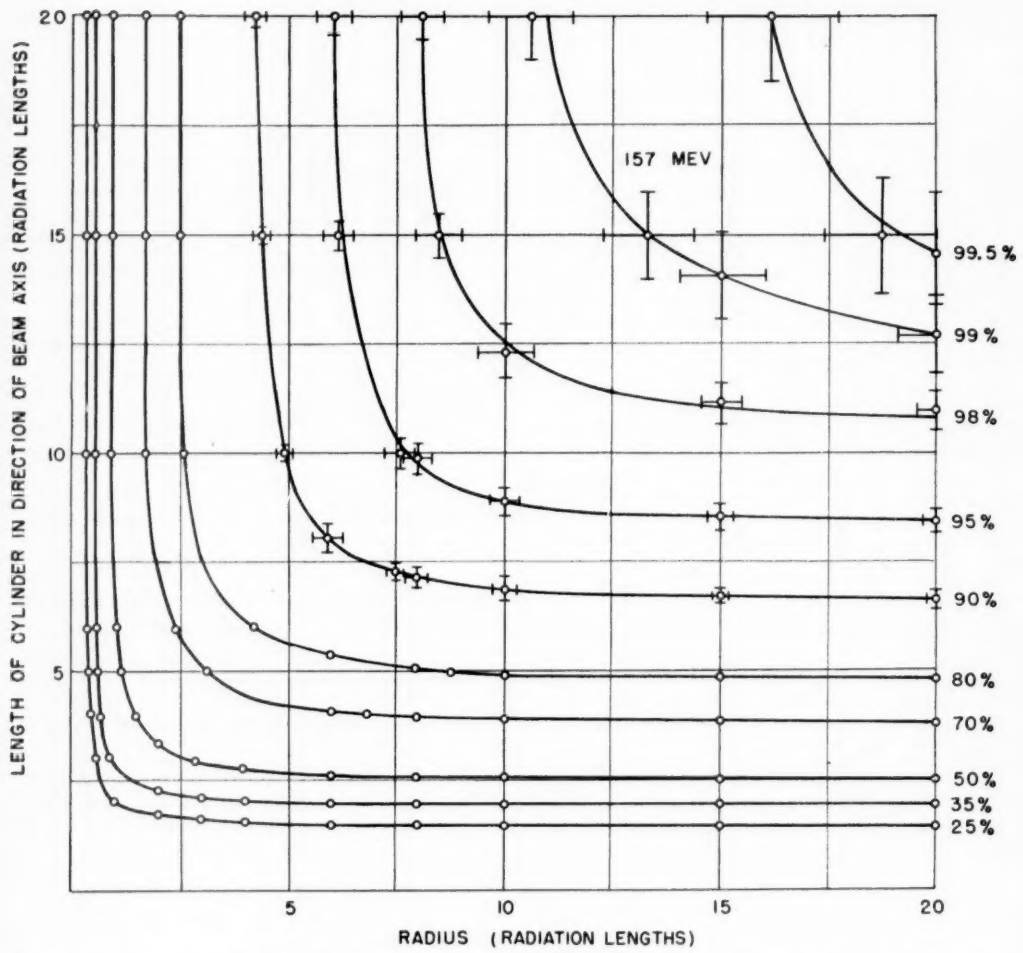

FIG. 15. Average total energy loss in copper cylinders of various dimensions for incident electrons of 157 Mev. These curves were calculated from the data in Fig. 12.

cantly, i.e., before the maximum. We have, however, reconstructed intensity curves based on our finite crystal size, taking into account the elliptical shape, and, thereupon, have obtained the dotted portions of the curves. Probably the true distribution lies in between these values.

While the experiments were in progress, it was not realized that a good check on the over-all transition curve could be obtained by using the initial value of energy loss A or B (Fig. 13), whichever is proper (depending on beam shape), to obtain a value of the total energy content in the beam. For example, if we consider that the electrons are very close to minimum ionization, we can obtain a figure for the linear range assuming only theoretical collision loss dE/dX. The intensity (A or B) times the theoretical range gives an area proportional to the energy in the beam. The area under the experimental transition curve should then be equal to the area calculated above. A simple graphical integration shows that the area under B is 9 percent greater than the simple collision loss integral, while the area under A is 18 percent less than the same. The agreement is considered quite satisfactory in view of the numerous integrations required.

A comparison was made of the integrated areas under the transition curves for 118 and 157 Mev and showed that the areas were in the ratio 1.35. The ratio of energy in the beam was actually 1.33. The ordinates of the transition curves were normalized to the same initial value for this comparison.

It is clear that with a small crystal and circular beam quite exact measurements and checks would become available. We have plans to carry out such experiments at the present and also higher primary energies.

Calculation for Scintillation Crystal

We can use the data given in Figs. 11 and 12 to calculate the fraction of total energy going into any given volume of copper. In this way we can discover the dimensions required to contain on the *average* a certain portion of the total energy. If we imagine cylinders of radius R and length L both measured in radiation lengths, we obtain Figs. 14 and 15 by graphical integration of the suitable fragments of curves (11) and (12). For example, if we assume a primary energy of 157 Mev and a copper cylinder of radius $R=5$ rad. lengths $=5$ (0.58 in.) $=2.9$ in. and $L=10$ rad. lengths $=5.8$ in., this cylinder will on the average capture 91 percent of the shower or 143 Mev. No fluctuation can give more than 100 percent or 157 Mev, while a fluctuation due to escaping gamma-rays can probably yield a lower energy of perhaps (20 percent lower) 120 Mev or so.

While our work has not been carried out with NaI(Tl), nevertheless, the main characteristics of the shower will probably be similar if expressed in radiation lengths.[14] For NaI(Tl) one radiation length equals approximately one inch: thus, a cylinder 10 in. in diameter and 10 in. long of NaI(Tl) will capture on the average 91 percent of a 157-Mev shower. Calculations for 118 Mev show similar results.

It is easily recognized that the outer parts of the cylinder are not particularly effective near the beginning of the shower. In other words, a conical section near the beginning would not be particularly disadvantageous. This is fortunate since crystals are actually grown with a conical tip.

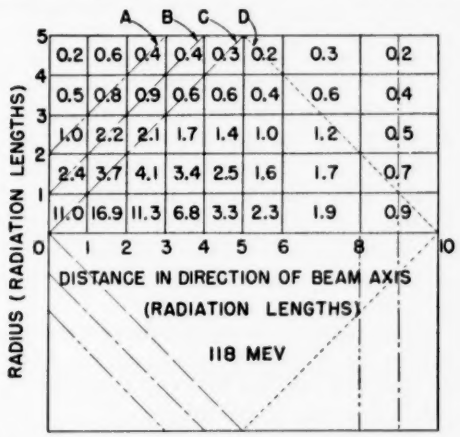

FIG. 16. A block diagram showing the average percentage of total energy captured in various regions of a copper cylinder for electron initiated showers at 118 Mev. A given block refers to a figure of revolution about the beam axis with the boundaries shown, A, B, C, D refer to different conical tips on large NaI(Tl) crystals, as explained in the text.

[14] The critical energy of NaI(Tl) is approximately equal to that of copper.

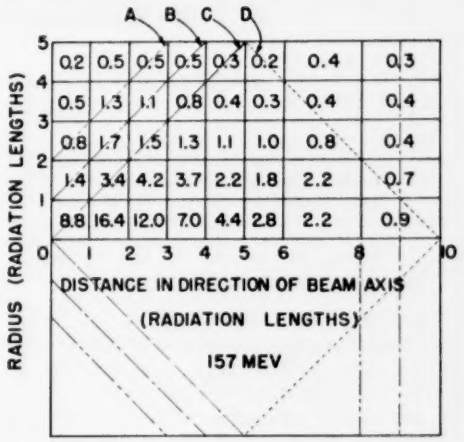

FIG. 17. Same as in Fig. 16 except for 157 Mev.

Figures 16 and 17 show how the energy is divided up into the various volume elements of a crystal. Particularly favorable conical crystals with conical tips have been sketched in the figures. In position C the conical tip of the crystal is directly in the beam, and in this position 73.8 percent of the total energy in the shower would be captured at 118 Mev and 74.9 percent at 157 Mev. In position B one radiation length has been cut off the conical tip, and this crystal now being nine radiation lengths in length would actually capture more energy than position C. At 118 Mev this crystal captures 85.2 percent and at 157 Mev it captures 83.1 percent of the total energy in the shower. Position A shows two radiation lengths cut off the conical tip and this crystal would capture even a greater percentage; 87.9 percent at 118 Mev and 85.6 percent at 157 Mev. By turning the crystal around so the conical tip is near the end of the shower we can take advantage of the hard core of the shower for a longer length. Position D shows this arrangement, and this crystal would capture 90.0 percent of the total energy in the shower at 118 Mev and 87.9 percent at 157 Mev.

We wish to thank H. R. Fechter, R. A. Helm, J. Jasberg, R. Kyhl, G. Masek, and Phyllis Hanson for their kind help in running the accelerator and taking data. We wish also to thank W. K. Panofsky for interesting discussions.

The Gyromagnetic Ratio of Supermalloy

G. G. Scott
Research Laboratories Division, General Motors Corporation, Detroit, Michigan
(Received September 24, 1952)

The gyromagnetic ratio of supermalloy has been determined by a highly refined magneto-mechanical method. The value obtained is 1.030±0.001 times the mass-to-charge ratio of the electron. Within the limits of experimental error, this is the same value as has recently been reported for pure iron.

INTRODUCTION

IT has been known for some time that the gyromagnetic ratio of a material determined by microwave techniques does not agree with the value determined by magnetomechanical methods. In an earlier paper[1] the author published values for the gyromagnetic ratios of Fe, Co, and Ni, as determined by a highly refined mechanical method.[2] In discussing these results with Dr. C. Kittel he suggested that this work be extended to include supermalloy since unusually sharp absorption lines are obtained by microwave methods for this material.[3] Arrangements were therefore made through Dr. S. O. Morgan whereby the Bell Telephone Laboratories very kindly furnished the author a heat treated supermalloy rod 1.5 cm in diameter and 22 cm long. This rod was wound with a magnetizing winding and supported as a torsional pendulum as indicated in reference 2.

TABLE I. Condensed data for the determination of the gyromagnetic ratio of supermalloy.

Date	Double amplitude change per reversal d (cm)	Element current i_e (amp)	Element magnetic moment M_e (amp cm²)	Period P (sec)	Gyromagnetic ratio in terms of m/e for the electron
Dec. 3, '51	0.03562	0.004311	23 154	26.937	1.032
Dec. 4, '51	0.03571	0.004309	23 147	26.925	1.036
Dec. 5, '51	0.03566	0.004310	23 149	26.923	1.034
Dec. 6, '51	0.03563	0.004310	23 150	26.936	1.033
Jan. 18, '52	0.03528	0.004308	23 056	26.927	1.027
Jan. 21, '52	0.03546	0.004309	23 147	26.946	1.028
Jan. 22, '52	0.07395	0.009011	48 370	26.951	1.025
Jan. 24, '52	0.07454	0.009012	48 375	26.928	1.034
Jan. 25, '52	0.07420	0.009012	48 377	26.950	1.029
Feb. 4, '52	0.07356	0.009011	48 372	26.928	1.021
Feb. 5, '52	0.03573	0.004312	23 163	26.941	1.035
Feb. 8, '52	0.03534	0.004311	23 156	26.919	1.025
				Average	1.030

Area summation of element winding: 75 378. cm²
Moment of inertia: 210.52 gram cm²
Length of light beam: 1589.2 cm

RESULTS

The results obtained for this supermalloy sample are based on readings taken on 12 different days. On each day four runs were obtained—one for each of four azimuthal positions separated from each other by 90°. This method eliminated errors caused by magnetic coupling between any small uncorrected fields and the magnetized sample. To eliminate any possible errors caused by the magnetizing current passing through the suspension system, readings were taken on alternate days with opposite positions for the small reversing switch located on the pendulum system.[2]

The value for the gyromagnetic ratio of supermalloy as determined in this series of experiments, is $(1.030\pm0.001)m/e$. The data from which this value has been calculated are condensed and tabulated in Table I. This value corresponds to a Landé factor of 1.942. Within the limits of accuracy of these experiments, this is the same value as has previously been reported by the author for the gyromagnetic ratio of pure iron (1.946).

It will be noted that the gyromagnetic ratios as determined by microwave techniques are also very nearly the same for both iron and supermalloy, and that the magnitude of the departure from 2 is very nearly three times as great in microwave experiments as it is in the present magnetomechanical experiments.

[1] G. G. Scott, Phys. Rev. **87**, 697 (1952).
[2] G. G. Scott, Phys. Rev. **82**, 542 (1951).
[3] W. A. Yager and R. M. Bozorth, Phys. Rev. **72**, 80 (1947).

PHYSICAL REVIEW VOLUME 89, NUMBER 3 FEBRUARY 1, 1953

The Symmetry of the S Matrix

F. COESTER
Department of Physics, State University of Iowa, Iowa City, Iowa
(Received September 29, 1952)

It is proven that any Heisenberg S matrix is symmetric for an appropriate choice of arbitrary phases in a representation in which the square and one component of the total angular momentum are diagonal. The consequences of this symmetry for the complex phases of the matrix elements are discussed.

I. THE SYMMETRY OF THE S-MATRIX

WIGNER and Eisenbud[1] have shown that the collision matrix for simple nuclear reactions is symmetric, provided arbitrary phases in the nuclear wave functions are chosen appropriately. This symmetry is a consequence of the time reversal invariance of the quantum mechanical formalism. The proof of Wigner and Eisenbud applies only to reactions in which there are two heavy fragments in the initial and final states.

It is the purpose of this note to prove that any Heisenberg S matrix[2] is symmetric for an appropriate choice of arbitrary phases in a representation in which the square and one component of the total angular moment $\mathbf{J}$ are diagonal. This proof will be developed by combining the theory of time reversal in quantum mechanics given by Wigner[3] with the methods of transformation theory.

Time reversal for a classical system can be defined by stating the transformation properties of a complete set of dynamical variables: velocities, momenta, angular momenta, and the electromagnetic vector potential change their sign as $t\rightarrow -t$. Position coordinates and energies remain unchanged. This determines the transformation property of any dynamical variable Q: $Q(t)\rightarrow Q^{\tau}(-t)$ as $t\rightarrow -t$ (e.g., $\mathbf{v}^{\tau}=-\mathbf{v}$, $\mathbf{x}^{\tau}=\mathbf{x}$). The operator of time reversal in quantum mechanics K must then satisfy for every Q and every state $\psi(t)$ the requirement

$$(K\psi(t), QK\psi(t))=(\psi(-t), Q^{\tau}\psi(-t)). \tag{1}$$

According to Wigner,[3] this operator takes the form

$$K\psi(t)=U\psi^{*}(-t), \tag{2}$$

where U is a unitary operator determined by the requirement (1). In a Schrödinger representation Q and U will be time independent, and from (1) it follows that

$$U^{+}QU=\tilde{Q}^{\tau}, \tag{3}$$

where $\tilde{Q}$ is Q transposed. If $Q^{\tau}=Q$, we call Q invariant under time reversal. The Hamiltonian of any system is invariant in this sense. The invariance of the S matrix is the mathematical expression of the principle of detailed balance. It can be shown to follow from the time reversal invariance of the Hamiltonian.[4]

A change in representation affects U in the following manner. Let ψ and ψ' be two representations of the same state related by the unitary transformation T:

$$\psi'=T\psi, \quad (K\psi)'=TK\psi. \tag{4}$$

From (2) and

$$(K\psi(t))'=U'\psi'^{*}(-t), \tag{5}$$

one finds with (4) that

$$U'=TU\tilde{T}.^{5} \tag{6}$$

For a system consisting of any number of particles (including photons), we specify the states by the quantum numbers J, M of the total angular momentum and other quantum numbers collectively denoted by A, $B\cdots$. Since $\mathbf{J}^2$ is invariant under time reversal,

$$U^{+}\mathbf{J}^2U=\mathbf{J}^{2*}. \tag{7}$$

Hence, U must be diagonal in the quantum number J. The quantum numbers A, $B\cdots$ are chosen such that they label the eigenvalues of time reversal invariant operators, for instance, the squares of the angular momenta of parts of the system. U must therefore also be diagonal in A. The M dependence of U can be determined from the condition

$$U^{+}\mathbf{J}U=-\mathbf{J}^{*}. \tag{8}$$

With the help of the known matrix representation[6] for J, one finds from (8), with some simple algebra,

$$(J'M'A'|U|JMA)=\delta_{A'A}\delta_{J'J}\delta_{-M'M}e^{i\pi[\alpha(J,A)+M]}, \tag{9}$$

where $\alpha(J, A)$ is an undetermined real function of J and A. The fact that U is unitary has, of course, also been used in the derivation of (9). α is, however, not only undetermined but completely arbitrary: we may always change the phases of the wave function by operating with the unitary matrix,

$$(J'M'A'|T|JMA)=\delta_{J'J}\delta_{M'M}\delta_{A'A}e^{-i\pi\beta(J,A)}. \tag{10}$$

[1] E. P. Wigner and L. Eisenbud, Phys. Rev. **72**, 29 (1947).
[2] W. Heisenberg, Z. Physik **120**, 513, 673 (1943).
[3] E. P. Wigner, Gött. Nach. **31**, 546 (1932).
[4] F. Coester, Phys. Rev. **84**, 1259 (1951).
[5] It is easy to generalize this for time dependent transformations $T(t)$, where

$$U'(t)=T(t)U\tilde{T}(-t).$$

With this equation one can show that U is time independent in any interaction representation in which H_0 is real.
[6] E. U. Condon and G. H. Shortley, *The Theory of Atomic Spectra* (Cambridge University Press, Cambridge, 1951), p. 48.

If we transform U with (10) according to (6), we get

$$(J'M'A'|U'|JMA)=\delta_{J'J}\delta_{M'M}\delta_{A'A}e^{i\pi(\alpha-2\beta+M)}. \quad (11)$$

β is arbitrary; we may therefore choose α conveniently in the first place. The choice

$$(J'M'A'|U|JMA)=\delta_{A'A}\delta_{J'J}\delta_{-M'M}e^{i\pi(J+M)} \quad (12)$$

makes U real and has the following advantage: Consider two systems, respectively, described by the quantum numbers $J_1M_1A_1$ and $J_2M_2A_2$; $\mathbf{J}_1+\mathbf{J}_2=\mathbf{J}$. The matrix U for the combined system in a $JMJ_1J_2A_1A_2$ representation can be obtained by taking the outer product of the U's for the separate systems and transforming according to (6) with the Clebsch-Gordan coefficient $(J_1J_2M_1M_2|JM)$. We assume (12) for the individual systems. Since the conventional Clebsch-Gordan coefficients are real and satisfy the symmetry relation[7]

$$(J_1J_2-M_1-M_2|J-M)=(-1)^{J_1+J_2-J}(J_1J_2M_1M_2|JM), \quad (13)$$

we again find (12) for the combined system if A is understood to stand for $J_1J_2A_1A_2$. No additional phase transformation is needed.

The time reversal invariance of the S matrix is, according to (3), expressed in the form

$$U^+SU=\bar{S}. \quad (14)$$

Since S is invariant under rotations of the coordinate system, it is diagonal in J and M and independent of M. It can therefore be written in the form $(B|S_J|A)$. From (12) and (14) it follows that

$$(B|S_J|A)=(A|S_J|B). \quad (15)$$

This establishes the symmetry of the S matrix which we set out to prove.

II. THE PHASES OF REACTION MATRIX ELEMENTS

If we substitute in (14) and (15) for S any invariant Hermitian operator, the matrix elements must be real. This is important in those cases where perturbation theory is applicable.[8] Whenever perturbation theory is applicable, the matrix elements are real. In general, the phases of the elements of S are not determined by (15), but for reactions involving the formation of a compound nucleus further conclusions can be drawn.

For resonance reactions elements of a certain finite submatrix of $R=S-1$ are large compared to all other elements. The picture of the compound nucleus suggests that all large elements belong to the same J. Neglecting small terms, we have a finite unitary and symmetric matrix $(B|S|A)$ to consider.[9] Any such matrix can be written in the form

$$S=(1+i\pi K)^{-1}(1-i\pi K), \quad (16)$$

where K is a real symmetric matrix. K and consequently S can be diagonalized by a real unitary matrix $T_{\lambda A}$. If K_λ are the eigenvalues of K, we have

$$R_\lambda=-2\pi iK_\lambda/(1+i\pi K_\lambda). \quad (17)$$

Assuming that $|K_\lambda|\gg 1$ at resonance for some values of λ, one finds

$$(B|R|A)=-2\sum_\lambda{}' T_{\lambda B}T_{\lambda A}, \quad (18)$$

where $\sum_\lambda{}'$ indicates summation over those values of λ for which $|K_\lambda|\gg 1$.

More can be said if the picture of the compound nucleus is further exploited. We describe the initial ensemble of particles capable of forming a compound nucleus of spin J by the density matrix[10] $(AJM|\rho_0|BJM')$. The ensemble of decay products of the compound nucleus is described by $(CJM|\rho_f|DJM')$. Since $(1/2\pi)|(B|R|A)|^2$ is the probability per unit time for the transition $A\to B$, ρ_0 and ρ_f are related by[11]

$$(CJM|\rho_f|DJM')=\text{const}\sum_{AB}(C|R|A)(AJM|\rho_0|BJM')(B|R^+|D). \quad (19)$$

The picture of the compound nucleus suggests that ρ_f should be independent of the way in which the compound nucleus is formed. That means it should be independent[12] of ρ_0. This requirement is satisfied if and only if R is proportional to a projection operator P which projects all states into a one-dimensional subspace. That means R has only one nonvanishing eigenvalue. $\sum_\lambda{}'$ in (18) reduces then to one term. The reality of $(B|R|A)$ in (18) is, however, independent of the assumption just discussed. On the other hand, off resonance the compound nucleus assumption formulated above gives us

$$(B|R|A)=-\frac{2\pi i\kappa}{1+i\pi\kappa}T_{\lambda B}T_{\lambda A}, \quad (20)$$

where κ is the nonvanishing eigenvalue of K. Since $T_{\lambda B}$ is real, this means that the matrix elements for all reactions which go through the same compound nucleus have the same phase. To what extent the basic assumption is valid must be decided ultimately by experiment. A resonance in the cross section is not sufficient to guarantee its validity. It rests at present mainly on its plausibility.

[7] G. Racah, Phys. Rev. **62**, 438 (1942).

[8] S. P. Lloyd has shown [Phys. Rev. **81**, 161 (1951)] that the relative phase of the matrix elements for multipole emission is either 0 or π. This result is a special case of our theorem.

[9] We drop the subscript J here for the sake of simplicity.

[10] For a definition of the density matrix and discussion of its formal properties see for instance R. C. Tolman, *The Principles of Statistical Mechanics* (Clarendon Press, Oxford, 1938), Chap. IX.

[11] This follows directly in a representation in which both ρ_0 and ρ_f are diagonal; if ρ_f and ρ_0 do not commute, they can both be diagonal if A, B and C, D refer respectively to different coordinate systems in Hilbert space. Equation (19) itself is then obtained by appropriate change of the representation. See also L. Wolfenstein and J. Ashkin, Phys. Rev. **85**, 947 (1952).

[12] T. D. Newton, Can. J. Phys. **30**, 53 (1952). See in particular assumption (A), p. 57.

The $Zr^{92}-Mo^{92}$ and $Zr^{94}-Mo^{94}$ Pairs and the $Zr^{96}-Mo^{96}-Ru^{96}$ Triplet

JAMES S. GEIGER,* BENJAMIN G. HOGG,† HENRY E. DUCKWORTH, AND JOHN W. DEWDNEY‡
Department of Physics, McMaster University, Hamilton, Ontario, Canada

(Received August 27, 1952)

Mass spectrographic measurements are reported of the following mass differences; $\frac{1}{4}W^{184}-Zr^{92}$, $\frac{1}{2}W^{184}-Mo^{92}$, $\frac{1}{2}Os^{188}-Zr^{94}$, $\frac{1}{2}Os^{188}-Mo^{94}$, $\frac{1}{2}Os^{192}-Zr^{96}$, $\frac{1}{2}Os^{192}-Mo^{96}$ and $\frac{1}{2}Os^{192}-Ru^{96}$. These results are used to check and supplement existing transmutation and disintegration data in the region of the $Zr^{92}-Mo^{92}$ and $Zr^{94}-Mo^{94}$ isobaric pairs and the $Zr^{96}-Mo^{96}-Ru^{96}$ isobaric triplet.

INTRODUCTION

THIS paper describes a mass spectrographic determination of the $Zr^{92}-Mo^{92}$, $Zr^{94}-Mo^{94}$, $Zr^{96}-Mo^{96}$, and $Ru^{96}-Mo^{96}$ mass differences. The information so obtained is useful in checking the correctness of certain transmutation and disintegration data and in estimating the energy available for unobserved reactions.

EXPERIMENTAL

The measurements herein reported were made by the doublet method using our large Dempster-type mass spectrograph.[1] The ion source was a high frequency spark. One electrode of the spark consisted of a thin-walled nickel tube which was packed with the elements to be studied. Exposure times ranged from 5–10 minutes The mass differences obtained in this way are shown in Table I.

The $Zr^{92}-Mo^{92}$ Stable Isobaric Pair

Nb^{92} has been found to decay to both Zr^{92} and Mo^{92}, in the former case by K-capture. There is a 0.93-Mev gamma-ray in the K-capture branch,[2] which represents all but 0.05 percent of the transitions, while the end point of the negatron group leading to Mo^{92} has been reported[3,4] to be 1.38 Mev.

It is possible to compute the energy available for the K-capture decay in two ways using existing transmutation data. The first calculation is based on the $Nb^{93}(\gamma,n)$ threshold[5] of 8.7±0.2 Mev, a Q[6] of 4.33±0.2 Mev for the $Zr^{92}(d,p)$ reaction, and values of 0.19[7] and 0.06[8] Mev for the end point of the Zr^{93} negatrons, *viz.*:

$$Nb^{93}-Nb^{92}=0.99964\pm21 \text{ amu};$$
$$Zr^{93}-Zr^{92}=1.00193\pm21 \text{ amu};$$
$$Zr^{93}-Nb^{93}=0.00013\pm\ 7 \text{ amu}.$$

Therefore,

$$Nb^{92}-Zr^{92}=0.00216\pm30 \text{ amu}=2.0\pm0.3 \text{ Mev}.$$

The second calculation is based on 2.5±0.2 Mev for the $Zr^{92}(p,n)Nb^{92}$ threshold,[9] and gives the value $Nb^{92}-Zr^{92}=1.7\pm0.2$ Mev. These two figures are in satisfactory agreement and appear consistent with a K-capture branch containing a 0.93-Mev gamma-ray. We shall assume a value of 1.8±0.2 Mev for the $Nb^{92}-Zr^{92}$ mass difference.

It is likewise possible to compute a value for the $Nb^{92}-Mo^{92}$ decay energy. The pertinent data are 8.7±0.2 Mev[5] for the $Nb^{93}(\gamma,n)$ threshold, 6.08±0.2 Mev[6] for the Q of the $Mo^{92}(d,p)$ reaction, 3.7±0.2 Mev[9] for the $Nb^{93}(p,n)Mo^{93m}$ (6.75 hr) threshold, and 2.5–2.7 Mev[10,11] for the $Mo^{93m}\rightarrow Mo^{93}$ transition. Thus,

$$Nb^{93}-Nb^{92}=0.99964\pm21 \text{ amu};$$
$$Mo^{93}-Mo^{92}=1.00005\pm21 \text{ amu};$$
$$Mo^{93m}-Nb^{93}=0.00309\pm21 \text{ amu};$$
$$Mo^{93m}-Mo^{93}=0.00279\pm10 \text{ amu}.$$

TABLE I. Mass spectrographic mass differences.

Nuclides	Mass difference mMU	Mev	Previous measurements
$\frac{1}{4}W^{184}-Zr^{92}$	69.79±0.14		74.1±1.8[a] 69.3±0.4[b]
$\frac{1}{4}W^{184}-Mo^{92}$	68.45±0.22		——
$Mo^{92}-Zr^{92}$ [c]	1.34±0.26	1.25±0.25	
$\frac{1}{2}Os^{188}-Zr^{94}$	71.34±0.12		——
$\frac{1}{2}Os^{188}-Mo^{94}$	72.56±0.16		73.1±2.8[a]
$Zr^{94}-Mo^{94}$ [c]	1.22±0.20	1.14±0.2	
$\frac{1}{2}Os^{192}-Zr^{96}$	71.83±0.24		——
$\frac{1}{2}Os^{192}-Mo^{96}$	75.46±0.14		72.8±2.9[a]
$\frac{1}{2}Os^{192}-Ru^{96}$	72.44±0.17		75.9±1.9[a] 73.4±1.3[d]
$Zr^{96}-Mo^{96}$ [c]	3.63±0.28	3.4 ±0.3	
$Ru^{96}-Mo^{96}$ [c]	3.02±0.22	2.8 ±0.2	

[a] A. J. Dempster, Phys. Rev. **53**, 64 (1938).
[b] Duckworth, Kegley, Olson, and Stanford, Phys. Rev. **83**, 1114 (1951).
[c] These values are computed from the other values which are the experimentally determined ones.
[d] A. C. Graves, Phys. Rev. **55**, 863 (1939).

* Holder of a Research Council of Ontario Scholarship. Present address: Sloane Laboratory of Physics, Yale University, New Haven, Connecticut.
† Holder of a National Research Council of Canada Fellowship.
‡ Holder of a Research Council of Ontario Scholarship.
[1] H. E. Duckworth, Rev. Sci. Instr. **21**, 54 (1950).
[2] P. Preiswerk and P. Stähelin, Helv. Phys. Acta **24**, 300 (1951).
[3] Sagane, Kojima, Niyamoto, and Ikawa, Proc. Phys. Math. Japan **22**, 174 (1940).
[4] D. N. Kundu and M. L. Pool, Phys. Rev. **71**, 140 (1947).
[5] Sher, Halpern, and Mann, Phys. Rev. **84**, 387 (1951).
[6] J. A. Harvey, Phys. Rev. **81**, 353 (1951).
[7] G. E. Boyd and Q. V. Larson, Oak Ridge National Laboratory Report ORNL-685 (1950) (unpublished).
[8] E. P. Steinberg and L. E. Glendenin, Phys. Rev. **78**, 624 (1950).
[9] Blaser, Boehm, Marmier, and Scherrer, Helv. Phys. Acta **24**, 441 (1951).
[10] *Nuclear Data*, National Bureau of Standards Circular 499 (1950), p. 100.
[11] L. Ruby and J. R. Richardson, Phys. Rev. **83**, 698 (1951).

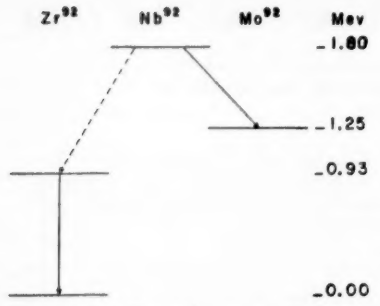

FIG. 1. Energetics at mass 92.

Therefore,

$$Nb^{92}-Mo^{92}=0.00011\pm38 \text{ amu}=0.1\pm0.4 \text{ Mev}.\S$$

It appears from this result that the 1.38-Mev beta-ray is not a transition from the ground state of Nb^{92} to the ground state of Mo^{92}.

These calculations indicate that the $Mo^{92}-Zr^{92}$ mass difference is $(1.8\pm0.2)-(0.1\pm0.4)=1.7\pm0.4$ Mev. From our experiments, as seen from Table I, this difference has been found to be 1.25 ± 0.25 Mev. These results are in satisfactory agreement, especially when one considers that the computed values are based on a chain of several measurements, each of which is subject to an error of 0.1–0.2 Mev. The energy relationships between Zr^{92}, Nb^{92}, and Mo^{92} are shown in Fig. 1. No attempt has been made to fit the 0.1 ± 0.4 Mev $Nb^{92}-Mo^{92}$ mass difference into this figure.

The $Zr^{94}-Mo^{94}$ Isobaric Pair

The state of knowledge of Nb^{94} is shown in Fig. 2.[10] It is not possible to compute the $Zr^{94}-Mo^{94}$ mass difference from disintegration or transmutation data. From Table I it is seen that the measured $Zr^{94}-Mo^{94}$ mass difference is 1.14 ± 0.2 Mev. This leaves 0.12 Mev of energy available for the K-capture mode of decay from the ground state of Nb^{94}, a figure which explains the lack of success[12] with which experiments to detect it have met.

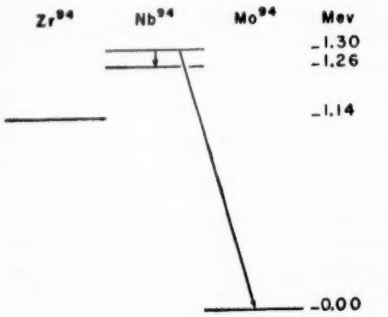

FIG. 2. Energetics at mass 94.

§ *Note added in proof:* Blaser *et al.* (see reference 9) have also made a calculation of this mass difference and have obtained substantially the same result.

[12] Hein, Fowler, and McFarlane, Phys. Rev. **85**, 138 (1952).

The $Zr^{96}-Mo^{96}-Ru^{96}$ Isobaric Triplet

Some knowledge of the $Zr^{96}-Mo^{96}$ mass difference may be obtained from the $Zr^{96}(p,n)$ threshold plus the various studies of the decay scheme of Nb^{96}.

Regarding the $Zr^{96}(p,n)$ threshold, this has been found by Blaser *et al.*[9] to be 2.6 ± 0.2 Mev. When this is compared to 2.5 Mev for the $Zr^{92}(p,n)$ threshold, obtained in the same laboratory, it is difficult to believe that both can be correct. One would expect the figure for Zr^{96} to be much lower than that for Zr^{92}. The latter has been seen above to be consistent with the other data at mass number 92. Consequently, we are assuming that the reported $Zr^{96}(p,n)$ value is to an excited state of Nb^{96}.

Concerning the $Nb^{96}-Mo^{96}$ decay, three values have been reported for the total decay energy: these are 3.14 Mev,[10] 3.16 Mev,[2] and 1.98 Mev.[13] Our value for the $Zr^{96}-Mo^{96}$ mass difference is 3.4 ± 0.25 Mev, which is larger than any of the figures for the $Nb^{96}-Mo^{96}$ difference. This implies either that there is more energy in the Nb^{96} decay than is presently realized, or that Zr^{96} is unstable against beta-decay to Nb^{96}. The former possibility does not seem very likely since two recent independent measurements agree closely on the total decay energy for Nb^{96}. The second possibility, which is the more likely, is analogous to the case of Ca^{48} which does not decay to Sc^{48}, although energetically possible, because of the large spin change involved.[14] Further, it is interesting to note that McCarthy[15] has obtained preliminary evidence for an activity of 3.3–4.3 Mev in Zr^{96}. This activity, if authentic, would represent the double beta-decay of Zr^{96} to Mo^{96}.

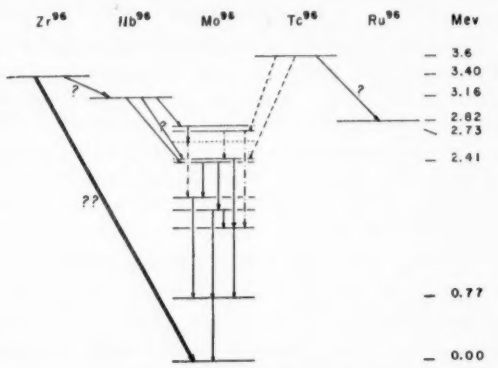

FIG. 3. Energetics at mass 96.

Turning now to the $Ru^{96}-Mo^{96}$ pair, it is known that Tc^{96} decays to Mo^{96} by K-capture and possibly to Ru^{96} by negatron emission. In the former case, 2.73

[13] M. L. Pool (private communication).

[14] T. P. Kohman, Phys. Rev. **73**, 16 (1948); T. P. Kohman, Phys. Rev. **73**, 1223 (1948); J. W. Jones and T. P. Kohman, Phys. Rev. **85**, 941 (1952); D. Kurath, Phys. Rev. **87**, 528 (1952); Hammermesh, Hummel, Goodman, and Engelkemeir, Phys. Rev. **87**, 528 (1952).

[15] J. A. McCarthy (private communication, August 10, 1952).

Mev[16] of gamma-rays follow the K-capture event, while the negatron group, if it exists, has an end point of ~0.8 Mev.[17,18] Both these data are consistent with our measurement of 2.8±0.2 Mev for the $Ru^{96}-Mo^{96}$ mass difference. Figure 3 shows the level schemes at mass number 96.

It is interesting to use our values for the $Zr^{96}-Mo^{96}$ and $Ru^{96}-Mo^{96}$ mass differences to construct at mass 96 the even-even parabola, which is predicted by the semi-empirical mass formula. This is done in Fig. 4, where it is compared to the parabola resulting from the use of the computed masses (with suitable vertical displacement) of Metropolis and Reitwiesner.[19]

The experimental parabola is seen to be wider than the predicted one. This also follows from the experiments of the Columbia group[20] who have found the sides of the valley of stability at constant Z (for $Z=32$ and $Z=34$) to be less steep than given by the computed masses.

Discussion of the Mo−Zr Mass Differences

In some cases at odd mass number, the Mo−Zr mass differences have been found by studying the decay schemes involved, *viz*: $Mo^{91}-Zr^{91} \geqslant 3.6$ Mev,[21]|| $Zr^{95}-Mo^{95}=2.04$ Mev,[22] and $Zr^{97}-Mo^{97}=4.59$ Mev.[23] In Fig. 5, where these values are plotted together with our $Mo^{92}-Zr^{92}$, $Zr^{94}-Mo^{94}$, and $Zr^{96}-Mo^{96}$ results, the mass difference appears to be a linear function of the mass number.

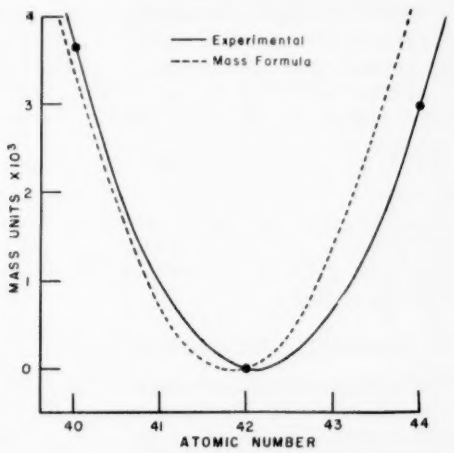

FIG. 4. The experimental and theoretical parabolae at mass 96. Assuming a form $({}_zM^A-{}_{Z_0}M^A)=\frac{1}{2}B(Z-Z_0)^2$, the parameters in the experimental case are $B=1.55$, $Z_0=42.1$, and in the theoretical case $B=1.94$, $Z_0=41.8$. *Note added in proof:* Charles D. Coryell, in a paper entitled "Beta Decay Energetics," to be published in Vol. II of *Annual Reviews of Nuclear Science*, gives in the region $70<A<90$, a curve of B *versus* A, derived from decay energies. This curve, when extrapolated to $A=96$, gives the value $B\sim1.5$, in good agreement with our experimental one.

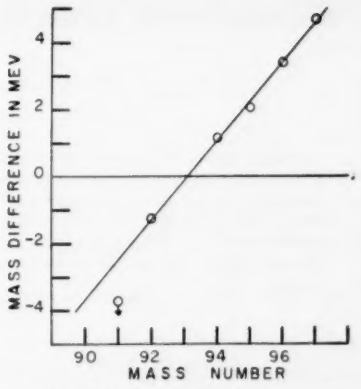

FIG. 5. A plot of the isobaric Zr−Mo mass differences *vs* mass number.

The widespread existence of linear relationships of this type has been pointed out to us by Dr. Katharine Way and Miss Marion Wood, and will, we understand, be described in detail by them in a future publication. The semi-empirical mass formula also predicts an approximately linear curve. We, therefore, regard Fig. 5 as an indication of the general correctness of our results.¶ The departure of the point at mass number 91 from the straight line curve is adequately explained by the extra energy involved in the $Mo^{91}-Nb^{91}$ transition, owing to the ease with which Mo^{91} is transformed into the 50 neutron configuration, Nb^{91}.

These results indicate that Zr^{93} and Mo^{93} are practically equal in mass. This is compatible with the fact that Zr^{93} has a half-life of $>4\times10^6$ years and Mo^{93} decays by K-capture with presumably a long lifetime.

The authors are grateful to Dr. Katherine Way and her colleague, Miss Marion Wood, both for sending us helpful preliminary reports on their beta-ray systematics in the mass 90–100 region, and for drawing to our attention pertinent experimental work. We also appreciate receiving prepublication accounts from John A. McCarthy of his studies of double-beta decay in Zr^{96}. These experiments have been generously supported by the National Research Council of Canada, the Research Council of Ontario, and the Research Corporation of New York.

[16] Medicus, Preiswerk, and Scherrer, Helv. Phys. Acta **23**, 299 (1950).
[17] Medicus, Mukerji, Preiswerk, and de Saussure, Phys. Rev. **74**, 839 (1948).
[18] J. E. Edwards and M. L. Pool, Phys. Rev. **72**, 384 (1947).
[19] N. Metropolis and G. Reitwiesner, *Table of Atomic Masses* (Argonne National Laboratory, Chicago, 1950).
[20] Geschwind, Minden, and Townes, Phys. Rev. **78**, 174 (1950), and S. Geschwind and R. Gunther-Mohr, Phys. Rev. **81**, 882 (1951).
[21] R. B. Duffield and J. D. Knight, Phys. Rev. **76**, 573 (1949).
|| *Note added in proof:* A recent study of the 15.5-min Mo^{91} positrons has given an end point of 3.32±0.05 Mev (Leon Katz, private communication, September 13, 1952). The $Mo^{91}-Zr^{91}$ mass difference is, therefore, $\geqslant 4.4$ Mev.
[22] J. S. Levinger, *Radiochemical Studies: The Fission Products* (McGraw-Hill Book Company, Inc., New York, 1951), Paper No. 94, National Nuclear Energy Series, Plutonium Project Record, Vol. 9, Div. IV; and C. Y. Fay, Phys. Rev. **81**, 300 (1951).
[23] Burgus, Knight, and Prestwood, Phys. Rev. **79**, 104 (1950).
¶ *Note added in proof:* In current mass spectrographic investigations of the Na−Sm isobaric differences at mass numbers 144, 148, and 150, we have found that a similar linear relationship appears to exist in this heavier region.

Magnetic Crystal Anisotropy and Magnetostriction of Iron-Nickel Alloys

R. M. Bozorth and J. G. Walker
Bell Telephone Laboratories, Murray Hill, New Jersey
(Received October 21, 1952)

Single crystals of a number of iron-nickel alloys were prepared, and measurements made of the magnetic crystal anisotropy, and of the magnetostriction at saturation in different crystallographic directions, as dependent on the rate of cooling of the specimens after annealing. There is a large effect of the cooling rate on the anisotropy, for compositions near $FeNi_3$, where atomic ordering occurs. There is a definite but smaller effect of cooling rate on the magnetostriction. The composition for highest initial and maximum permeabilities is nearly that for which λ_{111}, the magnetostriction in the direction of easy magnetization, is equal to zero.

INTRODUCTION

In any theory of the magnetic properties of the iron-nickel alloys, one should take into account the magnetic crystal anisotropy and the magnetostriction at saturation in different crystallographic directions. Some data on these quantities have already been reported. Grabbe[1] showed that the anisotropy constants of quenched alloys are larger (more positive) than those of alloys slowly cooled, and Lichtenberger[2] measured the magnetostriction in the [111], [110], and [100] directions for alloys having one heat treatment.

In the present work the magnetic crystal anisotropy and the magnetostriction in various crystallographic directions are determined on the same specimens, which are subjected to different heat treatments. In confirmation of the work by Grabbe, K is found to depend markedly on heat treatment on account of the atomic ordering that occurs in these alloys, especially in those near in composition to $FeNi_3$. Some effect of heat treatment on saturation magnetostriction is also observed.

The results are discussed briefly in their relation to the "Permalloy problem" which is to explain the various peculiar magnetic properties of iron-nickel alloys having the face-centered cubic structure, especially the high permeabilities of commercial alloys containing about 78 percent nickel, and their variation with heat treatment. It is pointed out that when magnetization proceeds by domain boundary displacement, magnetization gives rise to a minimum of strain energy when the magnetostriction is zero in the *direction of easy magnetization*. In pure quenched alloys this occurs at 79 to 80 percent nickel. This is close to the optimum composition of the alloys of ordinary purity.

PREPARATION AND TREATMENT OF CRYSTALS

Specimens of alloys containing 35 to 90 percent nickel were prepared as described by Walker, Williams, and Bozorth,[3] by slow cooling of the melt in an atmosphere of pure dry hydrogen. The raw materials used were Armco iron and selected Mond nickel, in both of which the metallic impurity content is low; the nonmetallic impurities C, N, O, and S are known to be removed by dry hydrogen at the temperatures used.

Specimens were cut in the form of disks, usually in the (100) plane, and were normally about 1 cm in diameter and 2 mm thick as prepared for use. After careful grinding with a carborundum wheel, and deep etching, the orientation was checked using x-ray spectrometry and back-reflection Laue photographs, the latter for determining the position of the crystal axes in the plane of the disk. When a variation of the surface from the desired crystallographic plane was more than 0.5°, a further correction was made.

Specimens were cooled at two standard rates: (1) they were withdrawn from the furnace at about 700°C and placed quickly on a cold copper plate, or (2) they were cooled from above 600°C to below 300°C at 2°C/hr. In (1) the estimated cooling rate was 300 000°C/hr. The known order-disorder transformation of $FeNi_3$ is 506°C.[4] Presumably, (1) gives a high degree of disorder, (2) a high degree of order, but some of our experiments indicate that a definitely higher degree of order is obtained by cooling at 1°C/hr.

MAGNETIC CRYSTAL ANISOTROPY

The magnetic crystal anisotropy constant K of cubic crystals is defined by the expression for the energy density of crystal anisotropy,

$$E=K(\alpha_1^2\alpha_2^2+\alpha_2^2\alpha_3^2+\alpha_3^2\alpha_1^2),$$

the α's being the direction cosines of the magnetization with respect to the crystal axes. In our experiments K was determined by measuring the torque per unit volume L acting upon the crystal when it was placed in a uniform field sufficiently strong to saturate it. If θ is the angle, measured in the (100) plane between the direction of magnetization and the [001] axis,

$$L=-\partial E/\partial\theta=-\tfrac{1}{2}K\sin 4\theta,$$

and K is then twice the maximum amplitude of L. K and L are expressed in ergs/cm³.

Measurement of L was carried out with apparatus

[1] E. M. Grabbe, Phys. Rev. **57**, 728 (1940).
[2] F. Lichtenberger, Ann. Physik **15**, 45 (1932).
[3] Walker, Williams, and Bozorth, Rev. Sci. Instr. **20**, 947 (1949).
[4] O. Källbäch, Arkiv Mat. Astron. Fysik **34B** (17), 1 (1947).

designed by Williams,[5] and similar in principle to that used by Sixtus.[6] The torsion fiber was a phosphor-bronze wire 0.38 mm in diameter and was found to have a constant of 59 dyne-cm/degree of torque. Reproducible settings could be made to less than 0.1° in the torque angle, therefore in a crystal having a volume of 0.1 cm³ the value of K could be determined with an accuracy of about 100 ergs/cm³, provided there were no other errors.

The magnetic field strength normally used was 9000 oersteds. This was more than sufficient to saturate the specimens of alloys measured, as shown by the constancy of the torque upon reduction of the field to one-half or less.

Often the final specimen was found to have a section that was not exactly circular; consequently, the maxima and minima of the torque curve did not have equal amplitudes. In such a case, only the 4θ component of the curve was used, as determined by a simple procedure: the observed torque curve was displaced horizontally by 90° and superposed on the original, and the average of the two curves taken. Such a procedure also allows for any small holes or imperfections that may or may not be visible on the surface. A specimen of one alloy (74 percent Ni) was prepared parallel to the (110) plane, the geometrical form of the disk being maintained with great care. The torque curve was found to depart only slightly from the theoretical form calculated with the second anisotropy constant K_2 equal to zero.[7] (The data gave $K_2/K<0.06$.)

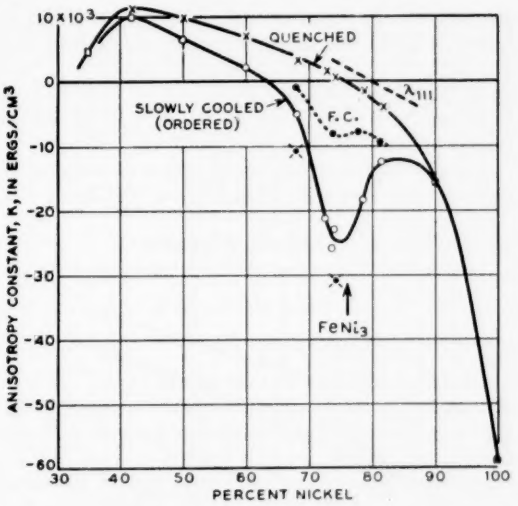

FIG. 1. Magnetic anisotropy constants of quenched and of slowly cooled alloys. Approximate rates of cooling, 10^5 and 2.5°C/hr, respectively, from 600 to 300°C. Broken line F.C. shows values for 55°C/hr. Line λ_{111} shows composition at which magnetostriction in [111] direction goes through zero. Single low points at 68 and 74 percent nickel are for cooling rate of about 1.5°C/hr.

[5] See R. M. Bozorth, *Ferromagnetism* (D. Van Nostrand Company, Inc., New York, 1951), p. 556.
[6] L. P. Tarasov, Phys. Rev. **56**, 1224 (1939).
[7] See reference 5, p. 563, for expression containing K_2.

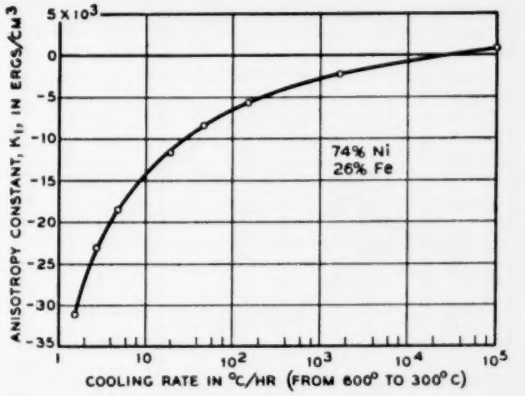

FIG. 2. Anisotropy constants of 74 percent nickel crystal as dependent on rate of cooling from 600 to 300°C. Highest cooling rate is approximate only (quenched on copper plate).

DISCUSSION OF ANISOTROPY

Data for alloys cooled at different rates are shown in Fig. 1. It is noted at once that the slowly cooled alloys have lower (more negative) anisotropy constants, especially in a range of composition near $FeNi_3$, at which a deep minimum occurs. Atomic ordering was detected by x-rays in the slowly cooled alloys containing 74 and 68 percent nickel, and it was not observed either in quenched alloys of the same compositions or in a slowly cooled specimen containing 90 percent nickel. It seems probable then that some ordering occurs in alloys containing as little as 40 percent nickel but not in those containing over 85 percent nickel.

Recently, Corliss, Hastings, and Weiss,[8] using neutron diffraction, have observed ordering in a single crystal of 68 percent nickel. After heat treatment in a magnetic field along a [110] direction, they observed ordering when the neutrons were reflected from the plane perpendicular to this [110] direction, and also when they were reflected from planes parallel to this direction. They thus find no indication of the "directional ordering" postulated by Chikazumi[9] as a possible explanation of the effect of magnetic anneal.

Alloys cooled at the intermediate rate of 50°C/hr, a rate often used in practice in "furnace cooling," have intermediate values of K, as shown by the broken line F.C. in Fig. 1. The alloy containing 74 percent nickel was cooled at various rates, and the resultant anisotropy constants are plotted in Fig. 2. This shows that the degree of ordering is still increasing as the cooling rate falls below 2°C/hr.

The composition at which the anisotropy is zero depends on cooling rate as follows:

Cooling rate (°C/hr)	2	55	10^5,
Composition for $K=0$ (percent Ni)	63	67	75.

[8] Corliss, Hastings, and Weiss, private communication.
[9] S. Chikazumi, Phys. Rev. **85**, 918 (1952).

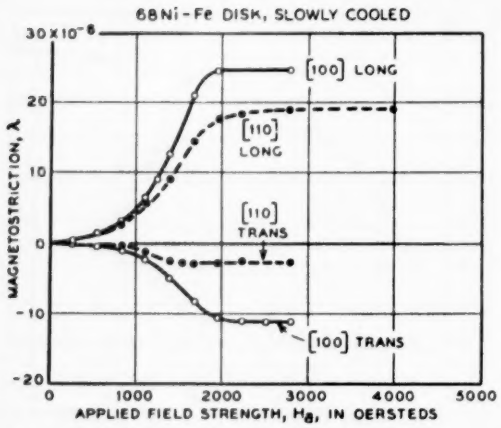

FIG. 3. Longitudinal and transverse magnetostriction of 68 percent nickel crystal, measured in [100] and [110] directions, as dependent on applied field strength. Ratio of diameter to thickness of specimen used is $m=4.4$.

It has previously been pointed out that a low value of the anisotropy constant is related to other magnetic phenomena, for example, low remanence,[10] high strain-sensitivity,[11] and susceptibility to magnetic anneal.[12] More quantitative tests of these relations can now be made.

MAGNETOSTRICTION

Magnetostriction was measured by strain gauges according to the method described by Goldman.[13] Usually $\frac{1}{8}$-in. gauges were employed, fastened to a disk surface with Duco cement and cured at 120 to 160°F as recommended by the maker.[14] The gauge was oriented so that it measured the change in length in a [001] or [011] direction in the (100) plane of the disk.

The magnetization was accomplished in an electromagnet having a 5-in. square section that was tapered to a $3\frac{1}{4}$-in. round section at the pole tips. A valuable increase in the uniformity of the field at the specimen was obtained by turning the pole tips in a lathe so that they presented to the specimen concave surfaces having a radius of curvature of 6 in. With a gap of 2 in., a specimen could be placed on a brass surface at the center, and the non-uniformity of the field would not move it against the friction resulting from its weight. Actually, the specimen was cemented at its edge to a small piece of brass which was held in place by a weight of about 100 g. The cement was allowed to harden with the field on so that the specimen was held parallel to the field; this was done to eliminate bending during the change in field during measurement. The maximum field readily attainable, with 20 amperes through the magnet coils, was about 5000 oersteds. Normally, 3000 oersteds was sufficient for obtaining the desired data.

Leads from the strain gauge led to the three other resistances of the bridge, and one of these, and also the strain gauge, were paralleled with precision resistance boxes that could be varied in steps of 1 ohm to 100 000 ohms. The detector was a Rubicon Photoelectric Galvanometer, with contained dc amplifier, the output of which was connected to a dc voltmeter used with 0–50 or 0–10 volt scales. After balancing the bridge with a given magnetic field applied, we observed the unbalance caused by reducing the field to zero.

Calibration was made by observing the unbalance caused by a known change in the resistance in parallel with the gauge. The change ΔR_g in the gauge resistance R_g that produces the same unbalance as a known change ΔR in the parallel resistance R is determined by

$$\Delta R_g/R_g^2=\Delta R/R^2,$$

provided $\Delta R \ll R$ and $\Delta R_g \ll R_g$. Since $\Delta R_g/R_g$ is strictly proportional to the fractional change in length of the specimen, $\Delta l/l$, we have

$$\frac{\Delta l}{l}=\frac{\Delta R_g}{R_g F}=\frac{R_g \Delta R}{R^2 F},$$

F being the "gauge factor," $(\Delta R_g/R_g)/(\Delta l/l)$, which is supplied by the manufacturer. The calibration curve, linear for small outputs, relates the output to ΔR. In our experiments $R_g \approx 120$, $R \approx 10\,000$ ohms and $F \approx 1.9$. Since the output voltage unbalance $V \approx 1.2\Delta R$, 0.1 volt corresponds to about 0.07×10^{-6}. A fraction of this change in length could be measured when desired.

The effect of the form of the specimen on its magnetostriction was determined as follows. Following Carr

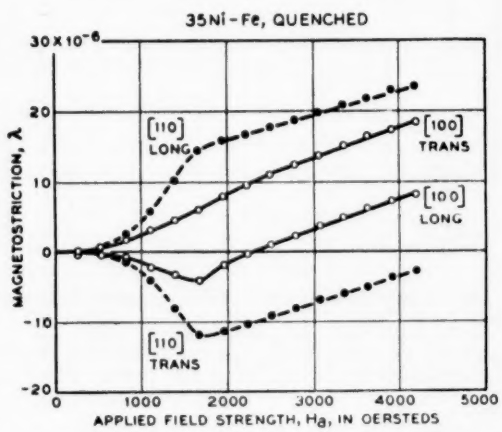

FIG. 4. Magnetostriction of 35 percent nickel crystal, showing large volume effect in high fields. Ratio $m=3.9$.

[10] R. M. Bozorth, Z. Physik **124**, 519 (1948).
[11] R. M. Bozorth and H. J. Williams, Revs. Modern Phys. **17**, 72 (1945).
[12] R. M. Bozorth and J. F. Dillinger, Physics **6**, 285 (1935). See also J. S. Marsh, *Alloys of Iron and Nickel* (McGraw-Hill Book Company, Inc., New York, 1938), pp. 214–19.
[13] J. E. Goldman and R. Smoluchowski, Phys. Rev. **75**, 140 (1949).
[14] The Baldwin-Lima-Hamilton Corporation, Philadelphia, Pennsylvania.

and Smoluchowski,[15] we calculate from the axis of an oblate ellipsoid its eccentricity ϵ

$$a=b=c/(1-\epsilon^2)^{\frac{1}{3}},$$

and the quantity

$$\mu=(3\pi/2\epsilon^4)[(1-\epsilon^2)(3+2\epsilon^2)-(3/\epsilon)(1-\epsilon^2)^{\frac{1}{2}}\sin^{-1}\epsilon].$$

The magnetostriction caused by the form is then

$$\lambda_f=\mu I^2/3(c_{11}-c_{12})$$

for the [100] direction, I being the intensity of magnetization and the c's the elastic constants. In the [111] direction $2c_{44}$ replaces $c_{11}-c_{12}$. The form effect λ_f is an expansion and must be subtracted from the observed change in length to give the required magnetostriction of an infinite sheet. In the crystals here measured $a=b\approx 5c$, $\mu\approx 0.8$, $I\approx 1000$, $c_{11}-c_{12}\approx 10^{12}$, and $\lambda_f\approx 0.2\times 10^{-6}$. In most cases the precision of the measurements does not warrant subtraction of this amount.

Measurements of magnetostriction were usually made in the [100] and [110] directions on the same specimens as those used to measure the magnetic anisotropy. After measuring $\Delta l/l$ parallel to the field, the crystal and attached gauge were turned 90° in their plane and the "transverse" magnetostriction recorded. We denote the longitudinal magnetostriction by λ_l, the transverse by λ_t. For the [100] measurements we then have the desired constant

$$\lambda_{100}=2(\lambda_l-\lambda_t)/3,$$

a result that is independent of the domain distribution before magnetization. Similarly, but not quite so obviously, when λ_l and λ_t are the measured changes in length in the [110] direction when the field is applied, respectively, parallel and perpendicular to [110], we have

$$\lambda_{111}=2(\lambda_l-\lambda_t)/3.$$

These expressions follow from the two-constant formula[5] for magnetostriction:

$$\lambda_s=(3/2)\lambda_{100}(\alpha_1^2\beta_1^2+\alpha_2^2\beta_2^2+\alpha_3^2\beta_3^2-\tfrac{1}{3})+3\lambda_{111}(\alpha_1\alpha_2\beta_1\beta_2+\alpha_2\alpha_3\beta_2\beta_3+\alpha_3\alpha_1\beta_3\beta_1),$$

λ_{100} and λ_{111} being the saturation magnetostriction in the [100] and [111] directions, for material with domains oriented initially at random, and the α's and β's the direction cosines of the magnetization and the measured change in length, respectively, with respect to the crystal axes. Also, $\lambda_{110}=(3\lambda_{111}+\lambda_{100})/4$.

A typical curve showing $\Delta l/l$ as dependent on the magnetizing field H_a, generated by the electromagnet is shown in Fig. 3 for the specimen containing 68 percent nickel. The demagnetizing field of the specimen must be taken into account if one desires to know H inside of the specimen. However, in order to determine the desired constants λ_{100} and λ_{111}, it is only necessary to know the limit which $\Delta l/l$ approaches in high fields. For the case illustrated, $10^6\lambda_{100}=\frac{2}{3}(24.5+11.3)=23.9$, and $10^6\lambda_{111}=\frac{2}{3}(18.7+2.8)=14.3$.

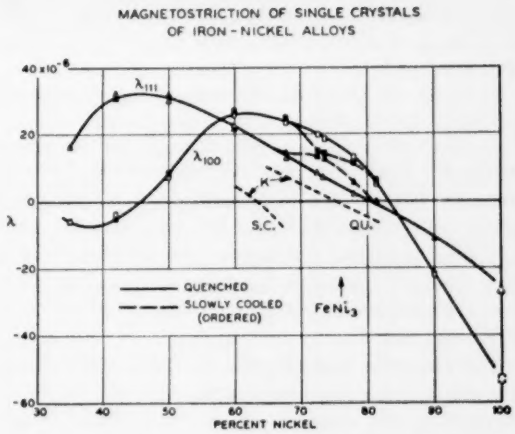

FIG. 5. Magnetostriction of quenched and of slowly cooled alloys. Broken lines show compositions at which anisotropy of quenched (QU.) and slowly cooled alloys (S.C.) goes through zero.

Figure 4 shows the magnetostriction *vs* field strength curves for the single crystal containing 35 percent nickel. All of the curves continue to rise in high fields, a trend that is obviously the result of volume magnetostriction, an expansion that is known to be equal in all directions independent of the direction of the field but approximately proportional to the increase in field-strength. Since this is also known to be most marked near the Curie point, it is not surprising that the material with the lowest Curie point should show the greatest effect.

The volume expansion calculated from the average slopes of the curves in high fields is 12×10^{-9}/oersted, a value that compares reasonably well with the value 15×10^{-9}/oersted reported by Masiyama.[16]

The presence of a large volume magnetostriction does not interfere with the determination of the constants λ_{100} and λ_{111}, for the difference between the longitudinal and transverse magnetostrictions is the desired quantity, and this approaches a definite limit in the high fields used.

DISCUSSION OF MAGNETOSTRICTION

Values of λ_{100} and λ_{111} as dependent on composition are shown in Fig. 5. Results for the quenched alloys are similar to those of Lichtenberger,[2] but λ_{111} is substantially higher in the 40 to 50 percent nickel range.

The effect of ordering is definite but not large, as shown by the broken lines in Fig. 5. The greatest observed change caused by ordering is about 5×10^{-6} in λ_{100} and λ_{111}, but the ratio of the λ_{111}'s can be more

[15] W. J. Carr and R. Smoluchowski, Phys. Rev. **83**, 1236 (1951).

[16] Y. Masiyama, Sci. Repts. Tôhoku Imp. Univ. **20**, 574 (1937).

than 2/1. No definitely established change, attributable to ordering, was observed outside of the range 68 to 80 percent nickel.

Data for alloys in the interesting region near 79 percent nickel are shown on an enlarged scale in Fig. 6. For quenched alloys, λ_{111} goes through zero at about 80 percent nickel; however, the reliability of the two-constant formula for magnetostriction is not great enough to establish the composition for zero λ_{111} with any great precision, and separate measurements have been made[17] to establish this composition. These show that the composition for zero λ_{111} is slightly less than 80 percent nickel.

The change in magnetization by the moving-boundary process takes place most easily when the magnetostriction in the direction of easy magnetization approaches zero.[18] Since [111] is the direction of easy magnetization in quenched iron-nickel alloys containing more than 75 percent nickel, it is to be expected that the composition for highest permeability will coincide with that for $\lambda_{111}=0$. Experiment now shows that these compositions do not differ by more than 1 or 2 percent.

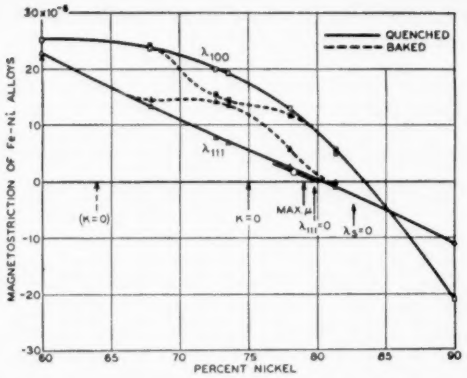

FIG. 6. Magnetostriction of alloys in range 60 to 90 percent nickel, showing unique points in series. Single point near λ_{111} curves is for specimen containing 0.5 percent manganese.

This small shift is probably effected by the nearby point for zero anisotropy at 75 percent nickel.

The relation of the magnetic anisotropy and the magnetostriction to the "Permalloy problem" has been discussed at length in another place.[18] Many of the changes in magnetic properties with composition and heat treatment of alloys of ordinary purity can now be explained in terms of the data here reported.

[17] R. M. Bozorth and R. W. Hamming, Phys. Rev. **87**, 209 (1952).
[18] R. M. Bozorth, Revs. Modern Phys. (to be published).

The Spectrum of Discrete Eigenvalues in a Negative Atomic Ion*

TA-YOU WU
Division of Physics, National Research Council, Ottawa, Canada
(Received June 25, 1952; revised manuscript received October 24, 1952)

It is pointed out that the usual argument for a finite number of stable discrete states in a negative atomic ion is not conclusive, and it is suggested that the question whether there are infinitely many discrete states in a negative ion, of hydrogen for example, calls for an investigation of the behavior of the spectrum of eigenvalues of the Hamiltonian for a two-electron atomic system at the point $Z=1$.

WHILE it is well known that many atoms, such as the halogens, oxygen, hydrogen, and even the alkali metal atoms, have a positive electron affinity and hence form stable negative atomic ions, the question as to whether there exist other stable states (stable in the sense that they are not subject to auto-ionization, i.e., they lie below the ionization limit which is the normal state of the neutral atom) in a negative ion does not seem to have been much investigated. On the experimental side, evidence for the existence of excited states of negative ions is very meager and uncertain.[1] On the theoretical side, no calculation has been made which is of the necessary accuracy to answer this question. It seems to be generally believed that at most a few stable states can exist in a negative ion. The argument seems to be the following.[1] Consider the negative ion of hydrogen H^-. The field on one electron resulting from the nucleus and the other electron falls off very much more rapidly with distance than a Coulomb field, and in such a field there can be only a finite number of discrete states. A similar argument applies to other negative ions.

The purpose of the present note is to emphasize that such an argument as given above is qualitative and inconclusive, and that the assumption of the continuity of the spectrum of eigenvalues of the Hamiltonian of the helium-like system at $Z=1$ would lead to the existence of infinitely many discrete states.

The Hamiltonian of a two-electron atomic system is

$$H=-\nabla_1^2-\nabla_2^2-2Z(1/r_1+1/r_2)+2/r_{12}. \quad (1)$$

Consider first $Z=2$ for the helium atom. The discrete part of the spectrum of eigenvalues of (1), which contains the infinitely many states described as $1snl\ ^{1,3}L$ in spectroscopic notation, may be defined by the following boundary conditions of the symmetrized wave functions $\psi_n(r_i, r_j)$:

$$\phi_n^2(r_i)=\int|\psi_n(r_i, r_j)|^2dr_j\to 0 \text{ for large } r_i,\ i=1,\ 2. \quad (2)$$

The first ionization limit may be defined as the lowest state satisfying the boundary condition:

$$\phi_k^2(r_i)=\int|\psi_k(r_i, r_j)|^2dr_j$$
$$\to\text{finite and oscillatory for large } r_i,\ i=1,\ 2. \quad (3)$$

The limit so defined will be very close to the one-electron state $1s\ ^2S$ of He^+.

Let us now vary the parameter Z in (1) adiabatically from 2 to

$$Z=1+\epsilon,\quad 0<\epsilon\leq 1. \quad (4)$$

The number of discrete states in the spectrum can be shown to remain infinite on the following considerations. For any value of Z in (4), one can first make the less optimistic estimate of the eigenvalues of (1) by separating the Schrödinger equation corresponding to (1) and studying the motion of one electron in the field of the nucleus and the other electron. This field obviously has the following limiting forms:

$$\lim_{r\to 0}V(r)\to-\frac{2Z}{r},$$
$$\lim_{r\to\infty}V(r)\to-\frac{2(Z-1)}{r}. \quad (5)$$

In such a field, there are infinitely many discrete states, even when $Z-1=\epsilon$ is an infinitesimal.[2] The exact treatment of the system (1) allowing for what is ordinarily called the polarization will give a spectrum of discrete states which are lower than the corresponding ones obtained on the above one-electron problem, and the number of discrete states is certainly infinite. From these considerations it is plausible to assume that the spectrum of eigenvalues of (1) is continuous with respect to the parameter Z for all values of $Z>1$, in the sense that no discrete states disappear when Z is varied adiabatically to $1+\epsilon$, where ϵ is a positive number, finite or infinitesimal.

When $Z=1$, the above method would lead, instead of the second limiting form in (5), to

$$\lim_{r\to\infty}V(r)\to-\frac{e^{-ar}}{r}, \quad (6)$$

* Contribution No. 2906 from the National Research Council of Canada.

[1] H. S. W. Massey, *Negative Ions* (Cambridge University Press, Cambridge, 1950), second edition, 1.2, 1.5.

[2] The above argument may be replaced by the mathematically more rigorous argument of Tosio Kato, Trans. Am. Math. Soc. **70**, 212 (1951).

and in such a field, there is no discrete state at all. It is clear, however, that this method is increasingly more grossly in error as Z approaches 1, since the nonseparability of the Schrödinger equation for (1) as represented by the term in r_{12} is increasingly more important as Z approaches 1. Thus, by taking this effect partly into account by using nonseparable wave functions in a variational calculation, Bethe, Hylleraas, and others[3] are able to establish the stability of the state corresponding to $1s^2\,{}^1S$. For $Z=1$, the method of using central field, one-electron approximation indicated above becomes completely inadequate and it is hence not entirely certain that the argument based on it for only a finite number of discrete states in H^- is conclusive.[4] The disappearance of an infinite number of discrete states in the spectrum of (1) at $Z=1$, while possible, cannot be proved by the above considerations. On the other hand, if one makes the assumption that the spectrum of (1) is continuous[5] in Z not only up to, but including, the value 1, there would exist infinitely many discrete states in H^-, although they are all very close together and to the limit defined by (3). We must emphasize, however, that to justify or to disprove this assumption, an exact mathematical investigation of the behavior of the spectrum of the operator (1) at the point $Z=1$ is necessary.[5]

The question whether there exist infinitely many discrete states in a negative ion is mainly of academic interest. In special cases, however, the existence of stable states may have practical significance. Thus it has been well established that H^- plays a very important role in the theory of the observed intensity distribution of stellar spectra.[3] The theory is based on the theoretical absorption coefficient of H^- resulting from transitions from the state "$1s^2\,{}^1S$" to the ${}^1P$ states in the continuum. Another stable state, such as $1s2s\,{}^3S$ in the conventional notation, will also contribute to the continuous absorption and must be included in the theory. Thus, it is of great interest to investigate the stability of such a state.[6] A calculation is being made with the nonseparable wave functions of Hylleraas.

[3] For references, see S. Chandrasekhar, Revs. Modern Phys. **16**, 301 (1944).

[4] The particular method of Kato, reference 2, when applied to the case $Z=1$, would lead only to the conclusion that the minimum number of discrete states would lie between 0 and infinity, and is thus not of help in the present question.

[5] There are potentials for which the spectrum of discrete states is discontinuous with respect to certain parameters in the following sense. Consider the square well or the exponential potential. By decreasing the parameter measuring the depth of the well, a discrete state can be made to approach the ionization limit. On further decreasing this parameter, one usually says that the state has become a "virtual" level. But the "virtual" level is not a level in any sense in the continuum; the asymptotic behavior $\exp(-ar)$ of the wave function of the discrete state passes over into $\exp(ar)$ for the wave function of the "virtual" state. (For a discussion of this "virtual" level from the standpoint of the S matrix, see a forthcoming paper of S. T. Ma.) Such a wave function is physically inadmissible. One must say that the spectrum is discontinuous at certain values of the parameter, at each of which a discrete state disappears.

On the other hand, the spectrum of eigenvalues is continuous for such potentials as the Coulomb and the simple harmonic oscillator, the number of discrete states remaining the same, in fact infinite, for all variations of the parameter Z or k except when that parameter is exactly zero. The value zero for Z is a singularity at which the nature of the field changes.

According to the argument based on (5) and (6), the point $Z=1$ for the Hamiltonian (1) would be similar to the point $Z=0$ for the Coulomb field (hydrogen atom problem) in that infinitely many discrete states disappear at their corresponding values 1 and 0 of Z. This similarity, however, is only suggestive and a mathematical proof is lacking. In fact, the existence of the "$1s^2\,{}^1S$" state in H^- renders the similarity incomplete since the whole discrete spectrum of the Coulomb field disappears at $Z=0$.

[6] Professor Hylleraas and Professor Chandrasekhar inform the writer that they had made similar calculations some years ago with negative result. The question, however, still remains whether the state "$1s2s\,{}^3S$" becomes stable when more appropriate trial wave functions are employed. The writer wishes to express his appreciation for their interest and correspondence concerning this problem.

Variations in Isotopic Abundances of Strontium

L. T. ALDRICH AND L. F. HERZOG
Department of Terrestrial Magnetism, Carnegie Institution of Washington, Washington, D.C.
AND
W. K. HOLYK, F. B. WHITING, AND L. H. AHRENS
Department of Geology, Massachusetts Institute of Technology, Cambridge, Massachusetts

(Received June 2, 1952)

Isotopic abundances of mineral sources of Sr have been measured. Variations in the ratio Sr^{86}/Sr^{88} of unknown origin have been found from 0.1160 to 0.1220. In Rb free minerals, the variation of the ratio Sr^{87}/Sr^{88} (0.0832 to 0.0868) is small enough to be completely attributable to the decay of Rb^{87} in geologic time. The large Sr^{87}/Sr^{88} variation in Rb minerals (biotite) from 0.0840 to 0.2629 indicates their suitability for use in the determination of mineral age.

SR isotope abundances have been determined in the minerals biotite and feldspar extracted from crystalline rocks of varying age and from celestites of sedimentary origin. The determination of the relative Rb-Sr content of biotite[1] showed the possibility of using this mineral in age determination work. The feldspar and celestite analyses were made to determine variations in Sr^{87} content of Sr in Rb-free minerals. The mineral fractions were separated and treated chemically at the Massachusetts Institute of Technology; Sr separation from Ca-Sr concentrates and mass spectrometric analysis were done at the Department of Terrestrial Magnetism.

The mass spectrometer used was adapted from that described by Nier.[2] Ion current ratios were measured by the null method from which the ratios 87/88, 86/88, and 88/(87+86+84) could be determined. From these the atom-percent of each isotope could be calculated. The ions were formed by thermal evaporation of 20–100 μg of $SrCl_2$ or $SrSO_4$ from a nickel-plated tungsten filament. The only residual peaks present during runs were those due to Rb. The Rb^{85} peak height for the work reported here was always less than 0.05 that due to Sr^{86}, so that the small correction to the mass 87 ion current owing to Rb^{87} could be made. For example, the error in the ratio, Sr^{87}/Sr^{86} attributable to Rb could be made less than 0.5 percent under these conditions if the ratio Rb^{85}/Sr^{86} is known within 15 percent. The smaller the latter ratio, the less accurately it need be measured to correct the Sr isotope ratios.

Peaks were also found on occasion at masses 83, 87, and 89 at temperatures below which Sr^+ ions were emitted. These were not present during runs on Sr from which these data are taken.

TABLE I. Relative abundance of isotopes of commercial strontium.

	88	87	86	84
Abundance this work	100	8.50±0.04	11.95±0.03	0.67±0.05
Nier	100	8.50	11.94	0.68

Table I shows the results of 6 separate analyses of Sr obtained as $SrCO_3$ from Eimer and Amend. They are compared with the results of Nier[3] obtained by electron bombardment of Sr metal. The agreement is remarkable. The error shown is the mean deviation of 6 determinations and is less than the error of each determination, which is of the order of 0.5 percent. Repeat measurements on minerals where sufficient material was available were consistent to the same precision as shown for commercial Sr.

Figure 1 is a histogram showing the variation in the ratio Sr^{87}/Sr^{88} in the minerals celestite and feldspar which, in general, have large ratios of Sr to Rb. The two lowest values for the ratio Sr^{87}/Sr^{88} are for feldspars whose ages are thought to be greater than 1.5×10^9 years and, therefore, should be representative of the change in this ratio for these rocks in over half the earth's history. Figure 2 is a histogram showing the variation in the ratio Sr^{86}/Sr^{88} for all the minerals tested. The variation in this ratio cannot at present be correlated with the age of the mineral or with any other known parameter. In both figures the interval chosen is the error in isotope determination.

Figure 3 is a histogram showing the number of

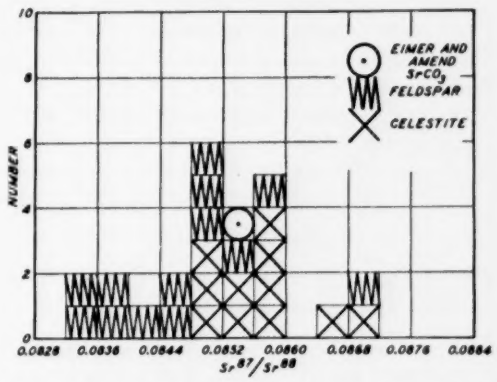

FIG. 1. The ratio Sr^{87}/Sr^{88} in celestite and feldspar mineral samples.

[1] L. H. Ahrens and F. B. Whiting, Bull. Geol. Soc. Am. **61**, 1439 (1950).
[2] A. O. Nier, Rev. Sci. Instr. **18**, 398 (1947).
[3] A. O. Nier, Phys. Rev. **54**, 275 (1938).

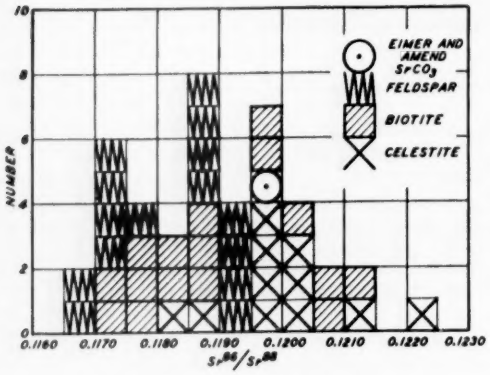

FIG. 2. The ratio Sr^{86}/Sr^{88} in celestite, feldspar, and biotite mineral samples.

biotites with a given Sr^{87}/Sr^{88} ratio. The scale of the abscissa is compressed. The variation in this ratio for biotites is seen to be many times that found in Rb-low minerals. Biotites appear to fulfill the promise predicted for them as suitable for use in the measurement of mineral age.

Two obvious conclusions may be made from these results. First, any age method requiring a measurement of small amounts of radiogenic Sr^{87} in the presence of preponderant amounts of common Sr will be subject to considerable error because of variations of undetermined origin in the relative abundances of the Sr isotopes. Secondly, for Rb rich minerals such as biotites, the Sr^{87} of radiogenic origin is sufficient to make these uncertainties unimportant for age determinations.

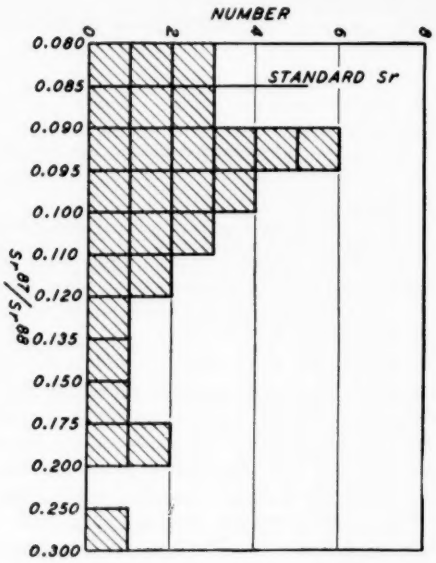

FIG. 3. The ratio Sr^{87}/Sr^{88} in biotite, a Rb-rich mineral. Note nonlinear scale.

PHYSICAL REVIEW VOLUME 89, NUMBER 3 FEBRUARY 1, 1953

Magnetic Susceptibility of a Diamagnetic Electron Gas—The Role of Small Effective Electron Mass

E. N. Adams II
Institute for Nuclear Studies, University of Chicago, Chicago, Illinois
(Received July 21, 1952)

An exact formula for the "steady" bulk susceptibility of a degenerate electron gas is derived. The deviations from the Landau-Peierls formula are studied for several situations in which the effective electron mass is small. It is concluded that, in any case for which the Landau-Peierls susceptibility differs from the Landau susceptibility, the total susceptibility differs from the Landau-Peierls susceptibility by an amount of the same order of magnitude.

The magnetic susceptibility of solid Bi is discussed on a model developed by H. Jones. It is found that for several reasons, Jones' model requires major modification. A particular modification is suggested as a possible basis for a theory of the Bi susceptibility.

Some implications of our conclusions are discussed in connection with Bardeen's theory of superconductivity and the theory of the de Haas-van Alphen effect.

1. INTRODUCTION

ALTHOUGH some metals are ferromagnetic or strongly paramagnetic, most metals have rather small magnetic susceptibilities of the order of 10^{-6}. The suceptibility of such an "ordinary" metal arises partly from the magnetic moments of electrons bound to lattice ions and partly from the moments of the conduction electrons, the two kinds of susceptibility being of roughly the same order of magnitude. If the conduction electrons behaved as a gas of free electrons, the second contribution would be paramagnetic and one would expect that the sign of the susceptibility would depend on whether the diamagnetism of the ions or the paramagnetism of the conduction electrons predominates. Actually, certain metals, e.g., Bi, exhibit a diamagnetism which, although weak, is conspicuously greater than any which could be accounted for as a contribution of electrons bound to lattice ions. In such cases it is necessary to attribute the additional diamagnetism to the conduction electrons. Clearly, if the large diamagnetism results from the orbital moments of the conduction electrons, however, the electronic motions in the lattice potential must be quite different from the motions in a free electron gas. Thus, in order to understand the susceptibility of a diamagnetic metal, one must know something of the way in which the electrons move in the lattice potential of the metal.

The basic theoretical analysis of the "orbital" susceptibility of conduction electrons is a result of the efforts of Peierls,[1] who worked in the approximation of "tight binding." The same problem has been worked through by Wilson,[2] who has discussed it in the approximation of nearly free electrons, although his analysis is quite general. The only serious assumption in these treatments is that the electron-electron interaction may be ignored except in so far as it can be represented by a potential which has the periodicity of the lattice and which is the same for every electron. That assumption will also be made in this paper. The results of their analyses may be summarized as follows: the calculated susceptibility splits naturally into two parts, the first part, given by the Landau-Peierls formula, being

$$\chi_{LP}=-\tfrac{1}{3}\mu_B{}^2 n(\zeta)\langle\alpha^{xx}\alpha^{yy}-[\alpha^{xy}]^2\rangle. \qquad (1.1)$$

Here μ_B is the Bohr magneton, ζ is the Fermi energy, $n(\zeta)$ is the level density at the Fermi surface, and, for example, α^{xy} is the product of the electron mass by the xy component of the reciprocal mass tensor; the angular bracket denotes an average over the free Fermi surface, which need not lie in a single band. The second contribution to the susceptibility is much more complicated, and will be discussed in detail later. At this point, it is sufficient to remark that it gets its greatest contribution from terms which have the general appearance of second-order energies so it may be thought of as arising because of virtual transitions between bands.

A number of attempts have been made to account for the observed susceptibilities of some of the diamagnetic metals on the basis of the theory referred to above.[3] In the applications it has usually been assumed that the major contribution to the orbital susceptibility is given by Eq. (1.1). On this assumption, it is easy to show that a large diamagnetism cannot arise solely as a consequence of a high level density $n(\zeta)$. For if one replaces the angular bracket in (1.1) by unity, its value for free electrons, one obtains for the susceptibility

$$\chi_L=-\tfrac{1}{3}\mu_B{}^2 n(\zeta). \qquad (1.2)$$

Formula (1.2) was first derived by Landau[4] for the case of a gas of free electrons. The susceptibility χ_L is just one-third as large as the Pauli[5] susceptibility χ_S,

[1] R. Peierls, Z. Physik **80**, 763 (1933).
[2] A. H. Wilson, *The Theory of Metals* (Cambridge University Press, Cambridge, 1936).
[3] See, for example, N. F. Mott and H. Jones, *The Theory of the Properties of Metals and Alloys* (Clarendon Press, Oxford, 1936), for a discussion of some applications.
[4] L. Landau, Z. Physik **64**, 629 (1930).
[5] W. Pauli, Z. Physik **41**, 81 (1926).

given by

$$\chi_S = \mu_B^2 n(\zeta). \tag{1.3}$$

The susceptibility χ_S is derived from the spin magnetic moment of the electron. A comparison of the expressions (1.2) and (1.3) shows clearly that a free electron gas is paramagnetic, and that a mere change in level density does not lead to diamagnetism. Thus, if the electron gas model is adequate for an understanding of the observed susceptibilities of the diamagnetic metals, it must be supposed that for some metals the angular bracket in Eq. (1.1) has a value considerably in excess of three.

The angular bracket in Eq. (1.1) has a simple physical interpretation. Because the electron gas is in a potential, a magnetic field does not cause an electron to precess in the manner of a free electron, but rather in a more complicated manner. Thus in the expression (1.2) for the susceptibility one should not use the Bohr magneton computed from the free electron mass, since the electron precesses as though its mass were quite different from that of a free electron. The angular bracket in Eq. (1.1) tells how the effect of the more complicated precession may be taken account of properly. It consists of a modification of the factor μ_B^2, so that $(1/m)^2$ is replaced by the proper combination of components of the reciprocal effective mass tensor. A large value of the angular bracket is associated with a small effective mass. Thus the argument of the previous paragraph is equivalent to the statement that a degenerate electron gas can be diamagnetic only if the average effective mass of the electrons at the Fermi surface is considerably smaller than the free electron mass.

The possibility that a really large diamagnetic susceptibility might arise as a consequence of the activities of a few electrons of very small effective mass has been contemplated by Bardeen,[6] who has envisaged a situation in which the susceptibility would be great enough to drive out the magnetic field. In Bardeen's problem the interaction of electrons with lattice vibrations splits the group of electron states at the Fermi surface into two groups. Bardeen treated the electrons in the energetically lower groups as electrons in an ordinary conduction band and used the formula Eq. (1.1) to calculate the magnetic susceptibility. He considered the possibility that the $\alpha^{\mu\nu}$ of Eq. (1.1) are of the order 10^4 corresponding to energy gaps in the electron spectrum of 10^{-3} ev. It seemed to the writer that the existence of such small energy gaps made the application of the ordinary susceptibility formula very doubtful, and it is in this doubt that the present work had its origin. However, the writer has not attempted a detailed application to Bardeen's theory, because he does not understand in what sense Bardeen can apply ordinary band theory in his particular problem. Instead, therefore, a detailed investigation was made of another theory which accounts for a large diamagnetism in terms of a small number of electrons with small effective masses, to wit, the theory given by Jones[7] to account for the susceptibility of Bi. In examining Jones' theory, we have been particularly interested in estimating the order of magnitude of other terms in the susceptibility than those leading to Eq. (1.1) because it is not obvious that such terms are really negligible when the effective masses of some electrons are very small. In fact, we will see immediately that these terms ought to be large when the effective masses are small.

An electron state which has a very small effective mass is located at a point in wave-number space where the curvature of the energy surface is large. Such regions of high curvature are small and are associated with energy gaps corresponding to planes of the reciprocal lattice. If the effective mass is very small, its magnitude is directly proportional to the size of the energy gap with which the high curvature is associated, and some or all of the α's which occur in Eq. (1.1) are large with magnitudes proportional to the reciprocal energy gap. Thus the large contributions to the Landau-Peierls susceptibility, Eq. (1.1), come from regions on the Fermi surface where electron states in two or more bands are almost degenerate. Now two states which are nearly degenerate can be appreciably admixed by what would otherwise be a very weak perturbation, and the second-order energy resulting from this admixing will have a magnitude proportional to the reciprocal energy gap. The magnetic perturbation is a weak perturbation which can cause such an admixture of states in different bands, and the second-order energy associated with this admixing makes a contribution to the susceptibility. Such contributions are not included in the susceptibility given by Eq. (1.1), and have usually been neglected in the theoretical studies of the observed susceptibilities of the diamagnetic metals. Wilson[2] has given a brief argument to the effect that one is justified in ignoring these contributions under most circumstances. It will be shown below that one should not neglect these contributions in the case of the diamagnetic metals, if it is true that most of the susceptibility is contributed by a few states. In fact, we will show that in such a case the Landau-Peierls formula, Eq. (1.1), does not give any reasonable approximation to the susceptibility.

In subsequent sections we derive an expression for the "steady" diamagnetic susceptibility, i.e., that part of the susceptibility which is independent of temperature and field strength, and use this expression to study the contribution to the susceptibility from the kinds of configurations of states which are believed to occur in the diamagnetic metals. The starting point in the derivation is the Hamiltonian of the generalized Wannier theory.[8] In Sec. 2 this Hamiltonian is diagonalized to order $3C^2$ by a unitary transformation. In Sec. 3 the diagonalized Hamiltonian is used in a statistical treatment to deduce a general expression for the steady susceptibility. The formula found here cannot well be compared with

[6] J. Bardeen, Phys. Rev. **80**, 567 (1950); **81**, 829 (1951).

[7] H. Jones, Proc. Roy. Soc. (London) **147**, 395 (1934).

[8] E. N. Adams, Phys. Rev. **85**, 41 (1952); **86**, 427 (1952).

Wilson's,[2] since some integrals which occur in his final formulas do not occur in the Wannier theory. In Sec. 4 a discussion is given of the effective mass tensor. In particular, we examine a special case in which the off-diagonal matrix elements can be expressed in terms of the effective mass. In Sec. 5 a calculation is made of the contribution to the susceptibility made by the simple configuration which occurs when the Fermi surface just overlaps the face of a Brillouin zone. This configuration is of interest because all terms in the susceptibility can be calculated almost exactly. The discussion of Sec. 5 shows that under certain circumstances a filled zone can make large contributions to the susceptibility. In Sec. 6 a discussion is given of the configuration which Jones[7] hypothesized to exist in Bi. While the complete calculation cannot be carried through for this configuration, it is shown that the terms which Jones neglected are of the same order as those which he kept. It is argued that in general the susceptibility contributions which are usually neglected are of the same order as the difference between the Landau susceptibility, Eq. (1.2), and the Landau-Peierls susceptibility, Eq. (1.1). It is concluded that Jones' theory of Bi is probably wrong; a modification of his model is suggested, but not investigated.

2. THE HAMILTONIAN

The Hamiltonian which will be used in calculating the susceptibility is that of the Wannier theory.[8] While the validity of this theory has been established only approximately, the applications to be made here do not depend on the approximations of the theory. The same results could be obtained from the Schrödinger theory by more tedious means. For an electron in a uniform constant magnetic field, the Schrödinger Hamiltonian will be written:

$$H=(p^2/2m)+V_L(x)+\tfrac{1}{2}\omega\delta_{\mu\nu\lambda}u^\mu\{x^\nu, p^\lambda\} +\tfrac{1}{8}m\omega^2\delta_{\mu\nu\lambda}\delta_{\alpha\beta\gamma}u^\mu u^\alpha\{x^\nu, \{x^\beta, \delta_{\gamma\lambda}\}\}. \quad (2.1)$$

Here $V_L(x)$ is the periodic potential of the unperturbed lattice, ω is the Larmor frequency ($e\mathfrak{H}/2mc$), u^μ is a unit vector in the direction of the magnetic field, $\delta_{\mu\nu\lambda}$ is the Levi-Civita δ symbol which is antisymmetric on all pairs of indices, and the curly brackets signify anticommutators. It is, of course, unnecessary to introduce the explicit symmetrization, but it will prove convenient subsequently because of the manifestly Hermitian character of the symmetrized terms. From the Schrödinger Hamiltonian, the Wannier Hamiltonian can be written down immediately.[8] First a slight change of notation from that used in reference 8 will be made. The notational change is simply to use Latin capitals instead of Greek letters to denote the operators for the electron momentum and coordinate. Thus $\mathbf{P}^\mu$ denotes the Wannier operator for the μ component of electron momentum, P_n^μ denotes that part of the operator which is diagonal in bands, P^μ that part which is nondiagonal in bands. Similarly, $\mathbf{X}^\mu$ denotes the operator for the μ-component of the electron coordinate, $x^\mu+X_n^\mu$ the part which is diagonal in bands, X^μ the part which is nondiagonal in bands. As previously, p^μ denotes the μ-component of the "crystal momentum" and x^μ the μ-component of what we might call the "crystal coordinate." P_n^μ, P^μ, and X^μ are functions of the p^ν but not not of the x^ν. X_n^μ is independent[8] of p^ν and x^ν. The explicit forms of $\mathbf{X}^\mu$, $\mathbf{P}^\mu$ are given in reference 8. The Wannier Hamiltonian is now obtained from the Schrödinger Hamiltonian by the following rules of substitution:

$$p^2/2m+V_L(x)\rightarrow\mathbf{E}(p), \quad x^\mu\rightarrow\mathbf{X}^\mu, \quad p^\mu\rightarrow\mathbf{P}^\mu. \quad (2.2)$$

Thus the Wannier Hamiltonian corresponding to (2.1) is:

$$\mathbf{H}=\mathbf{E}(p)+\tfrac{1}{2}\omega\delta_{\mu\nu\lambda}u^\mu\{\mathbf{X}^\nu, \mathbf{P}^\lambda\} +\tfrac{1}{8}m\omega^2\delta_{\mu\nu\lambda}\delta_{\alpha\beta\gamma}\{\mathbf{X}^\nu, \{\mathbf{X}^\beta, \delta_{\gamma\lambda}\}\}. \quad (2.3)$$

The operator $\mathbf{E}(p)$ is diagonal in the bands and its diagonal element in the jth band $\langle jp|E(p)|pj\rangle$ is just the energy of an unperturbed state of the electron in the jth band and with wave number p. However, the other terms are not diagonal, so before doing any statistical treatments it is convenient to diagonalize the Hamiltonian (2.3) to the second order in ω. As a preliminary step we transform $\mathbf{H}$ by the operator:

$$\mathbf{u}_1=\sum_n \tau_{nn}\exp\{-iX_n^\mu p^\mu\}. \quad (2.4)$$

The operator $\mathbf{u}_1$ is *not* periodic with the reciprocal lattice periodicity, so the transformed operators are no longer periodic functions of p. It can be seen, however, that the diagonal parts of the transformed operators remain periodic in p. The principal results of the transformation (2.4) is to remove the constants X_n^μ from $\mathbf{X}^\mu$.

$$\mathbf{u}_1(x^\nu+X_n^\nu)\mathbf{u}_1^{-1}=x^\nu. \quad (2.5)$$

The transformation (2.4) considerably simplifies the calculation of the formula for the susceptibility. In addition, it shows that the X_n^μ need not appear in the final formula. Because we make this transformation, however, we cannot easily compare our final formula with Wilson's,[2] which still contains the X_n^μ in the form of the integral $\int(\psi_{pn}^*\partial u_{pn}/\partial p^\mu)d\tau_0$. The existence of the transformation (2.4) shows that Wilson's formula could be simplied by the use of sum rules and relations among matrix elements.

Even after the transformation (2.4) we can continue to write the Hamiltonian in the form (2.3), but with the understanding that the transformed $\mathbf{X}$, $\mathbf{P}$ now occur therein. The next step is to transform $\mathbf{H}$ by a unitary transformation which removes all parts of $\mathbf{H}$ which are nondiagonal in the bands and are of order ω. The transformation which does this will be called $\mathbf{u}_2$. Writing $\mathbf{u}_2=\exp\{i\mathbf{S}_2/\hbar\}$, we find that a possible choice of $\mathbf{S}_2$ is

$$\mathbf{S}_2=\tfrac{1}{2}m\omega\delta_{\alpha\beta\gamma}u^\alpha[\{X^\beta, x^\gamma\} +\sum_{jj'}{}'\tau_{jj'}1(\hbar/miE_{jj'})(2\{P_n^\gamma, X^\beta\}_{jj'} +\{P^\gamma, X^\beta\}_{jj'}]. \quad (2.6)$$

The transformed Hamiltonian takes the form:

$$\begin{aligned}\mathbf{u}_2\mathbf{H}\mathbf{u}_2^{-1}=&[\mathbf{E}(p)+\tfrac{1}{2}\omega\delta_{\mu\nu\lambda}u^\mu\{x^\nu, P_n{}^\lambda\}\\&+\tfrac{1}{8}m\omega^2\delta_{\mu\nu\lambda}\delta_{\alpha\beta\gamma}u^\mu u^\alpha\{x^\nu,\{x^\beta,\partial P_n{}^\lambda/\partial p^\gamma\}\}]\\&+\omega h_1+\tfrac{1}{8}\omega^2\delta_{\mu\nu\lambda}u^\mu\{x^\nu, h_{21}{}^\lambda\}\\&+\tfrac{1}{8}\omega^2 h_2+O(\omega_0{}^3)+\cdots. \quad (2.7)\end{aligned}$$

h_1, $h_{21}{}^\lambda$, and h_2 are Hermitian functions of p; nondiagonal terms of order ω_2 have been neglected.

The bracketed quantities are just the development[9] of $\mathbf{E}(p^\mu-m\omega\delta_{\mu\nu\lambda}x^\nu u^\lambda)$ to order ω^2. If this were the complete Hamiltonian, the electrons in a given band would move about in a complicated way which could be described by attributing to the electron a velocity-dependent mass tensor. Transitions between bands would not occur as a result of the magnetic forces, and wave packets would move on constant energy surfaces. The complete expression for the steady susceptibility would be the Landau-Peierls susceptibility, which is given by (1.1).

The chief concern of this paper will be with the remainder of the susceptibility which arises from the terms h_1, $h_{21}{}^\lambda$, and h_2 in the Hamiltonian. These terms are of a rather complicated form, even after the maximum simplification has been made. In order to express these terms, it is convenient to define four real dimensionless tensor operators $l^{\mu\nu}$, $d^{\mu\nu}$, $r^{\mu\nu}$, and $s^{\mu\nu}$.

$$\begin{aligned}&l_{jj'}{}^{\mu\nu}\equiv(1/\hbar)\textstyle\sum_{j''}{}'(X_{jj''}{}^\mu P_{j''j'}{}^\nu+P_{jj''}{}^\nu X_{j''j'}{}^\mu),\\&d_{jj'}{}^{\mu\nu}\equiv(i/\hbar)\textstyle\sum_{j''}{}'(X_{jj''}{}^\mu P_{j''j'}{}^\nu-P_{jj''}{}^\nu X_{j''j'}{}^\mu),\\&r_{jj'}{}^{\mu\nu}\equiv(1/\hbar)\{X^\mu, P_n{}^\nu\}_{jj'},\\&s_{jj'}{}^{\mu\nu}\equiv(i/\hbar)[X^\mu, P_n{}^\nu]_{jj'}. \quad (2.8)\end{aligned}$$

The straight brackets denote commutators.

In terms of the operators (2.8) we may write

$$\begin{aligned}h_1=&(\hbar/2)\delta_{\mu\nu\lambda}u^\mu l_n{}^{\nu\lambda},\\h_{21}{}^\lambda=&m\delta_{\alpha\beta\gamma}u^\alpha[\{\partial X^\lambda/\partial p^\beta, P^\gamma\}+\{X^\beta, s^{\gamma\lambda}+d^{\gamma\lambda}\}\\&+3\{X^\beta, s^{\lambda\gamma}\}+2i[X^\lambda, l^{\beta\gamma}]]_n,\\h_2=&\textstyle\sum\tau_{nn}\hbar^2\delta_{\mu\nu\lambda}\delta_{\alpha\beta\gamma}u^\mu u^\alpha[\{X^\nu,\{X^\beta,\delta_{\gamma\lambda}+3\alpha_n{}^{\gamma\lambda}\}\}_n\\&\times(m/\hbar^2)-(2m/\hbar)\{X^\lambda,\partial l^{\beta\gamma}/\partial p^\nu\}\\&+\textstyle\sum_{n'}{}'(1/E_{nn'})\{-d_{nn'}{}^{\beta\nu}d_{n'n}{}^{\lambda\gamma}\\&-d_{nn'}{}^{\beta\nu}(2s_{n'n}{}^{\lambda\gamma}+s_{n'n}{}^{\gamma\lambda})+l_{nn'}{}^{\beta\gamma}l_{n'n}{}^{\nu\lambda}\\&+3l_{nn'}{}^{\beta\gamma}r_{n'n}{}^{\nu\lambda}+\text{c.c.}\}\\&+\textstyle\sum_{n'}{}'(1/iE_{nn'})\{3r_{nn'}{}^{\beta\nu}d_{n'n}{}^{\gamma\lambda}-s_{nn'}{}^{\gamma\beta}l_{n'n}{}^{\nu\lambda}-\text{c.c.}\}\\&+\textstyle\sum_{n'}{}'(1/E_{nn'})\{-s_{nn'}{}^{\nu\beta}s_{n'n}{}^{\gamma\lambda}\\&+2r_{nn'}{}^{\nu\lambda}r_{n'n}{}^{\beta\gamma}+\text{c.c.}\}\\&+\textstyle\sum_{m'}{}'(1/iE_{nn'})\{r_{nn'}{}^{\beta\nu}(3s_{n'n}{}^{\gamma\lambda}\\&+5s_{n'n}{}^{\lambda\gamma})-\text{c.c.}\}]. \quad (2.9)\end{aligned}$$

Here $E_{nn'}$ denotes $E_n-E_{n'}$ and the subscript n on an operator means the diagonal part of its matrix. Although the operator h_2 is complicated, it has several characteristics which can be described qualitatively. In the first place, h_2 vanishes for free electrons, since each of its terms involves off-diagonal matrix elements of the electron coordinate. In the second place, there are qualitatively different kinds of terms in h_2. For example, the first term involved $\delta_{\mu\nu\lambda}\delta_{\alpha\beta\gamma}u^\mu u^\alpha\{X^\nu,\{X^\beta,\delta_{\gamma\lambda}\}\}_n$ is always positive, while some of the other terms may have either sign according as the predominant energy denominators are positive or negative. This remark is made to emphasize the fact that h_2 is not simply a second-order energy correction, since the sign of a second-order energy must depend on whether the important intermediate states lie above or below the state corrected. What such behavior means will be discussed further when we obtain a formula for the susceptibility.

3. THE SUSCEPTIBILITY

The steady magnetic susceptibility may be defined in terms of the free energy F by

$$\chi=-\frac{\partial^2 F}{\partial\mathfrak{IC}^2}\bigg|_{\mathfrak{IC}=0}. \quad (3.1)$$

For a Fermi gas,

$$F=N\zeta-kT\textstyle\sum_i\ln[1+\exp\{-(E_i-\zeta)/kT\}]. \quad (3.2)$$

Since ζ depends on $\mathfrak{IC}$ quadratically, and since $\partial F/\partial\zeta=0$, ζ may be treated as a constant. In evaluating the susceptibility one makes use of the fact that the expression for χ may be converted into a trace which can then be evaluated in any convenient representation. It is easily seen because of the constancy of ζ and N, that the required form of the susceptibility is

$$\chi=-\frac{\partial^2}{\partial\mathfrak{IC}^2}\operatorname{Tr}[g(\mathbf{H})], \quad (3.3)$$

in which

$$g(\mathbf{H})\equiv-kT\ln[1+\exp\{-(\mathbf{H}-\zeta)/kT\}]. \quad (3.4)$$

Introducing the Larmor frequency here, (3.3) can be written as

$$\begin{aligned}\chi=&-\left(\frac{\mu_B}{\hbar}\right)^2\frac{\partial^2}{\partial\omega^2}\operatorname{Tr}[g(\mathbf{H})]\bigg|_{\mathfrak{IC}=0}\\=&-\left(\frac{\mu_B}{\hbar}\right)^2\operatorname{Tr}\left[\frac{\partial^2}{\partial\omega^2}g(\mathbf{H})\bigg|_{\mathfrak{IC}=0}\right]. \quad (3.5)\end{aligned}$$

Since the value of a trace is invariant against changes of representation, we may use the transformed Hamiltonian (2.7) in $g(\mathbf{H})$. In addition, in getting (3.5) we have assumed a choice of representation for which the wave functions do not depend on ω. It is clearly most advantageous to take the trace using the representation in terms of eigenfunctions of the unperturbed Hamil-

[9] J. M. Luttinger, Phys. Rev. **84**, 814 (1951).

tonian. At this point one can see why the Wannier formalism is especially suitable for the susceptibility calculation. Whereas with the Schrödinger Hamiltonian the unperturbed eigenfunctions are the complicated Bloch functions, with the Wannier formalism the unperturbed eigenfunctions are plane waves. Thus in setting up the Wannier formalism all of the complications of the problem have been put into the Hamiltonian, leaving the wave functions as simple as possible. Since we have already diagonalized $g(\mathbf{H})$ in the band indices, the trace will just involve a sum over bands of integrals on p of the diagonal parts of $g(\mathbf{H})$. Because the eigenfunctions are plane waves these integrals are very much like phase space integrals in classical statistical mechanics. The density of states in p space is just $2/(2\pi\hbar)^3$, provided that the integrals over p are restricted to the first Brillouin zone.

To facilitate calculating the trace, imagine that $g(\mathbf{H})$ has been developed as a formal power series in $\mathbf{H}$. It is not difficult to take the trace of the general term, and after doing so to sum the series. Thus we need first to calculate

$$T^{(N)}\equiv-\left(\frac{\mu_B}{\hbar}\right)^2\mathrm{Tr}\left[\frac{d^2\mathbf{H}^N}{d\omega^2}\right]_{\mathfrak{IC}=0}$$

$$=-\left(\frac{\mu_B}{\hbar}\right)^2\frac{2}{(2\pi)^3}\sum_n\int_{B.Z}d^3k e^{-ik\cdot x}\left[\frac{d^2H_n{}^N}{d\omega^2}\right]_{\mathfrak{IC}=0}e^{ik\cdot x}. \tag{3.6}$$

$T^{(N)}$ naturally breaks into two parts, one the result of first-order terms, the other the result of second-order terms. Call these $T_a{}^{(N)}$ and $T_b{}^{(N)}$, respectively. Since $\partial\mathbf{H}/\partial\omega$ commutes with $\mathbf{E}$, it is readily found that

$$T_a{}^{(N)}=-(\mu_B/\hbar)^2\,\mathrm{Tr}[(\tfrac{1}{2}\delta_{\mu\nu\gamma}u^\mu\{x^\nu,P_n{}^\lambda\}+h_1)^2 \times N(N-1)\mathbf{E}_n{}^{N-2}]. \tag{3.7}$$

Using the fact that only terms which are real and even in x can survive, this is found to be

$$T_a{}^{(N)}=(\mu_B/\hbar)^2\,\mathrm{Tr}[\{\tfrac{1}{4}(\delta_{\mu\nu\lambda}u^\mu\{x^\nu,P_n{}^\lambda\})^2+h_1{}^2\} \times\partial^2\mathbf{E}^N/\partial\mathbf{E}^2]. \tag{3.8}$$

The calculation of $T^{b(N)}$ will now be described. It is found that the term in $(h_{21}{}^\lambda)^2$ can give nothing. The term in h_2 leads to a contribution which will be called $T_{b_2}{}^{(N)}$ and is

$$T_{b_2}{}^{(N)}=-(\mu_B/\hbar)^2\,\mathrm{Tr}[\tfrac{1}{4}h_2\partial\mathbf{E}^N/\partial\mathbf{E}]. \tag{3.9}$$

$T_{b_1}{}^{(N)}$, the remaining trace, can be written as

$$T_{b_1}{}^{(N)}=-(\mu_B/\hbar)^2\,\mathrm{Tr}[N\langle\mathbf{E}^{N-1},(m/4)\delta_{\mu\nu\lambda}\delta_{\alpha\beta\gamma} \times u^\mu u^\alpha\{x^\nu,\{x^\beta,\partial P_n{}^\gamma/\partial p^\lambda\}\rangle_S]. \tag{3.10}$$

The notation $\langle\mathbf{E}^{N-1},o\rangle_S$, means that the N factors are to be completely symmetrized as to order, so that o occurs once in each of the N ordinal positions. Now the operator in the face bracket (3.10) is to be commuted through all the $\mathbf{E}$'s until it stands on the left. After the factors have been ordered in this way the plane wave eigenfunctions can be dropped and p treated merely as an integration variable. The surviving part of $T_{b_1}{}^{(N)}$ is:

$$\begin{aligned}T_{b_1}{}^{(N)}=&-(\mu_B/\hbar)^2\delta_{\mu\nu\lambda}\delta_{\alpha\beta\gamma}u^\mu u^\alpha \\ &\times\mathrm{Tr}[(m/4)\{x^\nu,\{x^\beta,\partial P_n{}^\gamma/\partial p^\lambda\}\}(d\mathbf{E}^N/d\mathbf{E}) \\ &-(\hbar^2/2)(\partial P_n{}^\beta/\partial p^\nu)(\partial P_n{}^\gamma/\partial p^\lambda)(d^2\mathbf{E}^N/d\mathbf{E}^2) \\ &-(\hbar^2/3m)P_n{}^\nu P_n{}^\beta(\partial P_n{}^\gamma/\partial p^\lambda)(d^3\mathbf{E}^N/d\mathbf{E}^3)]. \end{aligned}\tag{3.11}$$

The last term in $T_{b_1}{}^{(N)}$ may be integrated by parts using $(1/m)P_n{}^\nu d^3\mathbf{E}^N/\partial\mathbf{E}^3\equiv\partial(\partial^2\mathbf{E}^N/\partial\mathbf{E}^2)\partial p^\nu$. Finally, we get

$$\begin{aligned}T_{b_1}{}^{(N)}=&-(\mu_B/\hbar)^2\delta_{\mu\nu\lambda}\delta_{\alpha\beta\gamma}u^\mu u^\alpha \\ &\times\mathrm{Tr}[(m/4)\{x^\nu,\{x^\beta,\partial P_n{}^\gamma/\partial p^\lambda\}\}d\mathbf{E}^N/d\mathbf{E} \\ &-(\hbar^2/6)(\partial P_n{}^\beta/\partial p^\nu)(\partial P_n{}^\gamma/\partial p^\lambda)d^2\mathbf{E}^N/d\mathbf{E}^2. \end{aligned}\tag{3.12}$$

Now, before collecting terms, it can be shown that adding the first term of $T_{b_2}{}^{(N)}$ to the first term of $T_a{}^{(N)}$ will give something which eventually contributes no susceptibility. The proof consists in observing that these terms are just the ones which would have survived if we had assumed from the outset that $[p,x]=0$ and the Hamiltonian had the form $\mathbf{E}[p+(e\mathfrak{A}/c)]$. Thus these terms lead to the susceptibility which one gets on "nonquantum" mechanics for a Hamiltonian of the form $\mathbf{E}[p+(e\mathfrak{A}/c)]$. Van Leeuwen[10] has given an argument which shows that for such a Hamiltonian the susceptibility is precisely zero, since the energy depends only on the velocity. The argument is quite independent of statistics and can be used here to show that the two terms must cancel. There remains of $T^{(N)}$

$$\begin{aligned}T^{(N)}=&-(\mu_B/\hbar)^2\,\mathrm{Tr}[h_1{}^2(d^2\mathbf{E}^N/d\mathbf{E}^2) \\ &+\tfrac{1}{4}h_2(d\mathbf{E}^N/d\mathbf{E})]+\mu_B{}^2\tfrac{1}{6}\delta_{\mu\nu\lambda}\delta_{\alpha\beta\gamma}u^\mu u^\alpha \\ &\times\mathrm{Tr}[(\partial P_n{}^\beta/\partial p^\nu)(\partial P_n{}^\gamma/\partial p^\lambda)d^2\mathbf{E}^N/\partial\mathbf{E}^2]. \end{aligned}\tag{3.13}$$

$T^{(N)}$ was a typical term in the power series development of the trace (3.5). It is a trivial matter to sum the series again. While doing so, we will split the susceptibility into several parts for convenience of subsequent discussion. In re-expressing the last term, we introduce the usual notation:

$$\partial P_n{}^\gamma/\partial p_\lambda\equiv\alpha_n{}^{\gamma\lambda}, \tag{3.14}$$

and set the $u^\alpha=\delta_{\alpha 3}$, thus choosing axes so that the Z direction is along the magnetic field. Then from the last term we get

$$\chi_1=+\tfrac{1}{6}\mu_B{}^2\delta_{\nu\lambda 3}\delta_{\beta\gamma 3}\,\mathrm{Tr}[\alpha_n{}^{\beta\nu}\alpha_n{}^{\gamma\lambda}d^2g(\mathbf{E})/d\mathbf{E}^2]. \tag{3.15}$$

Denoting as x and y two directions perpendicular to the field, we may write (3.15) as

$$\chi_1=+[2\mu_B{}^2/3(2\pi\hbar)^3]\textstyle\sum_n \times\int d^3p(\alpha_n{}^{xx}\alpha_n{}^{yy}-[\alpha_n{}^{xy}]^2)d^2g(E_n)/dE_n{}^2. \tag{3.16}$$

[10] For a discussion see J. H. Van Vleck, *Electric and Magnetic Susceptibilities* (Oxford University Press, London, 1933), p. 94.

Now if $f(E)$ denotes the Fermi function, we have $dg(E)/dE = f(E)$. The integral in (3.16) can be performed using the δ function character of df/dE. In order to do this, one introduces the energy as a variable of integration to replace the component of p normal to the energy surface. Then (3.16) becomes

$$\chi_1 = -\tfrac{2}{3}\mu_B^2/(2\pi\hbar)^3 \int_{SF} dS_P(\alpha^{xx}\alpha^{yy} - [\alpha^{xy}]^2)/|\nabla_p E|. \tag{3.17}$$

Equation (3.17) just gives the Landau-Peierls susceptibility, Eq. (1.1):

$$\chi_1 = -\tfrac{1}{3}\mu_B^2 n(\zeta)\langle \alpha^{xx}\alpha^{yy} - [\alpha^{xy}]^2\rangle. \tag{1.1}$$

Next we get the contributions to the susceptibility from the first term of expression (3.13), using the expression for h_1 given in Eq. (2.9). By arguments analogous to those used above it is easily found that

$$\chi_2 = \tfrac{1}{4}\mu_B^2 n(\zeta)\langle (l^{xy} - l^{yx})^2\rangle. \tag{3.18}$$

Here as in Eq. (1.1) the angular bracket denotes an average over the Fermi surface which need not lie in a single band.

Finally, from the second term in the expression (3.13) we get a contribution

$$\chi_3 = -(\mu_B^2/4\hbar^2)[2/(2\pi\hbar)^3] \int_{VF} d^3p h_2(p). \tag{3.19}$$

The integral in Eq. (3.19) goes over all occupied states, so over the occupied regions in every zone.

The complete susceptibility is given as the sum of χ_1, χ_2, and χ_3. However, in most cases the bulk of the contribution is made by χ_1, since χ_2 and χ_3 contain energy denominators which make their contributions negligible. We will subsequently investigate special cases in which such is not the case. At this point, however, we want merely to characterize these three susceptibilities. χ_1 is the susceptibility which one derives from quantum statistical mechanics using a Hamiltonian $\mathbf{E}[p + (e\mathfrak{A}/c)]$. χ_1 includes certain effects caused by interaction between states in different bands, *viz.*, those which can be described in terms of an effective mass which is velocity dependent. χ_1 may be of either sign since the angular bracket may be either positive or negative. χ_2 is always positive. Its form suggests that it results from something like the orbital moment of the electron about the center of whatever unit cell the electron is momentarily in. If we set $l \sim 1$, we see that χ_2 is of the same order of magnitude as χ_1. χ_3 consists of two kinds of terms, *viz.*, terms which are always diamagnetic, and terms which have a sign determined by the distribution of neighboring states in the energy spectrum. It is probable that χ_3 could only be evaluated for the simplest cases, since it contains terms corresponding to complicated "roundabout" transitions. The condition that χ_3 be important is that the energy gaps between some occupied bands be much smaller than the Fermi energy. We will see in a later section that small energy gaps between bands can result in a quite large value of χ_3.

4. THE EFFECTIVE MASS

We have earlier introduced the effective mass ratio tensor $\alpha^{\mu\nu}$ defined by

$$\alpha_n{}^{\mu\nu} \equiv m\partial^2 E_n(p)/\partial p^\mu \partial p^\nu. \tag{4.1}$$

In this section we will discuss the effective mass for a case in which it is possible to evaluate the susceptibility completely by expressing the off-diagonal matrix elements which occur in the expression (3.18) in terms of the effective mass ratio tensor. We will first write down the derivation of another expression for $\alpha_n{}^{\mu\nu}$. Observe that the operators $\mathbf{P}^\mu$ and $\mathbf{X}^\nu$ are operators for the momentum and coordinate of the electron, so they have the commutation relation

$$[\mathbf{P}^\mu, \mathbf{X}^\nu] = (\hbar/i)\delta_{\mu\nu}. \tag{4.2}$$

In the Wannier theory these operators have the following matrix forms:[9]

$$\begin{aligned} \mathbf{P}^\mu &= \textstyle\sum_n \tau_{nn} P_n{}^\mu + \sum'_{nn'} \tau_{nn'} P^\mu{}_{nn'}, \\ \mathbf{X}^\nu &= x^\nu + \textstyle\sum'_{nn'} \tau_{nn'}(\hbar/miE_{nn'}) P^\nu{}_{nn'}. \end{aligned} \tag{4.3}$$

The expressions (4.3) give the correct forms after the transformation $\mathbf{u}_1$ given by Eq. (2.4). Calculating the commutator and making use of the fact that $\alpha_n{}^{\mu\nu} = \partial P_n{}^\mu/\partial p^\nu$, one gets

$$\alpha_n{}^{\mu\nu} = \delta_{\mu\nu} - \sum'_{n'}(1/mE_{n'n})(P_{nn'}{}^\mu P_{n'n}{}^\nu + P_{nn'}{}^\nu P_{n'n}{}^\mu). \tag{4.4}$$

We want to discuss the size and sign of $\alpha_n{}^{\mu\nu}$ for several cases of interest. In the first place, the $\alpha^{\mu\nu}$ should ordinarily be smaller than unity for the valence band of a metal. This is so because the few intermediate states which are of lower energy and which could, therefore, lead to larger values of $\alpha^{\mu\nu}$ actually lie so much lower in energy that their contributions are small. On the other hand, there are many excited states in higher bands, all of whose contributions have such a sign as to lower the value of $\alpha^{\mu\nu}$. There can quite easily be such states which are not much higher in energy, so it is reasonable to expect that for some values of p in the band the reduction of $\alpha^{\mu\nu}$ should become appreciable. Thus for a valence electron band $\alpha^{\mu\nu}$ is probably of the order of unity or somewhat smaller, being perhaps considerably smaller for a fraction of the states. If the excited band should lie very close for some values of p, the values of $\alpha^{\mu\nu}$ in that part of the band could be very much smaller than unity, but of absolute value very much greater than unity. In the case of a conduction band which lies not too far above a valence band, we ex-

pect large positive values of the $\alpha^{\mu\nu}$ for states in the neighborhood where the bands are very close together. Where a number of bands are close in energy, we simply expect $|\alpha^{\mu\nu}| \gg 1$, but we do not known the sign except for the highest and lowest bands.

In order to calculate the $\alpha_n{}^{\mu\nu}$ from Eq. (4.4), one would need to know the off-diagonal matrix elements of the electron momentum. Such knowledge would in turn involve a more detailed knowledge of the wave functions than one can ordinarily hope to attain. It is, in fact, more likely that one could get information about $\alpha^{\mu\nu}$ directly from the energy spectrum. In this section we will actually consider the $\alpha^{\mu\nu}$ as known, and express the off-diagonal elements in terms of the $\alpha^{\mu\nu}$. Of course, we can do so only in an especially simple situation. As will be seen, however, in this situation we can still learn something about the $\alpha^{\mu\nu}$ from Eq. (4.4). The simple case to be considered is one which arises when, in a certain region of p space, two bands and only two lie very close together. What we are interested in here is a configuration for which the energy gap is extremely small so that values $|\alpha| \gg 1$ occur. In such a case a very good approximation may be had by entirely neglecting the influence of other bands. In Fig. 1 we describe the configuration using the unreduced zone description of the bands. The near degenerate states are distributed along the faces of a plane in the momentum space, the plane being represented in cross section by a solid line. Another solid line represents the cross section of an energy surface which overlaps into the second band, while a dotted line indicates how the cross section might look in the absence of the energy discontinuity across the zone face. The large curvature of the energy surface near the zone face is proportional to one of the $\alpha^{\mu\nu}$. Because the curvature is high, the energy separation between bands grows rapidly with p in the direction normal to the face. Taking an origin of momentum coordinates at the point 0 and designating the normal direction as then x direction, one can say that for p_x about equal to p_m, the energy gap has already doubled.

$$p_m = (m\Delta E_0/|\alpha^{xx}|)^{\frac{1}{2}}. \tag{4.5}$$

The significance of p_m will be discussed again later. The dashed lines of Fig. 1 are intended to be at a distance p_m from the zone face and thus to show what states in the momentum space have large α values. The calculation to be made next applies only to states lying between the planes represented by the dashed lines.

ΔE will denote E_{21}, hence will be a positive number. Let us calculate the commutator $[\mathbf{X}^\mu, \mathbf{X}^\nu]$ using the form (4.3) and noting that because of the energy denominators only one intermediate state is important. All matrix elements of this commutator vanish identically because the $\mathbf{X}^\mu$ are electron coordinate operators. The vanishing of the diagonal element of the commutator gives

$$P_{12}{}^\mu P_{21}{}^\nu - P_{12}{}^\nu P_{21}{}^\mu = 0. \tag{4.6}$$

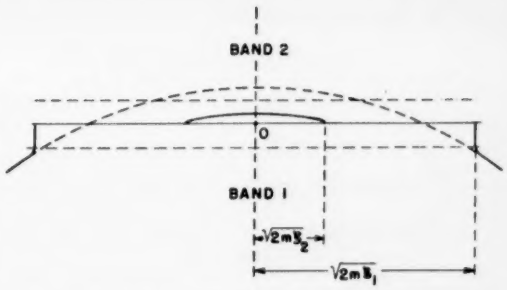

FIG. 1. Profile of an energy surface which just overlaps the face of a zone. $\zeta_1 = \zeta_2 + \Delta E_0$, where ΔE_0 is the energy discontinuity at 0. $pm = (m\Delta E_0/\alpha)^{\frac{1}{2}}$ gives the separation of the dashed lines from the plane.

Using Eq. (4.6) and the one intermediate state approximation, one gets from Eq. (4.4)

$$\begin{aligned} \alpha_1{}^{\mu\nu} &= \delta_{\mu\nu} - 2(P_{12}{}^\mu P_{21}{}^\nu/m\Delta E), \\ \alpha_2{}^{\mu\nu} &= \delta_{\mu\nu} + 2(P_{12}{}^\mu P_{21}{}^\nu/m\Delta E), \end{aligned} \tag{4.7}$$

or

$$2P_{12}{}^\mu P_{21}{}^\nu = (\delta_{\mu\nu} - \alpha_1{}^{\mu\nu})m\Delta E. \tag{4.8}$$

It will be seen later that Eqs. (4.7) and (4.8) and several equations deducible therefrom are all that we need to calculate the complete susceptibility when the Fermi surface overlaps a zone face.

Some equations which follow from (4.7) will be useful later. Adding the two Eqs. (4.7), one gets

$$\alpha_1{}^{\mu\nu} + \alpha_2{}^{\mu\nu} = 2\delta_{\mu\nu}. \tag{4.9}$$

Equation (4.9) can be integrated near $p = 0$ to give

$$P_1{}^\mu + P_2{}^\mu = 2p^\mu. \tag{4.10}$$

Also one can write from (4.9),

$$(\alpha_2{}^{\mu\nu} - \alpha_1{}^{\mu\nu}) = 2(\delta_{\mu\nu} - \alpha_1{}^{\mu\nu}),$$

which integrates to

$$(P_2{}^\mu - P_1{}^\mu) = 2(p^\mu - \alpha_1{}^{\mu\nu}p^\nu). \tag{4.11}$$

Finally, we will prove that if $\alpha^{\mu\nu}$ is diagonalized only one component can be large. In a weak potential theory with the potential represented by a single cosine this is obvious. However, the point here is to show that there is no conceivable set of circumstances under which we get more than one large α with only one excited state, no matter how many Fourier components are important. The proof follows immediately if one squares the two sides of Eq. (4.8) for $\mu \neq \nu$ and then uses Eq. (4.8) to rewrite the left-hand side. One gets, for example,

$$(\alpha_1{}^{\mu\nu})^2 = (1 - \alpha^{\mu\mu})(1 - \alpha^{\nu\nu}), \quad (\mu \neq \nu). \tag{4.12}$$

Equations (4.12) must hold when axes are chosen so

that $\alpha^{\mu\nu}$ is diagonal, so one gets

$$\begin{aligned}(1-{}^{xx}\alpha_1)(1-\alpha_1{}^{yy})&=0,\\(1-\alpha_1{}^{zz})(1-\alpha_1{}^{zz})&=0,\\(1-\alpha_1{}^{yy})(1-\alpha_1{}^{zz})&=0.\end{aligned}\tag{4.13}$$

Choosing $1-\alpha_1{}^{xx}\neq 0$, it follows that $\alpha_1{}^{yy}=\alpha_1{}^{zz}=1$.

5. THE COMPLETE SUSCEPTIBILITY FOR A SPECIAL CASE

If the Fermi surface slightly overlaps the face of a zone boundary across which there is a small gap, the electrons in the neighborhood of the gap will, under certain circumstances, make an unusually large contribution to the susceptibility. Equation (1.1) indicates that this will be the case when the field is oriented perpendicular to the direction in which $\alpha^{\mu\mu}$ is large. Clearly, $\alpha^{\mu\mu}$ is largest when μ refers to the direction normal to the zone face. This direction we denote as the x direction. The solid curve of Fig. 1 describes a cross section of the Fermi surface perpendicular to the magnetic field. Figure 2 shows a yz cross section, the circles being the intersections of the Fermi surface with the zone face.

We wish to calculate the contribution of this overlap configuration to the magnetic susceptibility for the case that the magnetic field direction lies in the zone face. What we will actually calculate is the excess above the Landau susceptibility as given by Eq. (1.2). In order to get the excess, we merely replace α^{xx} by $(\alpha^{xx}-1)$ in the susceptibility χ_1. Equation (4.8) shows that $(\alpha^{xx}-1)$ is a particularly simple expression which has a sharp maximum (as a function of p_x) at the zone face. We make one more elaboration in that together with the contribution of the overlap configuration discussed above we will take the identical contribution which comes from overlapping the opposite zone face. Then we can say that for small overlap the occupied states in the second band fill the ellipsoidal region

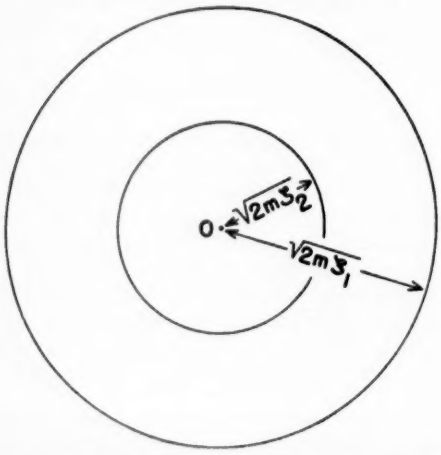

FIG. 2. Intersection of Fermi surface with plane discontinuity.

inside of an energy surface corresponding to an overlap energy ζ_2. The ellipsoid, because of the large value of $\alpha_2{}^{xx}$, is greatly flattened along the x axis.

In order to evaluate χ_2 and χ_3, we must evaluate certain sums over intermediate states. As we saw in the previous section, this becomes possible when there is but a single important intermediate state. Introducing the notation,

$$(\alpha_1{}^{xx}-1)\equiv-\alpha,\tag{5.1}$$

we can see from Eq. (4.9) that

$$(\alpha_2{}^{xx}-1)=\alpha.\tag{5.2}$$

In terms of α we can rewrite Eq. (4.8) as

$$2P_{12}{}^{\mu}P_{21}{}^{\nu}=m\alpha\Delta E\delta_{\mu x}\delta_{\nu x}.\tag{5.3}$$

We can now use Eq. (5.3) to rewrite the four expressions (2.8) so they involve only diagonal matrix elements. In our approximation,

$$\begin{aligned}l_{jj'}{}^{\mu\nu}&=0,\quad d_{jj'}{}^{\mu\nu}=0,\\r_{jj'}{}^{\mu\nu}&=(1/miE_{jj'})P_{jj'}{}^{\mu}(P_{j'}{}^{\nu}+P_j{}^{\nu}),\\s_{jj'}{}^{\mu\nu}&=(1/mE_{jj'})P_{jj'}{}^{\mu}(P_{j'}{}^{\nu}-P_j{}^{\nu}).\end{aligned}\tag{5.4}$$

Since $l_{jj'}{}^{\mu\nu}$ vanishes, the susceptibility χ_2 vanishes for our problem. We must simplify χ_3 which is given by (3.18). Inserting Eq. (5.4) into h_2 of Eq. (2.9), one gets for χ_3,

$$\begin{aligned}\chi_3=(\mu_B{}^2/4)&(2/(2\pi\hbar)^3)\delta_{\nu\lambda z}\delta_{\beta\gamma z}\delta_{\lambda x}\delta_{\gamma x}\\&\times\Big[\int_{(1)}\alpha d^3p\{-(1/\Delta E)(2\delta_{\beta\nu}+3\alpha_1{}^{\beta\nu}+3\alpha_2{}^{\beta\nu})\\&+(1/m\Delta E^2)[(P_2{}^{\beta}-P_1{}^{\beta})(P_2{}^{\nu}-P_1{}^{\nu})\\&+2(P_2{}^{\beta}+P_1{}^{\beta})(P_2{}^{\nu}+P_1{}^{\nu})\\&+5(P_2{}^{\beta}+P_1{}^{\beta})(P_2{}^{\nu}-P_1{}^{\nu})]\}\\&+\int_{(2)}\alpha d^3p\{-(1/\Delta E)(2\delta_{\beta\nu}+3\alpha_1{}^{\beta\nu}+3\alpha_2{}^{\beta\nu})\\&+(1/m\Delta E^2)[-(P_2{}^{\beta}-P_1{}^{\beta})(P_2{}^{\nu}-P_1{}^{\nu})\\&-2(P_2{}^{\beta}+P_1{}^{\beta})(P_2{}^{\nu}+P_1{}^{\nu})\\&+5(P_2{}^{\beta}+P_1{}^{\beta})(P_2{}^{\nu}-P_1{}^{\nu})]\}\Big].\end{aligned}\tag{5.5}$$

The integrals $\int_{(1)}d^3p$, $\int_{(2)}d^3p$ are over the occupied states in the first and second bands, respectively. Already in the form (5.5), it can be seen that χ_3 has two different kinds of terms. The first and last integrals in each bracket have the same sign in either band while the others are of opposite signs in the two bands. The terms of the second kind will contribute only if there is a region of p space for which the states are occupied in one band but not the other.

We can simplify Eq. (5.5) still further. Using Eqs. (4.9), (4.10), and (5.3), we reduce (5.5) to

$$\chi_3=(2\mu_B^2/(2\pi\hbar)^3)\Big[\int_{(1)} d^3p\alpha\{-(2/\Delta E)+(2/m\Delta E^2)p_y^2\}$$

$$+\int_{(2)} d^3p\alpha\{-(2/\Delta E)-(2/m\Delta E^2)p_y^2\}\Big]. \quad (5.6)$$

The total susceptibility is the sum of χ_3 and the surface integrals χ_1:

$$\chi_1=+(2\mu_B^2/3(2\pi\hbar)_3)\int_{(1)} dS_p\alpha/|\nabla_p E|$$

$$-(2\mu_B^2/3(2\pi\hbar)^3\int_{(2)} dS_p\alpha/|\nabla_p E|. \quad (5.7)$$

Note that in both Eqs. (5.6) and (5.7) α is a function of p which vanishes strongly when p_z is large. The strong energy dependence of α comes about partly because α contains an energy denominator and partly because the nondiagonal matrix elements fall off away from the zone face. It is difficult to estimate the energy dependence of the matrix elements without some kind of model of the potential so we will merely note that there is such energy dependence; later in the section we describe the results obtained on a specific model. In any case we can say that when p_z gets large enough α drops sharply to zero. We can estimate the value of p_z for which the drop-off occurs by noting that when the kinetic energy $\alpha p_z^2/2m$ equals half the gap energy $(\Delta E/2)$ it is no longer energetically profitable for the electrons to try to be in standing wave type states, so α will fall off. The critical value of p_z we have denoted as p_m; it was given in Eq. (4.5). We will do the integrals χ_1 and χ_3 on the assumption that α has the constant value α_0 for $p_z<p_m$ and the value 0 for $p_z>p_m$. This assumption cannot introduce any large errors. However, because of the different energy dependences of the different terms, we may get relative values of various terms which are wrong by as much as a factor 2. It will become clear that such errors will not affect the qualitative description of the dependence of the susceptibility on overlap.

We calculate the excess susceptibility due to overlap for two cases (a) and (b). In case (a) the overlap is small so the occupied states in the upper band occupy a flattened ellipsoid. A central cross section of the Fermi surface looks like the solid curve of Fig. 1. In case (b) the overlap is so large that the Fermi surface in the second band is more like a spherical cap sitting on a narrow collar cut from an ellipsoid. A central cross section looks like the solid curve of Fig. 3.

(a) The integral $\chi_1^{(2)}$ is easily found to be

$$\chi_1^{(2)}=-\tfrac{1}{3}\mu_B^2N(\zeta_2)\alpha_0. \quad (5.8)$$

Here

$$N(\zeta_2)\equiv 8\pi m(2m\zeta_2)^{\frac{1}{2}}(2\pi\hbar)^{-3}\alpha_0^{-1}, \quad (5.9)$$

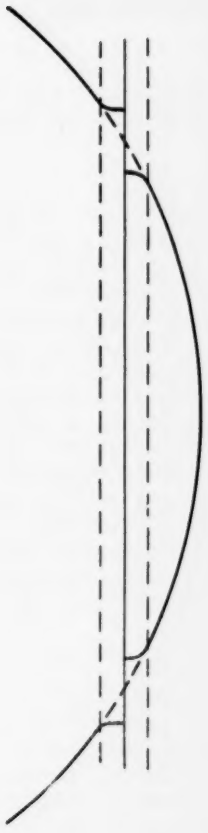

FIG. 3. Cross section of energy surface for large overlap. The dotted line shows the corresponding energy surface in the absence of interaction.

and the superscript (2) denotes the contributions from the second band. In order to evaluate $\chi_1^{(1)}$, we notice that the bulk of the integral comes from the "collar" on the surface (1). This collar is of radius $(2m\zeta_1)^{\frac{1}{2}}$ and width $2p_m$ when we take a pair of zone faces together. Carrying out the surface integral, one gets

$$\chi_1^{(1)}=\tfrac{1}{3}\mu_B^2\alpha_0N(\Delta E_0/2). \quad (5.10)$$

Thus

$$\chi_1=\tfrac{1}{3}\mu_B^2\alpha_0[N(\Delta E_0/2)-N(\zeta_2)]. \quad (5.11)$$

Equation (5.11) is valid for $\zeta_2\lesssim\Delta E_0/2$. χ_3 is easily calculated to be

$$\chi_3^{(1)}=\mu_B^2N(\Delta E_0/2)\alpha_0[(\zeta_1/\Delta E_0)^2-(2\zeta_1/\Delta E_0)], \quad (5.12)$$

$$\chi_3^{(2)}=-\tfrac{1}{3}\mu_B^2N(\zeta_2)\alpha_0[(4\zeta_2/\Delta E_0)+(8/5)(\zeta_2/\Delta E_0)^2]. \quad (5.13)$$

In case (b) the overlap is very large, so the upper band integrals must be recalculated. $\chi_1^{(2)}$ now comes from a "collar" integral also, and is found to be

$$\chi_1^{(2)}=-\tfrac{1}{3}\mu_B^2\alpha_0N(\Delta E_0/2). \quad (5.14)$$

$\chi_3^{(2)}$ is an integral over all occupied states inside the

upper collar region.

$$\chi_3^{(2)} = -\mu_B^2 N(\Delta E_0/2)\alpha_0[(\zeta 2/\Delta E_0)^2 + (2\zeta_2/\Delta E_0)]. \quad (5.15)$$

The lower band integrals are still given by Eqs. (5.10) and (5.12). In case (b) we have

$$\chi_1 = \chi_1^{(1)} + \chi_1^{(2)} \sim 0. \quad (5.16)$$

We can now survey the trend of the various contributions to χ, beginning with small overlap and proceeding to large overlap. For small overlap the Landau-Peierls susceptibility is paramagnetic as shown by Eq. (5.11). As the number of overlapping electrons increases, the susceptibility χ_1 decreases monotonically until for large overlap χ_1 is practically zero as shown by Eq. (5.16). Thus, surprisingly, the excess Landau-Peierls susceptibility is always paramagnetic. The susceptibility χ_3 is negative as overlap begins. The contribution from the lower band becomes less negative as the overlap proceeds since the term $(\zeta_1/\Delta E_0)^2$ in Eq. (5.12) is always greater than 1. At the same time the diamagnetic contribution from the upper band states is steadily growing. As the overlap becomes large, the susceptibility χ_3 finally takes on the simpler form

$$\chi_3 = -\mu_B^2 N(\Delta E/2)\alpha_0[1 + (2\zeta_2/\Delta E_0)]. \quad (5.17)$$

This susceptibility is diamagnetic and grows linearly with the maximum overlap energy. In Fig. 4 the general behavior is shown. Figure 4 is not plotted directly from the formulas above, since the method of integration used there permits relative errors between terms of a factor 2. As noted above such errors arise because of the energy dependence of the matrix elements. Therefore, we have again carried through the susceptibility calculation using the explicit form of the matrix elements obtained for the well-known case of a weak cosine potential. Thus in Fig. 4 the relative magnitudes of the various terms are correct. The formulas for this special case show that the integrations above are not bad. We label these formulas to correspond to those above.

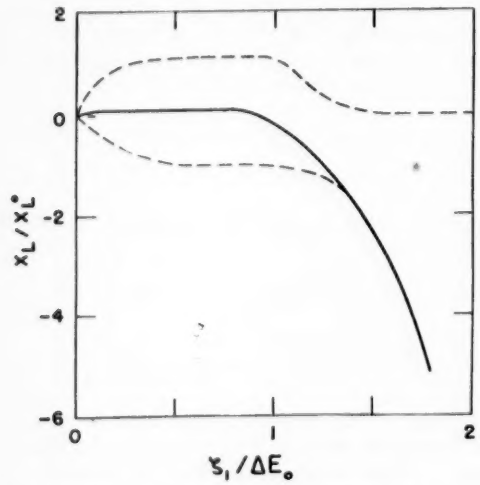

FIG. 4. Susceptibility as a function of ζ_1. Overlap begins for $\zeta_1 = \Delta E$. The upper dashed curve represents χ_1, the lower dashed curve χ_3. The solid curve is the total susceptibility. All susceptibilities are measured in units of $\chi_L^0 = \frac{1}{3}\mu_B^2 N(\Delta E/2)\alpha_0$.

(a) $$\chi_1 = \tfrac{1}{3}\mu_B^2\alpha_0[N(\Delta E_0/2) - N(\zeta_2)], \quad (5.11)\text{cp}$$

$$\chi_3^{(1)} = \mu_B^2 N(\Delta E_0/2)\alpha_0[(\sqrt{2}/3)(\zeta_1/\Delta E_0)^2 - (3\pi\sqrt{2}/16)(\zeta_1/\Delta E), \quad (5.12)\text{cp}$$

$$\chi_3^{(2)} = -\tfrac{1}{3}\mu_B^2 N(\zeta_2)\alpha_0[(3\zeta_2/\Delta E_0) + (8/5)(\zeta_2/\Delta E_0)^2]; \quad (5.13)\text{cp}$$

(b) $$\chi_1^{(2)} = -\tfrac{1}{3}\mu_B^2\alpha_0 N(\Delta E_0/2), \quad (5.14)\text{cp}$$

$$\chi_3^{(2)} = -\mu_B^2 N(\Delta E_0/2)\alpha_0[(\sqrt{2}/3)(\zeta_2/\Delta E_0)^2 + (3\pi\sqrt{2}/16)(\zeta_2/\Delta E_0)]. \quad (5.15)\text{cp}$$

The asymptotic behavior for large overlap is surprising, because it indicates that under certain circumstances one might get a very large contribution to the susceptibility from states which lie far below the Fermi surface. We will now see how large the effects are when an entire zone face is overlapped. We will assume that α satisfies

$$\alpha \sim 4E_K/\Delta E. \quad (5.18)$$

Relation (5.18) is true for a weak cosine potential[3] if E_K is the energy corresponding to the center of the face. Then $\Delta E/2 \sim 2E_K/\alpha$, and by (5.8)

$$\alpha_0 N(\Delta E_0/2) = 8\pi m(2mE_K)^{\frac{1}{2}}(2\pi\hbar)^{-3}. \quad (5.19)$$

The right-hand side of (5.19) is just the density of energy levels for a degenerate free electron gas with states occupied for all energies below E_K, so the susceptibility described by Eq. (5.17) is

$$\chi_3 \sim \chi_L^{(0)}(6\zeta_2/\Delta E), \quad (5.20)$$

in which $\chi_L^{(0)}$ is the Landau susceptibility for a free electron gas with Fermi energy E_K. If the complete face of a lower zone were thus overlapped, we would attain a value $\zeta \sim E_K/2$ at least, and find

$$\chi_3 \sim \chi_L(3E_K/\Delta E) \sim \alpha\chi_L^0. \quad (5.21)$$

Equation (5.21) describes the contribution to the total susceptibility which would be made by a pair of zone faces which are completely overlapped by the Fermi surface, no matter how far below that surface. For comparison it can be noted that the maximum value of χ_1 as given by Eq. (5.11) is about $\chi_L^{(0)}$, using the same approximation (5.18) for α.

The calculation as given in this paper does not give much insight into the physical process which leads to the large contribution to χ_3. However, an examination of the detailed deduction of the results in Sec. 3 shows that $\frac{1}{4}$ of the contribution comes from the $\mathfrak{A}^2$ term in the original Hamiltonian and $\frac{3}{4}$ from the $P\cdot\mathfrak{A}$ terms

taken in second order. While it is not easy to say what sign the latter contribution should have, it is clear that the result found here is qualitatively correct for the α^2 term which is positive for all states and hence must lead to a diamagnetic contribution to the susceptibility from all bands. That the order of magnitude of the contribution arising from a filled band is correct can be verified by noting that in the face of a zone there are of the order of $N\alpha^{-\frac{1}{3}}$ states whose magnetic energies are each of the order

$$\epsilon \sim \tfrac{1}{2}m\omega^2 X_{nn'}{}^2 \sim \tfrac{1}{2}\hbar^2\omega^2\alpha/\Delta E, \qquad (5.22)$$

where N is the number of electrons per unit volume on the metal. Thus the magnetic energy of this group of states is $U \sim \mu_B{}^2 \mathfrak{H}^2 \alpha N(E)$ which gives $\chi \sim \alpha\chi_L$ as found above. This large susceptibility contribution from a filled band corresponds to a physical situation in which there is a large ionic susceptibility because the ion has a low-lying excited state.

If in a metal there were a large susceptibility arising from overlap of weak gaps, a large magnetic anisotropy effect could easily result. For, as a result of a 90° rotation of the magnetic field direction, the susceptibility contribution of that face could be made to go from an original large value to zero. It is thus conceivable that a number of weak faces oriented in a simple pattern could rise to a rather complicated pattern of magnetic anisotropy in a single crystal specimen. We think it possible that such a situation exists in Bi, which we will discuss in detail in the next section.

6. APPLICATION TO BISMUTH

In the last section it was shown for a certain simple configuration of the Fermi surface in which the effective electron masses are very small that the Landau-Peierls formula, Eq. (1.1), does not give a good approximation to the total susceptibility. In this section we will argue that for any configuration of electron states with small effective masses the susceptibility contributions χ_2 and χ_3 are as important as the Landau-Peierls susceptibility. Naturally, we cannot calculate these susceptibilities for any very complicated configuration of states, so what we will do is to discuss an example of a more complicated configuration and show that the order of magnitude of the terms in χ_3 is the same as that of the Landau-Peierls susceptibility. The example which we will discuss comprises two configurations which are of general interest, *viz.*, the top of a band which is almost full and the bottom of a band which is almost empty.

The complicated situation we chose to discuss is the Fermi surface of Bi. For several reasons Bi seemed especially suitable for our purpose. A detailed analysis of the Bi susceptibility had already been made by Jones.[7] He had found that some of the electrical and magnetic properties could be understood in a simple manner as resulting from the anomalous behavior of very small groups of electrons with very small effective masses. Jones had developed a specific set of hypotheses giving a correlation of the various anomalous electric and magnetic properties with specific sites on the Fermi surface and had thereby reached quantitative conclusions concerning the values of the $\alpha^{\mu\nu}$ which would be required to explain the observations. Finally, Jones had apparently been able to reach reasonable agreement with experiment taking account of only the Landau-Peierls part of the susceptibility. Thus Bi was very satisfactory for our purpose since practically important configurations seemed to occur in Bi, small electron masses play an important role, and the effects which we are concerned with had not previously been studied for Bi.

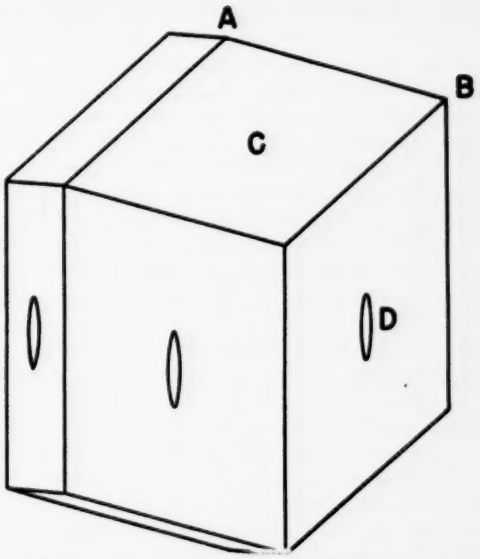

FIG. 5. Brillouin zone of bismuth containing five electrons: $E_A = 12.5$ ev; $E_B = 15$ ev; $E_0 = 9.2$ ev; $E_D = 7.5$; $E_F = 10$ ev.

Jones believed that the smallness of the electrical conductivity of Bi was evidence that most of the electrons in Bi occupy a nearly full Brillouin zone, so that the free Fermi surface is very small. The Brillouin zone which Jones suggested is shown in Fig. 5. If full, it would contain exactly the five valence electrons per atom which are present in pure Bi. Jones supposed that the zone is not quite full, but that there is a small number of holes in the inner zone at A and a small number of electrons overlapping into the outer zone at D. The number of overlapping electrons was estimated to be of the order of 10^{-4} per atom.[11] The overlapping electrons were supposed to occupy greatly elongated ellipsoids as indicated in Fig. 5. The large diamagnetic susceptibility which is observed when a magnetic field is applied along the principal axis of a single crystal of Bi was attributed to the diamagnetic precession of the

[11] See reference 3 for this estimate which is different from that of the original paper reference 6. Jones' theory is discussed in some detail in this reference.

overlapping electrons at the sites D. Jones decided that these electrons would have to have effective mass ratios $\alpha^{zz}\sim\alpha^{yy}\sim 200$ for motion perpendicular to the principal axis and $\alpha^{xx}\sim 1$ for motion along the principal axis. The large diamagnetic susceptibility which is observed when a magnetic field is applied perpendicular to the principal axis was attributed to the holes at A. Jones did not attempt a quantitative discussion of the holes or the susceptibility perpendicular to the principal axis.

A number of experiments give information which is in at least qualitative agreement with Jones' model.[10] The susceptibility of crystalline Bi is diamagnetic and about 25 times the value of χ_L which one calculates assuming that the 5 valence electrons per atom constitute a free electron gas having the electron density of Bi. It is difficult to account for such a large diamagnetism except on the assumption that some of the valence electrons have small effective masses. Furthermore, this large diamagnetism disappears almost completely when the Bi is melted so it is hard to avoid the conclusion that the diamagnetism is intimately associated with the lattice structure and it is reasonable to suppose it to be associated with the Brillouin zone structure. The ratio of susceptibilities parallel and perpendicular to the principal axis can be changed by a factor 2 by alloying with the pure Bi a small fraction of an atomic percent of Pb, which has one less valence electron per atom than Bi. This observation is compatible with the hypothesis that the principal axis susceptibility arises from the motions of a very small number of overlapping electrons, and that this number is substantially reduced percentage-wise by the substitution of the small number of Pb atoms. Finally, the field dependence of the Bi susceptibility is very spectacular (the de Haas-van Alphen effect);[12] the susceptibility oscillates in high fields and the oscillatory behavior persists to rather high temperatures. The reason for the oscillation was first recognized by Peierls and has since been studied in great detail.[13,14] Existing theories of the effect are not really applicable to metals because in the theories the electrons are treated as free. However, these theories show that a free electron gas could not have such an oscillation of the susceptibility at the field strengths used unless some electrons had extremely small masses. The totality of the evidence strongly suggests, therefore, that the anomalous magnetic properties of Bi originate from some configuration or configurations of conduction electrons which have small effective masses, probably as a consequence of the structure of the Brillouin zones.

In the following paragraphs we will discuss the two configurations which occur in Jones model of the Fermi surface from the point of view of the "neglected" susceptibilities. We will begin by discussing the hypothetical configuration of the electrons overlapping at the sites D. Figure 5 shows that for these electrons states all components of the diagonal reciprocal effective mass tensor are necessarily positive, and Jones found that agreement with experiment is only possible if precisely two components are large. Now it follows from Eq. (4.4) that if $\alpha^{\mu\mu}$ is large and positive for some state, then there exists a nearby state for which $\alpha^{\mu\mu}$ is large and negative. For suppose there are M states which are close together and interact strongly so that the sum is Eq. (4.4) gets its chief contribution from these states. Summing Eq. (4.4) over those states we find

$$\sum_{n=1}^{M} \alpha_n{}^{\mu\nu} = M\delta_{\mu\nu}. \tag{6.1}$$

M is always a small number, so it is clear that the positive and negative contributions must approximately cancel. The form of the right-hand side of (4.4) indicates that the lower-lying states will have negative $\alpha^{\mu\mu}$ while the higher-lying states will have positive $\alpha^{\mu\mu}$. Finally, the $\alpha^{\mu\mu}$ of the lowest state must be either smaller than one or negative. It would seem likely then, that on Jones' model the overlapping states at D are not in the lowest state of the set of near degenerate states responsible for the great size of the $\alpha^{\mu\nu}$. In that case, it must be that the lower band states on the other side of the zone face also have large (but negative) $\alpha^{\mu\nu}$, hence that there is only a small energy gap across the zone face. We can estimate the gap energy by noting that the free electron kinetic energy at the D site is about 7.5 volts and the α corresponding to the direction normal to the zone face is 200 for the upper band states. The corresponding α in the lower band must be also of the order 200, so we could conclude by Eq. (5.18) that the energy discontinuity across the zone face was of the order of 0.15 ev. An examination of the kinetic energies at various points in the zone of Fig. 5 shows that such a small gap would be insufficient to restrain the electrons within the rather oblong Brillouin zone. A further point is that, since more than one of the $\alpha^{\mu\nu}$ was assumed to be large, at least one additional excited band would have to be supposed to lie within a small fraction of a volt of the overlapping states at the sites D. Mr. Joel McClure and the writer have constructed all of the reciprocal lattice planes which are relevant to the D sites and have found that no other planes come at all close. It would seem most improbable, then, that the situation with regard to the D sites could be quite as Jones has supposed.

Even though we do not believe that Jones description of the overlap configuration is quantitatively correct, we want to discuss the order of magnitude of the terms χ_2 and χ_3 which would have been expected for such a configuration. We will show that for any configuration like that at the D sites χ_1 would be a poor approximation to the total susceptibility. In order to demonstrate that the terms in χ_2 and χ_3 could not be ignored, we will

[12] de Haas-van Alphen, Leiden Comm. **212a** (1930).
[13] E. H. Sondheimer and A. H. Wilson, Proc. Roy. Soc. (London) **A210**, 173 (1952). In this paper can be found references to much of the work beginning with Peierls original paper.
[14] R. B. Dingle, Proc. Roy. Soc. (London) **211**, 500 (1952); **212**, 38 (1952).

simply select one of the terms from χ_3' and show that it alone could give a susceptibility as large as χ_1. From the expression (2.9) for we can select the term

$$h\equiv-\sum_{n'}(\hbar^2/E_{nn'})[s_{nn'}{}^{\nu\beta}s_{n'n}{}^{\gamma\lambda}+\text{c.c.}]\delta_{\nu\lambda z}\delta_{\beta\gamma z}. \quad (6.2)$$

Using the definition of $s_{jj'}{}^{\mu\nu}$ given in (2.8), we can write (6.2) as

$$h=-\sum_{n'}(2\hbar^2/m^2E_{n'n}{}^3)(P_{n'}{}^\beta-P_n{}^\beta)(P_{n'}{}^\nu-P_n{}^\nu) \times P_{nn'}{}^\gamma P_{n'n}{}^\lambda\delta_{\nu\lambda z}\delta_{\beta\gamma z}. \quad (6.3)$$

Since we want to see the order of magnitude, we will ignore off-diagonal components of the $\alpha^{\mu\nu}$ and write

$$P_n{}^\beta\doteqdot p^\beta\alpha_n{}^{\beta\beta}. \quad (6.4)$$

Then

$$h=-\sum_{n'}(2\hbar^2/m^2E_{nn'}{}^3)[p_x{}^2(\alpha_{n'}{}^{xx}-\alpha_n{}^{xx})^2|P_{nn'}{}^y|^2 + p_y{}^2(\alpha_{n'}{}^{yy}-\alpha_n{}^{yy})^2|P_{nn'}{}^x|^2]. \quad (6.5)$$

For simplicity, let us set $|\alpha^{xx}|\sim|\alpha_{yy}|\sim\alpha$. Then (6.5) is of the order

$$h\sim-4\hbar^2(p_x{}^2+p_y{}^2)\alpha^3/m\Delta E^2, \quad (6.6)$$

in which ΔE denotes some average excitation energy which is of the order of the excitation from the first to second band. Now if ζ_2 is the energy to which an ellipsoid in zone 2 is filled, there will be occupied in the lower band a volume of about

$$V_{K1}\sim(2m)^{\frac{3}{2}}\Delta E\alpha^{-1}(\Delta E+\zeta_1)^{\frac{1}{2}}. \quad (6.7)$$

Inserting h as given by (6.6) into Eq. (3.18) and using the volume given by Eq. (6.7), we get an estimate of the susceptibility contribution of the term Eq. (6.2) from the low band. This is

$$\chi\sim\mu_B{}^2[2/(2\pi\hbar)^3](2m)^{\frac{3}{2}}\Delta E\alpha^2(\Delta E+\zeta_1)^{\frac{1}{2}}(p_x{}^2+p_y{}^2/m\Delta E^2);$$

or, setting $(p_x{}^2+p_y{}^2)_{\max}\sim m\Delta E/\alpha$, $\Delta E\sim E_F/\alpha$, we find

$$\chi\sim\chi_L\alpha^{\frac{1}{2}}. \quad (6.8)$$

We can compare the susceptibility Eq. (6.8) with the surface integral χ_1 over the ellipsoid in the second zone. This is

$$\chi_1=-(\mu_B{}^2/3)(8\pi/(2\pi\hbar)^3)m(2m\zeta_2)^{\frac{1}{2}} \times|\alpha^{xx}\alpha^{yy}|^{\frac{1}{2}}|\alpha^{zz}|^{-\frac{1}{2}}. \quad (6.9)$$

Now as we saw in the last section, $\Delta E/2=\zeta_2$ in (6.9) gives the approximate maximum value which χ_1 will attain for a single ellipsoid, regardless of the value of ζ_2, in view of the fact that $\alpha^{\mu\mu}$ approach unity for very large ζ_2. Putting $\zeta_L\sim\Delta E/2$ into (6.9), we get

$$\chi_{1\max}\sim-\chi_L\alpha^{\frac{1}{2}}. \quad (6.10)$$

We see that for the kind of overlap configuration which Jones considered, the susceptibility χ_3 is of the same order as the susceptibility χ_1. As it is, we considered only those occupied states in the lower band which lay in a "collar" around the central point of overlapping. If we had assumed that the gap was small all the way across a zone face and that the lower band states were occupied across the face, we would find for χ_3 something larger in powers of α than what we wrote in Eq. (6.8); such a result emphasizes the incompatibility of the assumption of large α and of small overlap.

We have shown that it is doubtful that for a configuration of the type at the D sites one can get a useful interpretation of the susceptibility merely on the basis of the Landau-Peierls formula in the case that the gap across the zone face is small. We have also shown the assumption that the zone of Fig. 5 *is* about full to be incompatible with the assumption that any small groups of overlapping electrons at D sites would have very small effective masses. We will now discuss the holes in a zone corner like A or B. We need not go into great detail in such a discussion since the arguments are very much the same as we have used before. In the first place, if the $\alpha^{\mu\nu}$ are really large for the corner states, it means that the energy of excitation to the next band is very small. In an unreduced zone picture this must mean that there is a very small gap across one or more of the faces which make up the corner. Since a corner is always energetically higher than the points on the faces which form it, we would find that because of the smallness of the gap across one face the Brillouin zone would not be "strong" enough to keep the electrons in. This again is a special argument applying only to the model of Bi in which high corners and small gaps are both assumed. The argument that if the $\alpha^{\mu\nu}$ are large χ_3 has terms of the same order as χ_1 applies to this configuration also. While we can hardly discuss χ_2, it is a fair assumption that it too may be appreciably large in both configurations. For if two or more of the $\alpha^{\mu\mu}$ are large, there must be at least two important intermediate states. With two intermediate states, "roundabout" transitions need not be small so χ_2 need not be small.

The discussion which we have given for the special configurations which occur in Jones' model of Bi can easily be recast to apply to other configurations. It will always be found that when the excitation energy from a group of occupied states to other states is much smaller than the Fermi energy, the Landau-Peierls formula does not contain a good approximation to the total susceptibility contribution from that group of states. So goes the general conclusion. In the course of this investigation the writer has come to doubt that Jones' theory of Bi is even qualitatively correct. One may even question whether a zone picture of energy bands is appropriate in Bi, since Bi shows some tendency toward covalent bonding. Without attempting to settle this question the writer would like to suggest that there is a modification of Jones' scheme which appears to offer the possibility of accounting in a rough way for both the parallel and perpendicular susceptibilities. The modified model might well retain some degree of validity, even

if there is a tendency towards forming a covalent bond between nearest neighbors, since the electrons which provide the diamagnetism are distinct from those which provide the covalent bond. Suppose that we use the Brillouin zone description of the bands, but admit that the gaps across some of the zone faces may be rather large. Let us suppose that the energy gaps across the $(1\bar{1}0)$ faces at D amount to several volts so that indeed there is little or no overlap at D. In such a case any overlapping electrons at D would not have especially small masses so would not contribute any great diamagnetism. In fact, if the density of energy levels were quite high, such electrons might give an appreciable *paramagnetic* contribution on account of their spin moments. The source of the observed large diamagnetism of Bi would then have to be elsewhere, and we suggest that the probable source is a group of regions, one of which we have labeled C in Fig. 5. The details of the Bi zone structure indicate that if the overlap at D is not too great there will be appreciable overlap at C. A number of "strong" planes at about the Fermi radius intersect the energetically high corners of the zone shown in Fig. 5 and effectively prevent any electrons from getting near the corners. With the corners of the zone thus cut off there is not room in the zone for five electrons per atom so overlap must occur somewhere. Assuming that the $(1\bar{1}0)$ faces are strong enough to restrict the amount of overlap at D, then the overlap could only occur at C. Let us suppose that it happens so, and consider what the energy level structure might be like in the neighborhood of C. The top faces of the zone are formed by the (221) planes. One of these planes would be expected to have a gap across it which is smaller than that across the $(1\bar{1}0)$ planes but still substantial. The gap would not be small enough in itself to explain any very small effective masses. However, there is another feature of the zone structure which could provide the required complexity of energy levels at the C sites. The strong (211) planes intersect in lines which pass obliquely through the zone faces formed by the (221) planes, and the point at which the line passes through the (221) face is very close to the point where we would have expected overlap to occur most easily. It would not be strange if there are electron states of very small mass in the neighborhood of the intersection point. Thus it would appear that the C sites are naturally endowed with the kind of energy structure which could contribute to a large diamagnetism.

No attempt has been made to work out the consequences of such a model in detail, but some of them can be foreseen without calculation. One of the most striking is that the angle which the (221) faces make with the principal axis is favorable for explaining the observed anisotropy effect of the diamagnetism, without bringing in two separate sites as sources of large diamagnetism. In this respect the model proposed here is even simpler than Jones' original model. On the other hand, other results of the present work make it clear that the diamagnetism could not be simply characterized by a set of effective mass values and a number of overlapping electrons, since off-diagonal matrix elements would play an important role. It would probably be quite difficult to establish the proposed model on a quantitative basis just because of the complications which come into the calculation of the susceptibility when the effective mass is very small. There would be analogous anomalies in a calculation of the electrical properties, so it is not clear whether or not the electrical properties would follow naturally from the model. At the moment all we claim for the model is that it is not palpably absurd, it involves only the most natural hypothesis about the energy structure, and it probably leads to magnetic anomalies of the kind observed for Bi.

7. SUMMARY AND CONCLUSIONS*

In this paper we have derived an expression for the orbital magnetic susceptibility of an electron gas which moves in a periodic potential. The derivation makes use of the Wannier formalism. The final formula for the susceptibility is somewhat simpler than previous formulas, because the Wannier formalism contains implicitly certain sum rules which were not previously noticed.

Using our formulas for the susceptibility we have studied the question as to whether the Landau-Peierls formula, Eq. (1.1), gives a good approximation to the total orbital susceptibility. What we have found is that if any portion of the Landau-Peierls susceptibility is the result of electrons with small effective masses, then the total orbital suceptibility differs from the Landau-Peierls susceptibility by an amount of the same order as that portion. More precisely, if the energy gaps between bands are appreciably smaller than the Fermi energy, the total susceptibility differs from the Landau-Peierls susceptibility by an amount which is of the same order of magnitude as the difference between the Landau-Peierls susceptibility and the Landau susceptibility, Eq. (1.2).

We have treated in detail the case of a weak plane in the reciprocal lattice and shown that such a plane can give large contributions to the orbital diamagnetism when it is overlapped by the Fermi surface. The large diamagnetism resulting from such a plane was shown to be not identical with the Landau-Peierls diamagnetism[6] in fact, for large overlap this diamagnetism was much larger than the Landau-Peierls diamagnetism. If one or more such planes formed the boundary of a filled zone, the zone could make a large contribution to the susceptibility, even though there is no Fermi surface in the zone. This part of the susceptibility could be expected to be anisotropic in a manner determined by the arrangement of the weak planes. It was pointed out that the occurrence of such a susceptibility would cor-

* See also "Note added in proof" at end of this section.

respond to some electrons being weakly bound to the lattice ions forming larger ions with very low-lying excited states.

We have examined Jones' theory of the Bi diamagnetism and concluded that his hypothesis concerning the location of the Fermi surface is incompatible with his assumptions concerning the effective masses. We have suggested a modification of Jones' hypothesis which we believe to be more in accord with the detailed structure of the Brillouin zones and the evidences of strong binding in Bi. It was indicated how the modified model may give a simpler explanation of the over-all features of the Bi susceptibility.

In conclusion, we would like to briefly discuss two theories on which we believe our discussion has some bearing but to which we cannot make a detailed application. The first in Bardeen's theory[6] of superconductivity which was referred to earlier. Bardeen has discussed a case in which the α's were supposed to be so large that the diamagnetism, Eq. (1.1) would be more than sufficient to drive out the field. While we cannot discuss Bardeen's theory itself, it should be clear from the examples discussed in this paper that (Eq. (1.1) is unreliable when the electron effective mass is very small. Another feature of Bardeen's theory which we can comment on in this connection is his "self-consistent field" argument showing that electrons with small effective mass can keep the magnetic field out of a metal because the penetration depth is considerably smaller than the electron wave function. In making this argument, Bardeen set up a Hamiltonian which was the same as the ordinary free electron Hamiltonian except that the effective mass occurred in the place of the free electron mass. The approximation involved in writing such a Hamiltonian is known,[8,9] and the terms neglected are just the terms which give the additional contributions to the susceptibility which are the subject of this paper. As we have seen when the effective mass is very small, the neglected terms are just as important as those which are kept. Thus we can conclude that Bardeen's calculation concerning the penetration of the magnetic field is based on an incomplete Hamiltonian, and that the terms which have been omitted are so large as to bring into question the outcome of a calculation made with the correct Hamiltonian.

There is another matter to which our results cannot be applied and yet about which they indicate something significant, namely the interpretation of the de Haas-van Alphen effect in the diamagnetic metals. At attainable field strengths the effect cannot be observed except in those substances for which there exist electrons of very small electron mass. Dingle[13] has done a careful analysis of a number of factors which cause the magnetic susceptibility of a real material to differ from the ideal crystal-bulk susceptibility considered here. He has included, for example, the effects of finite level width and of finite crystal size, and has done the calculation so as to get the complete temperature dependence and field dependence of the susceptibility. The apparent purpose of his work is to lay the foundation for a study of the de Haas-van Alphen effect in a real metal. Dingle worked in the approximation that the electrons are completely free, and in this approximation obtained the result quoted above that electrons of very small mass must be responsible for the observed de Haas-van Alphen effects. The part of his work which has as yet been published indicates that he considers the effective mass approximation adequate even for very refined calculations. The results of our work, on the other hand, make it certain that the effective mass approximation should be completely inadequate for an interpretation of observed de Haas-van Alphen effects. We have shown that if the effective masses are small there is an important additional term in the steady susceptibility arising from the term in the Hamiltonian which is neglected in the effective mass approximation. There will be similar contributions to each term in the development of the susceptibility in powers of the field, these contributions corresponding to higher order correction effects of the "neglected" term in the Hamiltonian (2.7) which explicitly involves the magnetic field rather than the vector potential. Accordingly, we must conclude that the effective mass approximation is not adequate for interpreting the de Haas-van Alphen effect in real metals. It unfortunately appears that an adequate calculation which takes into account multiple transitions between bands is almost outside the range of possibility.

The writer expresses his appreciation of enlightening discussions with a number of persons in the Institute for the Study of Metals and in particular the assistance of Mr. Joel McClure in constructing the Fermi surface of Bi.

Note added in proof.—After a number of conversations on the subject of this paper, I think it well to restate explicitly just what is claimed to be the validity of these conclusions. In the first place it is not claimed that the example which is carried through to the end is necessarily directly analogous to the situation obtaining in any of the diamagnetic metals. This example is given to show that in the one case for which the off diagonal terms can be readily computed, they are really as big as the Landau-Peierls term. The calculation cannot readily be made for more interesting configurations, but the estimates given show that sizes of matrix elements and numbers of states of large matrix element are such as to make it probable that in these cases, too, the off diagonal terms are really as large as the Landau-Peierls term. I think these last arguments extremely suggestive of the conclusions but it cannot be claimed that they quite prove the conclusions. However, irrespective of the detailed arguments presented, it can be seen that the key fact in the case of interest is that there exist off diagonal terms which, before integration over k, are large like the inverse cube of the energy gap.

For ordinary energy gaps such terms are negligible but for very small energy gaps they become dominant, unless, of course, they cancel one another. I have looked for and failed to find a reason for such a cancellation.

Finally, it is certainly not concluded that observed diamagnetic susceptibilities are not to be interpreted in terms of effective masses. However, it is concluded that the relation of an empirically determined effective mass to the reciprocal curvature of an energy surface will not be simple when the mass is very small.

PHYSICAL REVIEW VOLUME 89, NUMBER 3 FEBRUARY 1, 1953

The Proton-Proton Reaction and Energy Production in the Sun*

E. A. FRIEMAN,† *Polytechnic Institute of Brooklyn, Brooklyn, New York*
AND
L. MOTZ, *Rutherfurd Observatory, Columbia University, New York, New York*

(Received September 9, 1952)

The proton-proton capture cross section is recalculated using the recently computed deuteron wave functions of Feshbach and Schwinger and the most recent value of the Fermi G factor. The energy production of the p-p cycle is redetermined and applied to the sun, using the luminosity calculations of Epstein. It is shown that the p-p cycle outweighs the carbon cycle by a considerable factor under the assumed conditions of temperature and density.

I. INTRODUCTION

IN view of recent results which affect the conclusions of Bethe and Critchfield[1] on the proton-proton reaction,

$$H^1+H^1\rightarrow H^2+\beta^++\nu,$$

this process is recalculated and its astrophysical implications discussed for the sun. Epstein[2] showed recently that the energy production in the sun arising from the p-p cycle outweighs that arising from the carbon cycle by at least a factor of 12. This calculation utilized the new determination of the cross sections for the carbon cycle by Hall and Fowler[3] extrapolated from their measurements at 100 kev. In the present calculation the most recent value of the Fermi constant as well as new deuteron wave functions were used in the calculation of the cross section. The energy production per process also differs from that described in reference 1 because the He^3 reaction replaces the sequence used there.

II. THE CROSS SECTION FOR THE $P-P$ REACTION[4]

The cross section for the process, expressed as a function of the relative velocity v, is

$$\sigma(v)=(G/v)\,|\bar{M}|^2 f(W), \tag{1}$$

where $\bar{M}$ is the nuclear matrix element,

$$\bar{M}=\int \Psi_f \bar{\Gamma} \Psi_i d\tau, \tag{2}$$

and $\bar{\Gamma}$ is the Gamow-Teller interaction operator,

$$\bar{\Gamma}=(3)^{-\frac{1}{2}}\sum_i \tau^i\bar{\sigma}^i. \tag{3}$$

The proton space wave functions are those given by Yost, Wheeler, and Breit[5] for a square well and are given in concise form in reference 1. We can represent them as

$$\Psi_p(r,\bar{\sigma},\tau)=\Psi_p(r)\,{}^1(\sigma)_0\,{}^3(\tau)_{-1}, \tag{4}$$

where we have used Rosenfeld's[6] notation to represent the spin and isotopic spin wave functions.

The deuteron wave functions used are those computed by Feshbach and Schwinger[7] for "Yukawa well" interactions of different ranges for both the central and tensor portions of the interaction potential. These eigenfunctions can be represented by

$$\Psi_d=(4\pi)^{-\frac{1}{2}}\left[\frac{u(r)}{r}+(2)^{-\frac{1}{2}}S_{12}\frac{w(r)}{r}\right]{}^3(\sigma)_{m_S}\,{}^1(\tau)_0. \tag{5}$$

Using the well-known property of the tensor operator S_{12}, namely, that its average over all angles vanishes, it is seen that there is no D wave contribution to the matrix element. The spin summation is then easily performed using the Hermitian character of the G-T operator, since the sum over the final states of $|\bar{\Gamma}|^2$ is just the expectation value in the original state. The contribution to the cross section from the sum is simply a factor of two. The square of the matrix element can then be written

$$|\bar{M}|^2=8\pi\left|\int_0^\infty \psi_p(r)u(r)rdr\right|^2. \tag{6}$$

---

* This paper is based on a Ph.D. thesis submitted to the Graduate School of the Polytechnic Institute of Brooklyn. A preliminary report of this work was presented at the May, 1951, meeting of the American Physical Society.

† Now at the James Forrestal Research Center, Princeton University, Princeton, New Jersey.

[1] H. A. Bethe and C. Critchfield, Phys. Rev. **54**, 248 (1938).

[2] I. Epstein, Astrophys. J. **112**, 207 (1950).

[3] R. N. Hall and W. A. Fowler, Phys. Rev. **77**, 197 (1950).

[4] The symbols used here are the same as those given in reference 1 unless otherwise stated.

[5] Yost, Wheeler, and Breit, Phys. Rev. **49**, 174 (1936).

[6] L. Rosenfeld, *Nuclear Forces* (Interscience Publishers, Inc., New York, 1949).

[7] H. Feshbach and J. Schwinger, Phys. Rev. **84**, 194 (1951). We wish to thank Professor Feshbach for a prepublication copy of his paper.

The numerical tables of the deuteron eigenfunctions are given in terms of the dimensionless variable,

$$x=r/r_0, \quad r_0=2.76\times10^{-13} \text{ cm}, \tag{7}$$

for $0\leq x\leq 4.968=x_1$. The integrations were performed numerically up to the table limit and thence analytically, using the asymptotic form of the deuteron eigenfunctions

$$\begin{aligned} u(x)&=Ae^{-\xi(x-x_1)},\\ w(x)&=Be^{-\xi(x-x_1)}[1+3/\xi x+3/(\xi x)^2], \\ \xi&=(M\epsilon)^{\frac{1}{2}}r_0/h=0.64. \end{aligned} \tag{8}$$

The normalization condition on the deuteron wave functions,

$$1=r_0\int_0^\infty (u^2+w^2)dx, \tag{9}$$

allows the determination of A and B in terms of an auxiliary constant C_1 introduced to effect the normalization in the range 0 to x_1. The matching condition at $x=x_1$ further determines C_1. With the aid of the integrals

$$\begin{aligned} I_1&=\int_0^{x_1}(u^2+w^2)dx=1047.94,\\ I_2&=\int_{x_1}^\infty u^2(x)dx=A^2/2\xi, \\ I_3&=\int_{x_1}^\infty w^2(x)dx=(B^2/2\xi)[1+6(1+\xi x_1)^2/(\xi x_1)^3], \end{aligned} \tag{10}$$

one obtains

$$C_1=5.87\times10^4, \quad A=11.54\times10^4. \tag{11}$$

The proton space wave functions can be denoted following reference 1,

$$\psi_p(r)=\begin{cases} C[\Phi(r)+\theta(r)\lambda r_2/r], & r>r_2=e^2/mc^2; \\ C\dfrac{r_2}{r}[\Phi(r_2)+\theta(r_2)\lambda]\dfrac{\sin(\nu r/b)}{\sin(\nu r_2/b)}, & r<r_2; \end{cases} \tag{12}$$

where the values of the constants are given in Table I. The functions Φ and θ are given by

$$\begin{aligned} \Phi(y)&=y^{-\frac{1}{2}}I_1(2y^{\frac{1}{2}}),\\ \theta(y)&=-2y^{\frac{1}{2}}K_1(2y^{\frac{1}{2}}), \\ C&=(2\pi\eta)^{\frac{1}{2}}e^{-\pi\eta}, \quad \eta=e^2/hv. \end{aligned} \tag{13}$$

Introducing the proton and deuteron wave functions into the expression for the square of the matrix element, we obtain

$$|\bar{M}|^2=16\pi^2\eta e^{-2\pi\eta}\Lambda^2, \quad \Lambda^2=|\sum_{i=1}^5 a_i\Lambda_i|^2. \tag{14}$$

TABLE I. The values of the constants and the integrals appearing in the matrix element.

$\Lambda_1=4.222\times10^{-13}$,	$\lambda=2.63$,
$\Lambda_2=6.843\times10^{-21}$,	$\nu=2.18$,
$\Lambda_3=6.278\times10^{-12}$,	$b=4.37\times10^{-13}$ cm,
$\Lambda_4=4.441\times10^{-25}$,	$\Phi(r_2)=1.050$,
$\Lambda_5=0.707\times10^{-14}$,	$\theta(r_2)=0.769$.

The integrals appearing in (14) are

$$\begin{aligned} \Lambda_1&=\int_0^{r_2}\sin(\nu r/b)u(r)dr, \\ &\qquad a_1=C_1r_2[\Phi(r_2)+\theta(r_2)\lambda]/\sin(\nu r_2/b), \\ \Lambda_2&=\int_{r_2}^{x_1r_0}\Phi(r)u(r)rdr, \quad a_2=C_1. \\ \Lambda_3&=\int_{r_2}^{x_1r_0}\theta(r)u(r)dr, \quad a_3=C_1\lambda r_2, \\ \Lambda_4&=\int_{x_1r_0}^\infty \Phi(r)\exp[-\xi r/r_1]dr, \quad a_4=Ae^\xi, \\ \Lambda_5&=\int_{x_1r_0}^\infty \theta(r)\exp[-\xi r/r_1]dr, \quad a_5=Ae^\xi\lambda r_2. \end{aligned} \tag{15}$$

Using the above values, one finds

$$\Lambda^2=0.818\times10^{-36}. \tag{16}$$

This can be compared to the value of Λ^2 (corrected for the spin summation), given by Bethe and Critchfield, 1.25×10^{-36}.

The Fermi constant G can be calculated from Wu's[8] experiments on He^6. The reaction,

$$He^6\rightarrow Li^6+\beta^-+\nu^*, \tag{17}$$

has a half-life of 0.823 sec. The f function for this reaction is 990 ± 85, and the nuclear matrix element squared for a pure Gamow-Teller transition is 2. Thus

$$G=\frac{\log 2}{ft_{\frac{1}{2}}|\bar{M}|^2}\cong(2200 \text{ sec})^{-1}. \tag{18}$$

The recent determination of the neutron half-life of 12.8 ± 2.5 min by Robson[9] also makes this value trustworthy. $f(W)$ for the p-p reaction is 0.134.

III. ENERGY PRODUCTION

Following reference 1, one integrates $\sigma(v)v$ over the thermal distribution of the protons to obtain the number of reactions per cm^3 per sec and thence the energy production. One finds that the number of

[8] C. S. Wu, Revs. Modern Phys. **22**, 386 (1950); Wu, Rustad, Perez-Mendez, and Lidofsky, Phys. Rev. **87**, 1140 (1952). For the half-life of He^6, see J. E. R. Holmes, Proc. Phys. Soc. (London) **62**, 293 (1949).

[9] J. M. Robson, Phys. Rev. **83**, 349 (1951).

processes per g per sec is

$$\rho=(16\pi/3^{5/2})\rho N_A{}^2C_{\rm H}{}^2Gf(W)\tau^2e^{-\tau}\Lambda^2, \quad (19)$$

where

$$\tau=3(\pi^2Me^4/4h^2kT)^{\frac{1}{3}}. \quad (20)$$

The original cycle studied by Bethe and Critchfield was

$$\begin{aligned} &H^1+H^1\rightarrow H^2+\beta^++\nu,\\ &H^1+H^2\rightarrow He^3+\gamma,\\ &He^3+He^4\rightarrow Be^7+\gamma,\\ &Be^7+\beta^-\rightarrow Li^7+\nu+\gamma,\\ &Li^7+H^1\rightarrow He^4+He^4, \end{aligned} \quad (21)$$

with an energy release of 4.3×10^{-5} erg. However, Fowler[10] has pointed out that the reaction,

$$He^3+He^3\rightarrow He^4+H^1+H^1, \quad (22)$$

should have a much higher probability than the He^3+He^4 reaction because of the emission of three particles in the former case, while the latter is a radiative capture. Osterbrock[11] has shown that the sequence of reactions ending in (22) reduces the energy release of the cycle by a factor of 0.514; the difference between this factor and 0.50 is due to the energy carried off by the neutrinos.

The energy produced per g per sec is then given by

$$\epsilon=1244\rho C_{\rm H}{}^2\tau^2e^{-\tau}. \quad (23)$$

The recent investigation by Epstein,[12] using a dual source for the sun, i.e., both the carbon and the p-p cycles operative, gives a central density of $\rho=150$ g/cm^3, a concentration of H, $C_{\rm H}=82$ percent, and a central temperature of 15×10^6 °K. The energy released is then found to be

$$\epsilon=265 \text{ ergs per g per sec.} \quad (24)$$

For small ranges of temperatures in the neighborhood of 15×10^6 degrees, we can approximate Eq. (23) by

$$\epsilon=9.37\times10^{-6}\rho C_{\rm H}{}^2T^4, \quad (25)$$

where T is in millions of degrees. This is to be compared with the results of Bondi and Salpeter[13] and still more recently Salpeter[14] who give the expressions

$$\epsilon=(55\pm8)(\rho/100)X_{\rm H}{}^2(T/15)^4$$

and

$$\epsilon=50(\rho X_{\rm H}{}^2/100)(T/15)^4,$$

respectively. In our notation these two expressions become the same as (25) with the coefficient in that equation replaced by 10.8×10^{-6} and 9.88×10^{-6}, respectively.

The corresponding expression for the carbon cycle[2] is[15]

$$\epsilon=5.1\times10^{-23}\rho C_{\rm H}\alpha_{14}T^{20}, \quad (26)$$

where α_{14} is the N^{14} abundance and has the value 0.0025.[12]

The relative roles of both these cycles in solar energy production can best be determined by comparing their respective contributions to the luminosity. The integration of the luminosity relation

$$L=4\pi\int_0^R\rho\epsilon r^2dr \quad (27)$$

was first carried out by Epstein,[2] assuming the temperature and density distributions to be given by a polytrope of index $\frac{3}{2}$. Upon revising his results to take into account the new value of ϵ for the p-p reaction, we find

$$L_p/L_c=(C_{\rm H}/\alpha_{14})(1.1\times10^{18}/T_c{}^{16}). \quad (28)$$

If we use the values quoted above, this yields

$$L_p/L_c=55. \quad (29)$$

IV. CONCLUSIONS

Although our results indicate that the C−N cycle is no longer of great importance in the sun, this conclusion may have to be revised as a result of the recent work on N^{14} cross section.[16] The experimentally obtained cross sections for the $N^{14}(p,\gamma)O^{15}$ reaction in the range 0.25 to 2.6 Mev were extrapolated to the approximate energy of interest in stellar calculations (28 kev). This procedure is valid only if there are no low energy resonances present in this reaction. Although the available data on this point is still inconclusive, a rough estimate of the effect of resonances can be obtained by assuming that the N^{14} reaction goes much faster than the C^{12} reaction, and that the latter nuclei now have the longest lifetime in the cycle. The energy production can then be calculated by taking the upper limit given by Bondi and Salpeter,[13] which becomes in our notation

$$\epsilon=44\times10^{-20}C_{\rm H}C_{\rm CN}T^{18}.$$

If we then take the value 0.0025 for $C_{\rm CN}$, we find that

$$L_p/L_c\sim1.4.$$

In considering this last result, we must keep in mind that it holds for a central temperature of 15×10^6 degrees. With both cycles contributing equally, however, this means that the release of energy at this temperature would be greater than the observed value. We should therefore have to consider models of the sun with smaller central temperatures, with the result that the p-p reaction would again be dominant.

[10] W. A. Fowler, Phys. Rev. **81**, 655 (1951).
[11] D. E. Osterbrock, unpublished.
[12] I. Epstein, Astrophys. J. **114**, 438 (1951).
[13] H. Bondi and E. E. Salpeter, Nature **169**, 304 (1952).
[14] E. E. Salpeter, Astrophys. J. (to be published).

[15] In reference 2 the coefficient given by Epstein in the expression for the energy generation for the carbon cycle is 1.0×10^{-23} instead of the value given in (26). The reason for the difference is that Epstein uses $E_0=Z^2$ instead of the correct expression $0.993\ Z^2\mu$, where μ is the reduced mass of the colliding particles. If this expression is used and the reduced mass for H and carbon 12 is taken, then the temperature, which enters to the twentieth power, has to be divided by 0.92, and this gives the corrected coefficient.
[16] D. B. Duncan and J. E. Perry, Phys. Rev. **82**, 809 (1951).

Interpretation of α-Values in p–n Junction Transistors

F. S. GOUCHER AND M. B. PRINCE
Bell Telephone Laboratories, Murray Hill, New Jersey

(Received October 20, 1952)

By the measurement of five parameters in several p-n junction transistors, *viz.*, the conductivities and diffusion lengths of minority carriers in the emitter and base regions and the widths of the base regions, the current amplification factor α of the transistors has been computed from theory. Previous to this investigation two of the parameters associated with the thin p-layer had not been measured. The quantity α also was obtained independently by two alternate methods: (1) by measuring the collector-emitter current characteristic, and (2) by measuring the apparent quantum efficiency of the transistor as a two-electrode photocell with a floating base. The three determined values of α for each sample agree within the experimental error.

INTRODUCTION

THE p-n junction transistors studied in this investigation[1] consist of a single crystal of germanium in which normally a thin layer of p-type semiconductor is sandwiched between two n-type end sections. Electrons from one n-type section, the emitter, are injected into the p region where some or most of them diffuse to the boundary between the p layer and the second n section, the collector. With a reverse bias across this second junction, electrons reaching this junction fall down hill into the collector and are registered as collector current.

For this device the current amplification factor α is defined as $-\partial I_c/\partial I_e$ at constant collector voltage. I_c and I_e are collector and emitter currents, respectively. It is apparent physically that α depends on three factors: (1) γ: the fraction of the current carried by electrons, across the emitter junction, (2) β: the fraction of the electrons emitted into the p region which arrive at the collector junction, and (3) α^*: the ratio of change in total current to change in electron current reaching the collector junction.

It has been shown theoretically by Shockley[2] that α^*, β, and γ are simple functions of five parameters characteristic of the semiconducting material. Measurement of these parameters obviously would afford an additional check on the consistency and applicability of the theory. Such has been the purpose of this experimental investigation.

The relations can be expressed as

$$\gamma=\frac{1}{1+(\sigma_b/\sigma_e)(L_b/L_e)\tanh(w/L_b)}\simeq\frac{1}{1+(\sigma_b/\sigma_e)(w/L_e)},$$

$$\beta=\operatorname{sech}(w/L_b)\simeq 1,$$

$$\alpha^*=1 \quad \text{for} \quad \sigma_c\gg\sigma_i,$$

$$\alpha=\gamma\beta\alpha^*,$$

where σ_c = conductivity of collector region, σ_b = conductivity of base layer, σ_e = conductivity of emitter region, σ_i = conductivity of intrinsic germanium, L_b = diffusion length for minority carriers in base layer, L_e = diffusion length for minority carriers in emitter region, and w = width of base layer. The approximations are valid for $w\ll L_b$.

When the transistor is used as a phototransistor, the apparent quantum efficiency (Q.E.) is related to α uniquely by the same theory.[2]

$$\alpha=(\text{Q.E.}-1)/\text{Q.E.}$$

Q.E. will be defined later in the paper.

Thus, we have been able to measure α for five n-p-n and one p-n-p transistors by three independent experimental methods. 1. Measurement according to the definition: $\alpha=(\partial I_c/\partial I_e)_{V_c}$. 2. Calculation of α from measured values of the five parameters—w, L_e, L_b, σ_e, σ_b. 3. Calculation of α from measured Q.E.

For all six samples, the three determinations of α agree within the experimental errors.

EXPERIMENTAL PROCEDURE

A. Specimens

All the specimens used in these experiments were slabs cut from various single crystals of germanium.[3] They varied in thickness from 0.028 in. to 0.051 in. and were approximately one-half inch in width. The crystals were grown with a base layer width of at least 0.004 in. so that L_b could be measured.

B. Direct Measurement of α

This value of α was determined by taking the slope of the plot of I_c *vs* I_e at constant V_c. As α is insensitive to V_c, $V_e=3$ volts was used since it was convenient.

C. Calculation of α from Measured Values of the Five Parameters

1. σ_e was measured using a four-point probe method (Fig. 1). The general formula[4] for this method is

[1] All the samples had four terminals (two terminals to the base region) and the dimensions of the samples were chosen to be large in comparison with the dimensions of production transistors. However, these samples can be and have been operated as three terminal devices in the manner of conventional n-p-n transistors (the two base region contacts tied together).

[2] Shockley, Sparks, and Teal, Phys. Rev. **83**, 151 (1951).

[3] Teal, Sparks, and Buehler, Phys. Rev. **81**, 637 (1951).

[4] See Appendix.

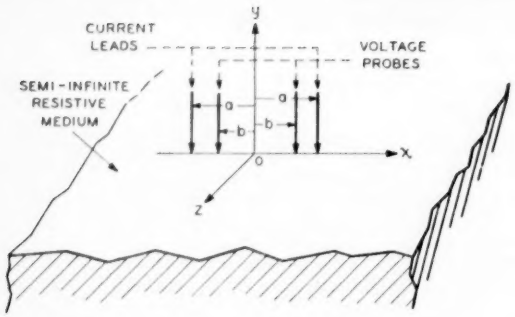

FIG. 1. Four-point probe resistivity measuring device.

$\sigma=[2b/\pi(a^2-b^2)](I/V)$, where a and b are distances shown in Fig. 1, I is the current flowing in the current probes, and V is the voltage across the potential probes. In this investigation, $a=3b=0.19$ cm; therefore $\sigma_s=1.25I/V$. The above relation holds for samples whose dimensions are large compared to 2a.

2. σ_b and w were measured by potential probes. Two contacts were made to the base layer of an n-p-n junction transistor (Fig. 2), and the two junctions were biased in the reverse direction. This resulted in small reverse currents flowing across the junctions. The principal current flowed in the base layer between the two contacts. A voltage probe connected to a potentiometer was drawn across the junctions in the x direction for various values of y. A typical set of plots of these probe voltages is shown in Fig. 3. The parameter w is determined directly from these plots and σ_b from

$$\sigma_b=(I/tw)(\Delta y/\Delta V),$$

where I = current flowing in region of base layer, t = thickness of slab, w = width of base layer, Δy = distance between two probes in the x direction, and ΔV = voltage difference in base layer between two probes.

3. L_e and L_b were obtained from measurements of the distance variation of the photocurrent produced by scanning the specimen with a small spot of "chopped" light, in a direction normal to the junctions. The light spot was 2–3 mils in diameter, the frequency of chopping 90 cps, the light and dark intervals of equal duration, and the biasing voltage sufficient to saturate the collector current. In these measurements the specimen was biased as in Fig. 4(a). The 90-cycle component of current was measured by means of the ac voltage it generated across a series resistance small in comparison

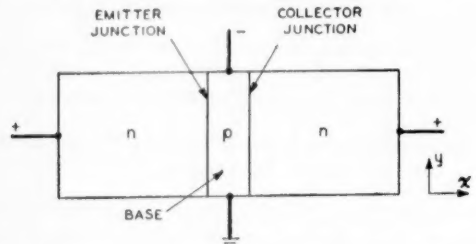

FIG. 2. Electrical polarities for measuring base layer conductivity in n-p-n junction transistor.

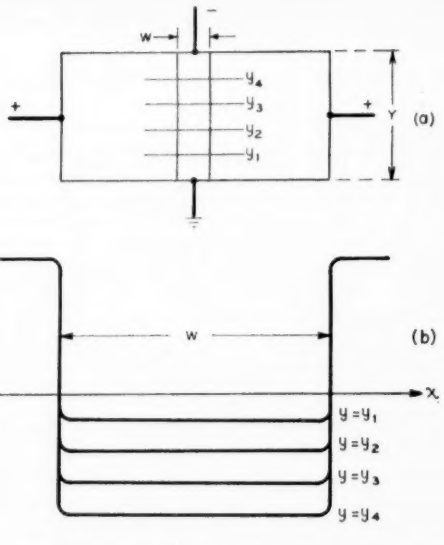

FIG. 3. Probe plots for determining base layer conductivity. (a) Position of probe lines on the crystal. (b) Potential *vs* position for probes.

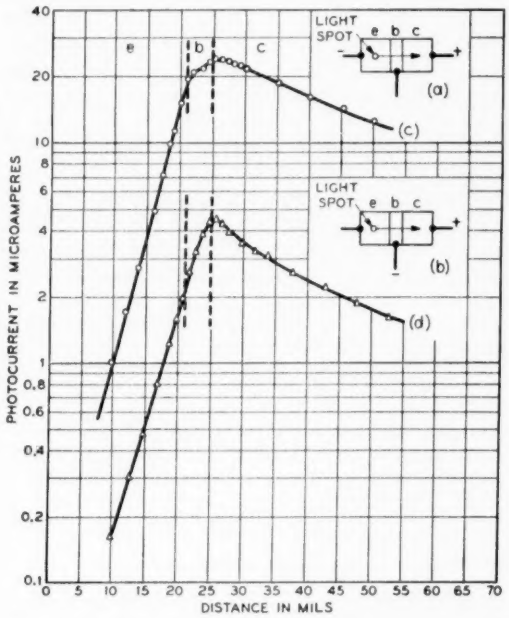

FIG. 4. Diffusion length determinations. (a) Transistor biased for phototransistor operation. (b) One junction biased in reverse for unit quantum efficiency. (c) Photocurrent when transistor is biased as a phototransistor. (d) Photocurrent when one junction is biased in reverse.

TABLE I. Tabulation of experimental data and calculated results.

Specimen	1 Type	2 σ_e mho/cm	3 σ_b mho/cm	4 L_e microns	5 L_b microns	6 w microns	7 Calc. γ	8 Calc. β	9 Q.E.	10 Calc. α	11 Direct measurement α	12 Q.E. α
16	n-p-n	0.098	0.43	216	1020	210	0.19	0.98	1.14	0.19	0.22	0.12
17A	n-p-n	2.8	0.50	97	452	103	0.84	0.97	5.4	0.81	0.81	0.82
19A	n-p-n	2.6	0.32	266	710	200	0.92	0.96	10.0	0.88	0.79	0.90
19B	n-p-n	2.6	0.35	187	687	110	0.93	0.98	11.1	0.91	0.90	0.91
25A	n-p-n	15.1	0.44	45	495	600	0.72	0.55	1.68	0.40	0.40	0.40
43	p-n-p	29.5	4.9	130	58	161	0.93	0.25	1.27	0.23	0.25	0.21

with the resistance of the collector junction, which was biased in reverse. Under these conditions characteristics such as Fig. 4(c) were obtained. Since the response falls off exponentially from the emitter junction in the emitter region, in agreement with diffusion theory, L_e is determined as that distance which reduces the photoresponse to $1/e$ of its original value.[5] Similarly L_b is determined from the photoresponse data in the base region. However, in this region, it can be shown that L_b must be determined from a more complicated function of L_e, w, and the photoresponse *vs* distance curve, than in the emitter region.

D. Determination of α from the Apparent Quantum Efficiency

The theory of the operation of a p-n junction phototransistor using a p-n hook collector is discussed in reference 2. The apparent quantum efficiency or amplification factor is defined as the ratio of the peak photocurrent when the light spot falls on the collector junction with the transistor biased as a phototransistor [Fig. 4(a)] to the photocurrent obtained when the same light spot falls on the collector junction biased as in Fig. 4(b). The latter is best obtained by scanning both junctions as in Fig. 4(b). It has been shown[6] that when the light spot is small compared to the diffusion length, the photocurrent with the spot at a p-n junction corresponds approximately to unit quantum yield for the absorbed quanta. Therefore, the apparent quantum efficiency is a measure of the amplification factor of the p-n junction phototransistor.

TABLE II. Tabulation of probable errors in measured quantities.

Quantity	Probable error percent
σ_e	5
σ_b	2
L_e	10
L_b	20
w	2
Direct measurement α	2
Q.E.	10

[5] F. S. Goucher, Phys. Rev. **81**, 475 (1951).
[6] F. S. Goucher, Phys. Rev. **81**, 637 (1951).

EXPERIMENTAL RESULTS AND DISCUSSION

The dependence of α upon σ_e, σ_b, L_e, L_b, and w found in the experiments described above is summarized in Table I. In Table II, there is a listing of the probable errors associated with the measured quantities. Previously reported results[2] indicate that the current voltage relationships are in agreement with theory. The results of these experiments demonstrate that the parameter α can be deduced from measured properties of the structure. The modified experimental structures are in every way similar to an actual transistor structure except in the width of the sample. On the basis of these facts, there can be little doubt as to the soundness of the present theory of the functioning of junction transistors.

We are indebted to W. Shockley, who proposed this investigation, for his advice and support, to M. Sparks for supplying the crystals and suggesting experimental techniques, and to R. Mikulyak who helped in the preparation of the experimental samples.

APPENDIX

Theory of 4-Point Probe Resistivity Measuring Device[7]

Consider a semi-infinite homogeneous resistive medium (Fig. 1) with a pair of current probes at $x=\pm a$ and a pair of potential probes at $x=\pm b$. The potential at any point r due to the two current sources is

$$V(r)=V(a)+\frac{I}{2\pi\sigma|a-r|}+V(-a)-\frac{I}{2\pi\sigma|-a-r|}.$$

Therefore

$$V=V(b)-V(-b)=\frac{I}{\pi\sigma}\left[\frac{1}{a-b}-\frac{1}{a+b}\right]=\frac{2b}{a^2-b^2}\frac{1}{\pi\sigma},$$

or

$$\rho=\frac{1}{\sigma}=\frac{\pi(a^2-b^2)}{2b}\frac{V}{I}.$$

[7] For a more general discussion see L. B. Valdes, to be published in the near future.

Letters to the Editor

PUBLICATION of brief reports of important discoveries in physics may be secured by addressing them to this department. The closing date for this department is five weeks prior to the date of issue. No proof will be sent to the authors. The Board of Editors does not hold itself responsible for the opinions expressed by the correspondents. Communications should not exceed 600 words in length and should be submitted in duplicate.

Some Properties of Superconductors below 1°K*

T. S. SMITH,† W. B. GAGER, AND J. G. DAUNT
Department of Physics and Astronomy, Ohio State University, Columbus, Ohio
(Received December 15, 1952)

IN a previous paper[1] we reported some properties of superconductors below 1°K. After that paper was completed, we measured magnetically the superconducting properties below 1°K of a recently required sample of titanium obtained from the Foote Mineral Company and bearing the type number "Lot Number 203.8."

This sample of Ti was in the form of a crystal bar, produced by deposition from the iodide, and was of stated purity 99.99 percent. The measured hardness, used at Tukon machine, of a sample cut from the bar on arrival averaged 76 dph numbers. After annealing at 670°C in vacuum for 3 hours, the measured hardness averaged 67 dph numbers. This relative softness of the material indicated that it was of high purity and, in particular, relatively free from gaseous occlusions.

Using the vacuum annealed Ti, we obtained by methods previously reported,[1,2] the results shown in Table I. The differences between the temperatures T^* computed from Curie's law and the temperature T_c^* on the Curie scale for a spherical sample were calculated using measured data of the filling factor and axial lengths of the ellipsoidal chrome potassium alum pill employed in the experiment.

The results indicated a transition temperature T_c of 0.387° curie and a slope of the magnetic threshold curve dh/dT at $T=T_c$ of 89.5 gauss/deg. The magnetic threshold curve was approximately parabolic and indicated a magnetic threshold field value H_0 at 0°K of 20 gauss.

These values for T_c and dH/dT for Ti are considerably smaller than those which we have previously reported,[1,2] and indicate that the present Ti sample was of higher purity, both physically and chemically, than the samples previously employed, as can be assessed also by comparison of the measured hardness of the samples. The results serve to emphasize the care which must be taken in establishing superconductive data for metals which are difficult to prepare in a pure state; and these results, by reflection, emphasize again the very preliminary character of the data[1] obtained for hafnium, as we have previously pointed out.[1]

If one assumes that the measured magnetic threshold curve for Ti represents an equilibrium boundary between superconducting and normal states, which seems reasonable in view of the high purity of the sample, we can compute therefrom the specific heat of the electrons in the normal state to be

$$C_{el,n}=\gamma T=1.1\times10^{-4}T \text{ cal/mole-deg.}$$

TABLE I. The magnetic transition in titanium. Temperatures on Curie scale and critical field values.

T^*	T_c^*	H_c gauss
0.369	0.387	0
0.31	0.328	6.6
0.276	0.294	8.25
0.254	0.272	9.9

This value is considerably smaller than that reported by Estermann, Friedberg, and Goldman,[3] who made calorimetric measurements in the liquid helium temperature region. A similar discrepancy between the values of γ obtained by magnetic measurements on the superconducting state and those obtained calorimetrically has been previously noted and extensively discussed by us[1] in the case of Zr. It is to be noted here for Ti that, as in the case of Zr, the magnetically computed γ-values are the lower ones. It is possible that the origin of the discrepancies lies in the fact that both for Ti and Zr the two sets of measurements were performed in temperature regions different from one another by a factor of 5 or more. Support for this view comes from the well-known[4] agreement between magnetic and calorimetric determinations of γ for superconducting elements for which the determination can be made in both cases in the same temperature regions, as has been shown for example for Sn by Daunt, Horseman, and Mendelssohn.[4]

We wish to acknowledge our thanks to The Research Corporation for a grant which has greatly aided this research.

* Assisted by contract between the U. S. Atomic Energy Commission and the Ohio State University Research Foundation.
† Now at the Department of Physics, Ohio University, Athens, Ohio.
[1] T. S. Smith and J. G. Daunt, Phys. Rev. **88**, 1172 (1952).
[2] J. G. Daunt and C. V. Heer, Phys. Rev. **76**, 715 (1949).
[3] Estermann, Friedberg, and Goldman, Phys. Rev. **87**, 582 (1952).
[4] Daunt, Horseman, and Mendelssohn, Phil. Mag. **27**, 754 (1939).

Air Mass between an Observer and Outer Space

E. C. PRESSLY
Naval Research Laboratory, Washington, D. C.
(Received December 11, 1952)

THE mass of air encountered in traveling rectilinearly from outside the atmosphere to certain stations within the atmosphere is of interest in a number of fields of experimentation, for example, cosmic rays and the scattering of light. In recent years rocket flights have provided atmospheric densities to great altitudes, which can now be used to calculate values for the air mass. Tables are given which show the effect of zenith angle and height of station above the surface of the earth on the total mass traversed. The calculations are based on density data obtained from rocket experiments by Havens.[1,2] These data are for conditions over White Sands, New Mexico. A single rocket flight at the equator showed little variation. However, it is known that a difference does exist between the latitudes of Massachusetts and New Mexico.[3] According to Whipple, meteor studies indicate a higher density over Massachusetts, the difference starting at 50–60 km and amounting to a factor of about 2 between 75 and

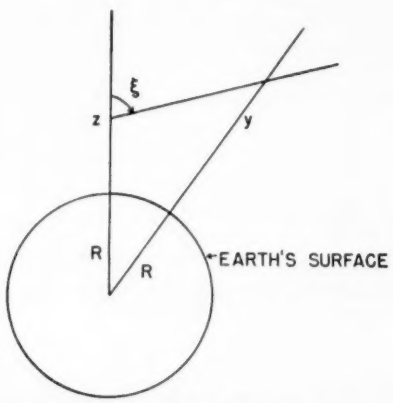

FIG. 1. Coordinates used in the calculation.

TABLE I. Mass of air contained in a column of unit cross section from outside the earth's atmosphere to a specific station within the atmosphere z kilometers above the surface along a path of zenith angle ξ.

	$M(z, \xi)$ g/m²									
z km	$\xi=0°$	30°	60°	75°	80°	85°	87.5°	90°	Max ξ	$M(z, \xi_{max})$
0	1.07×10^{7}	1.24×10^{7}	2.13×10^{7}	4.07×10^{7}	5.95×10^{7}	1.09×10^{8}	1.78×10^{8}	3.74×10^{8}	90°	3.74×10^{8}
5	5.73×10^{6}	6.61×10^{6}	1.14×10^{7}	2.18×10^{7}	3.20×10^{7}	5.90×10^{7}	9.72×10^{7}	2.14×10^{8}	92°16.3′	6.45×10^{8}
10	2.81×10^{6}	3.24×10^{6}	5.58×10^{6}	1.07×10^{7}	1.57×10^{7}	2.90×10^{7}	4.82×10^{7}	1.10×10^{8}	93°12.5′	7.07×10^{8}
15	1.30×10^{6}	1.50×10^{6}	2.60×10^{6}	4.97×10^{6}	7.28×10^{6}	1.35×10^{7}	2.24×10^{7}	5.16×10^{7}	93°55′	7.32×10^{8}
20	5.93×10^{5}	6.84×10^{5}	1.18×10^{6}	2.26×10^{6}	3.31×10^{6}	6.11×10^{6}	1.01×10^{7}	2.33×10^{7}	94°32′	7.41×10^{8}
30	1.32×10^{5}	1.53×10^{5}	2.64×10^{5}	5.04×10^{5}	7.37×10^{5}	1.35×10^{6}	2.22×10^{6}	4.96×10^{6}	95°33′	7.47×10^{8}
40	3.54×10^{4}	4.09×10^{4}	7.06×10^{4}	1.35×10^{5}	1.97×10^{5}	3.59×10^{5}	5.82×10^{5}	1.24×10^{6}	96°24.5′	7.48×10^{8}
50	1.05×10^{4}	1.21×10^{4}	2.08×10^{4}	3.98×10^{4}	5.81×10^{4}	1.06×10^{5}	1.73×10^{5}	3.70×10^{5}	97°0.5′	7.48×10^{8}
60	3.00×10^{3}	3.46×10^{3}	5.99×10^{3}	1.14×10^{4}	1.67×10^{4}	3.07×10^{4}	5.02×10^{4}	1.09×10^{5}	97°50′	7.48×10^{8}
70	770	890	1.54×10^{3}	2.93×10^{3}	4.30×10^{3}	8.00×10^{3}	1.34×10^{4}	3.13×10^{4}	98°27.5′	7.48×10^{8}
80	141	163	282	538	789	1.47×10^{3}	2.49×10^{3}	5.97×10^{3}	99°2′	7.48×10^{8}
100	5.92	6.82	11.8	22.5	32.9	60.2	98.5	222	100°5′	7.48×10^{8}
120	0.539	0.622	1.08	2.03	2.94	5.25	8.25	16.4	101°2′	7.48×10^{8}
150	0.0493	0.0569	0.0907	0.184	0.264	0.455	0.680	1.21	102°19′	7.48×10^{8}

90 km. This factor would be reflected in the total air mass beginning gradually at stations somewhat below 50–60 km.

The mass $M(z, \xi)$ of a column of unit cross section of air in a given direction ξ degrees from the zenith above a station z kilometers above the surface of the earth is

$$M(z, \xi)=\int_{z}^{\infty}\rho(y)dy\Big/\left[1-\left(\frac{R+z}{R+y}\right)^{2}\sin^{2}\xi\right]^{\frac{1}{2}},$$

where $\rho(y)$ is the density at each altitude y along the given path as seen in Fig. 1. R, the radius of the earth was taken to be 6368 km. In this calculation the upper limit of integration was 220 km, the last altitude for which Havens quoted a density. For $\xi<75°$, relatively no error is involved in assuming a flat earth such that

$$M(z, \xi)=\sec\xi M(z, 0°).$$

At $\xi=85°$ this method gives about an 11 percent error. Table I gives mass in grams per meter squared for various stations above the earth for several zenith angles—including the value of ξ for which the path is tangent to the earth. In all the large angle cases, and especially for the maximum angle cases, the path traverses latitudes and longitudes quite far away from White Sands, where presumably different atmospheric conditions prevail. The effect on $M(z, \xi)$, however, should be within the accuracies quoted, these being based upon the accuracy claimed by Havens. Figure 2 shows, for a station at z kilometers altitude, the ratio of mass at various zenith angles to vertical mass.

Computation error up to 100 km is estimated to be not greater than 2 percent. In his density data, Havens claims an error of less than 5 percent up to 40 km and less than 10 percent up to 70 km.

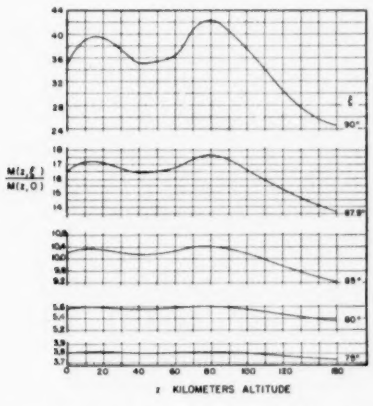

FIG. 2. Air mass ratio. ξ = zenith angle; z = altitude of observation point above the surface of the earth; $M(z, \xi)$ = mass of air in direction ξ between the observation point and outer space in a column of unit cross section; $M(z, 0)$ = mass of air vertically above observation point.

Values above 80 km are based on fewer measurements. A check was made using data on pressures, densities, and temperatures in the upper atmosphere by the Rocket Panel.[4] In general the air mass obtained from that atmosphere is slightly lower than that obtained here, but the difference is well within the limit of error stated above.

[1] Havens, Koll, and LaGow, J. Geophys. Research **57**, 59 (1952).
[2] R. J. Havens, and O. Berg, Trans. Am. Geophys. Union **316** (1952).
[3] Fred L. Whipple, Bull. Am. Meterol. Soc. **33**, 13 (1952).
[4] The Rocket Panel, Phys. Rev. **88**, 1027 (1952).

The Electric Scattering of Deuterons*

U. E. KRUSE, N. F. RAMSEY, AND B. J. MALENKA
Harvard University, Cambridge, Massachusetts
(Received December 12, 1952)

A LETTER on the above subject by French and Goldberger[1] which has recently appeared in the *Physical Review* was apparently written without the authors' knowledge of the existence of a letter on the same subject by one of us[2] a year earlier. As a result, there is one difference in the conclusions of the two articles which arises from the invalidity of one of their approximations in some cases. In particular, French and Goldberger conclude that there should be simple Rutherford scattering by $n=Ze^{2}/\hbar v\gg1$, whereas in Ramsey's[2] earlier paper a small departure is predicted.

This discrepancy arises from the approximations used by French and Goldberger being just such as to conceal the non-Rutherford scattering which arises from the distortion of the deuteron by the electric field, i.e., from the polarizability of the deuteron. Their conclusion about the Rutherford nature of the scattering for $n\gg1$ is based on an analysis of their Eq. (4) which is only an approximation to their earlier Eq. (3). The exact wave function of the deuteron in the process of the scattering is replaced by a wave function whose dependence on the deuteron's internal coordinates is just that of the ground state of the deuteron in the absence of any strong electric field. Then, because of the spherical symmetry of the latter state, it is argued that the average value of $[1/|\mathbf{R}-\frac{1}{2}\mathbf{s}|-1/R]=0$ except for $R\leqslant\frac{1}{2}s$ and that this high penetration of the deuteron is improbable for large n.

However, the use of the ground-state wave function for the deuteron is only approximately valid in the presence of the strong electric field of the scattering nucleus, and higher deuteron states must be included. The admixture of the higher states corresponds to a distortion or polarization of the deuteron by the electric field of the scattering nucleus. When these terms are included, the bracketed quantity above no longer equals zero when $R>\frac{1}{2}s$ and the disagreement with Ramsey's[2] conclusions disappears. That there should be considerable admixture of higher states is apparent from the fact that the electric field at the deuteron multiplied by the product of the deuterons charge and diameter is comparable to the binding energy of the deuteron.

Experiments with $n \gg 1$ have the advantage[2] that then the circumstances can sometimes be such that the Coulomb barrier prevents appreciable overlap of the nuclei and all departures from the Rutherford scattering law must be attributed to the distortion of the deuteron by the electric field in scattering. On the other hand, under the conditions of the French and Goldberger[1] theory, the calculated departure from Rutherford scattering due to the deuteron structure occurs along with a large and unknown departure due to nuclear forces; the separation of the two effects experimentally would be very difficult. The importance of direct nuclear interaction is apparent from the fact that in their example of 14-Mev deuterons on aluminum the classical distance of closest approach of these nuclei considered as point charges is 1.34×10^{-13} cm which is much less than the radius of either the deuterium or the aluminum nucleus, so that large effects from nuclear forces should occur.

We have calculated the polarizability of the deuteron quantum mechanically, and we have interpreted the polarizability scattering by a classical approximation. The validity of the calculations are limited by the assumptions that the Coulomb field is adiabatically applied and that $n \gg 1$. In so far as these assumptions hold for the scattering of 8-Mev deuterons on bismuth, we find approximately a 3 percent departure from Rutherford scattering in the backward direction.

* This work was partially supported by the joint program of the U. S. Office of Naval Research and the U. S. Atomic Energy Commission.
[1] J. B. French and M. L. Goldberger, Phys. Rev. **87**, 899 (1952).
[2] N. F. Ramsey, Phys. Rev. **83**, 659 (1951).

Search for "*T*-Tracks" in Photographic Plates

PAUL H. BARRETT, G. COCCONI, AND Y. EISENBERG*
Cornell University, Ithaca, New York
(Received December 5, 1952)

BLAU and Salant[1] have reported evidence for a type of event observed in photographic plates, which they called a *T*-track and tentatively interpreted as the break-up of a heavy particle at, or near, the end of its range into two fast, singly charged particles. Their evidence is based on the fact that *T*-tracks appeared to be more frequent than could be explained by the chance passing of a light track by the end of a black track.

In the last month we have scanned 112 cm² of 400 μ G-5 emulsion that was exposed vertically for about 10 hours at 90 000 ft and geomagnetic latitude of 41°N.

To find *T*-tracks, all stars with three or more prongs and with at least one prong longer than 100 μ were analyzed, and all the prongs ending in the emulsion were examined for minimum ionizing tracks passing at distances up to 5 μ. The minimum ionizing tracks were required not to scatter appreciably within 500 μ; this condition eliminates electrons of energy smaller than about 20 Mev.

A total number of 2191 stars were found, with 4246 prongs ending in the emulsion; of these, 335 had minimum ionizing tracks within 5 μ, subdivided as shown in Table I.

To determine the expected number of chance coincidences between the endings of the heavy tracks and tracks of minimum ionization, we have measured the number of minimum ionizing tracks crossing unit surfaces of developed emulsion, N_v in the vertical planes and N_h in the horizontal planes containing the shrunken coordinate.

It was found that $N_h \simeq N_v = 1.0\times10^{-3}\mu^{-2}$, which indicates an isotropic distribution of the minimum ionizing tracks. It follows that the expected number of chance *T*-tracks within a distance r is

$$n_{ch} = 2\pi\times0.86\times N_h\times r^2\times\text{No. of track endings observed.}$$

The factor 0.86 arises from taking into account that the emulsion has shrunk, after development, by a factor of about 2.5, so the sphere of developed emulsion was originally a prolate ellipsoid.

The estimated backgrounds are given in the lowest row of Table I. It seems that the observed number of *T*-tracks within 1 μ is well accounted for by chance coincidences.

TABLE I. Observed and expected track distributions.

Distances within which the minimum ionizing particles were found, in μ	0–1	1–2	2–3	3–4	4–5
No. of observed cases	19	47	86	87	96
Expected chance coincidences	22	66	110	156	198

The fact that the number of expected chance coincidences is higher than the observed coincidences at the larger distances is thought to be the result of a decrease in the efficiency of the scanner when looking at regions not very close to the end of the heavy track.

We did not try to subdivide further the 19 cases classified within 1 μ, as we felt very uncertain in determining the distances when they were smaller than this limit. One reason for this is that many of the minimum ionizing tracks are steep, and the distance from the end of the heavy track can be estimated by utilizing only a few of their grains. These are not enough to determine the trajectory of the fast particle within much less than 1 μ, as the grains may be displaced from the true trajectory by distances of the order of the dimension of a grain, i.e., by several tenths of a micron. Another reason is that it is often difficult to tell whether a grain is the last grain of the heavy track or a grain belonging to the light track. Finally, depths of field much less than the wavelength of the light (0.5 μ) cannot be realized, and this puts a limit on the precision of the depth measurements.

If we try to select among the 19 close cases the one which appear as "perfect *T*-tracks," three give unmeasurable distances. The value of r which corresponds to three chance coincidences is 0.37 μ, in reasonable agreement with the resolving power of the microscope.

We are thus led to the conclusion that, in order to explain the occurrence of the *T*-tracks observed in our plates, it is not necessary to postulate the existence of any special particle.[2]

We wish to thank the Aero-Medical Field Laboratory, Holloman Air Force Base, New Mexico, for conducting the balloon flight and J. de Vesty, C. Lipetz, S. Perry, and C. Sienko for helping us scan the plates.

* H.T.I. Fellow.
[1] M. Blau and E. O. Salant, Phys. Rev. **88**, 945 (1952); we are grateful to Dr. Blau and Dr. Salant for communicating to us their results before publication.
[2] In a private communication, Dr. Salant has stated to us that the number of *T*-tracks they observe within 1 μ is four times the calculated random background. Since in our plates the background of light particles is larger by about a factor four than that quoted by Blau and Salant, the detection of *T*-particles would be more difficult in our case.

The Lattice Expansion of Quartz Due to Fast Neutron Bombardment

M. WITTELS
Oak Ridge National Laboratory, Oak Ridge, Tennessee
(Received December 17, 1952)

THE progressive anisotropic expansion of α-quartz irradiated with increasing dosages of fast neutron flux has been observed and measured by x-ray and density methods of analysis. Bombardment produced by a neutron source that gave a total integrated neutron flux of 6.6×10^{19} *nvt* resulted in a density change of $(\Delta\rho/\rho)\times100 = 3.5\pm0.1$ as measured by the hydrostatic weighing method. The density change measured by the x-ray method gave $(\Delta\rho/\rho)\times100 = 4.8\pm1.5$. The crystal temperature was approximately 100°C during irradiation.

X-ray diffraction data taken from Debye-Scherrer, Laue, and precession photographs show that the expanded lattice belongs to the trigonal system. In addition, it appears likely that this lattice has the same space group, D_3^4 or D_3^6, as the nonirradiated crystal. The expanded lattice constants are $a_0 = 5.01\pm0.01$A and $c_0 = 5.41\pm0.02$A, as compared with the nonirradiated quartz $a_0 = 4.903$A and $c_0 = 5.393$A.

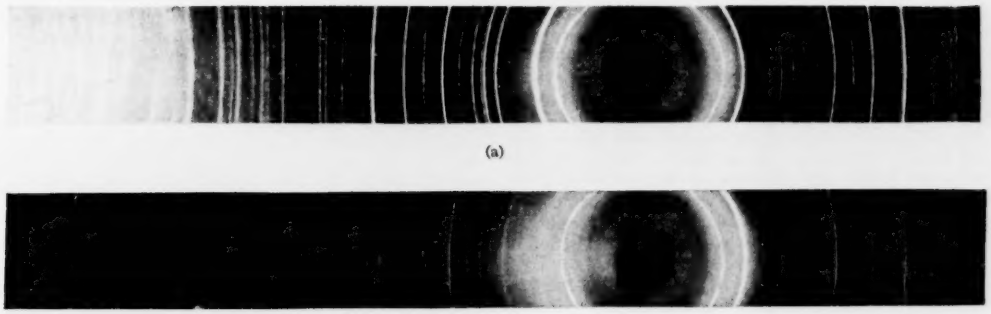

(a)

(b)

FIG. 1. Debye-Scherrer diffraction patterns of α-quartz (a) before irradiation; (b) after irradiation.

The strain imposed on the lattice by this expansion is evidenced in the back-reflection region of the Debye-Scherrer diffraction pattern (Fig. 1b). All reflections at $2\theta > 90°$ have been "smeared out" so that they are indistinguishable above background level. The inaccuracies in determining precise lattice constants and x-ray densities are due to the absence of these reflections at large Bragg angles.

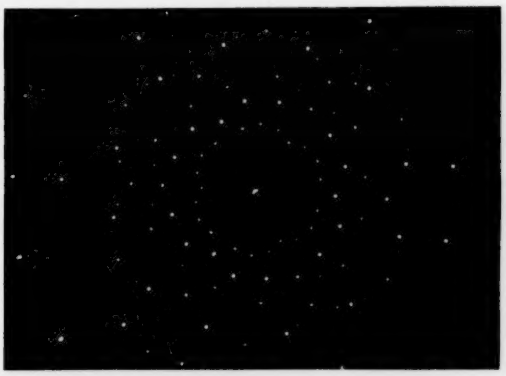

(a)

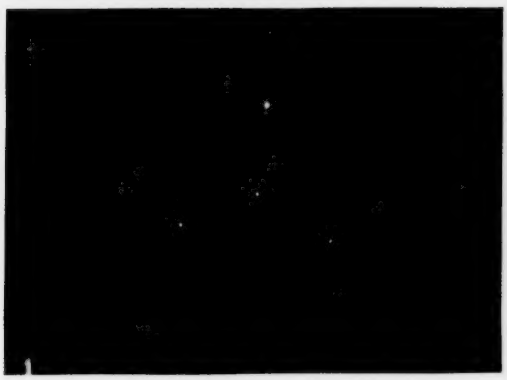

(b)

FIG. 2. Laue transmission photographs of α-quartz parallel to Z (a) before irradiation; (b) after irradiation.

The pseudo-hexagonal symmetry inherent in the Laue pattern of Z-cut quartz (Fig. 2a) is barely visible in the same pattern (Fig. 2b) of the irradiated crystal which shows its true trigonal symmetry. In addition, the apparent absence of many reflections in this latter pattern also indicates strain in the expanded lattice.

The thermal stability of this expanded lattice is of considerable magnitude. Annealing at 485°C for two hours produced no detectable relief from lattice strain, and no lattice contraction. Four hours of annealing at 650°C produced no lattice contraction, but the (33.1) and (23.4) reflections reappeared as broad, very weak peaks in the back-reflection diffraction pattern. The interest here lies in the fact that this annealing temperature is 77°C higher than the normal inversion temperature of $\alpha \rightarrow \beta$ quartz. Heating at 900°C for twelve hours relieved the lattice strain completely and contracted the lattice to normal parameters.

A model of the packing of atoms in α-quartz indicates that the largest interstitial spaces in the lattice form long irregular channels parallel to the principal axis. It seems likely that these sites are the most probable positions in which the dislocated atoms could be trapped. On the basis of this premise, the anisotropic expansion in the a direction is explained.

The writer is indebted to F. A. Sherrill, B. S. Borie, Jr., and G. E. Klein for valuable assistance during the course of the investigation.

The Thermal Neutron Absorption Cross Section of Scandium

E. E. LOCKETT
Atomic Energy Research Establishment, Harwell, Berkshire, England
AND
E. BOWELL
Chemical Inspectorate, Chatham, England
(Received December 8, 1952)

WE have made a measurement of the thermal neutron absorption cross section of scandium in an attempt to resolve the inconsistencies in the published literature on the cross section of this element.

The thermal neutron cross section is quoted by Pomerance[1] as 11.8 barns, and the pile neutron cross section by Harris *et al.*[2] as 31.8 barns. Sc^{45} is 100 percent abundant in natural scandium, and neutron capture in it leads to 85-day Sc^{46}, partly directly, and partly via a 20-second isomer of Sc^{46}.[3] The pile activation cross section for the production of 85-day Sc^{46} is, therefore, also the pile absorption cross section of scandium. Seren, Friedlander, and Turkel[4] have measured this activation cross section as 22 barns (±20 percent).

We have made a rough measurement of the cadmium ratio for scandium in the G.L.E.E.P., which shows it to be approximately a $1/v$ absorber. This is confirmed by Harris *et al.*[5] For a $1/v$ absorber the pile neutron cross section is the same as the thermal neutron cross section. We would, therefore, expect the three values quoted above to be in agreement.

In view of the violent disagreement between these values a new measurement was undertaken. The scandium used was in the form of "spec-pure" Sc_2O_3. The measurement was made using the G.L.E.E.P. oscillator by the method described by Colmer and Littler,[6] and the value obtained for the pile cross section was 23.2 barns (±4 percent), assuming the absorption cross section of boron at 2200 m/sec to be 710 barns (±2 percent).

The sample was then analyzed by the Chemical Inspectorate, Chatham, for forty elements, including the rare earths. It was found that the contribution to the cross section from impurities was less than 2.4 barns. Allowing for this, our value for the pile neutron absorption cross section, and also the cross section at 2200 m/sec, becomes $23\binom{+1}{-3}$ barns.

As a result of this measurement we communicated with Pomerance, and have heard from him that he has remeasured his sample and now obtains a value of 23 barns.[7] Since Harris *et al.* state that their scandium was impure, their measurement can presumably be discounted, and the values obtained by the other experimenters are now in agreement with our value of 23 barns.

[1] H. Pomerance, Phys. Rev. **83**, 641 (1951).
[2] Harris, Muehlhause, Rasmussen, Schroeder, and Thomas, Phys. Rev. **80**, 342 (1950).
[3] M. Goldhaber and C. O. Muehlhause, Phys. Rev. **74**, 1877 (1948).
[4] Seren, Friedlander, and Turkel, Phys. Rev. **72**, 888 (1947).
[5] Harris, Muehlhause, and Thomas, Phys. Rev. **79**, 11 (1950).
[6] F. C. W. Colmer and D. J. Littler, Proc. Phys. Soc. (London) **A63**, 1175 (1950).
[7] Private communication from H. Pomerance to D. J. Littler, October 3, 1952.

Intensities of Nuclear Magnetic Resonances in Cubic Crystals

G. D. Watkins* and R. V. Pound
Harvard University, Cambridge, Massachusetts
(Received December 11, 1952)

A RECENT communication[1] reports puzzling results from attempts to determine the spin of Si^{29} by comparing the intensity of its magnetic resonance absorption with that of I^{127}, of spin 5/2, in cubic crystalline KI. Some observations made a year ago on the shapes and intensities of the nuclear magnetic resonance lines of Br^{79}, Br^{81}, and I^{127} in crystalline KBr and KI are briefly reported here because they seem particularly relevant to the interpretation of the above results. The intensities were determined relatively and absolutely by use of the calibrating circuit briefly described previously.[2]

In well-annealed single crystals of optical quality, narrow, symmetrical lines were observed. However, it was discovered that the integrated observable intensities were considerably smaller than would be expected for their respective spins. The observed intensities of Br^{79} and Br^{81}, both of spin 3/2, were each only 0.4, and that of I^{127}, of spin 5/2, only 0.3 as large as expected. In powdered samples, or in single crystals which had been subjected to linear compression resulting in plastic flow and "work-hardening," the lines were found to be broader and unsymmetrical, with a stronger tail on the low frequency side. In these highly strained samples, the observed intensities of the resonances of bromine were still 0.4 of the full values and that of I^{127} had decreased to about 9/35.

These effects have been interpreted as arising from the interaction of the quadrupole moments of the nuclei with electric field gradients of random position and orientation produced by internal strains in the crystals. A quadrupole interaction introduced as a first-order perturbation causes the normal magnetic resonance line to split into $2I$ lines equally spaced by an amount determined by the magnitude and orientation of the field gradient relative to the direction of the magnetic field.[3] For odd half-integral spin, the central line occurs at the unperturbed magnetic absorption frequency. Field gradients having a range of intensities and random orientations would smear the satellite lines over a wide frequency range, leaving only the central line as observable. The fractional intensity associated with the central line is just 4/10 for $I=3/2$, and 9/35 for $I=5/2$. This suggests that only the central lines were observed in the single crystal of KBr. In the single crystal of KI, we were evidently observing, as well as the central line, a small residual contribution from the satellites. A broadening of the central line, with an asymmetry in the same direction as that observed in the highly strained samples, can be explained by carrying the perturbation to second order as required for larger gradients.

An attempt has been made to estimate the magnitude of the internal strains associated with lattice imperfections of the dislocation type. The changes in line shape found to accompany plastic flow seem consistent with the increase in concentration of dislocations required to account for the flow. However, if a concentration of 10^8–10^{10} cm^{-2} is assumed for the well-annealed crystal, using reasonable values for the nuclear quadrupole moments,[4] one finds that the field gradients at the nuclei must be a factor $\beta\sim 2$–20 times greater than would be produced by just the charged alkali neighbors displaced under strain. Another estimate of about 10 for this factor β was made from observations of a small reversible effect of linear compression upon the line shape of Br^{79} in a highly work-hardened crystal of KBr. Both of these observations indicate that the symmetry of the electronic wave function of the halogen ion itself is a larger contributant to the field gradient than is the direct effect of the displacement of the neighboring ions from cubic lattice sites. The details of this calculation as well as the experimental results quoted in this letter will be published later.

If this interpretation is correct, it is evident that a nucleus with a moderate quadrupole moment can serve as a very sensitive monitor of internal strains in crystals. The resonances observed here are poor for this because they are really too sensitive, the first-order smearing being almost completely effective even in the most perfect crystals. A nucleus with a smaller quadrupole moment (or smaller β) would be better. Detailed analysis of its line shape could give information about both the magnitude and distribution of internal strains in even the most "perfect" available single crystals. Intensity observations on Li^7 in LiF revealed no effects of this sort.

* Now at the Research Laboratory, General Electric Company, Schenectady, New York.
[1] R. H. Sands and G. E. Pake, Bull. Am. Phys. Soc. **27**, No. 5, 11 (1952).
[2] G. D. Watkins and R. V. Pound, Phys. Rev. **82**, 343 (1951).
[3] R. V. Pound, Phys. Rev. **79**, 685 (1950).
[4] I. E. Mack, Revs. Modern Phys. **22**, 64 (1950).

The Cross Section for $Ta^{181}(\gamma, 2n)Ta^{179}$ at 17.6 Mev

J. H. Carver, R. D. Edge, and D. H. Wilkinson
Cavendish Laboratory, Cambridge, England
(Received December 11, 1952)

THE variation with energy of the total nuclear absorption cross section of complex nuclei for gamma-rays has not yet been determined. The well-known "resonances" of the (γ, n) cross section alone may or may not persist when competing reactions are taken into account; if they persist, then it may be that some specific nuclear model[1] is needed or that some specific aspect of nuclear forces is involved. It is also important to determine whether there exists the considerable cross section for higher order processes needed[2] in the interpretation of the total neutron yield through the dipole sum rule.[3]

We have measured the ratio of the $(\gamma, 2n)$ cross section for Ta^{181} at 17.6 Mev to the (γ, n) cross section at 14.6 Mev and found 0.29 ± 0.11; the details of the method will be published elsewhere. We have used the *form* of the (γ, n) cross section as measured by Haslam, Smith, and Taylor.[4] If we make the assumption that the *form* of the $(\gamma, 2n)$ cross section above 18 Mev is the same as that of the (γ, n) process,[5] while that at lower energies is derivable from the total cross section and the statistical theory[6] of the (γ, n) *versus* $(\gamma, 2n)$ competition, we may from our measurement at one energy construct the $(\gamma, 2n)$ cross section and hence the total nuclear absorption cross section.[7] This is shown in Fig. 1. It is seen that there is a considerable $(\gamma, 2n)$ cross section above the threshold[2] (14.0 Mev) but that the total cross section retains a sufficiently sharp peak to warrant further consideration of specific theories such as that of Goldhaber and Teller.[1] The importance of the $(\gamma, 2n)$ process may be somewhat less than estimated indirectly by Eyges,[8] who suggests 0.41 for our measured ratio.

Since we completed our measurements, Halpern, Nathans, and Mann[9] have published a total neutron excitation function for tantalum. In Fig. 2 we compare their measured points with the neutron yield curve expected from the cross sections of Fig. 1.

Halpern, Nathans, and Mann have seen in their results evidence for a second maximum in the total cross section at about 20.5 Mev due to $(\gamma, 2n)$. If this second maximum indeed exists, it appears probable that two separate mechanisms are at work to produce the two maxima. We may seek to identify the second maximum with resonance dipole absorption in the alpha-particle or with the lowest quadrupole mode in the extension of the Goldhaber-Teller theory by Danos and Steinwedel[10] and Danos,[11] but in the latter case the experimental resonance energy spacing of 6.5 Mev is rather less than the theoretical 8.5 Mev, and the experimental cross section appears too large by a factor of order two. It is also difficult to understand why the $(\gamma, 2n)$ cross section should not rise from its threshold much more rapidly than suggested by Halpern, Nathans, and Mann whether or not there exists a second maximum. It seems, therefore, in view of the fair agreement between our own suggestions and the neutron yield results, that this second maximum must be treated with some reserve; its definite establishment would be of the greatest importance for the theory of these processes.

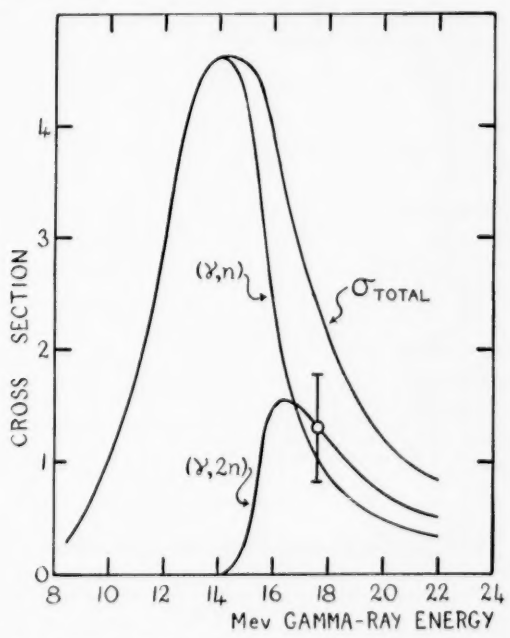

FIG. 1. $Ta^{181}(\gamma, n)Ta^{180}$ cross section (in arbitrary units) as a function of gamma-ray energy (measured by Haslam, Smith, and Taylor) with the present measurement of the $(\gamma, 2n)$ cross section at 17.6 Mev, the full $(\gamma, 2n)$ cross section constructed with its aid and the resultant total absorption cross section.

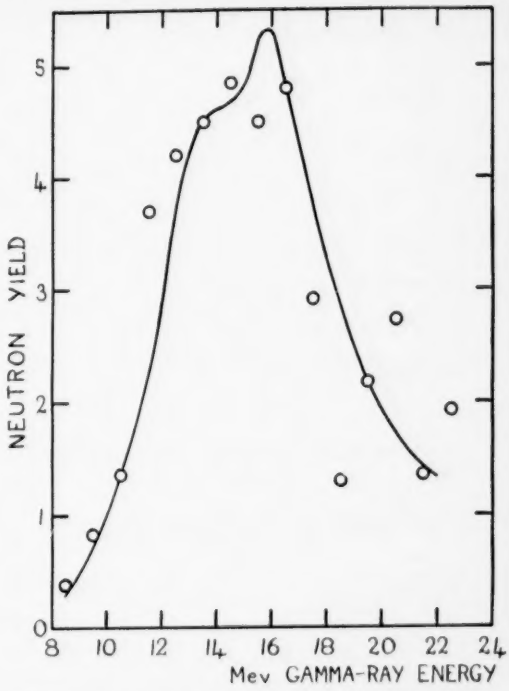

FIG. 2. Total neutron yield (in arbitrary units) as measured by Halpern, Nathans, and Mann (circles) compared with the yield expected from the cross sections of Fig. 1 (full line).

[1] M. Goldhaber and E. Teller, Phys. Rev. **74**, 1046 (1948); H. Steinwedel and J. H. D. Jensen, Z. Naturforsch. **5a**, 413 (1950).
[2] J. S. Levinger and H. A. Bethe, Phys. Rev. **85**, 577 (1952).
[3] J. S. Levinger and H. A. Bethe, Phys. Rev. **78**, 115 (1950).
[4] Haslam, Smith, and Taylor, Phys. Rev. **84**, 840 (1951).
[5] Above 18 Mev the (γ, n) cross section must be due almost wholly to direct interaction [E. D. Courant, Phys. Rev. **82**, 703 (1951)] since the neutron multiplicity for compound nucleus formation is almost two; it is reasonable that the probability of exciting a compound nucleus following an initial direct interaction should remain almost constant within the restricted range of interest here, so the $(\gamma, 2n)$ cross section should at any rate not fall less rapidly than the (γ, n).
[6] J. M. Blatt and V. F. Weisskopf, *Theoretical Nuclear Physics* (J. Wiley and Son, Inc., New York, 1952), pp. 365 ff.
[7] Charged particle emission may be neglected, the threshold for $(\gamma, 3n)$ is 22.2 Mev (see reference 2), and the contribution from (γ, γ) and (γ, γ') is small [M. B. Stearns, Phys. Rev. **87**, 706 (1952)].
[8] L. Eyges, Phys. Rev. **86**, 325 (1952).
[9] Halpern, Nathans, and Mann, Phys. Rev. **88**, 679 (1952).
[10] M. Danos and H. Steinwedel, Z. Naturforsch. **6a**, 217 (1951).
[11] M. Danos, Ann. Physik **10**, 265 (1952).

A Theory of the Paramagnetism of Uranyl-Like Ions*

R. J. ELLIOTT
Department of Physics, University of California, Berkeley, California
(Received December 15, 1952)

A CONSIDERABLE amount of data concerning the paramagnetic properties of the transuranic ions has recently been accumulated[1,2] in an attempt to ascertain the electronic configurations of these ions. However, a detailed theoretical discussion of any particular salt has not yet been given, and in some cases it is still in doubt whether the paramagnetism is due to $5f$

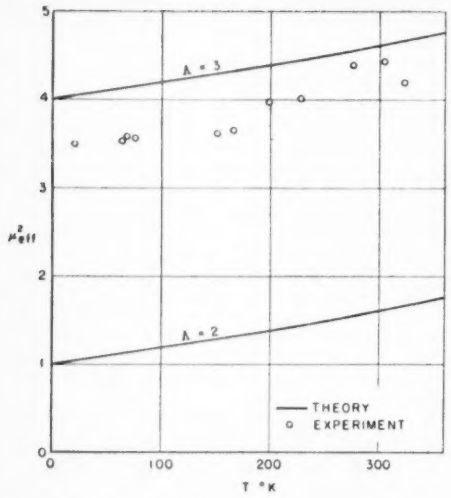

FIG. 1. The observed effective magnetic moment of sodium neptunyl acetate compared with theory.

or $6d$ electrons. It has proved possible to give a more thorough analysis of the paramagnetic susceptibility observed from the neptunyl[3] $(NpO_2)^{++}$ and plutonyl[4] $(PuO_2)^{++}$ ions in compounds isomorphous with sodium uranyl acetate $-Na(UO_2)(C_2H_3O_2)_3$, and to show that it is compatible with f electrons.

The crystal structure of these compounds is known,[5] and it is found that the transuranic ion lies between two oxygen atoms so that a linear molecule is formed. Since $(UO_2)^{++}$ is diamagnetic, all its electrons are presumably in closed shells, and one expects the paramagnetism of $(NpO_2)^{++}$ and $(PuO_2)^{++}$ to be due to one and two electrons, respectively, outside these shells. The neptunyl case should therefore be relatively simple. Neglecting the interaction between these ions and their surroundings in the crystal, as a first approximation, we are concerned with a set of linear molecules. The component of orbital angular momentum of the electron along the axis of the molecule will then be a constant, having the value $|\Lambda|=0, 1, 2, 3$, etc. Spin-orbit interaction $\zeta\mathbf{l}\cdot\mathbf{s}$ in the case of a single electron will cause the two states in which the orbital and spin momenta are aligned antiparallel to have an energy lower by $\Lambda\zeta$ than those states where they have parallel alignment. It can be shown by an argument similar to that used by Van Vleck[6] for the linear molecule NO that the effective magnetic moment μ_{eff} of a powdered crystal containing these ions should be given in units of Bohr magnetons β, by a formula

$$\mu_{eff}^2=\frac{3k\chi T}{N\beta^2}=\left[(\Lambda-1)^2+(\Lambda+1)^2e^{-\Lambda\zeta/kT}+4(1-e^{-\Lambda\zeta/kT})\frac{kT}{\Lambda\zeta}\right]\Big/(1+e^{-\Lambda\zeta/kT}),$$

where χ is the powder susceptibility, T the absolute temperature, N the number of molecules (the NO susceptibility is given by $\Lambda=1$). The theoretical dependence of μ_{eff}^2 on temperature is given in Fig. 1 for $\Lambda=2$ and 3 together with Hutchison's[3] measurements on $Na(NpO_2)(C_2H_3O_2)_3$. The slope of the curve is determined by ζ which is expected to be large in these heavy ions. The experimental points are in reasonable agreement with $\Lambda=3$, if ζ is chosen to be about 500 cm^{-1} as in the figure. This paramagnetism must therefore arise from an f electron with $l=3$.

$(PuO_2)^{++}$ will have two electrons of a similar kind, and if the electrostatic interaction between them is small, the lowest state will be $^3\Sigma$ with no orbital angular momentum and a total spin of one. This is in very good agreement with the experimental susceptibility[4] which gives $\mu_{eff}=2.82$ over the temperature range 0–300°K while the theoretical value is $2\sqrt{2}=2.83$.

Another way of formulating the problem, which is simpler to extend, is to assume that the extra electrons are f electrons on the heavy atoms and to consider the oxygens as causing a very strong electric field with axial symmetry. The electrostatic interaction between electrons, the spin-orbit coupling, and the interaction with the rest of the crystal which sets up a crystalline electric field of trigonal symmetry about the axis will add smaller terms to the Hamiltonian of the ion, which are considered by perturbation theory. To first order, the results are identical with the above. To higher orders it can be shown that in neptunyl the μ_{eff} at $T=0$ would be altered by a small amount, while the temperature dependence would remain approximately the same. By an adjustment of the magnitudes of the various terms in the Hamiltonian it is possible to obtain much better agreement with experiment than is shown in Fig. 1.

Such calculations will not have much significance until more detailed information, such as might be obtained from paramagnetic resonance, is available. To first order, the above theory gives the spectroscopic splitting factors of the lowest doublet level in neptunyl as $g_{\parallel}=4$, and $g_{\perp}=0$ (parallel and perpendicular to the axis of the molecule). No resonance would then be observable because of the zero g. Higher order effects will make $g_{\perp}$ nonzero but small; and this means that the resonance will have a very small transition probability when it appears in low fields, and a normal value only in very high fields, and may not therefore be easily observable. The plutonyl ion has a spin triplet for its lowest state, and its resonance spectrum should be similar in many ways to that of divalent nickel ions.[7] Higher order effects in the spin-orbit coupling will resolve the degeneracy of the triplet into a singlet $S_z=0$, and a doublet $S_z=\pm1$; and resonance is to be expected if this splitting is small (not greater than a few cm^{-1}). Preliminary measurements by Professor Kip (unpublished) have shown that a spectrum does exist, and more work is in progress.

It is interesting to note that although this interpretation is in favor of f electrons in these ions, the interaction between them and their surroundings is very strong and gives rise to spin-only paramagnetism in the plutonyl ions. It is possible that spin-only paramagnetism in other salts in this group might arise from f electrons interacting strongly with their surroundings rather than from d electrons as Dawson suggests.[3] This model would have a further test in measurements on the ions $(AmO_2)^{++}$ and $(AmO_2)^{+}$. If the first approximation as used above is valid here and the interaction between the electrons is still not too large, the former should have a result similar to $(NpO_2)^{++}$, except that the spin-orbit coupling constant ζ will effectively have the opposite sign and μ_{eff} will be 4 at low temperatures, while the latter should have a very small temperature-independent paramagnetism.

The author is indebted to Dr. G. Seaborg and Dr. B. Cunningham for instructive discussion.

* This work was supported in part by the U. S. Office of Naval Research.
[1] G. Seaborg, Nucleonics **5**, No. 5, 16 (1949).
[2] J. K. Dawson, Nucleonics **10**, No. 9, 39 (1952).
[3] C. A. Hutchison, Jr., U. S. Office of Naval Research Technical Report (1951), unpublished.
[4] J. K. Dawson, Atomic Energy Research Establishment Report C/R-876 (1952), unpublished.
[5] J. Fankuchen, Z. Krist. **91**, 473 (1935).
[6] J. H. Van Vleck, *The Theory of Electron and Magnetic Susceptibilities* (Oxford University Press, London, 1932).
[7] J. H. E. Griffiths and J. Owen, Proc. Roy. Soc. (London) **A213**, 459 (1952).

Influence of Electric Fields on Luminescence

FRANK MATOSSI AND SOL NUDELMAN
United States Naval Ordnance Laboratory, White Oak, Maryland
(Received November 24, 1952)

DESTRIAU[1] has reported on an extinguishing effect of an electric field on phosphors that are continuously excited by x-rays. Using a similar procedure, but with improved technique, we have obtained more detailed information about the light out-

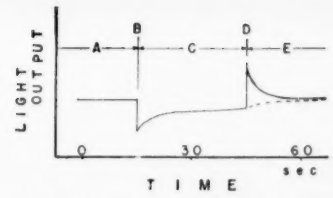

FIG. 1. Light output of ZnS:Cu phosphor *versus* time, schematic. *B*—field on; *D*—field off. Solid curve—10 000 cps; dashed curve—60 cps.

put from a near ultraviolet excited ZnS:Cu phosphor. This report gives the qualitative features of some of our observations.

A film of the powdered phosphor was obtained by immersing the phosphor in a parlodium-amylacetate solution and then pouring the mixture on a conducting glass plate. The phosphor film thickness was about 0.2 mm. After the film had dried, the outer uneven edges were cut away. An electrode of copper or some other metal was evaporated on the exposed surface of the phosphor film. We used potential differences from 0 to 400 volts with frequencies ranging from 0 to 10 000 cps. The output of a near ultraviolet source of constant energy excited the phosphor continuously. A photomultiplier responded to the light output from the phosphor with a filter arrangement designed to eliminate any ultraviolet which might be reflected by the phosphor-glass surface. The output from the photomultiplier was fed to an amplifier and then to the vertical plates of a cathode-ray oscilloscope.

If a potential difference of 400 volts and a frequency of 10 000 cps is applied across the phosphor film, a trace of the signal on the oscilloscope is obtained which is illustrated in Fig. 1. Regions *A* and *E* represent the light output before the field has been applied and after the field has been removed, respectively. *B* designates the time when the field is applied; *D* the time at which it is removed. *C* is the region during which the field is applied. The trace given in Fig. 1 is similar to those reported by Destriau with the exception of the momentary illumination at point *D*. The magnitude of this sudden light excess is a function of the field strength and of the frequency. At low frequencies, of the order of 60 cps and with the same high field strength, the momentary illumination at *D* disappears and the trace assumes the shape of the dashed curve. In Destriau's papers, however, this shape of the curve is reported for a fast decaying phosphor only; on the other hand, his slow decaying phosphors do show momentary illumination for 50 cps, the only frequency for which Destriau gives results.

Our preliminary investigation reveals that for decreasing field strength the magnitude of the overshoot at *D* decreases almost linearly. The rise at *D* is remarkedly steeper than the fall at *B*, with the decay beyond *D* being apparently of the power law type. The rise in region *C* is more complex. The extinguishing effect at *B* increases with frequency and field strength.

Application of a dc field yields only a momentary illumination of very short duration (about 10^{-4} sec), with another momentary illumination of reduced amplitude being obtained when the dc field is removed.

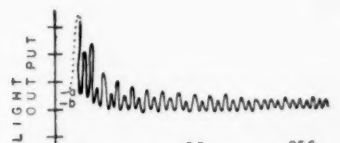

FIG. 2. "Blow-up" of region *B* of Fig. 1. *a* = light output before the field is applied; *b* = lowest average light output with field on; dotted curve = conjectured rise of output.

Point *B* is of further interest. If a fast sweep rate on the oscilloscope was used, we obtained a signal trace for *B* like that reproduced in Fig. 2 for a 60-cps field. Here we see another momentary illumination preceding the extinguishing effect. The light output fluctuates with twice the frequency of the electric field. These ripples alternate in intensity, probably because of the influence of the polarity of the electrodes. The general character of the trace was the same for all frequencies, but the amplitude of the ripples decreased with increasing frequency. The momentary illumination occurred always within 3–5 periods of the ac field.

Work is now in progress to obtain more quantitative information concerning the dependence of the effects on frequency, field strength, wave shape of the applied field, and on the nature of the phosphor. The time variation of light output in the regions *B*, *C*, and *E* will be investigated for possible correlations with the natural growth and decay processes of the phosphor.

[1] G. Destriau, Phil. Mag. **38**, 880 (1947); G. Destriau and J. Mattler, J. phys. et radium **9**, 258 (1948).

Anisotropic Susceptibility of Polycrystalline Graphite*

W. P. EATHERLY AND J. D. MCCLELLAND
Atomic Energy Research Department, North American Aviation, Inc., Downey, California
(Received November 24, 1952)

ALTHOUGH the spur invariance of the susceptibility tensor has been frequently used in the study of single crystals, it is apparently not generally realized that a similar property holds for anisotropic polycrystalline materials of arbitrary preferred orientation. That polycrystals possess this property is almost self-evident from the single crystal invariance, but the experimental conditions under which the elements of the spur may be determined for a polycrystal can be seen most easily by analysis.

The proof is quite simple: Let k_{ij} be the susceptibility tensor of a single crystal referred to its principal axes, and hence it is diagonal. A crystallite with orientation θ, ϕ, ψ will possess the susceptibility tensor $k_{ij}' = R_{im}^{-1} k_{mn} R_{nj}$, where $R(\theta, \phi, \psi)$ is the three-dimensional rotational operator. Let $w(\theta, \phi, \psi)$ be the normalized density function of crystallites with given orientation in the range $d\tau$. The potential energy is then

$$U = \tfrac{1}{2} \int_V \int_\tau H_i k_{ij}' H_j w d\tau dV,$$

where the integrations are over the space of θ, ϕ, ψ and over the volume V of the sample. The force exerted by the sample in the direction x_l is

$$F_l = -\frac{\partial U}{\partial x_l} = -\int_V \int_\tau H_i k_{ij}' \frac{\partial H_j}{\partial x_l} w d\tau dV,$$

since k_{ij}' is symmetric. If grad$|H|^2$ is sensibly constant over the volume V, and H also unidirectional over the volume, then we may without loss of generality take H to be in the direction x_1 and obtain

$$F_l = -\int_V H_1 \frac{\partial H_1}{\partial x_l} \int_\tau k_{11}' w d\tau dV.$$

Since this depends only on k_{11}', it serves to determine one element of the spur. If we make three determinations of F_l in three independent orthogonal directions by rotating the sample in the field, then their sum is

$$\sum_{m=1}^{3} (F_l)_m = -\int_V H \frac{\partial H}{\partial x_l} \text{ Spur } k' w d\tau dV = H(\partial H/\partial x_l)_{k_0} V \text{ Spur } k.$$

Defining the apparent susceptibility k_m as $(F_l)_m/(VH\partial H/\partial x_l)$, we obtain $\Sigma k_m = \text{Spur } k$, providing the sample is perfectly compact. This last restriction may be removed by using the specific susceptibility χ, for which

$$\Sigma \chi_m = \text{Spur } \chi.$$

The left side refers to the three orthogonal susceptibilities of the solid polycrystalline sample, the right to the single crystal susceptibility.

An apparatus of the Faraday type which satisfies the condition of uniformity for H and grad$|H|$ over a suitable volume has been designed[1] and applied to the measurement of polycrystalline graphite. A Honda-Owen correction has been employed to determine the effect of ferromagnetic impurities, using field strengths from 8000 to 16 000 oersteds. The total susceptibility $\Sigma\chi_m$ has been measured for various grades running from various petroleum base Atcheson graphites to natural and lampblack graphites. Although the accuracy of the measurements is of the order of 1 percent, the precision and relative values are correct to better than 0.5 percent. Small cubical samples $\frac{1}{8}$ inch on edge were employed. For a given type of graphite the invariance of the total susceptibility was verified to 0.5 percent, and all the Atcheson graphites examined fell in the range -20.5×10^{-6} to -21.2×10^{-6} cgs. For comparison, Guha and Roy[2] find for the spur of a single crystal the value -23.5×10^{-6} cgs. The "anisotropy ratio" for the manufactured graphites ranged from 1:1 to 9:1, whereas that reported for the single crystal was of the order of 60/1. One may interpret these results as suggesting that not more than 10 percent of the material in the artificial graphites is of a nongraphitic nature.

One should expect a single determination of the susceptibility of a powdered, and presumably randomly oriented, artificial graphite to be one-third of -21×10^{-6}, or about -7×10^{-6}. Values reported in the literature range from -3×10^{-6} to -5×10^{-6}. These low values are probably due to orientation of the powder either in packing or in the magnetic field, or possibly to a ferromagnetic impurity. The present results demonstrate that manufactured graphite yields the same susceptibility as natural graphite, up to a minor correction for intercrystallite carbon, or crystallites too minute to develop a crystalline field.

* This report is based on studies conducted for the U. S. Atomic Energy Commission.

[1] J. J. Donoghue (to be published).

[2] B. C. Guha and B. P. Roy, Indian J. Phys. **17**, 348 (1934).

The Statistics of a Two-Dimensional, Hexagonal Net

J. P. Hobson and W. A. Nierenberg
Department of Physics, University of California, Berkeley, California
(Received December 11, 1952)

In a recent paper,[1] Gurney discusses the specific heat of graphite and shows that for low temperatures, the specific heat goes as T^2 and is consistent with the model he proposes to describe the distribution of normal modes. In this model, the only contributing modes at these low temperatures are those that propagated in the plane of the hexagonal network of the carbon atoms and whose displacements are perpendicular to these planes. It is the two-dimensional nature of the problem that leads to the T^2 law, and the analysis of the problem is completed using a Debye frequency distribution and a Debye temperature.

However, for this problem, a closed analytic expression can be found for the frequency distribution by methods previously described[2] for the case of nearest neighbor interactions. The coupling constant between nearest neighbors can be evaluated from the comparison of the value of the distribution function at zero frequency and the low temperature behavior of the specific heat.

The distribution function is written as $g(\tilde{\omega}^2)d(\tilde{\omega}^2)$, where $\tilde{\omega}^2$ is the dimensionless frequency whose range is $0\leq\tilde{\omega}^2\leq1$ and is related to the maximum frequency $\omega=\omega_{\max}\tilde{\omega}$. In this expression $\omega_{\max}=(6\alpha)^{\frac{1}{2}}$, where α is the ratio of the force constant and the atomic mass and is described by writing the contribution to the acceleration of the nth atoms as $-\alpha(u_n-u_N)$, where u_n is the atomic coordinate and u_N is the coordinate of a nearest neighbor.

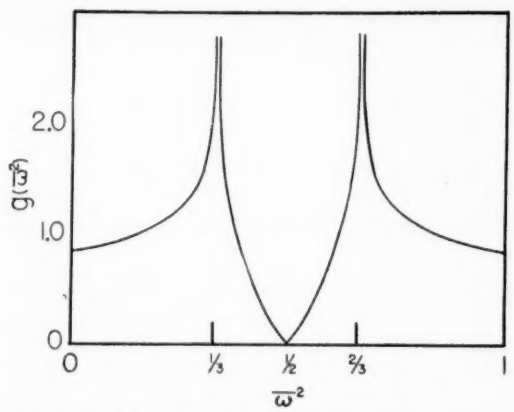

FIG. 1. The distribution function $g(\tilde{\omega}^2)$ *vs* $\tilde{\omega}^2$ for the two-dimensional hexagonal net in nearest neighbor interaction in normal vibration to the plane of the net.

With this notation, the expression for $g(\tilde{\omega}^2)$ is

$$g(\tilde{\omega}^2)=\frac{9}{\pi^2}\left[\frac{1-2\tilde{\omega}^2}{3}\right]^{\frac{1}{2}}K\left[\frac{\tilde{\omega}^2(2-3\tilde{\omega}^2)^2}{(1-2\tilde{\omega}^2)}\right]^{\frac{1}{2}},\quad 0\leq\tilde{\omega}^2\leq\tfrac{1}{3};$$
$$g(\tilde{\omega}^2)=\frac{9}{\pi^2}\frac{1-2\tilde{\omega}^2}{[3\tilde{\omega}^2(2-3\tilde{\omega}^2)^2]^{\frac{1}{2}}}K\left[\frac{1-2\tilde{\omega}^2}{\tilde{\omega}^2(2-3\tilde{\omega}^2)^2}\right]^{\frac{1}{2}},\quad \tfrac{1}{3}\leq\tilde{\omega}^2\leq\tfrac{1}{2};\qquad(1)$$

where

$$K(p)=\int_0^1\frac{dx}{[(1-x^2)(1-p^2x^2)]^{\frac{1}{2}}},$$

and the function is symmetric about $\tilde{\omega}^2=\frac{1}{2}$.

Figure 1 is a plot of $g(\tilde{\omega}^2)$. There are two symmetric infinite peaks whose asymptotic behavior is described by

$$g(\tilde{\omega}^2)\cong\frac{9}{2\pi^2}\log\frac{2}{1-3\tilde{\omega}^2},\qquad(2)$$
$$\tilde{\omega}^2\to\tfrac{1}{3}.$$

The specific heat at low temperatures is determined by $g(0)$, whose value is

$$g(0)=9/2\pi\sqrt{3}.\qquad(3)$$

The specific heat per mole at low temperatures can be found from the following expression for a two-dimensional lattice:

$$C_V=3.606Nkg(0)T^2/\theta^2,\qquad(4)$$

where $g(0)\neq0$ and is finite and $\theta=\hbar\omega_{\max}/2k$. Using the data[3] from reference 1, we find $\alpha=13.34\times10^{26}$ sec^{-2}, and $\omega_{\max}=8.95\times10^{13}$ sec^{-1}.

The details of the calculation will be published elsewhere.

[1] Ronald W. Gurney, Phys. Rev. **88**, 465 (1952).

[2] W. A. Nierenberg, J. Chem. Phys. **19**, 659 (1951).

[3] It can be remarked that the first entry in reference 1, Table I, for θ^2 should be 373 000, improving the T^2 fit and changing the mean θ^2 to 375 200.

Normal Fluid Concentration in Liquid Helium II below 1°K*

D. de Klerk,† R. P. Hudson, and J. R. Pellam
Cryogenics Laboratory, National Bureau of Standards, Washington, D. C.
(Received December 11, 1952)

Measurements of second sound velocity u_2 recently obtained by the authors[1] permit one to calculate the normal fluid concentration ρ_n/ρ at temperatures below 1°K. This has been done, employing the well-known relationship

$$\rho_n/\rho_s=\frac{S^2T}{C}\frac{1}{u_2^2},\qquad(1)$$

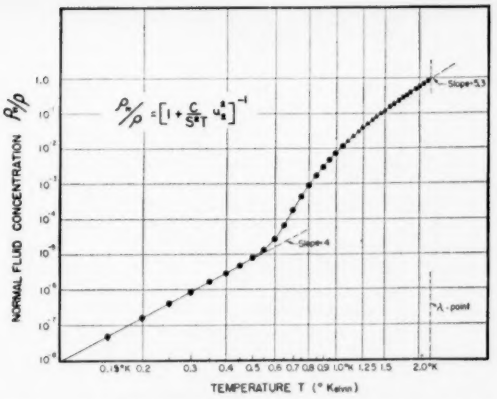

FIG. 1. Normal fluid concentration ρ_n/ρ *versus* temperature. Values of ρ_n/ρ are plotted *versus* temperature T (°K) on a log-log basis. The circles ● represent values of ρ_n/ρ computed from our recent second sound velocity measurements (see reference 1). Triangles ▲ represent those computed from earlier second sound data by Peshkov (see reference 4) and by Herlin (see reference 5). The squares ■ in the upper temperature range represent ρ_n/ρ measurements by Andronikashvilli employing the oscillating disk technique. To avoid confusion in presenting these data, we have not shown overlap between the three sets of measurements.

in terms of entropy S, specific heat C, and the density of normal fluid ρ_n and superfluid ρ_s. Since for temperatures well below 1°K liquid helium II is composed almost entirely of the superfluid component, Eq. (1) also holds effectively for the normal fluid concentration (i.e., $\rho_n/\rho_s \simeq \rho_n/\rho$).

Our second sound measurements were combined with the specific heat and entropy data of Kramers, Wasscher, and Gorter,[3] to determine the ratio ρ_n/ρ of normal fluid density to total fluid density. The results are given in Fig. 1, where ρ_n/ρ is plotted *versus* temperature T on a $\log_{10}$–$\log_{10}$ scale.

The large circles below 1.1°K are values computed from our second sound curve[1] at temperatures for which tabulated values of C and S are available.[3] At temperatures below 0.3°K, there is some uncertainty in the values of ρ_n/ρ (the extent of uncertainty being indicated by vertical lines), since the observed velocities display an anomalous increase in the 0.05°K–0.3°K range.[1] This is apparently a superficial effect, possibly a shock wave or phonon mean free path phenomenon, without thermodynamic significance to formula (1). Accordingly, below 0.3°K we have employed values of u_2 extrapolated from our more reliable measurements above 0.3°K; these values of ρ_n/ρ are indicated as the solid circles, with vertical lines extending down to values computed on the basis of our actual (anomalous) u_2 measurements.

The solid curve drawn through these circles represents our determination of the dependence of ρ_n/ρ on temperature. Above 1.3°K we have indicated by squares ■ Andronikashvilli's[3] original values of ρ_n/ρ measured by the oscillating disk technique. Finally, in the 1.1°K–1.5°K region, values represented by triangles ▲ were computed from Peshkov's[4] and Herlin's[5] earlier velocity measurements (and Kramers, Wasscher, and Gorter's values of C and S).

The slope of $\log_{10}(\rho_n/\rho)$ *versus* $\log_{10}T$ within various temperature regions is of interest. In the upper temperature range of liquid helium II, the original Andonikashvilli results show a slope of 5.3, whereas the best straight line through the Peshkov-Herlin data gives roughly 6. With decreasing temperature the steepness of this curve continues to increase, with the result that our slope eventually reaches a maximum value of about 13 at 0.7°K. For still lower temperatures, however, our slope decreases again, rapidly reaching an eventual limiting value of 4 below 0.5°K, as indicated by the dotted line.

This fourth power temperature dependence of ρ_n/ρ near absolute zero is, of course, a direct consequence [see Eq. (1)] of the T^3 entropy (and specific heat) relationship, plus the fact that the second sound velocity u_2 has become relatively constant at these temperatures. This represents the T^4 behavior of ρ_n/ρ originally predicted by Landau[6] for temperatures approaching absolute zero, where phonon effects should predominate. In fact it was Landau's correct deductions that ρ_n/ρ would vary as T^4, and specific heat and entropy as T^3, which originally led him to the conclusion that second sound velocity should approach a constant value at absolute zero.

Numerical values of our determination of ρ_n/ρ will be given in tabular form in our final publication.

* Supported in part by the U. S. Office of Naval Research.
† On a one-year leave of absence from the University of Leiden, Leiden, Holland.

[1] de Klerk, Hudson, and Pellam, Phys. Rev. **89**, 326 (1953).
[2] Kramers, Wasscher, and Gorter, Physica **18**, 329 (1952).
[3] E. L. Andronikashvilli, J. Phys. (U.S.S.R.) **10**, 201 (1946).
[4] V. Peshkov, J. Phys. (U.S.S.R.) **10**, 389 (1946); J. Exptl. Theor. Phys. (U.S.S.R.) **18**, 951 (1948).
[5] R. D. Maurer and H. A. Herlin, Phys. Rev. **76**, 948 (1949).
[6] L. Landau, J. Phys. (U.S.S.R.) **5**, 71 (1941); **8**, 1 (1944); **11**, 91 (1947).

Effects of *F* Centers on the Internal Friction of Rocksalt Single Crystals*

D. R. FRANKL AND T. A. READ
Columbia University, New York, New York
(Received December 15, 1952)

WE have studied the effects of introduction and removal of *F* centers on the internal friction of rocksalt single crystals. The specimens were pure synthetic crystals, obtained from the Harshaw Chemical Company. Internal friction measurements were made at room temperature over a range of strain amplitudes by the composite piezoelectric oscillator method described by Read.[1] Results for one specimen are shown in Fig. 1. In the "as grown" condition, after sawing and polishing to size, the increase of internal friction with strain amplitude (Fig. 1, curve *A*) is qualitatively similar to the behavior of any metals, for which the damping has been attributed to motion of dislocations.[1]

On mild x-irradiation at room tempertture the internal friction was markedly reduced (Fig. 1, curve *B*). The irradiation was carried out by placing the speciment directly before the beryllium window of an x-ray tube operating at 40 kv, 20 ma, for 20 minutes at each of six spots covering one entire face of the crystal. This dosage was sufficient to impart a deep amber coloration throughout the crystal with some decrease of intensity in the direction of incidence. Milder irradiations of similar specimens gave less intense coloration extending only partly through the crystal, and the consequent reduction of internal friction was smaller.

Removal of the *F* centers by bleaching with visible light, and removal by infrared irradiation of any *F'* centers that may have been formed did not return the internal friction to its initial value (Fig. 1, curve *C*). However, a mild anneal (30 minutes at 200°C, followed by slow cooling to room temperature) did increase the internal friction nearly to its initial value (curve *D*).

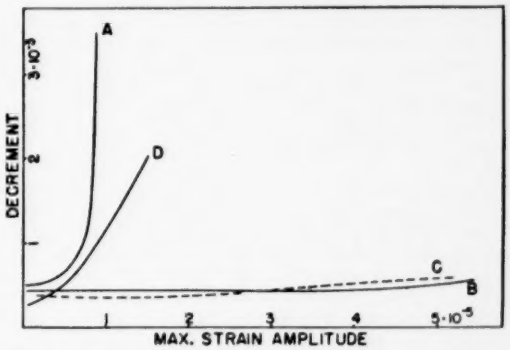

FIG. 1. Effect of room temperature x-irradiation on internal friction. *A*: before irradiation; *B*: irradiated; *C*: bleached; *D*: annealed.

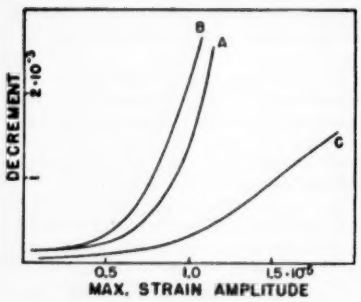

FIG. 2. Effect of cold x-irradiation on internal friction. *A*: before irradiation; *B*: cold irradiation and cold bleach; *C*: cold irradiation, and room temperature bleach.

Figure 2 shows the results obtained on another specimen which was x-irradiated at liquid nitrogen temperature. When the specimen was bleached while still cold, there was no reduction of internal friction (Fig. 2, curve *B*); but when the specimen was warmed to room temperature before bleaching, the internal friction was reduced (Fig. 2, curve *C*). These cold irradiations (40 kv, 35 ma, 20 minutes per spot) imparted only slight coloration to the crystal.

On lowering the internal friction by irradiation, the resonant frequencies of the specimens increased by a few parts in 10^4, i.e., the Young's modulus increased by about 0.1 percent.

These results may be interpreted in terms of a mechanism proposed by Seitz[3] in connection with *F* center formation. The crystal initially contains equal numbers of positive- and negative-ion vacancies, most of which are bound together in pairs. On trapping an electron in a negative vacancy, the associated positive vacancy is set free and, being mobile, will diffuse away if the temperature is high enough.

We propose that these free positive-ion vacancies diffuse to and interact with dislocations. Thus, the initial high damping is due to the motion of "free" or "loosely pinned" dislocations, and on trapping the positive-ion vacancies these dislocations become "firmly pinned," increasing the modulus and decreasing the internal friction. The binding energy of the pinning vacancies is small, since at slightly elevated temperatures they diffuse away and recombine with the negative-ion vacancies.

* This work was supported by the Office of Ordnance Research.
[1] T. A. Read, Phys. Rev. **58**, 371 (1940).
[3] F. Seitz, Revs. Modern Phys. **18**, 384 (1946).

Saturation in the X-Ray Coloration of Corundum Single Crystals*

R. ALLAN HUNT AND ROBERT H. S HULER
Departments of Physics and Chemistry, Canisium College, Buffalo, New York
(Received December 8, 1952)

THE coloration induced in single crystals of corundum (aluminum oxide) by x-radiation in the region of 0.2A wavelength has been investigated. During the course of many irradiations, it has been observed that the characteristic absorption bands rapidly approach a low but constant saturation level with additional irradiation, for the maximum dosages utilized, having no appreciable effect on the coloration.

Two single crystals, each having a thickness of 5.1 mm and optically polished faces 20 mm×10 mm, were used.[1] The crystals were irradiated at a distance of 9 cm from the target of an industrial x-ray unit operated at 120 kv and 5 ma. Energy was absorbed in the crystal at a rate of approximately 2×10^{17} ev per cc per min. During the irradiation a small blower served to keep the crystals at room temperature. In one series of irradiations, the gamma-radiation from 300 millicuries of Co^{60} was employed in the activation. The intensity here was about one one-hundredth as great as in the case of the experiments using x-radiation.

The induced coloration was visually observed to be homogeneous throughout the crystal and light brown in color, with the intensity of coloration being very low in all cases. The absorption spectrum was measured with the aid of a Beckman DU quartz spectrophotometer. In Fig. 1 are represented typical spectra (after correction has been made for the blank crystals) obtained for crystals irradiated to the saturation point. Two dominant absorption bands are noted with maxima at about 230 mμ and at 400 mμ with an additional weak band appearing in the region around 650 mμ. For the band at 400 mμ the wavelength and intensity of absorption appears to be very similar in both crystals, while at 230 mμ, although the band peaks occur at the same wavelength, the intensity of absorption in crystal 2 is about twice that in crystal 1. In regard to this point, it was found that before irradiation crystal 1 had a considerably lower transmission than crystal 2 in the region below 250 mμ. The saturation level was found to be about the same in the case of irradiation with Co^{60} gamma-radiation as for the more intense x-irradiation.

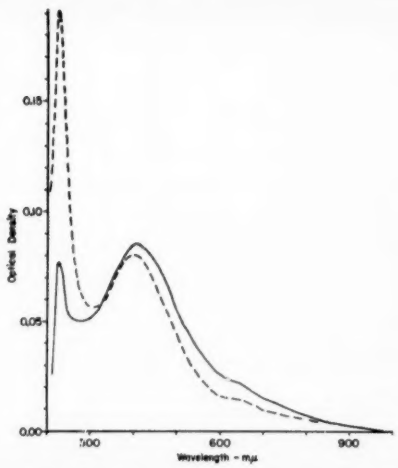

FIG. 1. Absorption spectra of x-irradiated single crystals of corundum. The optical density ($-\log I/I_0$) is corrected for the transmission of the blank crystal. The solid curve represents crystal 1; the broken curve crystal 2.

At 400 mμ the absorption coefficient of the saturated crystal is approximately 0.4 cm^{-1}. This is two orders of magnitude lower than the saturation coefficient for sodium chloride estimated at 41 cm^{-1} from the work of Alger.[2] Since the energy absorbed in producing the coloration is less by about a factor of one hundred than that utilized in the case of sodium chloride, it is believed that the low coloration level is due not to a decrease in the intensity of absorption of the individual centers but rather to a decrease in the number of centers. Assuming an oscillator strength of unity for the absorbing center, the color center concentration is estimated to be about 2×10^{15} centers per cc.

At room temperature the coloration seems to be relatively stable over moderate periods of time, i.e., weeks. The crystals were heated for periods up to 24 hours at 1000°C and found to bleach to a blank identical to that of the unirradiated crystal. Throughout the course of numerous processings of this type, there was no observable effect upon subsequent radiation coloration. Heating of the crystals on a hot plate at about 500°C was observed to produce a pinkish thermoluminescence of low intensity with the intensity being greater for crystal 2.

Further work is in progress on the thermal and optical bleaching of this radiation-induced coloration.

* Supported in part under contract with the U. S. Atomic Energy Commission.
[1] We wish to thank the Linde Air Products Company for their cooperation in supplying the crystals used here. The two crystals were obtained about one year apart and represent completely different samples.
[2] R. S. Alger, J. Appl. Phys. **21**, 30 (1950).

The Angular Momenta of the Excited States of Pt^{196}†

ROLF M. STEFFEN
Department of Physics, Purdue University, Lafayette, Indiana
(Received December 15, 1952)

THE angular correlation of the Pt^{196} gamma-rays has been measured before[1] and was interpreted as characteristic for two quadrupole transitions between levels of angular momenta I of 2, 2, and 0. Internal conversion data[2] indicate electric quadrupole radiation for both transitions.

Recently, a number of parity unfavored gamma-transitions were found to be a mixture of magnetic dipole and electric quadrupole radiation.[3-5] A similar mixed transition may be expected for the first gamma-ray of the Pt^{196} cascade, being due to a parity unfavored transition between states of the same angular momentum ($I=2$). The accuracy of the former Pt^{196} angular correlation measurements was not sufficient to allow a determination of the dipole admixture intensity; the Pt^{196} gamma-gamma correlation was therefore remeasured using much improved experimental techniques and evaluation methods.[6]

To avoid the detection of scattered radiation two techniques were employed which yielded the same angular correlation (within 1.5 percent): (1) the two NaI(Tl) crystals which were used to detect the Pt^{196} gamma-rays of 0.330 Mev and 0.358 Mev were covered with 0.2-cm lead on the front and 1.5-cm lead on the side, or (2) pulse-height discrimination was employed making the use of any lead absorber unnecessary. The discriminator bias was set at the lower edge of the 0.330-Mev photopeak. The data for the Pt^{196} gamma-gamma angular correlation are shown in Fig. 1.

The Au^{196} sources used were in the form of dilute solutions of $AuCl_3$ in order to obtain the maximum angular correlation;[7,8] however, sources of dry $AuCl_3$ and Au^{196} imbedded in gold (Au^{196} produced by the $Au^{197}(n, 2n)Au^{196}$ reaction) showed the same angular correlation as above (within 3 percent).

The data, fitted by least squares to an angular correlation function $W(\theta)=1+a_2\cos^2\theta+a_4\cos^4\theta$, taking the finite angular resolution of the apparatus into account,[9] give for the correlation coefficients: $a_2=-1.02\pm0.05$ and $a_4=+1.32\pm0.05$. The maximum anisotropy, calculated from the coincidence rate at $\theta=90°$, $\theta=270°$, and $\theta=180°$ after correction for the angular resolution was determined as $(a_2+a_4)=+0.28\pm0.03$. This correlation function is consistent with the assignment 2, 2, 0 for the angular momenta of the excited states and the ground state of Pt^{196}, the first transition being a mixture of 95 percent quadrupole and 5 percent dipole radiation and the two components being out of phase (in Lloyd's[10] notation; same sign of the reduced electric and magnetic matrix elements in the notation of Biedenharn and Rose[11]). The data on internal conversion are consistent with both transitions being mainly electric quadrupole (+5 percent magnetic dipole in the first transition), indicating the same parity for all three levels involved (Fig. 2).

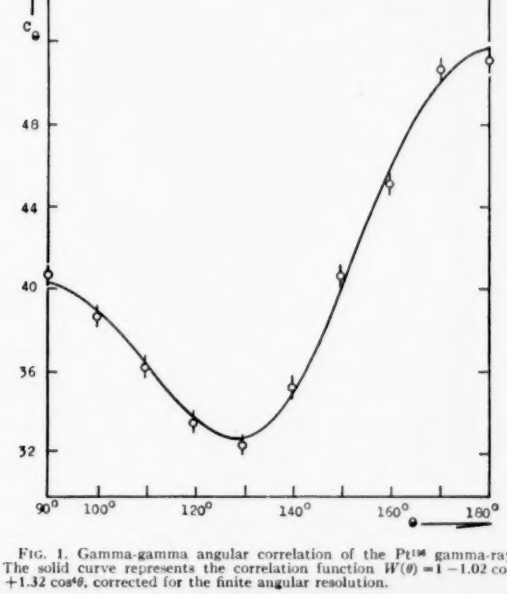

FIG. 1. Gamma-gamma angular correlation of the Pt^{196} gamma-rays. The solid curve represents the correlation function $W(\theta)=1-1.02\cos^2\theta+1.32\cos^4\theta$, corrected for the finite angular resolution.

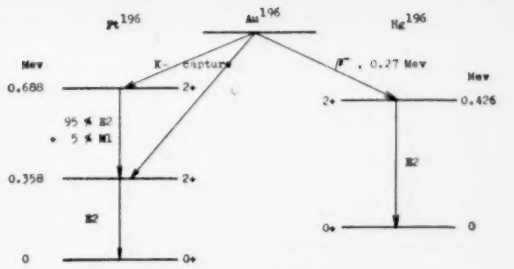

FIG. 2. Decay of Au^{196} and the angular momenta of the excited states of Pt^{196}.

These assignments would suggest a strong cross-over transition of 0.688-Mev energy to the ground state of Pt^{196}. The search for such a gamma-radiation with a scintillation spectrometer resulted in an upper limit for the intensity of the cross-over transition of less than 1 percent.

It is interesting to note that, in the very similar case of the Cd^{114} gamma-rays,[4,5] the magnetic dipole (96 percent) and electric quadupole (4 percent) components are in phase, whereas the case of Pt^{196} there is a phase difference of π.

Recently, an angular correlation of the Pt^{196} gamma-rays in agreement with these measurements has been observed by the Zurich group.[12]

† Supported by the U. S. Atomic Energy Commission.
[1] R. M. Steffen and D. M. Roberts, Phys. Rev. **82**, 332 (1951).
[2] Steffen, Huber, and Humbel, Helv. Phys. Acta **22**, 167 (1949).
[3] Aeppli, Frauenfelder, and Walter, Helv. Phys. Acta **24**, 335 (1951).
[4] E. D. Klema and F. K. McGowan, Phys. Rev. **87**, 524 (1952).
[5] Rolf M. Steffen and W. Zobel, Phys. Rev. **88**, 170 (1952).
[6] Rolf M. Steffen (to be published).
[7] J. C. Kluyver and M. Deutsch, Phys. Rev. **87**, 203 (1952).
[8] Rolf M. Steffen (to be published).
[9] Walter, Huber, and Zunti, Helv. Phys. Acta **23**, 697 (1952); see also H. Frauenfelder, *Annual Review of Nuclear Science*, Vol. 2, (to be published).
[10] S. P. Lloyd, Phys. Rev. **85**, 904 (1952).
[11] L. C. Biedenharn and M. E. Rose, Revs. Modern Phys. (to be published).
[12] E. Heer *et al.* (private communication by H. Frauenfelder).

States of S^{33} and Si^{29} from (d, p) Stripping

J. R. HOLT AND T. N. MARSHAM
Nuclear Physics Research Laboratory, University of Liverpool, Liverpool, England
(Received December 15, 1952)

WE have used a proportional counter telescope to examine the angular distributions within the range 0° to 90° of several groups of protons from the reactions $S^{32}(d, p)S^{33}$ and $Si^{28}(d, p)Si^{29}$ with 8-Mev deuterons. By comparing these distributions with the theories of the stripping process,[1,2] the appropriate value of the orbital angular momentum l of the captured neutron has been determined in each case. These values are given in Tables I and II, together with the excitation energies of the final states. The spins of these states have one of the values $l\pm\frac{1}{2}$. Some of the

TABLE I. $S^{32}(d, p)S^{33}$.

Proton group	Excitation (Mev)	l value	Relative neutron capture probability, A	A / $(2j_f+1)$	Shell model term
p_0	0	2	8.0	2.0	$1d_{3/2}$
p_1	0.85	0	1.5	0.75	$(2s_{1/2})^{-1}(1d_{3/2})^2$
p_4	2.90	3	20	2.5	$1f_{7/2}$
p_6	3.26	1	13	3.2	$2p_{3/2}$
p_7	4.21	1	1.6	0.8 or 0.4	...
p_9	4.89	1	0.8	0.4 or 0.2	...
p_{11}	5.72	1	9	4.5	$2p_{1/2}$

proton groups were too weak for measurement, and these are indicated by the gaps in the sequence of group numbers.

Using the theory of Bhatia *et al.* and the measured differential stripping cross sections, we have calculated the value of the quantity A for each proton group. This is proportional to the nuclear capture probability for the neutron within the deuteron when the neutron arrives at the nuclear surface with the correct angular and linear momenta to form the final state in question. Numbers proportional to A are given in the tables but are unrelated in the two cases.

It is expected that the capture probability will be greatest when the neutron is captured directly into an orbit, i.e., into a state of single-particle excitation. In such cases the relative capture probability may depend mainly on a statistical factor $(2j_f+1)$, where j_f is the spin of the final state.

In the reaction $S^{32}(d, p)S^{33}$ (Table I) the sequence of l values of the transitions with the greatest values of capture probability is 2, 3, 1, 1, where the first belongs to the transition to the ground state. The orbits available to the odd neutron in S^{33} according to the shell model are $1d_{3/2}$, $1f_{7/2}$, $2p_{3/2}$, $1f_{5/2}$, $2p_{1/2}$ in order of increasing energy. We suggest that the states of S^{33} corresponding to the proton groups p_0, p_4, p_6, p_{11} and having l values 2, 3, 1, 1 are states formed by capture of a neutron into the orbits $1d_{3/2}$, $1f_{7/2}$, $2p_{3/2}$, $2p_{1/2}$, while the core S^{32} remains unexcited. If we assume that the spins of these states are those given by the shell model and remove the factor $(2j_f+1)$ from the values of the capture probability, these become more nearly equal (Table I).

The proton groups associated with low values of the capture probability correspond to states requiring the excitation of one or more particles of the nuclear core. In particular, the first excited state with spin $\frac{1}{2}$ is probably produced by a neutron from the $2s_{1/2}$ level of the core being lifted to the $1d_{3/2}$ level to form a pair of resultant spin 0 with the captured neutron. In support of this we note that the first excited state of S^{33} has an energy of 0.6 ± 0.2 Mev[3] close to the value 0.85 ± 0.03 Mev for this state of S^{33}.

In the reaction $Si^{28}(d, p)Si^{29}$ the sequence of l values associated with the largest values of the capture probability is 0, 2, 3, 1. As before, we suggest that the states of Si^{29} corresponding to the proton groups p_0, p_1, p_5, p_9, with l values 0, 2, 3, 1 are formed by

TABLE II. $Si^{28}(d, p)Si^{29}$.

Proton group	Excitation (Mev)	l value	Relative neutron capture probability, A	A / $(2j_f+1)$	Shell model term
p_0	0	0	9.0	4.5	$2s_{1/2}$
p_1	1.278	2	15	3.7	$1d_{3/2}$
p_2	2.027	2	5.7	0.8	$(1d_{5/2})^{-1}(2s_{1/2})^2$
p_4	3.070	2	1.9	0.5 or 0.3	...
p_5	3.623	3	19	2.4	$1f_{7/2}$
p_9	4.934	1	16	4.0	$2p_{3/2}$
p_{12}	6.380	1	5.4	2.7 or 1.3	$2p_{1/2}$?

capture of a neutron into the orbits $2s_{1/2}$, $1d_{3/2}$, $1f_{7/2}$, $2p_{3/2}$. Comparison of the values of the capture probability after correcting for the factor $(2j_f+1)$ (Table II) suggests that the twelfth excited state may be the $2p_{1/2}$ state.

The second excited state having l value 2 and spin 5/2 or 3/2 is probably produced by a neutron from the $1d_{5/2}$ level of the core being lifted to the $2s_{1/2}$ level to form a pair with the captured neutron. Again we observed that the energy of the first excited state of the Si^{28} core is 1.8 ± 0.2 Mev,[4] close to the value 2.027 Mev for this state of Si^{29}.

A full account of this work will be published elsewhere.

[1] S. T. Butler, Proc. Roy. Soc. (London) **A209**, 461 (1951).
[2] Bhatia, Huang, Huby, and Newns, Phil. Mag. **43**, 485 (1952).
[3] S. C. Snowdon, Phys. Rev. **86**, 630 (1952).
[4] R. A. Peck, Phys. Rev. **76**, 1279 (1949).

The American [illegible] of Physics

[illegible]ORATED

57 East [illegible] Street, New York 22, N.Y.

MEMBER SOCIETIES:

American Physical Society
: Karl K. [illegible], *Secretary*, Columbia [illegible], New York 27, New York

Optical Society of America
: Arthur [illegible], *Secretary*, Massachusetts Institute of Technology, Cambridge [illegible], Massachusetts

Acoustical Society of America
: Wallace Waterfall, *Secretary*, 57 East [illegible] Street, New York 22, New York

Society of [illegible]
: G. J. D[illegible], *Secretary*, Brookhaven [illegible] Laboratory, Upton, Long Island, New York

American Association of Physics Teachers
: R. F. P[illegible], *Secretary*, University of [illegible], Urbana, Illinois

AFFILIATED SOCIETIES:

- American [illegible] Association
- American Society for Metals
- Electron Microscope Society of America
- Physical Society of Pittsburgh
- Physics Club of Chicago
- Physics Club of Philadelphia
- Cleveland Physics Society
- Physics Club of the Lehigh Valley
- Sigma Pi Sigma

ASSOCIATES:

Over seventy-[illegible] leading industrial [illegible] and other institutions which contribute to the support of the Institute.

JOURNALS:

The Physical Review
: S. A. Goudsmit, *Editor*, Brookhaven National Laboratory, Upton, Long Island, New York

Reviews of Modern Physics
: J. W. [illegible], *Editor*, University of Minnesota, Minneapolis, Minnesota

Journal of the Optical Society of America
: Wallace R. [illegible], *Editor*, National Bureau of Standards, Washington 25, D. C.

The Journal of the Acoustical Society of America
: Floyd A. [illegible], *Editor*, 57 East [illegible] Street, New York 22, New York

American Journal of Physics
: Thomas H. [illegible], *Editor*, Michigan State College, East Lansing, Michigan

The Review of Scientific Instruments
: Gaylord P. Harnwell, *Editor*, Randal Morgan Laboratory of Physics, University of Pennsylvania, Philadelphia, Pennsylvania

The Journal of Chemical Physics
: Clyde A. [illegible], Jr., *Editor*, Institute for Nuclear Studies, University of Chicago, Chicago 37, Illinois

Journal of Applied Physics
: Elmer [illegible], *Editor*, Case Institute of Technology, Cleveland 6, Ohio

Physics Today
: Gaylord P. Harnwell, *Editorial Director*; [illegible] R. Davis, *Managing Editor*, American Institute of Physics, 57 East 55 Street, New York 22, New York

OFFICERS

[illegible], *Chairman*
Massachusetts Institute of Technology

[illegible], *Treasurer*
[illegible] University

GOVERNING BOARD

[illegible]

Committee on Printing
[illegible]

ADMINISTRATIVE STAFF

[illegible], *Director*
Wallace Waterfall, *Executive Secretary*
[illegible], *[illegible] Manager*
[illegible], *Publication Manager*
[illegible], *Assistant Secretary*
[illegible], *Circulation Manager*
[illegible], *Assistant Treasurer*

The American Institute of Physics was founded in 1931 as a federation of leading societies in the field of physics. It combines into one operating agency those functions on behalf of physics which can best be done by the Societies jointly. Its purpose is the advancement and diffusion of physics and its application to human welfare. To this end it publishes for itself or the Societies the nine journals listed on this page; promotes unity and effectiveness of effort among all who are interested in physics; renders numerous direct services to physicists and to the public; and cooperates with government agencies, national associations, educational institutions, industrial laboratories, and others in such manner as to realize the opportunities and fulfill the responsibilities of physics as an important and constructive human activity.

CONTENTS

THE PHYSICAL REVIEW SECOND SERIES, VOLUME 89, NO. 3 FEBRUARY 1, 1953

Internal Pair Production of γ-Rays of Nuclear Origin; Alternate Modes of $^{16}O^{*}$ Decay . . . . . P. LIENHARD, A. SACHS, AND J. SCHNEIDERMAN 531

Blocked Capillary Method for Determining Melting Pressures: The Melting Curve of Helium from 1.8° to 4°K . . . . . C. A. SWENSON 538

Z-Dependence of the Pair Production Cross Section at 1.33 and 2.62 Mev . . . . . EUGENE E. DAYTON 544

Radiochemical Studies on the Fission of Th^{232} with Li+D Neutrons . . . . . A. TURKEVICH, J. B. NIDAY, AND ARTHUR TOMPKINS 562

Ionization Probability Curves for Krypton and Xenon near Threshold . . . . . R. E. FUNK, W. M. HICKAM, AND T. KJELDAAS, JR. 568

Gamma-Radiations from Zr^{95} and Nb^{95} . . . . . C. E. MANDEVILLE, E. SHAPIRO, R. I. MENDENHALL, E. E. ZUCKER, AND G. L. COWELIN 569

Neutron Scattering by Coupled Paramagnetic Ions . . . . . PHILIP J. ELICH 561

Genetics of the Ga^{69}—As^{75} Fission Chain . . . . . NATHAN SUGARMAN 570

Isomer Eb^{154m} . . . . . R. S. CAIRD AND ALLAN C. G. MITCHELL 573

Multiple Scattering and the Many-Body Problem—Applications to Photomeson Production in Complex Nuclei . . . . . KENNETH M. WATSON 575

Quasi-Relativistic Theory of Gravitation . . . . . MARVIN G. MOORE 587

Pion-Nucleon Scattering When the Coupling Is Weak and Extended . . . . . GEOFFREY F. CHEW 591

Heat Conduction of the Boundary Layer in Liquid Helium II . . . . . DAVID WHITE, O. D. GONZALES, AND H. L. JOHNSTON 598

Nuclear Gyromagnetic Ratios. IV . . . . . YU TING AND DUDLEY WILLIAMS 596

Some Points of the Theory of Liquid Helium II . . . . . LOUIS GOLDSTEIN 597

High Energy Photoneutron Production by 322-Mev Bremsstrahlung . . . . J. W. ROSENGREEN AND J. M. DUDLEY 603

Hyperfine Structure in the Paramagnetic Resonance of the Ion $(SO_3)_2NO^{---}$ . . . . . J. TOWNSEND, S. I. WEISSMAN, AND G. E. PAKE 606

Electron-Induced Showers in Copper . . . . . ASHER KANTE AND ROBERT HOFSTADTER 607

Gyromagnetic Ratio of Supermalloy . . . . . G. G. SCOTT 618

Symmetry of the *S* Matrix . . . . . F. COESTER 619

Zr^{91}—Mo^{91} and Zr^{93}—Mo^{93} Pairs and the Zr^{91}—Mo^{91}—Ru^{91} Triplet . . . . . JAMES S. GEIGER, BENJAMIN G. HOGG, HENRY E. DUCKWORTH, AND JOHN W. DEWDNEY 621

Magnetic Crystal Anisotropy and Magnetostriction of Iron-Nickel Alloys . . . R. M. BOZORTH AND J. G. WALKER 626

Spectrum of Discrete Eigenvalues in a Negative Atomic Ion . . . . . TA-YOU WU 629

Variations in Isotopic Abundances of Strontium . . . . . L. T. ALDRICH, L. F. HERZOG, W. K. HOLTZ, F. R. WHITING, AND L. H. ASHENS 631

Magnetic Susceptibility of a Diamagnetic Electron Gas—The Role of Small Effective Electron Mass . . . . . E. N. ADAMS II 633

Proton-Proton Reaction and Energy Production in the Sun . . . . . R. A. FERRMAN AND L. MOTZ 648

Interpretation of α-Values in p—n Junction Transistors . . . . . F. S. GOUCHER AND M. B. PRINCE 651

Letters to the Editor:

Some Properties of Superconductors below 1°K . . . T. S. SMITH, W. B. GAUGE, AND J. G. DAUNT 654

Air Mass between an Observer and Outer Space . . . . . E. C. PEARSLY 654

Electric Scattering of Deuterons . . . . . U. E. KRUSE, N. F. RAMSEY, AND B. J. MALENKA 655

Search for "7-Tracks" in Photographic Plates . PAUL H. BARRETT, G. COCCONI, AND Y. EISENBERG 656

Lattice Expansion of Quartz due to Fast Neutron Bombardment . . . . . M. WITTELS 657

Thermal Neutron Absorption Cross Section of Scandium . . . . . E. E. LOCKETT AND E. BOWELL 657

Intensities of Nuclear Magnetic Resonances in Cubic Crystals . G. D. WATKINS AND R. V. POUND 658

Cross Section for $Te^{122}(Y,2n)Te^{121}$ at 17.6 Mev . J. M. CARVER, R. D. EDGE, AND D. H. WILKINSON 660

Theory of the Paramagnetism of Ionic-Like Ions . . . . . R. J. ELLIOTT 699

Influence of Electric Fields on Luminescence . . . . . FRANK MATOSSI AND SIR. NUSSELMAN 660

Anisotropic Susceptibility of Polycrystalline Graphite . . W. P. KOTHERLY AND J. D. MCCLELLAND 661

Statistics of a Two-Dimensional, Hexagonal Net . . . . . J. P. HOBSON AND W. A. NIERENBERG 663

Normal Fluid Concentration in Liquid Helium II below 1°K . . . . . D. DE KLERK, R. P. HUDSON, AND J. R. PELLAM 663

Effects of *F* Centers on the Internal Friction of Rutile Single Crystals . . . . . D. R. FRANKL AND T. A. READ 663

Saturation in the X-Ray Coloration of Corundum Single Crystals . . . . . E. ALLAN HUNT AND ROBERT H. SCHULER 664

Angular Momenta of the Ruthenium Isotopes . . . . . ROLF M. STEFFEN 665

Shapes of S^{32} and Si^{28} from (d,p) Stripping . . . . . J. R. HOLT AND T. N. MARHAM 665

LANCASTER PRESS, INC., LANCASTER, PA.